

Alma Mater Studiorum – Università di Bologna

DOTTORATO DI RICERCA IN SCIENZE
DELLA TERRA DELLA VITA E DELL'AMBIENTE

Ciclo XXXI

Settore concorsuale: 04/A2

Settore Scientifico disciplinare: GEO/01

Stratigraphic paleobiology
of late Quaternary mollusk assemblages from the
Po Plain-Adriatic Sea system

Presentata da: Michele Azzarone

Coordinatore Dottorato:

Prof. Giulio Viola

Supervisore:

Dott. Daniele Scarponi

Esame Finale anno 2019

Abstract

Stratigraphic paleobiology - a relatively new approach for investigating fossiliferous sedimentary successions - is rooted on the assumption that the fossil record cannot be read at face value, being controlled not only by biotic, but also by sedimentary processes that control deposition and erosion of sediments. By applying the stratigraphic paleobiology tenets, this Ph.D. project focused on acquisition and analyses of macrofossils data to assess the response of late Quaternary ecosystems to environmental changes and enhance stratigraphic interpretations of fossiliferous successions. A primary activity of my Ph.D. research involved assembling a macrobenthic dataset from the latest Pleistocene glacial succession of the near-Mid Adriatic Deep (Central Adriatic, Italy). This dataset once combined with its counterpart from the Po coastal plain (Holocene), will offer a unique perspective on mollusk faunas and their dynamics during the current glacial-interglacial cycle. This thesis includes four papers. The first one assessed the quality and resolution of the macrofossil record from transgressive Holocene deposits of Po plain (Italy). The second paper focused on the Holocene fossil record of the Po coastal plain to evaluate the response of trematode parasites to high-frequency sea-level oscillations. The third study investigated distribution of last occurrences of macrobenthic species along a down-dip transect in the Po coastal plain and evaluate potential effects of sequence stratigraphic architecture on mass extinction pattern. The fourth is a case study to test the robustness of the paleoecological pattern derived by the application of different ordination analyses (DCA and nMDS) and to assess the main environmental driver(s) of faunal turnover in marine settings. In summary, my Ph.D. demonstrates that even if the fossil record cannot always be read literally, the stratigraphic paleobiology approach to the geologic record makes it possible to interpret biological trends from the fossil record and enhance the stratigraphic resolution of fossiliferous successions.

Index

1. Introduction	6
1.1. The Quaternary fossil record: an ideal laboratory for stratigraphic paleobiology.....	7
1.2. Mollusk fauna as a tool for stratigraphic paleobiology	8
1.3. The Milankovitch and sub-Milankovitch cyclicity	8
2. The Po Plain-Adriatic Sea system	13
2.1. The Po Delta and its southern coastal plain.....	15
2.1.1. Tectonic setting.....	16
2.1.2. Late Quaternary stratigraphic architecture	18
2.2. The Adriatic Sea and the Mid Adriatic Deep (MAD).....	25
2.2.1. Tectonic setting.....	26
2.2.2. Late Quaternary stratigraphic architecture	29
3. Research Outlines	34
4. The Mid Adriatic Deep (MAD) dataset.....	38
4.1. MAD data collection.....	39
4.2. MAD dataset structure	41
4.3. Future applications and outreach	44
5. Manuscript I	46
<i>“Systematic vertical and lateral changes in quality and time resolution of the macrofossil record: Insights from Holocene transgressive deposits, Po coastal plain, Italy”</i>	
6. Manuscript II.....	60
<i>“Surges in trematode prevalence linked to centennial-scale flooding events in the Adriatic”</i>	
7. Manuscript III.....	87
<i>“Stratigraphic signatures of mass extinction: ecological and sedimentary determinants”</i>	
8. Manuscript IV	113
<i>“Early-Middle Pleistocene benthic turnover and oxygen isotope stratigraphy from the Central Mediterranean (Valle di Manche, Crotone Basin, Italy): Data and trends”</i>	
9. Concluding remarks.....	129
References	132

*“It is interesting to contemplate an entangled bank,
clothed with many plants of many kinds, with birds singing on the bushes
with various insect flitting about,
and with worms crawling through the damp earth,
and to reflect that these elaborately constructed forms,
so different from each other, and dependant on each other in so complex manner,
have all been produced by laws acting around us [...].*

*There is a grandeur in this view of life,
with several powers, having been originally breathed into a few forms or into one;
and that, whilst this planet has gone cycling on according to the fixed law of gravity,
from so simple a beginning endless forms,
most beautiful and most wonderful have been,
and are being,
evolved”.*

*Charles Darwin
On the Origin of Species*

Chapter **1**

Introduction

1. Introduction

Since the last few decades, a new approach for investigating fossiliferous sedimentary successions has gained approval throughout the paleontological scientific community. This recent development in the field of paleontology relies on the assumptions that the fossil record cannot be read at face value and that fossil dynamics through time and space are easier to interpret when analyzed in conjunction with their stratigraphic context (e.g., Kidwell, 1993; Holland, 1995, 2000; Scarponi and Kowalewski, 2004; Dominici and Kowalke, 2007; Patzkowsky and Holland, 2012; Terry and Novack, 2015; Danise and Holland, 2017). This relatively new paradigm to the investigation of the fossil record is known as stratigraphic paleobiology (Patzkowsky and Holland, 2012), which is rooted on the postulation that interpretation of the fossil record should also consider a modern understanding of the principles of sediment accumulation (Patzkowsky and Holland, 2012). Indeed, the distribution of fossil taxa in time and space is controlled not only by biotic processes (e.g., taxa niches, taxa evolutionary strategies, extinctions/originations) but also by physical processes that govern where and when fossiliferous sedimentary bodies are deposited and preserved. Teasing apart the effects of these two suites of processes on structuring fossil associations or at least acknowledgement of their conjunct effects, is pivotal for understand and reconstructing the dynamics of environments and their organisms through time. This is the core of stratigraphic paleobiology. Such an integrated approach is intended primarily to augment the potential of paleontological investigations to answer core questions that lays buried in the geological record of the Earth.

A clear example on the assessment and magnitude of stratigraphic controls on fossil distribution is provided by Holland (1995). Here the author shows, by means of model data, that previously described paleobiologic patterns concerning mass extinction and evolutionary dynamics may be partly stratigraphic artifacts originating from the stratigraphic architecture of investigated successions. Specifically, the first and last occurrences (FOs and LOs, respectively) of marine fossil taxa cluster within intervals of strong time condensation or along sequence boundaries. This produces a distortion of the real time of appearance or extinction so that in the fossil record, such FOs and LOs will appear to be simultaneous even if they are not. Examples of such stratigraphic forcing on fossil records have been reported for decades (Patzkowsky and Holland, 1999; Holland, 2000; Kidwell and Holland, 2002; Scarponi and Kowalewski, 2007; Holland and Allen, 2008) and have reached full recognition in Patzkowsky and Holland (2012). The authors pointed out that the introduction of sequence stratigraphy concepts, which lead to a better understanding of sedimentary basin dynamics, will help to sort true biological signals from stratigraphic artifacts that shaped the fossil record. The last few years saw a growing wealth of case studies showing that fossil dynamics are strictly linked to the sequence stratigraphic framework of the encasing sedimentary successions (e.g., Bonelli and Patzkowsky, 2008; Scarponi et al., 2013; Boessenecker et al., 2014; Huntley et al., 2014; McMullen et al., 2014; Huntley and Scarponi, 2015; Danise and Holland, 2017; Dominici et

al., 2017) and that spatial and temporal completeness of the fossil record is scale dependent (Foote and Raup, 1996; Foote, 1996; Valentine, 2004). However, it is widely accepted that even if the fossil record is not a perfect recorder of history of life, that is, it cannot be read literally, important biological and environmental signals can be interpreted. On the contrary, consideration of the sedimentary succession as a perfect recorder of history is unrealistic and is a scenario that we have always known to be incorrect. In summary, stratigraphic paleobiology approach to the geologic record has proved to be of paramount importance for detecting biological trends and enhancing the stratigraphic interpretation of sedimentary successions worldwide. My Ph.D. research focuses on gathering data and applying the stratigraphic paleobiology approach to Quaternary sedimentary successions.

1.1. The Quaternary fossil record: an ideal laboratory for stratigraphic paleobiology

The dualistic stratigraphic paleobiology approach to the investigation of the fossil record has gained traction among paleontologists who investigate bio-sedimentary dynamics during the late Quaternary, which is a period characterized by strong climate fluctuations that had profound impacts on structuring the Earth's sedimentary and biological systems (Holland et al., 2001; Scarponi and Kowalewski, 2004; Holland and Christie, 2013). Indeed, late Quaternary climate-driven sedimentary successions represent an invaluable testing ground for evaluating tenets and applying tools of stratigraphic paleobiology. These successions are also dominated by extant taxa with well-understood ecology, biology and biogeography. This enables precious insight to be gained on the scale, magnitude, and significance of several past biological key issues such as the ecological response of communities to climate transitions, while providing a refined understanding of how allo- and auto-cyclic changes in sea-level affect the formation of sedimentary bodies. In addition, detailed reconstructions of past ecological and environmental dynamics relative to high-frequency climate fluctuations provide a reference baseline for evaluating the severity and significance of anthropogenic processes that threaten present-day ecosystems and their biodiversity.

Among the multitude of currently forming basins on the Earth, the Po Plain-Adriatic Sea system represents an ideal venue for investigating bio-sedimentary dynamics and for developing and testing investigative methodologies for sedimentary geology. Indeed, Quaternary successions of the Po Plain and Adriatic Sea record a strong climatic-driven cyclicality and were deposited in a subsiding setting that preserved an expanded record of high-quality stratigraphic and paleontological data (Ridente and Trincardi, 2002; Kowalewski et al., 2015; Amorosi et al., 2017; Pellegrini et al., 2017a, 2018 and references therein). Hence, the youngest geological record of the targeted system is uniquely complete, finely studied and resolved, and the least ambiguous to interpret. In addition, ^{14}C and racemization calibrated dating have been successfully used to establish a robust geochronological

framework for the entire targeted system (Piva et al., 2008; Maselli et al., 2010; Trincardi et al., 2011; Scarponi and Kowalewski, 2013; Amorosi et al., 2017).

1.2. Mollusk fauna as a tool for stratigraphic paleobiology

The Quaternary mollusks fauna is the object of this investigation. Mollusks constitute one of the largest and most diverse phyla in the animal kingdom with a remarkable fossil record that dates back to the early Cambrian, about 541 Ma (Ponder and Lindberg, 2008; Li et al., 2017). The extant species of marine mollusks number at around 50,000 (Oliverio, 2003; Bouchet, 2006; Bouchet et al., 2016 but see Haszprunar and Wanninger, 2012). Among Mollusca, many classes are characterized by organisms bearing an endo- or exoskeleton; hence, their potential of fossilization is high. Mollusks have adapted to nearly all habitats and conditions, from arid terrestrial to deep marine settings, and are highly sensitive to environmental variables (Morton, 1967; Gutierrez et al., 2003; Bolotov et al., 2012). Hence, their environmental plasticity along with their abundance and diversity in the fossil record makes this group an excellent descriptor of past and present benthic biocenoses and an excellent proxy for biodiversity studies through time (Gambi et al., 1982; Wells, 1998; Mikkelsen and Craft, 2001; Gladstone, 2002; Tyler and Kowalewski, 2017). Moreover, Mediterranean mollusk fauna have been widely investigated since the last century for various applications (see Table I in Oliverio, 2003). This century-long activity has yielded an impressive accumulation of ecological, biological and biogeographic data. Specifically, most of the common species retrieved in targeted sedimentary successions are well documented in terms of their bathymetric and environmental requirements (e.g., Nordsieck, 1968, 1972, 1982; Parenzan, 1970; 1974, 1976; ENEA, 2017).

1.3. The Milankovitch and sub-Milankovitch cyclicality

Earth's orbital geometry around the Sun is defined by three main astronomical parameters: precession, obliquity, and eccentricity. Taken in together, variations of these parameters modulate the solar radiation received by Earth, with averaged periodicities of ca. 23, 41 and 100 ka respectively (Bradley, 1999; Ruddiman, 2014). As postulated by Milankovitch (1930, 1941) and later by Berger (1988), long-term changes in solar radiation determine cyclical climatic oscillations on Earth that in turn trigger eustatic sea-level fluctuations (Chappell, 1974; Schwarzacher, 2000). Changes in Earth's orbit during the late Quaternary are considered to be the main drivers of climate shifts at the glacial-interglacial time-scale. On much a shorter time-scale of 10^1 yr- 10^3 yr, drivers of climate variation are commonly attributed to stochastic processes occurring in the climate system (e.g., volcanic dust loading), random phenomena outside the Earth's system (e.g., solar variability) and internal iterations/feedback between the multiple sub-systems of Earth, such as oceanic global circulation and ice-sheet dynamics. These millennial- or lower-scale perturbations of the climate system, such as Dansgaard- Oeschger or Bond events, are of smaller amplitude compared with those produced by

Milankovitch forcing (Fig. 1); pairwise, however, they can leave traces in the geologic record as well (Cruz et al., 2005; Deplazes et al., 2013). In general, climate changes that have periodicity or quasi-periodicity of less than 15 ka and durations of few thousand years to a few centuries, are commonly attributed to the sub-Milankovitch frequency band.

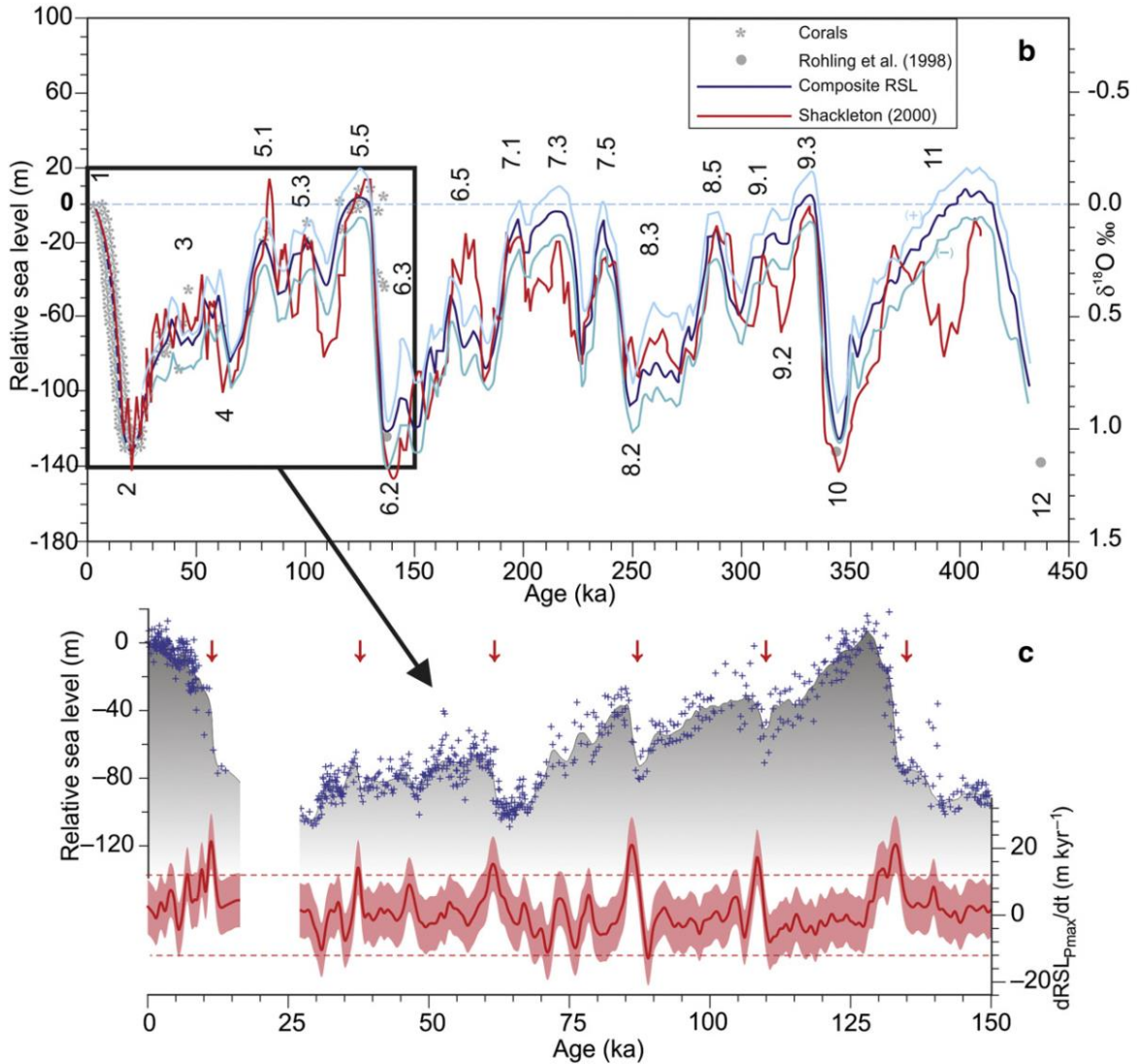


Figure 1 - Milankovitch and sub-Milankovitch cyclicality and sea-level oscillations during the last 450 ka (after Lobo and Ridente, 2014). Numbers in the upper panel represent the marine isotope stages (MIS). The lower panel displays a detail of the last 150ka (after Grant et al., 2012). Blue crosses represent relative sea-level, whereas the gray shaded areas record the maximum-probability of relative sea-level. The red line represents the rates of sea-level variation within the 95% confidence interval (pink shading). The rates of high sea-level variation (+12 and -8 m/ka) are indicated by horizontal dashed lines, whereas the red arrows point to sea-level variation higher than +12 m/ka.

In the past decades, increasing efforts have been spent on reconstructing the Milankovitch cyclicality within Quaternary shelf successions (e.g., Somoza et al., 1997; Carey et al., 1998; Bernè et al., 2004; Bassetti et al., 2008; Lobo and Ridente, 2014). Owing to their shallow depth, these deposits enable acquisition of reliable seismic imaging and are relatively obtainable by coring activities. Generally

speaking, the continental margins during the late Quaternary, were shaped by high-frequency and repeated astronomically-driven climatic oscillations. As reported by Lobo and Ridente (2014), the late Quaternary stratigraphic architecture of continental margins shows a dominant eccentricity cycle periodicity (about 100 ka), expression of major ice-volumes changes (Lisiecki and Raymo, 2005) - even though the depositional architecture of the Upper Pleistocene is better explained by precession-related signals of about 20 ka. These ~20 ka sea-level oscillations are well recorded in the sedimentary record of the last 125 ka, where they briefly interrupt the overall declining trend of sea-level by short pulses of sea-level increase (Lobo and Ridente, 2014).

Recently, high-resolution investigation of the recent sedimentary succession has revealed evidence that highlights the presence of short-lived prograding units framed by flooding surfaces that record sea-level fluctuations at the millennial time-scale. These sub-Milankovitch fluctuations coincide with quasi-periodic climate pulses and are known as Heinrich events (HE; Maslin et al., 2001; Bassetti et al., 2008; Sierro et al., 2009; Andrews and Voelker, 2018). These events are traceable in the sedimentary record of the North Atlantic by debris discharged by melting icebergs during their southward migration (Ziemen et al, 2018). These episodes are the results of the oscillations in the volume of warm and saline-rich tropical water conveyed by the thermohaline convective current from equatorial to polar regions (Little et al., 1997), under the background of unstable ice-sheets that rimmed the North Atlantic. Among the numerous proposed explanations (Little et al., 1997; Seidov and Maslin, 2001, Maslin et al., 2001), the overgrowth and collapse of Laurentide and Eurasia ice sheets, is one of the most often cited mechanisms responsible for destabilization of the thermohaline current (e.g., Broecker and Denton, 1989; Paillard and Labeyriet, 1994; Little et al., 1999; Zhang et al., 2014). The armadas of melting icebergs supplied an incredible volume of less-dense fresh water into the northern Atlantic Ocean, hampering the capability of the thermohaline current to sink and to maintain the convective overturn. This caused an abrupt cooling and renewed strong ice-sheet expansion with perturbation on the global climate (Little et al., 1997). In contrast with the hypothesis of the Laurentide ice-cap collapse, Rahmstorf and colleagues (2005) more recently proposed hysteresis in thermohaline circulation as an explanation for HEs. This means that profound variation in the pattern of global circulation was caused even by smaller changes in the fresh water supply in the North Atlantic region.

Between Heinrich events – which occurred on average every 7200 ± 2400 calendar years (Maslin et al., 2001), detailed investigation of ocean sediments and Greenland ice cores detected higher frequency episodes recurring every ~1500 years; such events are known as Dansgaard-Oeschger (D-O; Dansgaard et al., 1993; Bond et al., 1997). These events, roughly framed between two HEs, occurred 25 times during the Last Glacial and share the same causative mechanisms as those of HEs (Dowdeswell et al., 1995; Maslin et al., 2001; Marshall and Koutnik, 2006; Petersen et al., 2013). The presence of sub-Milankovich climatic fluctuations have also been documented during the Holocene and are known as Bond events. Bond and colleagues (1997) argued that these events, identifiable primarily by ice-rafting debris, can be defined as the interglacial counterparts of the D-

O glacial events and share the same forcing mechanism of quasiperiodic climate cyclicity as well as a comparable time of occurrence of ~1470 years.

These climatic fluctuations at the Milankovitch and sub-Milankovitch scale have been largely recognized also in the Adriatic and in the Po Plain sedimentary successions. For the Adriatic, Piva et al. (2008) recognized the signal related to glacial-interglacial fluctuations showing periodicities of 100 ka and 23 ka in the borehole PRAD 1-2. Within the last glacial interval, the authors were able to detect a sub-Milankovitch cyclicity interpreted as the Adriatic counterpart of the D-O events. Amorosi et al. (1999, 2004, 2008) reported that within the Po Plain, eight T-R cycles of the last 800 ka were produced in response to fourth-order cyclicity. More recently, Amorosi et al. (2017), identified a series of overall-prograding stratigraphic units (i.e., parasequences) showing short-term millennial-scale periodicity within the Holocene interglacial Po coastal sedimentary wedge.

Chapter 2

***The Po Plain–
Adriatic Sea system***

2. The Po Plain-Adriatic Sea system

The Po Plain–Adriatic Sea represents a unique and complex system of sedimentary basins that acts as a foreland for distinct mountain chains (Fig. 2.1). The Po Plain represents a foreland for the Southern Alps to the north and the Northern Apennine to the south (Ori et al., 1986; Vannoli et al., 2015). In contrast, the Adriatic Sea acts as a foreland region for both the Apennine to the west and the Dinarids to the east (Zecchin et al., 2015). The pre-Quaternary stratigraphic evolution of the Po Plain–Adriatic Sea system is dominated by a deposition of a thick succession of basin-floor turbidites owing to the growth of the Apennine chain (Rizzini and Dondi, 1979; Mattavelli et al., 1983; Ricci Lucchi, 1986, 1990; Antonioli et al., 2009; Ghielmi et al., 2013). During the Quaternary, the decreased uplift and reduced migration of the Apennines defined a switch of the Po Plain–Adriatic Sea toward a system in which the Po River was the most important sediment source (Amorosi et al., 2015). Thus, during this time, the targeted system experienced a progressive infilling by progradational marine and continental successions, along the basin major axis (i.e., northwest toward southeast; Fontana, et al., 2014; Amorosi et al., 2015).

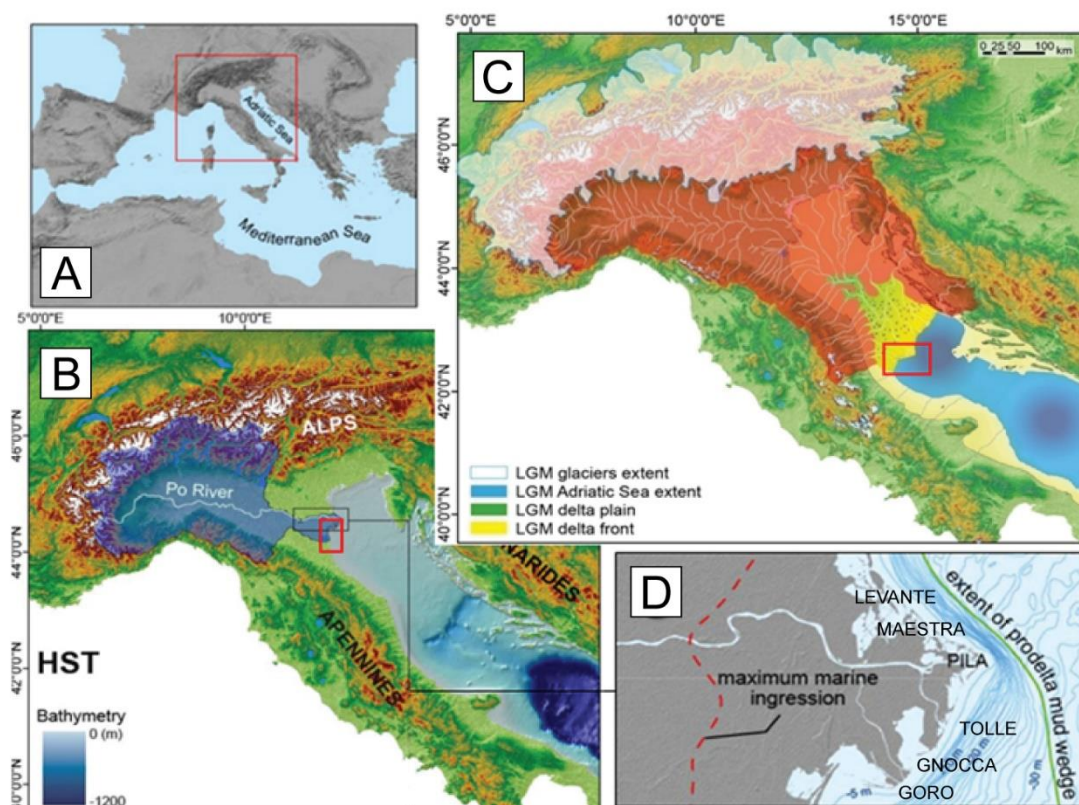


Figure 2.1 – Location and physiographic setting of the Po Plain–Adriatic Sea system at present (A–B) and (C) during the Last Glacial Maximum. Inset (D) shows the present-day morphology of the Po Delta along with its major distributaries. Red rectangles indicate the locations of the main study areas, and the red dashed line shows the coastline during the Holocene maximum marine ingression (after Amorosi et al., 2015, and Pellegrini et al., 2017a, slightly modified).

At present, the eastern area of the Po Plain is characterized by a relatively thin layer of continental deposits constituting the topset of the overall prograding sedimentary complex. The Po Plain passes eastward to a shallow epicontinental sea characterized by a gently dipping continental shelf (Cattaneo et al., 2003; Maselli et al., 2011). The shelf break is located approximately 300 km southeast of the modern Po Delta and marks the passage to the deeper Mid Adriatic Deep (MAD) basin (Fig. 2.1).

The two main sedimentary bodies of interest for this study are i) the Holocene coastal/shallow marine succession of the Po Delta and its southern coastal plain and ii) the late Pleistocene–Holocene succession of the Po Delta deposited close to the MAD basin during the last glacial phase (Fig. 2.1). Although they are connected in their geological and sedimentological evolution, particularly during the late Quaternary, these two key areas are treated separately in this thesis. This choice was dictated by the will to offer a clearer picture of these complex regions with main sediment accumulation phases occurring at different times. Indeed, the Po Delta/coastal plain records an expanded marine sedimentary succession that was deposited mainly during sea-level highstands, the MAD records an expanded marine succession that was stacked during sea-level lowstands (Amorosi et al., 2004; Pellegrini et al., 2018).

2.1. The Po Delta and its southern coastal plain

The Po Plain, with an extension of 46,000 km², is the largest alluvial plain in Europe (Astori et al., 2002) and is cut in two by the Po River, the longest and most relevant watercourse in the country (Vannoli et al., 2015). The modern Po Delta, with a surface of 54,000 ha, forms the largest complex of wetlands in Italy and is localized at the border between the Emilia-Romagna and Veneto regions (~ lat. 44.919937°N; ~ long. 12.387254°E; Fig. 2.1). The Po Delta includes an extensive delta plain, a wave-influenced delta front, and a broad asymmetric composite prodelta. The sediment dispersal is controlled by six main distributary channels including the Gnocca, Goro, Levante, Maestra, Pila, and Tolle (Correggiari et al., 2005) which form an equal number of main prodelta lobes.

The modern Po Delta is a relatively recent geomorphologic/geographic feature that evolved during the last 500 years in response to the Porto Viro diversion (1604 AD; Correggiari et al., 2005). The Porto Viro diversion was commissioned by the Doge of Venice to divert the main distributary channel southward to stop the gradual migration of the delta system toward the Venice lagoon. Since then, a 30 km coastal progradation of the area has been recorded (Correggiari et al., 2005). South of the Po Delta, the coastal plain shows a triangular shape and occupies a surface of approximately 244,000 ha extending from Pontelagoscuro (Ferrara) to the Adriatic Sea to the north and tapering southward, where the Apennine chain meets the coastline.

2002; Ghelmi et al., 2013; Vannoli et al., 2015). In contrast, the buried central Alpine margin is characterized by a simpler geometry represented by the Pedevalpine homocline, a gently southward dipping E–W-trending structure extending from Milan to Garda Lake (Burrato et al., 2003).

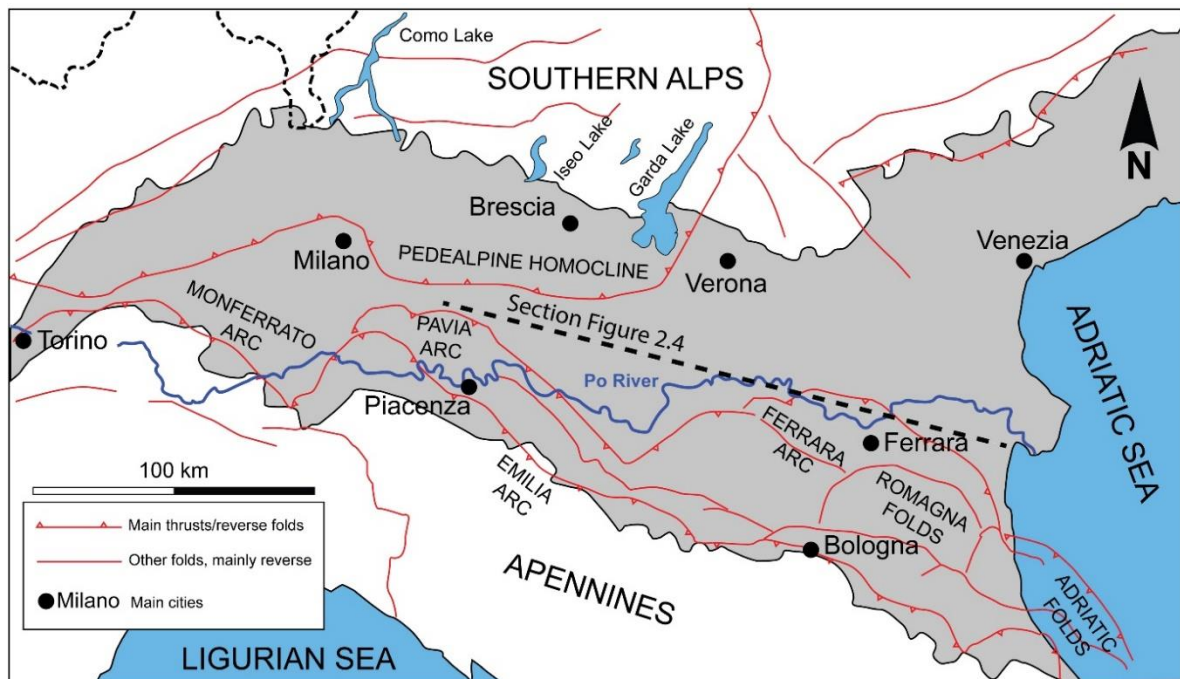


Figure 2.3 - Simplified structural setting of the Po Basin (gray area) showing the complex organization of buried folds, faults, and thrusts. The black dashed line is the trace of the transect reported in figure 2.4. (Burrato et al., 2003, slightly modified).

Regarding the Apennine front, several high-resolution seismic profiles acquired over years (Pieri and Groppi, 1981; Picotti et al., 2007; Picotti and Pazzaglia, 2008 and references therein) have enabled detailed reconstruction of its tectonic complexity and its impact on the sedimentary successions deposited in the Po Plain foreland (e.g., Rossi, 2017). Three large thrust sheets, arc-shaped in plain view, have been recognized (Pieri and Groppi, 1981; Castellarin, 2013; Livani et al. 2018) as the buried expression of the articulated northern Apennine front including the Monferrato, Pavia and Ferrara-Romagna arcs from west to east. Costa (2003) highlighted a different deformation style along each arc side such that, the western side of the arc is characterized by NW-verging thrusts, whereas the north-eastern side presents high-angle *en-echelon* reverse faults interpreted as dextral shear zones. The strike-slip component associated with these dextral shear zones is an inevitable result of the progressive activation and eastward migration of these arc-shaped structures, from the Oligocene to the Pliocene (Butler, 1982; Costa, 2003). In addition, Picotti and Pazzaglia (2008) determined that sedimentary successions deposited along the arc fronts lie in two different types of basins: a classic wedge-shaped type and a more symmetrical sag type. Specifically, in the western Po Plain, the growth of the Monferrato arc folded the Oligocene to Quaternary deposits into anticlines

and synclines, the latter typical of sag basin geometry (Kingston et al., 1983; Selley and Sonnenberg, 2014). Eastward in the central Po Plain, the arc growth is associated with a progressive transition from wedge-shaped to asymmetrical sag-type basins beginning from the Messinian. However, by the Middle Pleistocene, the wedge-shaped basins had evolved to sag-type throughout the Po Plain foreland; this suggests a stall in the convergence rates of the Apennine thrusts, followed by their subsidence (Picotti and Pazzaglia, 2008).

2.1.2. Late Quaternary stratigraphic architecture

Owing to the wealth of data derived by seismic, well-log, and borehole-based investigations, the large-scale stratigraphic and structural architecture of the Po Plain is well established (Fig. 2.4; Pieri and Groppi, 1981; Regione Emilia Romagna and ENI-AGIP, 1998; Muttoni et al., 2003; Garzanti et al., 2011).

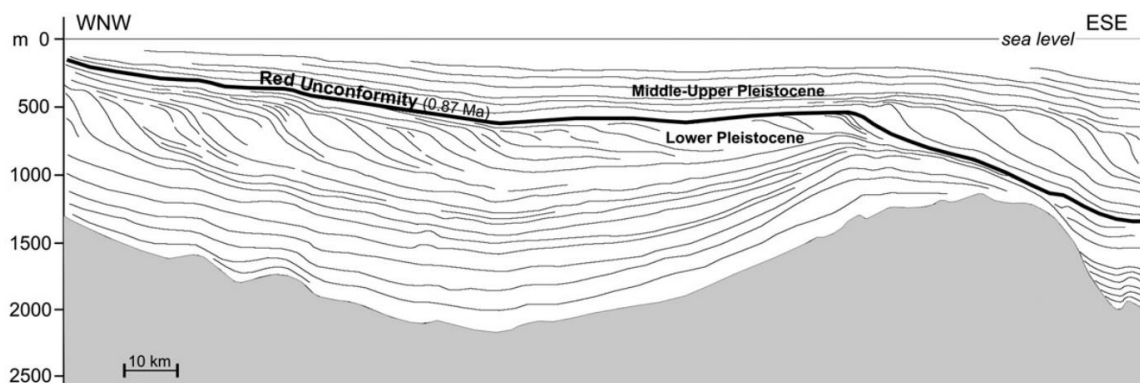


Figure 2.4 – Composite seismic profile across the Po Plain. The orientation and position of the transect are given in figure 2.3. The Adriatic Sea is on the right (after Garzanti et al., 2011).

In the Po Plain, the southward crustal tilting related to stacking of the Apennine enabled since the late Miocene strong subsidence in its southern foredeep (up to 2.4 mm/y; Antonioli et al., 2009; DeCelles and Giles, 1996; Fantoni and Franciosi, 2010). Hence, owing to this sustained rate of tectonic subsidence, the Quaternary deposits in the south-eastern Po Plain display an incredible maximum thickness of 2 km (Antonioli et al., 2009). This noticeable example of expanded stratigraphic record has been targeted in subsurface investigations for the last 50 years, since oil and water-driven geophysical research facilitated the first large-scale stratigraphic and structural reconstruction of the Po Plain Quaternary succession (AGIP, 1977; Aquater, 1976, 1977, 1978; Aquater-ENEL, 1981).

This integrated stratigraphic approach has had a noticeable impact on the geological reconstruction of the targeted area. The late Quaternary sedimentary succession of the Po Plain is currently subdivided into a series of basin-scale, third-order unconformity-bounded stratigraphic units (Fig. 2.2; UBSU in Regione Lombardia and ENI divisione AGIP, 2002; Amorosi et al., 2013). The recognized stratigraphic unconformities, which are dated around 1.6 Ma, 1.24 Ma, and 0.87 Ma

corresponding to blue, green, and red lines in Fig. 2.2, respectively, underlines strong phases of tectonic activity that resulted in significant modification of the basin geometry. Overall, the basin-infill shows progressively decreasing deformation from the bottom to top (Regione Lombardia and ENI divisione AGIP, 2002; Amorosi et al., 2008).

The post-0.87 Ma Quaternary succession (~800m thick beneath the Po coastal plain) represents the Po Supersynthem. This unit has been recently subdivided into a Lower and Upper Po Synthem by a fourth regional unconformity dated at 0.45 Ma (yellow line in Fig. 2.2; black line in Fig. 2.5). These syntems, in turn, include sub-syntems represented by sedimentary units tens of meters-thick that recorded a strong glacio-eustatic imprint (Fig. 2.6; Regione Emilia Romagna and ENI-AGIP, 1998; Amorosi et al., 1999; 2004; 2008; 2016; Scarponi and Kowalewski, 2004; Francani et al., 2016).

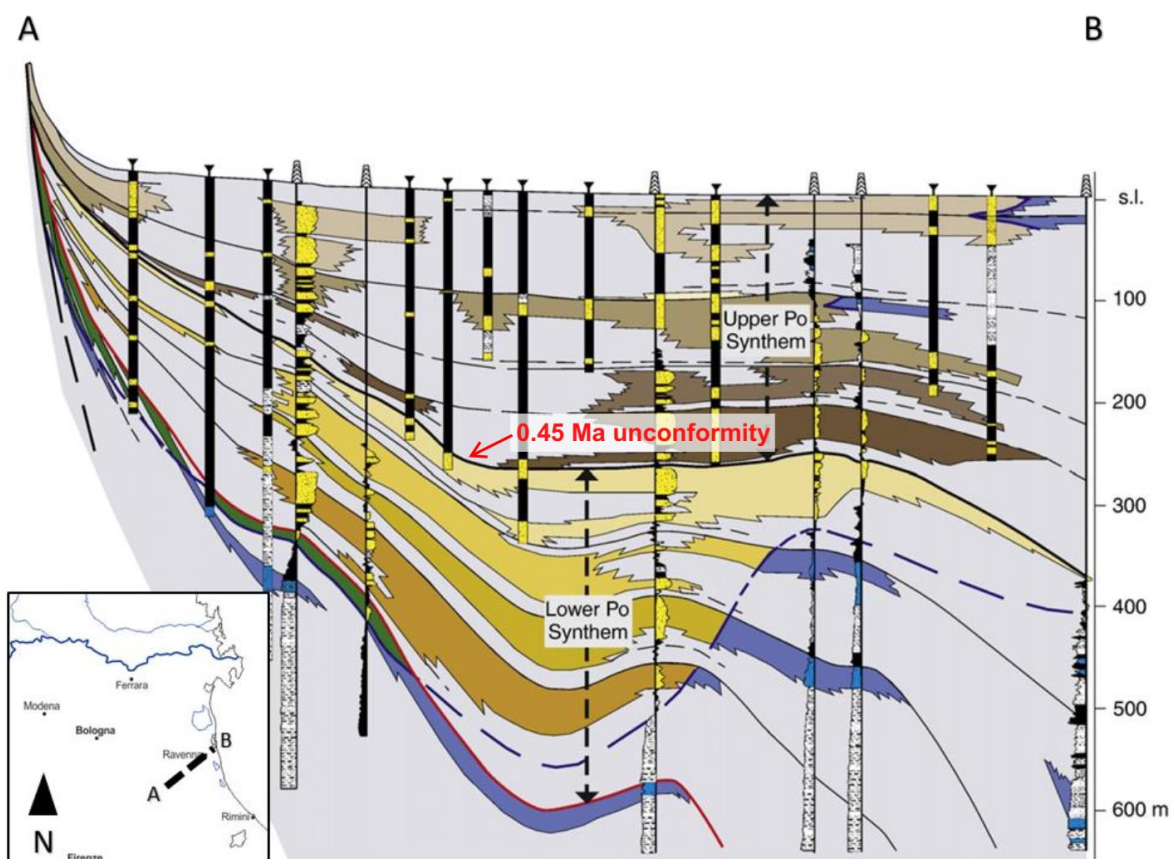


Figure 2.5 – Schematic stratigraphy of the Po Supersynthem, which is subdivided into Lower and Upper Po Synthem by means of the lower-rank regional unconformity dated 0.45 Ma. The internal organization of each synthem enable definition of a series of sub-syntems (after Amorosi et al., 2008).

The sub-syntems show characteristic wedge-shaped geometry as a result of the backstepping of transgressive nearshore-settings during the phases of rapid sea-level rise. This was followed by phases of aggradation and progradation of the coastal-deltaic systems during the deceleration phases of sea-level rise and subsequently sea-level fall and lowstand (Fig. 2.6). The internal stratigraphic architectures of the individual sub-syntems can be tracked from fluvial to marine realms through

identification of prominent bounding surfaces representing the onset of transgressive events (Fig. 2.6; Muttoni et al., 2003; Amorosi et al., 2008; 2016).

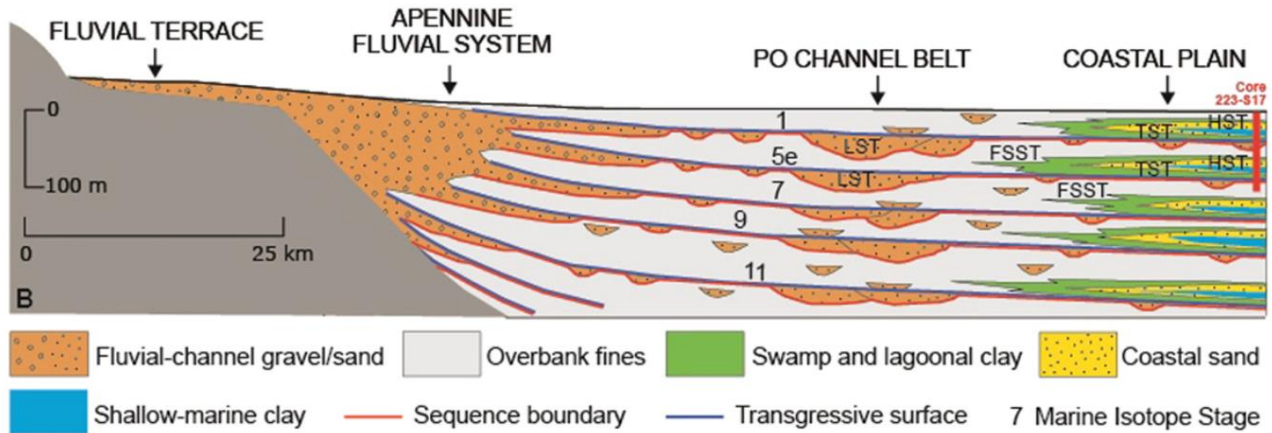


Figure 2.6 – Schematic reconstruction of the fourth-order transgressive – regressive sequences driven by Milankovitch cyclicity at 100 ka (after Amorosi et al., 2016).

Multidisciplinary investigations, based on integrated data of sedimentology; fauna such as mollusks, ostracods, and benthic foraminifers; and pollen document a strong climate-driven influence on stratigraphic architecture of the late Quaternary succession (Amorosi et al., 2008, 2014). The coastal-marine, landward-thinning bodies recorded in the subsurface of the Po coastal plain, represent the stratigraphic expression of shoreline transgression and ensuing deltaic progradation that occurred during interglacial phases (TST + HST in Fig. 2.6). Whereas, the pluri-decamic thick alluvial successions are related to phases of falling and lowstand of sea-level that occurred during glacial intervals (FSST + LST in Fig. 2.6).

Within the latest Quaternary (<150ka), two wedge-shaped coastal sedimentary bodies were located at respective core depths of approximately 0-30 m and 95-120 m (Fig. 2.7). These bodies show comparable T-R stacking patterns and were deposited during the two major transgressive pulsations and subsequent sea-level highstands of the last 150 ka (Amorosi et al., 2004; Amorosi and Colalongo, 2005). These two sedimentary bodies, assigned respectively to the Tyrrhenian marine isotope stage (MIS) 5e and the Holocene MIS 1, are separated by a 50-100 m thick succession of alluvial and fluvial sediments recording the overall sea-level fall and lowstand that occurred between about 116 ka and 14 ka, and resulted in extensive basinward shifts of alluvial facies.

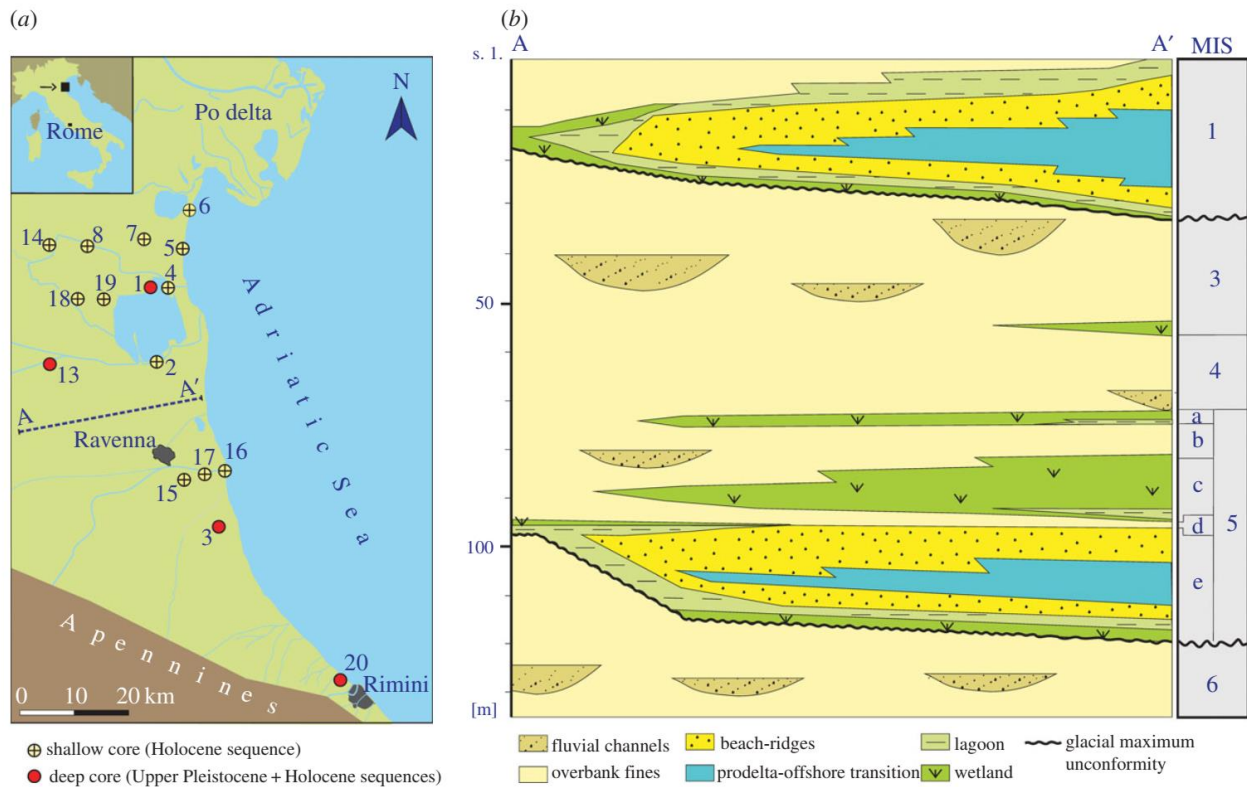


Figure 2.7 – (A) Location map of the investigated section. (B) Sketch of the subsurface facies architecture of the Po coastal plain for the last 150 ka and its correlation with $\delta^{18}\text{O}$ isotope stages (after Kowalewski et al., 2015).

This prolonged phase of overall sea-level fall (FSST = MIS 5d to 2) was punctuated by higher frequency transgressive pulses (see also paragraph 1.3), which led to widespread deposition of thin packages of organic-rich, lagoonal and swamp deposits chronologically constrained to MISs 5c, 5a, and 3 (Fig. 2.7; Amorosi et al., 2004; Kowalewski et al., 2015; Campo et al., 2017). At maximum glacial interval (MIS 2), the Po delta system was located in proximity to the Mid Adriatic Deep (MAD; Pellegrini et al., 2018) and the present-day Po coastal plain recorded a succession of laterally extensive sand fluvial bodies associated to pedogenically altered floodplain deposits (Bruno et al., 2017). Upward, the superposition of poorly-drained floodplain onto pedogenically altered deposits, marks the onset of an overall retrogradational stacking pattern of facies. This contact has been interpreted as the transgressive surface (TS) or maximum regressive surface (MRS; *sensu* Catuneanu, 2017), bounding at the base the currently forming fourth-order post-LGM T-R sequence (Fig. 2.7). The TS, being associated with a series of weakly developed paleosols attributed to the Younger Dryas cold event (McClennen et al., 1997; Amorosi et al., 1999, 2014; Bruno et al., 2016), is a striking regional stratigraphic surface that can be easily recognized in cores (Amorosi et al., 2004). The post-LGM T-R sequence was recently subdivided into eight millennial-scale depositional units (parasequences). Some of these units present a further recognizable internal subdivision, being

nested with higher frequency units bounded by flooding surfaces of centennial time-scale (Fig. 2.8; Amorosi et al., 2017).

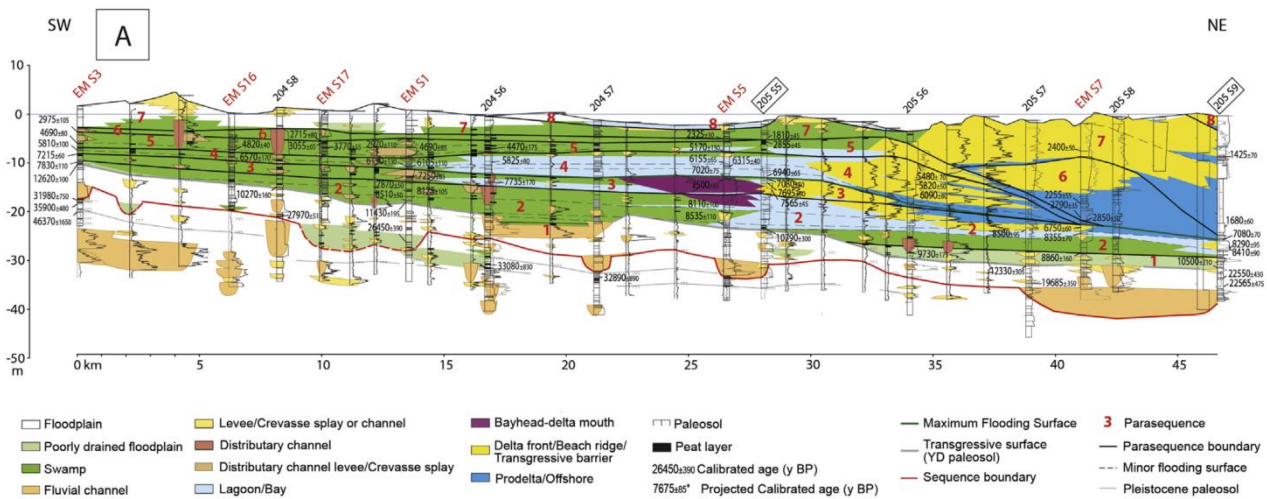


Figure 2.8 – Correlation panel (after Amorosi et al., 2017) showing the Holocene stratigraphic architecture of the Po coastal plain. The eight Holocene parasequences are numbered in red, and the maximum flooding surface corresponds to the green line separating parasequences 3 and 4.

A parasequence is a stratigraphic unit composed of a relatively conformable succession of genetically-related strata, bounded by a flooding surface across which a substantial facies dislocation is present (Van Wagoner, 1995; Amorosi, 2017; see also Catuneanu, 2017). It is widely accepted that a parasequence internal stacking pattern commonly displays a shallowing-upward trend representing an episode of progradation. However, in a high subsidence setting such as the Po coastal plain, the lowermost portion of these sequence-stratigraphic units might record a deepening upward trend (Zecchin and Catuneanu, 2013; Amorosi et al., 2017).

Following Amorosi et al. (2017; Fig. 2.8), parasequences 1 to 3 show clear retrogradational stacking of alluvial to estuarine and marginal marine facies across the targeted area, which is in agreement with a stepped post-glacial eustatic sea-level rise (Boyd et al., 2006; Amorosi et al., 2016). Units 4 to 8 show a multifaceted and aggradational-to-increasingly-pronounced progradational pattern of coastal/deltaic facies that developed under the action of more local autogenic forcing factors (Amorosi et al., 2017). The maximum flooding surface, marking the turnaround between transgressive and normal regressive stacking patterns, is placed at the base of parasequence 4 (Fig. 2.8)

1. Parasequence 1 (~11.5 to ~9.2 cal ka BP), records mainly poorly-drained floodplain deposits passing upward to swamp/salty-marshes/inner lagoon facies (Amorosi et al., 2017). The organic-rich deposits of parasequence 1 can be correlated to a transgressive barrier system

(~10.5 ka BP) locally preserved at a water depth of 42 m in the Adriatic Sea (Trincardi et al., 1994; Cattaneo and Steel, 2003; Correggiari et al., 2005; Storms et al., 2008).

2. Parasequence 2 (~ 9.2 to ~7.7 cal ka BP), is nested with several higher frequency (centennial-scale) parasequences. Seaward, the stacking pattern of these centennial units is distinctly retrogradational, as supported by the transition from poorly drained floodplain to lagoon and to transgressive sand sheets facies. Landward, these higher frequency units record alternating poorly drained floodplain and swamp facies (Amorosi et al., 2017).
3. Parasequence 3 (7.7 to 7.0 cal ka BP) preserves the maximum landward shift of the shoreface along the transect. In proximal settings, the development of a large bay-head delta filling the lagoon-barrier system has been detected. In distal settings the onset of a prolonged sediment starvation phase, will lead to the development of a multi-millennial condensed interval only a few decimeters-thick.
4. Parasequence 4 (~ 7.0 to 5.2 cal ka BP) is bounded at the base by the maximum flooding surface (MFS) that shows a strong degree of diachroneity both down-dip and across-strike (Amorosi et al., 2005, 2017). Indeed, Amorosi et al. (2017) reported that the initial progradation of the shoreline is paralleled inland by the 15 km landward expansion of the back-barrier settings. In proximal coastal and brackish settings, high-frequency centennial scales parasequences are also recorded (Fig. 2.8).
5. Parasequence 5 (~ 5.2 to 2.8 cal ka BP) records a phase of lobe switching, with main distributary channels delivering coarse sediment-loads in both southward and northward directions relative to the modern-day Po Delta. In the coastal settings, the stacking patterns of facies displays a slight progradational trend, as evidenced by the infill of the lagoons and the development of a wave dominated delta system. In the distal sector (i.e., shallow marine settings) substantial condensation was still observed.
6. Parasequence 6 (~ 2.8 to 1.5 cal ka BP) is still characterized by slow progradational rates. The parasequence was built up under the influence of sediment redistribution by longshore currents from the Adige River, as evidenced by geochemical data (Amorosi et al., 2007, 2017).
7. Parasequence 7 to 8 (< 1.5 cal ka BP) shows comparable internal architecture and display a strong progradation of the nearshore and upper delta plain environments. Parasequence 7 marks the transition from a wave dominated to river dominated delta. The fastest progradation rates were observed in unit 8, at time of the modern Po Delta building. Indeed, during the last 500 ka the delta front line advanced about 30 km in the Adriatic Sea.

The unparalleled resolution of these stratigraphic investigations provides a detailed picture of Holocene millennial- to sub-millennial-scale depositional dynamics of the Po coastal plain, which represents an ideal venue for investigating macrobenthic bio-sedimentary dynamics.

2.2. The Adriatic Sea and the Mid Adriatic Deep (MAD)

The Adriatic Sea occupies an ~800 km elongated and narrow semi-enclosed epicontinental basin, divided roughly in northern, central, and southern sectors (Fig 2.9). The northern sector of the basin is characterized by a wide shelf with a low topographic gradient of 0.02° and extends southward for ~350 km from the Gulf of Venice (Cattaneo et al., 2003; Ridente et al., 2008a, b).

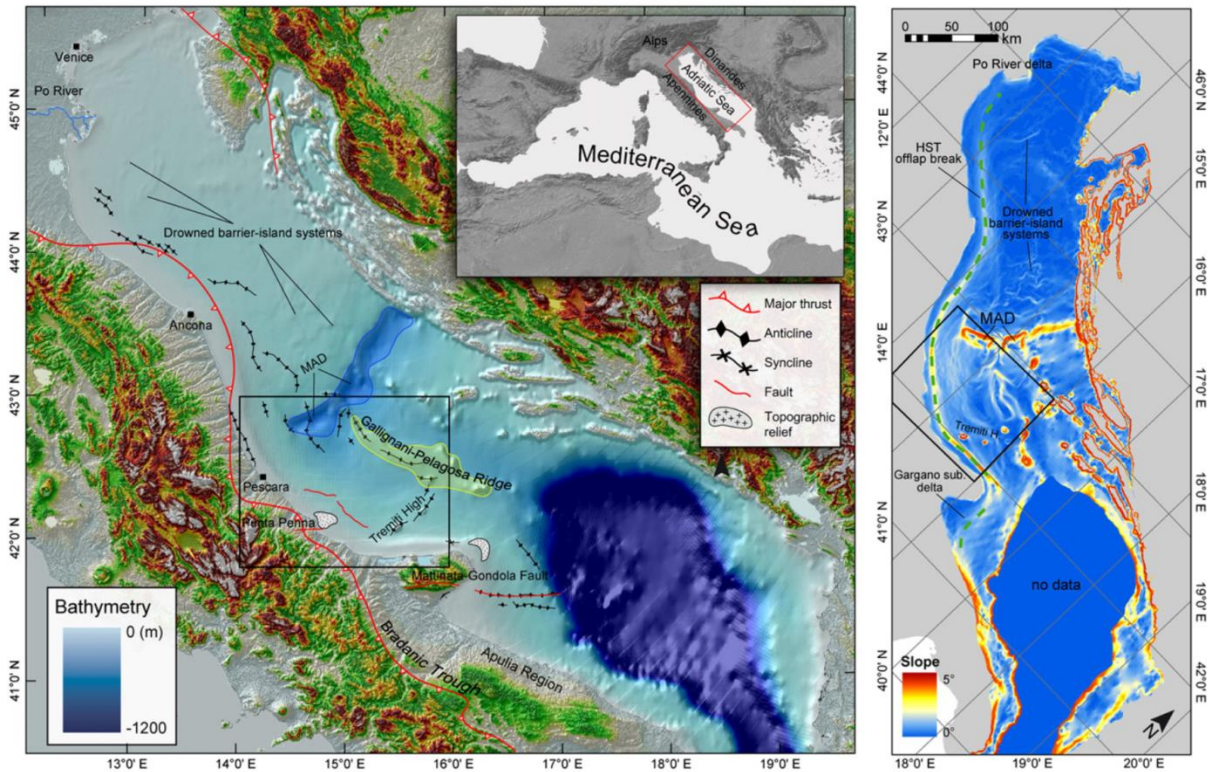


Figure 2.9 – Digital model of the Adriatic Sea and the main structural elements (after Maselli et al., 2011). The wide low-angle northern shelf limited the Mid Adriatic Deep (MAD) to the North, and the narrower shelf areas surround the Gargano Promontory. The digital model of the land surface is derived from SRTM 90m Digital Elevation Data (<http://srtm.csi.cgiar.org>).

The central sector of the basin, which is confined to the south by the Gallignani-Pelagosa ridge (Maselli et al., 2011), displays a narrower shelf at a maximum of 50 km, with steeper gradient of 0.2° to 0.5° that border a small remnant basin known as the Mid Adriatic Deep (MAD) (Fig. 2.9). During the late Quaternary this formerly larger and deeper basin has been partially filled by the Po River when, at times of sea-level lowstand, the Po Delta was repeatedly located at the edge of the MAD (Pellegrini et al., 2017a, 2018). The southern Adriatic sector, south of Pelagosa Sill has a maximum depth of 1200 m. The sea bottom in this area shows a very steep and narrow shelf (Cattaneo et al., 2002) with irregular topography characterized by such tectonic structures as the Gondola Fault/Gondola anticline, the Dauno seamount (Ridente et al., 2008a; Pellegrini et al., 2016) and the Bari Canyon; the latter acts as the main sediment conduit on the southwestern side of the Adriatic Sea (Ridente et al., 2007; Pellegrini et al., 2016). In the southernmost part of the Adriatic, the Otranto Strait enables connection with the Mediterranean Sea. As reported by Artegiani and

colleagues (1997a, b) this narrow passage (72 km wide, 780 m deep) plays a pivotal role in controlling the modern-day circulation pattern not only in the Adriatic but across the entire Mediterranean Sea (Storms et al., 2008).

2.2.1. Tectonic setting

The Adriatic Sea is the distal area of the Po Plain-Adriatic Sea system and acts as a foreland for the Apennines on the north-western margin and for the Dinaric orogen on the south-eastern margin (Ori et al., 1986; Cattaneo et al., 2003; Pace et al., 2015). From the Oligocene until the Pleistocene, a series of foredeep basins was created along the eastern border of the Apennine outer thrust arc (Ricci Lucchi, 1986; Doglioni et al., 1994, 1996; Ridente et al., 2008b). As the thrusts belt migrated eastward, deformation of the Miocene-Pliocene foredeep successions led to the formation of a series of piggy-back basins filled by late Pliocene to Pleistocene sediments (Ori and Friend, 1984; Bigi et al., 2013) whereas adjacent foredeep systems were created along the northeast edge of the Adriatic Sea (Fig 2.10).

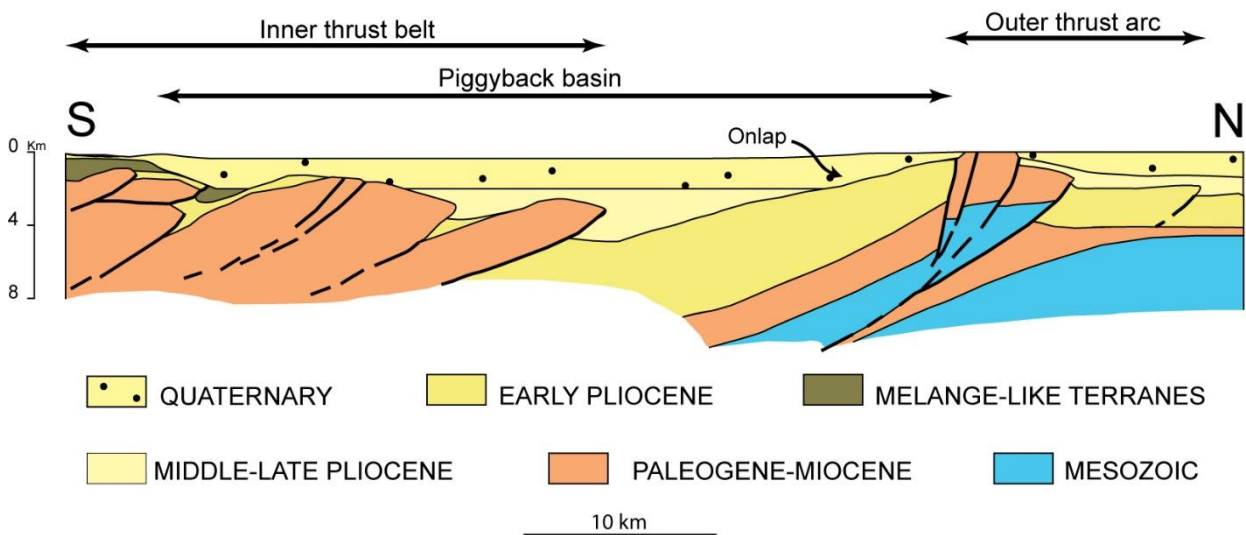


Figure 2.10 – Section of southern Po basin based on seismic profile realized by Agip. The piggy-back basin that originated by eastward thrusting of the growing Apennines. Shown on the right side of the figure is the outer thrust arc that represents the foredeep of the Apennine chain (redrawn and modified after Ori and Friend, 1984).

In this scenario, the modern central Adriatic is the most recent of a series of foredeep basins (Ricci Lucchi, 1986; Royden et al., 1987; Artoni, 2007; Bigi et al., 2013). Plio-Quaternary in age, this modern foredeep has an arcuate shape and is separated into two sub-depocenters by the Ancona structural high (Fig. 2.11; Ori et al., 1986; Argnani and Gamberi, 1995). The late Quaternary sedimentation in these sub-basins is controlled by the increased subsidence and sustained sediment supply, both due to the high rates of Apennine uplift (Cattaneo et al., 2003). The exceptional thickness (~8 km) of the Plio-Quaternary sedimentary succession preserved in these Adriatic

depocenters should be also linked to the presence of two areas overlying minimum Bouguer anomalies (Pieri and Groppi, 1981; Bally et al., 1986; Cattaneo et al., 2003).

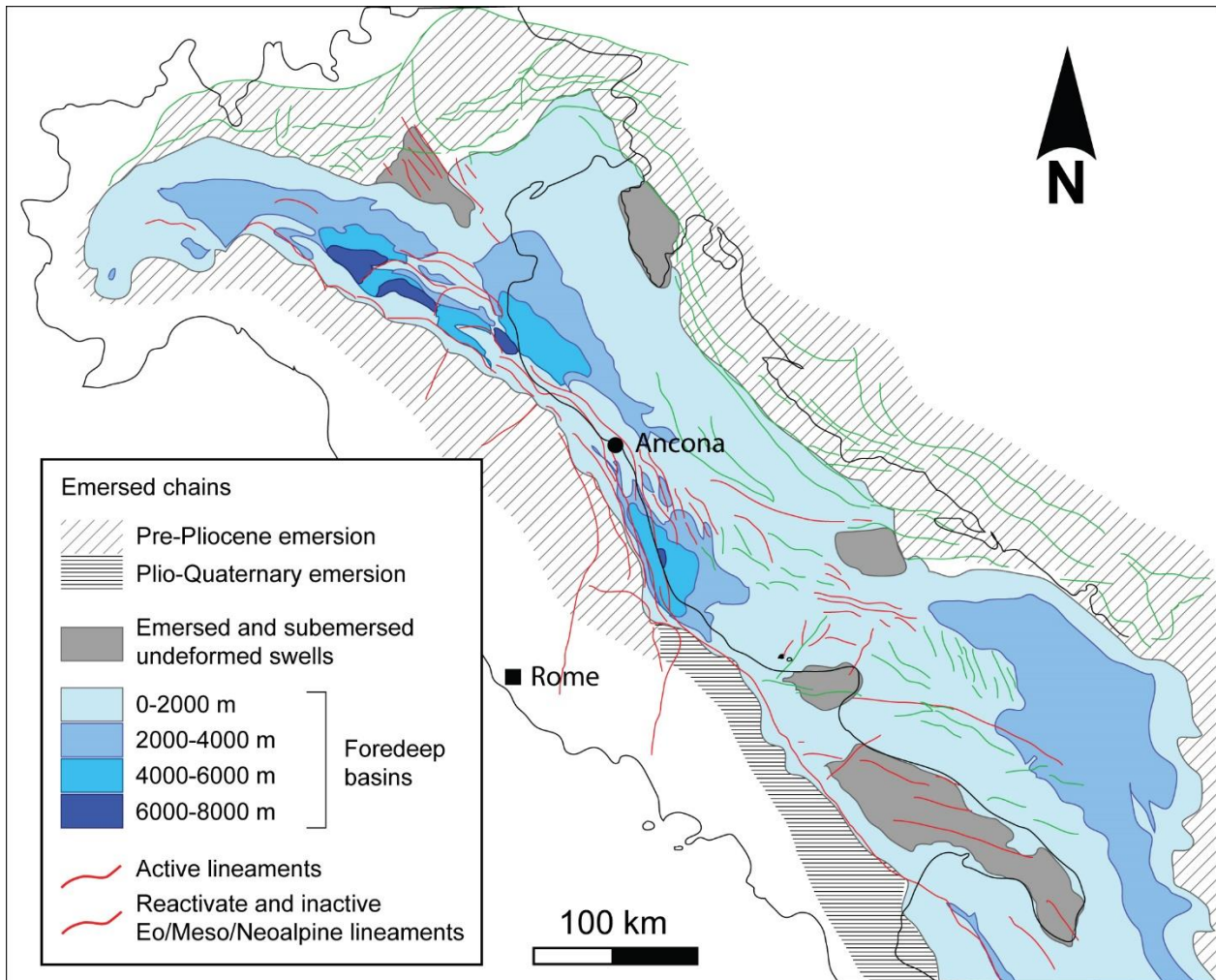


Figure 2.11 – Schematic reconstruction of the main tectonic lineaments within the Po plain– Adriatic Sea and the location of the main foredeep basins. Redrawn and modified after Fantoni and Franciosi (2010).

During the Quaternary, intense tectonic activity (Doglioni et al., 1994; Tinti et al., 1995; Trincardi and Correggiari, 2000) led to crustal deformation and uplift of structural highs in the central and southern portions of the Adriatic, to form the Gargano Promontory, Tremiti structural high and Gallignani Ridge (Figs. 2.9-2.12; Trincardi and Correggiari, 2000; Cattaneo et al., 2003; Ridente and Trincardi, 2006).

The Gargano area during the Pliocene was characterized by a wide and subsiding foredeep basin that surrounded the Gargano Promontory (Torre et al., 1988). Since the late Pliocene, the development of a NE-SW oriented transpressive lineament known as the Tremiti Line led to the growth of the Tremiti structural high (Fig. 2.12). This tectonic feature acted as a lateral transfer zone, separating two portions of the Adriatic plate that thus underwent distinct subduction histories (Fig. 2.12; Doglioni et al, 1994; de Alteriis, 1995).

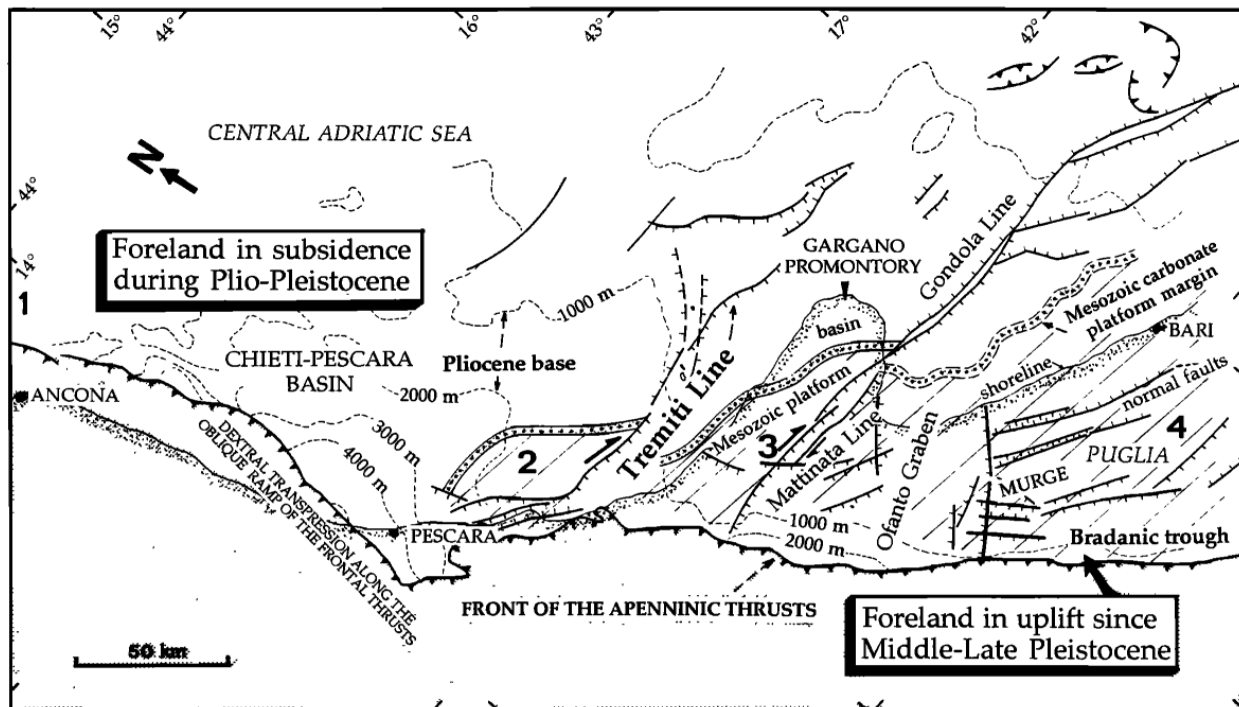


Figure 2.12 – Structural maps of the central/southern Adriatic Sea. Shown in the figure is the transpressive structure of the Tremiti Line, north of the Gargano Promontory, which acts as a transfer zone separating the two domains with different tectonic, subsidence and sedimentary evolution (after Doglioni et al., 1994).

As confirmed by the structural map, the northern area underwent tilting and experienced high subsidence rates through the Quaternary owing to the incipient position of the Apennine thrusts (Doglioni et al., 1994; Trincardi and Correggiari, 2000). In contrast, south of the Gargano Promontory, the Apennine thrusts were located inland and the foredeep insists on the Bradanic trough (Maselli et al., 2011). Thus, the southern area underwent low rates of subsidence owing to the mid-Quaternary uplift triggered by lithosphere buckling caused by the more inland stacking of the Apennine thrusts (Doglioni et al., 1994; Ridente et al., 2008a). Slightly south of the Gargano Promontory, reactivation and inversion of Mesozoic extensional faults formed the Gargano Deformation Belt, which controlled the tectonic deformation in the Pliocene. Inland its main lineament is represented by the Monte S. Angelo – Mattinata Fault, whereas offshore, it extends to the W-E oriented Gondola Fault (Ridente et al., 2008a). The Gondola Fault is roughly 140 km long and is subdivided in two sectors, with slightly different orientations (Fig. 2.13). This orientation discrepancy led to the formation of a compressional structure during the late Miocene to the Early Pliocene known as Grifone, which is roughly oriented NW-SE (Alteriis, 1995). Seaward with respect to the Tremiti High, the Gallignani Ridge is a NW-SE-oriented complex structure formed by buckling of the subducted lithosphere around the peripheral bulge. This lineament folds and faults both Pliocene and Quaternary deposits and acted as a boundary for sedimentation in the central Adriatic shelf area (Trincardi and Correggiari, 2000).

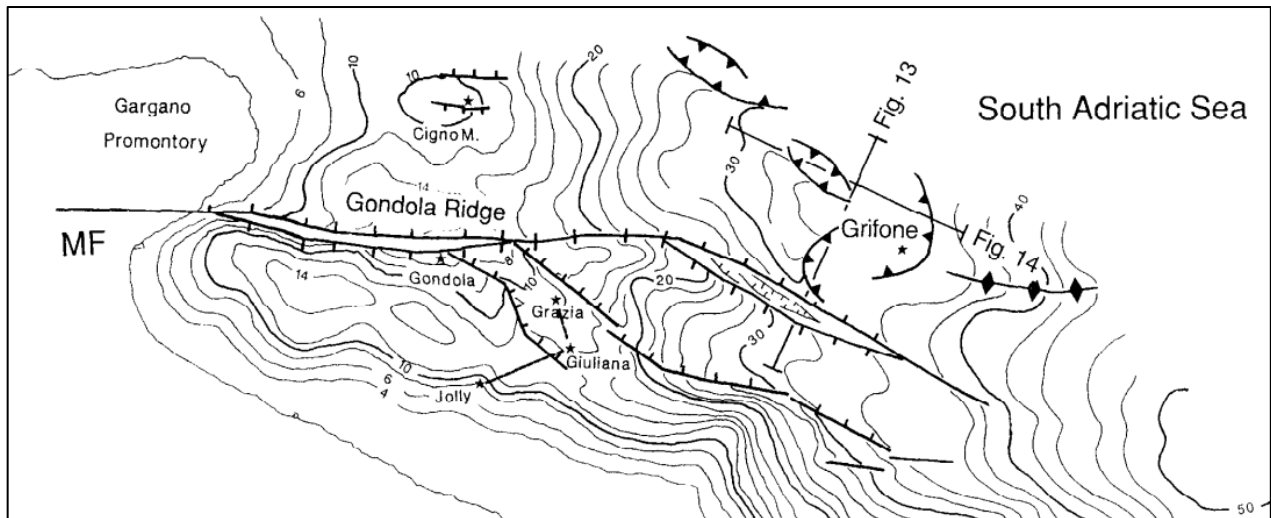


Figure 2.13 – Topographic map featuring the Monte S. Angelo - Mattinata Fault (MF) and its offshore extension, the Gondola Ridge. The map also shows the compressional structure of Grifone formed by the transpressive reactivation of this Mesozoic lineament (after Alteriis, 1995).

2.2.2. Late Quaternary stratigraphic architecture

A dense network of high-resolution Uniboom 3.5-khz and Chirp-sonar profiles (e.g. Trincardi et al., 1996; Cattaneo et al., 2003; Pellegrini et al., 2017a), combined with lithostratigraphic data from several short cores (Trincardi and Correggiari, 2000) and a few long cores (i.e., PRAD 1-2; Piva et al., 2008; Ridente et al., 2008b; Ridente et al., 2009; Pellegrini et al., 2017a, 2018), formed the basis for a detailed reconstruction of the Central Adriatic and MAD stratigraphic framework during the late Quaternary (Fig. 2.14). This stratigraphic framework is additionally constrained chronologically by numerous previously dated foraminifera bioevents, tephra layers and magnetostratigraphic polarity units (Asioli, 1996; Asioli et al., 2001; Ridente et al., 2008b; Bourne et al., 2010). Similar to that in the Po coastal plain, the middle Pleistocene to Holocene succession of the central Adriatic western margin records a cyclic stacking pattern with alternating coastal-to-shallow marine and deep marine deposits that accumulated during glacial and interglacial periods, respectively, described as eccentricity-driven depositional cycles in Ridente et al. (2008b) and Ghielmi et al. (2010). Indeed, during the late Quaternary, the Adriatic underwent repeated rearrangements owing to Quaternary strong eustatic fluctuations of 100-130 m that, during glacial periods, exposed the entire Northern Adriatic shelf. With reference to the Last Glacial Maximum in the targeted area, the huge amount of sediments transported by the Po River led to construction of the Po River Lowstand Wedge (PRLW), a ~350 m thick succession that prograded of about 40 km southward into the MAD in ~17 ka (Fig. 2.16; Trincardi et al., 2004; Pellegrini et al., 2017a, 2018).

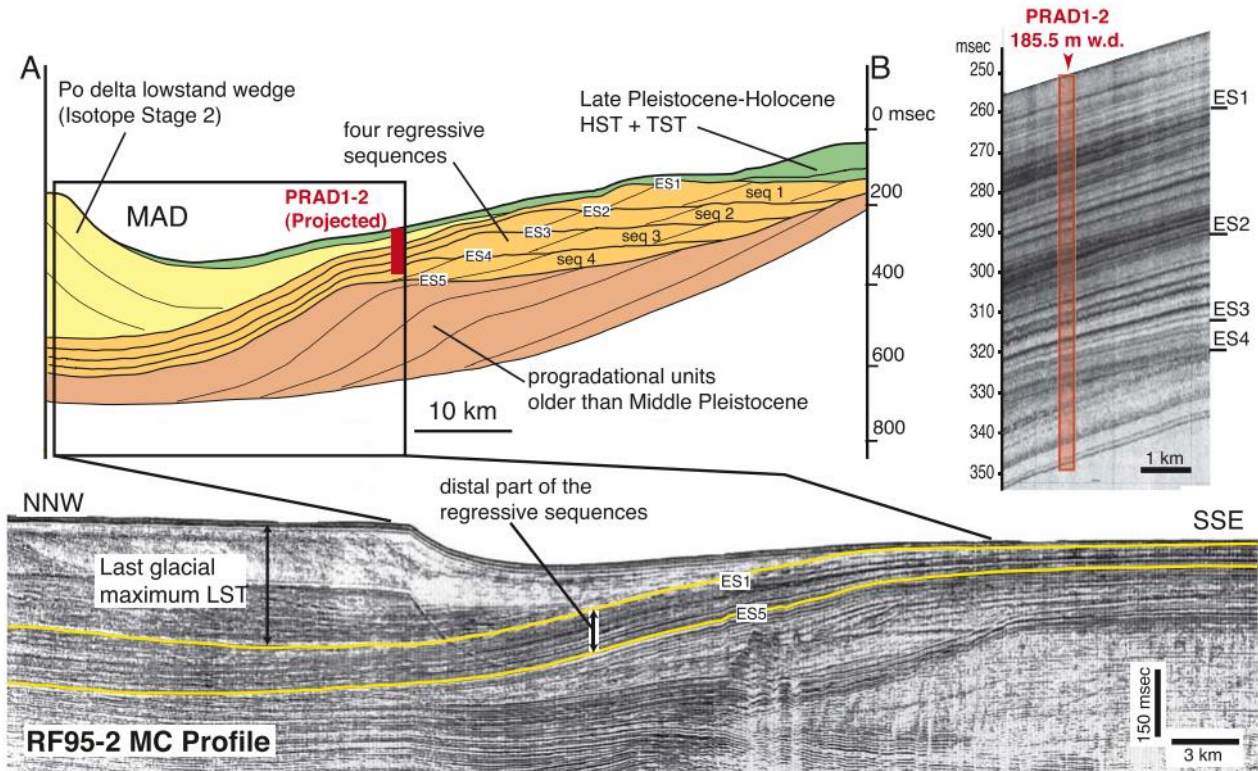


Figure 2.14 – Schematic reconstruction of the stratigraphy of the central Adriatic and MAD based on the high-resolution multichannel profile and PRAD 1-2 boreholes (detailed on the right; after Ridente et al., 2008b).

The southward progradation of the PRLW was accompanied by contemporary construction of minor sedimentary wedges on top of narrow shelves surrounding the flanks of the MAD (Ciabatti et al., 1987; Trincardi et al., 1994; Trincardi and Correggiari, 2000). These minor wedges were fed by rivers of the central Apennine chain (Trincardi and Correggiari, 2000). This concerted wedge building severely reduced the MAD extension and its depth from ~450m (Pellegrini et al., 2018) to the modern-day ~260m (Trincardi et al., 1996; Zecchin et al., 2015).

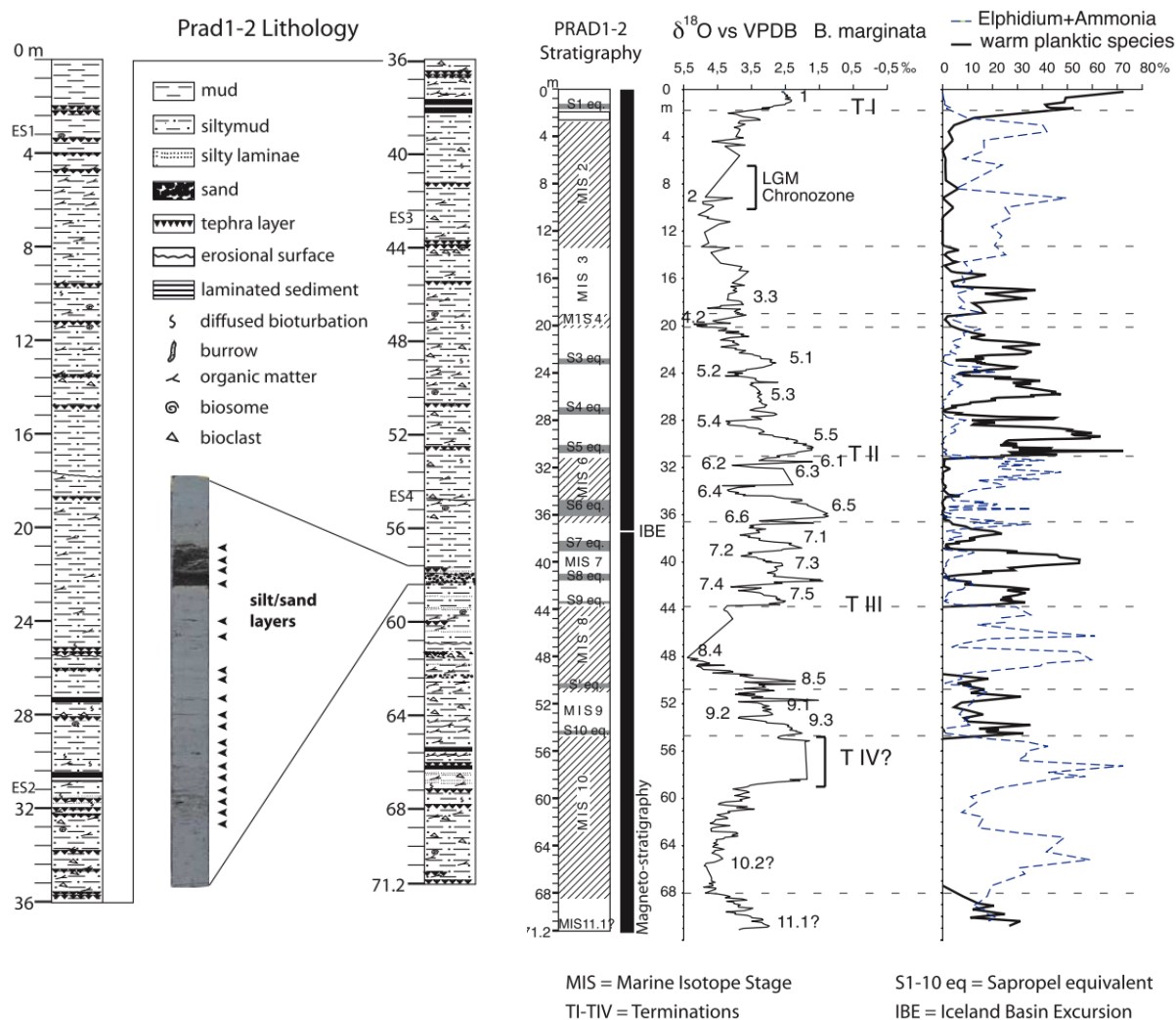


Figure 2.15 - Lithological interpretation of the boreholes PRAD 1-2 (left) and summarized stratigraphy of PRAD 1-2 (right) with integration of magnetostratigraphy, marine isotope stages (MIS) and abundance curve for planktonic foraminifera for the last 1.2 Ma (after Ridente et al., 2008b).

The PRLW is delimited at the base by the sequence boundary (SB in Fig. 2.16; dated at ~ 31.8 ka BP; Pellegrini et al. 2017b) and at the top by the TS (or MRS in Fig. 2.16) dated ~ 14 ka BP (Pellegrini et al., 2017a). The internal stratal architecture of the PRLW is composed of three main clinothem types shown as A-C in Fig. 2.16. In turn, they are organized in clinothem sets characterized by an overall progradational-to-aggradational stacking pattern (Pellegrini et al., 2017a).

Each clinothem type is characterized by peculiar features concerning topset geometry, shelf-edge and onlapping trajectory, internal structure (seismic-inferred) and bottomset geometry (Fig. 2.16). These different clinothem morphologies have been connected to significant eustatic, climate and environmental changes that punctuated the last glacial phase.

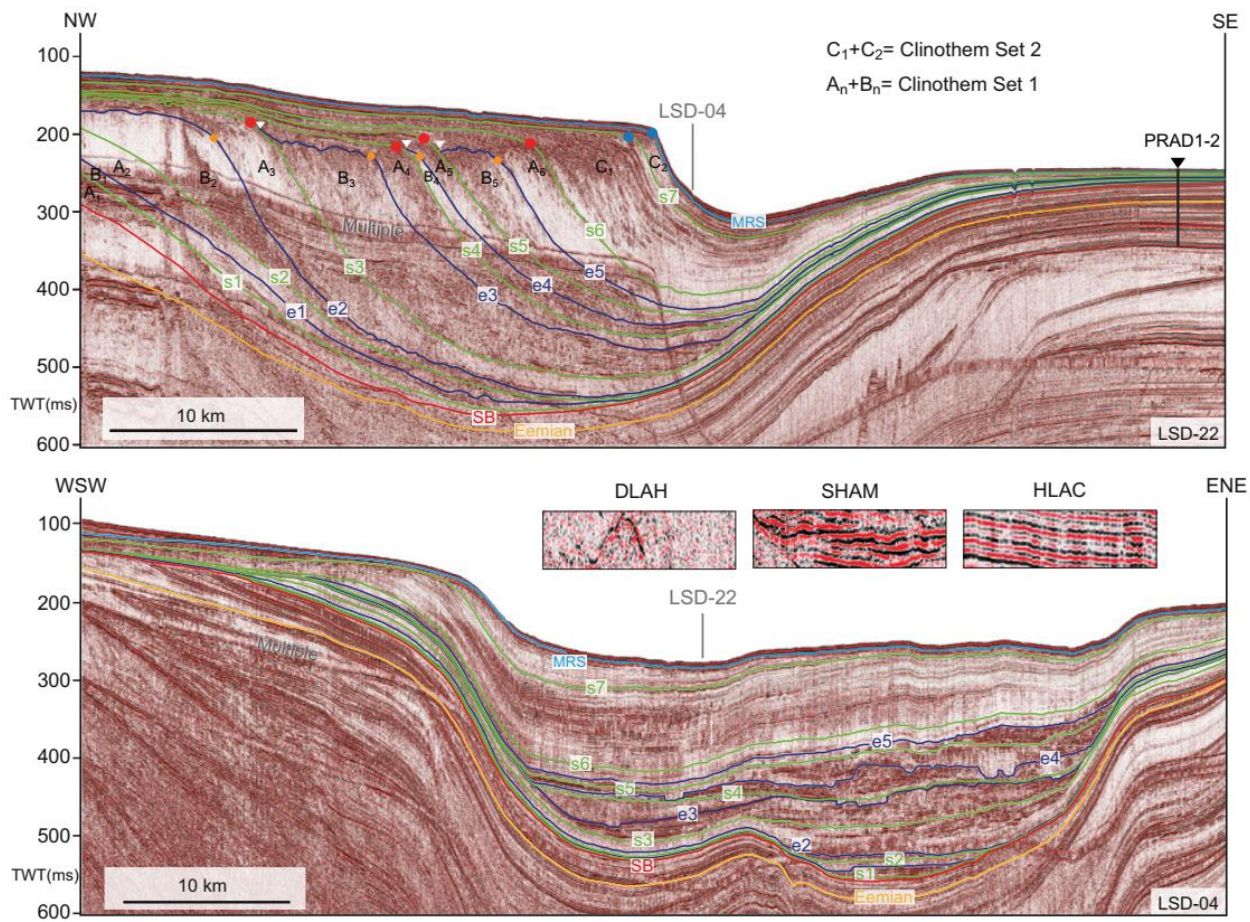


Figure 2.16 – Top: Down-dip multichannel profile LSD22 showing the Po River lowstand wedge clinothem architecture, along the main direction of progradation. Bottom: Along-strike profile LSD04 showing the succession in the basins. The three types of clinothems are described as A, B, and C. The red line indicates the sequence boundary (SB), and red orange and blue dots indicate the shelf-edge for type A, B and C clinothems, respectively. The white triangles indicate the onlap of type B clinothems. The insets show details of the basin facies associated with the different clinothems as highlighted by seismic reflectors (after Pellegrini et al., 2017a).

Briefly, type A clinothems show a topset with continuous strata. The high-amplitude reflectors of the topset diverge down-dip and then correlate with the bottomset deposits characterized by low-amplitude and discontinuous reflectors. The ascending shelf-edge trajectory records a maximum vertical offset of ~10m, which is indicative of low rates of sedimentation and progradation. The geometry of the type B clinothem differs from that of the type A because of the truncated toplap geometry that passes basinward to semi-continuous high-amplitude bottomset reflectors. Contrary to type A, the shelf-edge trajectory is descendant (meters over horizontal distance of kilometers). This is indicative of high sedimentation rates and the fastest progradation of the clinothems. Finally, type C clinothems feature continuous seismic reflectors within the topset and bottomset. Contrary to that of the topset reflectors, which is always at high amplitudes, the bottomset one is characterized by high and low amplitudes. Type C clinothems record the lowest progradation and sedimentation rates. Further details of these clinothem types are given in Pellegrini et al. (2017a, 2018).

The briefly outlined overall geometry of the above clinothems enabled them to be grouped into two sets. Pellegrini and colleagues (2017a, 2018) described the lower set as being composed mainly of the clinothem types A and B. These units indicate sustained progradation with a flat shelf-edge trajectory that led to progressive filling of the MAD depocenter. A moderate aggradation has been also recognized (Fig. 2.16). Conversely, the upper clinothem set is represented by two type C units that record limited progradation and strong aggradation as evidenced by the strong ascending trajectory of the shelf-edge that developed during the initial phase of sea-level rise following the Last Glacial Maximum, which occurred between 18 and ~14 ka BP (Pellegrini et al., 2017a, 2018).

Thus, during the last glacial phase, the MAD and central Adriatic shelf experienced sustained sedimentation in coastal to marine depositional settings, whereas the northern Adriatic was exposed completely and recorded episodic continental accumulation as evidenced by the development of a meter-thick alluvial succession. The subsequent deposition of the late Pleistocene-Holocene transgressive sedimentary succession occurred in the context of non-monotonic relative sea-level rise. In the central and especially the northern Adriatic, the resulting transgressive meter-thick deposits are represented by patchy sandy intervals with a coarsening-upward trend, overlaying widespread peat layers and topped by silty-muddy bay-to-marine deposits with highly irregular thickness (Correggiari et al., 1996; Storms et al., 2008; Amorosi et al., 2016; Trobec et al., 2018). The coarser bodies have been interpreted as almost completely recycled sand-barriers of drowned and rapidly backstepping barrier-lagoon-estuary complexes (Trincardi et al., 1994; Correggiari et al., 1996; Storms et al., 2008). Conversely, near the MAD, a rapid transgression associated with Melt-Water Pulse 1A (Amorosi et al., 2015 and references therein), produced a condensed, rapidly deepening upward coastal to marine and thin but generally thickening north-eastward marine succession that recorded the first of many rapid phases in sea-level rises through the latest Pleistocene and early Holocene.

At time of the highstand the northern and central Adriatic Sea experienced the deposition of a decametric-thick mud-dominated and fluvio-influenced sedimentary succession confined southward of the Po River Delta, in a narrow belt parallel to the modern eastern shoreline (Trincardi et al., 1996; Ridente and Trincardi, 2005; Goudeau et al., 2013; Amorosi et al., 2016). This muddy wedge passes eastward to thin muddy drapes 1-2m thick. Correggiari et al. (1996) reported that large parts of the northeast Adriatic shelf lack highstand units, and transgressive deposits have been found on the seafloor. For the MAD area, only the western shelf (i.e., the one closer to the HST mud wedge) records thin deltaic and shallow-marine progradational units composed of fine-grained sigmoidal clinofolds with gently dipping foresets of typically 0.5–1°. These units are likely a product of subaqueous progradation of muddy deposits supplied by the Po River and Apennine rivers. However, other sectors of the MAD lack a proper highstand unit and record only the distal condensed equivalent (Trincardi et al., 1996).

Chapter 3

Research Outlines

3. Research Outlines

The research activities developed over the course of my Ph.D. research and presented in this thesis explore how integrated paleontological and sedimentological investigations of the geologic record can enhance the understanding of sedimentary succession architecture as well as past and future biotic trends, mainly within the Po Plain-Adriatic Sea system. My research activity and the obtained results are tied by a common application of the stratigraphic paleobiology principles in the investigation of late Quaternary marine fossil assemblages and their encasing sedimentary successions.

The main goal of this Ph.D. was to acquire and use macrofossils to assess the response of late Quaternary ecosystems to environmental changes and to enhance the stratigraphic interpretations of fossiliferous sedimentary successions. Concerning data acquisition, my research activity focused on assembling an important dataset (chapter 4) from latest Quaternary succession of the Central Adriatic Sea (i.e., near Mid Adriatic Deep-MAD). In addition to the newly acquired macrobenthic dataset, this thesis presents four published papers that represent the fruitful results of stratigraphic paleobiology approach to Quaternary fossiliferous successions. They range from quantification of quality and resolution of the fossil record along an onshore-offshore transect (chapter 5), to assessment of host-parasite dynamics in relation to sea-level changes (chapter 6), to evaluate the impact of stratigraphic architecture on the shape of mass-extinction events (chapter 7). Finally, a brief methodological study focuses on the need to integrate different multivariate techniques to obtain robust stratigraphic paleobiological trends (chapter 8). A short introduction to the main results reported in this Ph.D. thesis is given below.

Mid Adriatic Deep - Macrobenthic dataset (chapter 4)

Azzarone M., and Scarponi D.

A relevant part of my Ph.D. activities was dedicated to assembling a dataset on the species retrieved in the central area of the Adriatic Sea, near the MAD (Italy). This targeted area is currently 100 m – 150 m below sea level. During the last glacial phase, however, it recorded the Po Delta and coastal dynamics at the time of lowstand. The MAD dataset has been completed and is composed of 187 samples and 12,126 specimens grouped in 190 species. This dataset will be merged with a previously acquired dataset recording Po Delta and costal dynamics during the present and previous interglacial periods. This composite glacial/interglacial Po dataset will enable a historical perspective to be formed on modern ecosystems that have been shaped by long-term (glacial/interglacial) climatic oscillations. Moreover, an understanding of the long-term dynamics of those ecosystems (i.e., resilience, persistence or stochastic reassembly) to the long-term natural changes will provide an

important reference framework for assessing recent anthropogenic changes affecting deltaic ecosystems.

Manuscript 1 (chapter 5)

Systematic vertical and lateral changes in quality and time resolution of the macrofossil record: Insights from Holocene transgressive deposits, Po coastal plain, Italy

Scarponi D., **Azzarone M.**, Kusnerik K., Amorosi A., Bohacs K. M., Drexler T. M. and Kowalewski M.

Marine and Petroleum Geology 87, 128-136

This study, based on macrobenthic data from cored transgressive deposits, integrates taphonomic, bathymetric, and fossil density patterns to characterize Holocene spatio-temporal trends in taphonomic degradation along a 30 km onshore-offshore depositional profile. The joint consideration of quantitatively-derived eco-taphonomic trends enhanced interpretation of past sedimentary environments and past biotic trends and enabled identification of surfaces/intervals of sequence stratigraphic significance.

Manuscript 2 (chapter 6)

Surges in trematode prevalence linked to centennial-scale flooding events in the Adriatic

Scarponi D., **Azzarone M.**, Kowalewski M., and Huntley J.W.

Scientific Reports 7(1), 5732

The study utilizes the high-resolution stratigraphic and (sub-) fossil record of Holocene-aged lagoon and estuarine environments in northern Italy to test the responses of complex life cycle parasites over geological short-lived, but societally-relevant, sea-level oscillations. We find that using the most recent geological deposits to gain insight into biotic responses to climate change has distinct advantages over ecological studies of shorter temporal scales. These advantages include a longer time scale of observation, a high-resolution record of ecosystem response, and the potential for elucidating the roles of numerous biotic and abiotic factors on this pattern and their changes through sea level changes.

Manuscript 3 (chapter 7)

Stratigraphic signature of mass extinction: ecological and sedimentary determinants

Nawrot R., Scarponi D., **Azzarone M.**, Dexter T. A., Kusnerik M. K., Wittmer J. M., Amorosi A., and Kowalewski M.

Proceedings of the Royal Society B, 285(1886), 20181191

The fossil record is the principal source of information on the causes and consequences of mass extinctions. This work investigated last occurrences (LOs) of macrobenthic species in four cores along a down-dip transect within the stratigraphically and chronologically well-resolved Holocene succession of the Po coastal plain. Given that a hypothetical catastrophic event caused the extinction of all molluscan fauna of the Adriatic Sea in recent times, this paper focuses on evaluating whether the observed LO positions follow an apparent gradual extinction pattern (i.e., Signor-Lipps effects) or if complex but entirely false patterns can emerge owing to sea-level driven facies shifts and non-random distributions of fossil-rich deposits.

Manuscript 4 (chapter 8)

Early-Middle Pleistocene benthic turnover and oxygen isotope stratigraphy from the central Mediterranean (Valle di Manche, Crotona Basin, Italy): Data and trends

Azzarone M., Ferretti P., Rossi V., Scarponi D., Capraro L., Macri P., Huntley J.W., and Faranda C.

Data in Brief, 17, 1099-1107

This fourth paper presents a methodological study applied on the fossil Pleistocene benthic fauna from the Valle di Manche section (southern Italy). The availability of an integrated mollusk and ostracod dataset from a candidate section for the Middle Pleistocene Subseries drove my investigation on this area although not connected with the Po Adriatic Sea system. This integrated mollusk and ostracod dataset provides a unique opportunity to test the robustness of the paleoecological pattern derived by the application of various ordination analyses and to assess the main environmental driver(s) of faunal turnover. To this end, detrended correspondence analysis (DCA) and non-metric multidimensional scaling (nMDS) were performed on a set of abundance matrices derived by varying sample and taxon thresholds. The investigation concludes that - even varying the analytical sample threshold - stratigraphic plots of nMDS and DCA axis 1 sample scores yielded consistent faunal trends, that in accordance with previously conducted investigation on Po Plain-Adriatic Sea system, invariably indicate bathymetry as the main driver of faunal turnover along shelf settings.

Chapter 4

***The MAD
macrobenthic
dataset***

4. The Mid Adriatic Deep (MAD) dataset

The MAD dataset described in this section and available on AMS Acta (<http://doi.org/10.6092/unibo/amsacta/6101>; protected access until 29 March 2022), is part of an ongoing larger project that aims to build a comprehensive macrobenthic dataset from the Po Plain–Adriatic Sea system by sampling both sedimentary successions and present-day depositional surfaces. During my Ph.D. research, I processed samples taken from the MAD and near-MAD cored sedimentary succession in the central Adriatic, that contain marine lowstand deltaic and costal deposits from the last glacial time interval. Although an abundance of data has been gathered from the sedimentary succession of the Adriatic Sea, the dynamics of the macrobenthic community preserved there has been little investigated. The MAD dataset will represent a keystone for enhancing the knowledge of the molluscan fauna during the last glacial period.

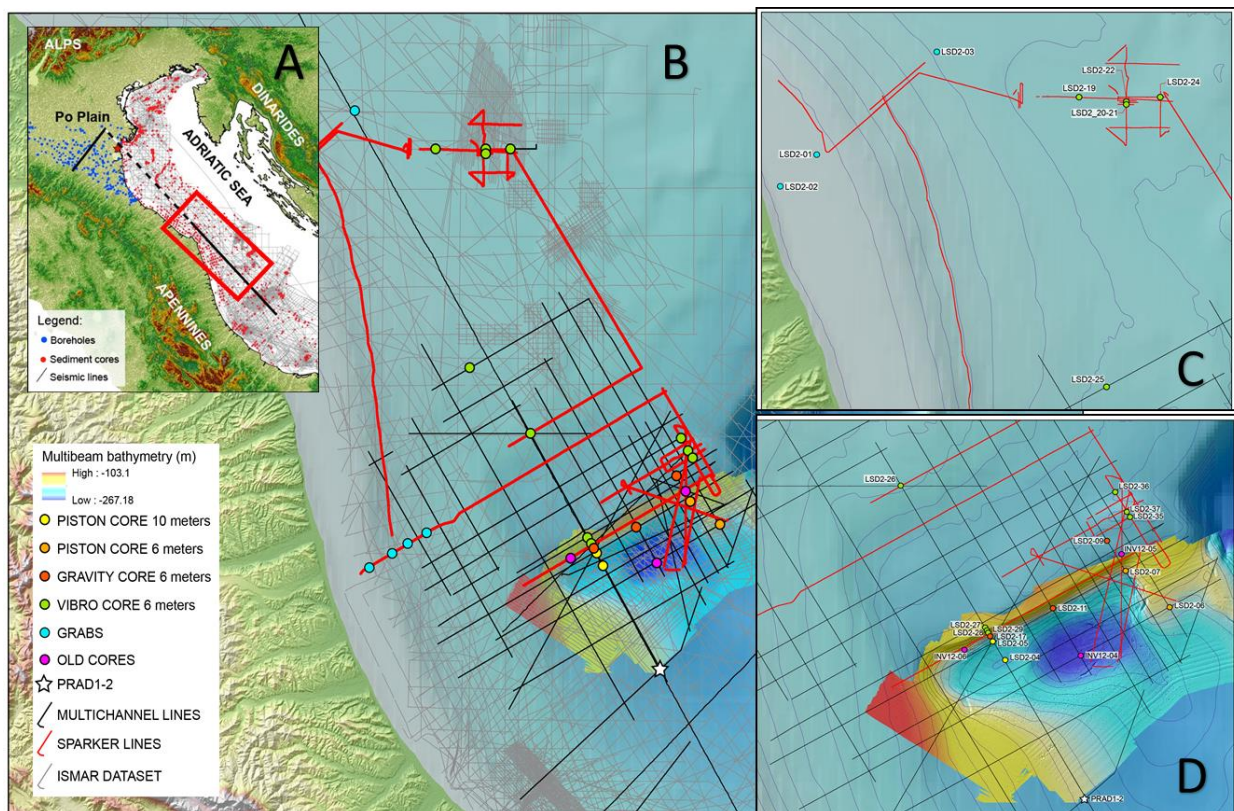


Figure 4.1– A) Network of seismic lines acquired in the last decades by Istituto di Scienza Marine – Consiglio Nazionale delle Ricerche (ISMAR-CNR) in the Adriatic Sea (after Amorosi et al., 2015). (B)–(D) Location of the investigated cores in the central Adriatic Sea and MAD (Pellegrini C. unpublished material).

4.1. MAD data collection

During the last 20 years, several oceanographic cruises conducted by Istituto di Scienze Marine (ISMAR-CNR) in Bologna collected a database of 80,000 km of high-resolution seismic profiles

obtained mainly by the Chirp Sub Bottom Profiler (Amorosi et al., 2015; Pellegrini et al., 2018). Morpho-bathymetric data were acquired by using a multibeam echosounder system. Moreover, more than 800 gravity and piston short cores (<10 m) and two borehole long cores (PRAD1 and PRAD2) were collected along the Adriatic Sea (Fig. 4.1). The MAD dataset was assembled by examining cores taken from the MAD and surrounding areas mainly during the cruise LSD2-2015 operated by the Research Vessel Minerva 1. The cruise resulted in a collection of 22 cores including piston, gravity, and vibro cores and six Van Veener grab samples. In addition, four previously acquired cores, one collected during the INVAS 2012 cruise and three collected during the AN 1997 cruise were considered. All of the investigated cores were stored in a refrigerated cell at ISMAR-CNR in Bologna and subdivided in 1m long segments. For each targeted core, ISMAR-CNR personnel provided lithological and facies descriptions, magnetic susceptibility profiles and a preliminary sequence stratigraphic interpretation.

Core Name	Latitude	Longitude	Device	Water Depth (m)	Recovery (m)	# of samples
LSD2-04	42.856494°N	14.626905°E	PC 10 m	230	8.97	14
LSD2-05	42.883066°N	14.602752°E	PC 10 m	199	8.33	14
LSD2-09	43.012104°N	14.806459°E	GC 6 m	136.7	2.32	5
LSD2-17	42.886148°N	14.600467°E	GC 6 m	192	3.06	5
LSD2-19	43.569592°N	14.232994°E	VC 6 m	84	5.3	11
LSD2-21	43.563881°N	14.316475°E	VC 6 m	87	5.69	6
LSD2-22	43.561092°N	14.317009°E	VC 6 m	88	5.9	15
LSD2-24	43.569952°N	14.377668°E	VC 6 m	84	5.6	7
LSD2-25	43.192624°N	14.286502°E	VC 6 m	83.1	5.6	10
LSD2-26	43.081668°N	14.440637°E	VC 6 m	98.6	5.21	8
LSD2-27	42.895910°N	14.592332°E	VC 6 m	146	5.4	9
LSD2-28	42.896907°N	14.591559°E	VC 6 m	145	5.6	12
LSD2-35	43.042674°N	14.848213°E	VC 6 m	123	5.7	10
LSD2-36	43.073539°N	14.822226°E	VC 6 m	130	5.7	9
LSD2-37	43.049098°N	14.842841°E	VC 6 m	117	5.4	12
LSD2-38	42.008205°N	16.281927°E	VC 6 m	64	5.6	9
AN97-31	43.669890°N	14.339024°E	GC 2.8m	80.5	2.29	6
AN97-32	43.669890°N	14.339357°E	GC 2.8m	80.5	2.8	5
AN97-40	43.588388°N	14.336859°E	GC 2.8m	86.2	2.35	5
INV-05	42.994021°N	14.831556°E	PC 10m	140	6.90	15

Table 4.1 – List of the 20 cores investigated for acquiring the MAD macrobenthic dataset. PC = piston corer, VC = vibrocorer, GC = gravity corer.

Unfortunately, not all cores were available or suitable for sampling: 20 out of 25 of the targeted cores mentioned above were sampled. Specific information on each targeted core is given in Table 4.1. The

resulting sampling effort consisted of 187 bulk samples (about 150 cm³ each), acquired from the targeted cores (Table 4.1) with average vertical spacing of 0.5 m. The samples were commonly taken from near the top and the bottom of each core-segment. In the case of fossiliferous intervals an additional sample was taken from the middle portion of the targeted segment. The samples were processed at the Department of Biological, Geological and Environmental Sciences of Bologna University. Each sample was soaked in ca. 10% H₂O₂ for 12 h or more, depending on the lithology. The resulting processed sediment was wet sieved by using 1 mm screens. For each sample, all mollusk specimens were identified to the species level (when possible) and were counted. In the case of bivalves, each valve was counted as one specimen. Only complete macrobenthic fossils or unique fossil fragments (e.g., umbo for bivalves and apex for gastropods) were counted. The sampling effort yielded 190 species grouped in 174 genera consisting of 12,126 specimens of mainly bivalves and gastropods. Details are given in Table 4.2.

# cores investigated	20
# samples collected	187
# taxa	294
# identified genera	174
# identified species	190
# bivalves species (total)	130 (44.2%)
# gastropods species (total)	155 (52.7%)
# other molluscs species (total)	9 (3.1%)
# specimens	12126

Table 4.2 – Salient abundance information about the MAD dataset. Results are clear showing the strikingly dominance of Gastropods and Bivalves, that together cover more than 95% of the recorded taxa.

4.2. MAD dataset structure

The MAD macrobenthic dataset consists of two main parts. The first part (i.e., the first 15 columns), reports all of the relevant chronological, environmental, geographic and stratigraphic information for each collected sample because, the main purpose of the MAD dataset is to explore mollusk dynamics in relation to time and space. For each sample, the main stratigraphic, temporal and geographic qualifiers are reported along with a brief explanation in Table 4.3.

Region	Italian region from which the core was taken
Samp_date	Date of collection (dd/mm/yyyy)
Depth_sampling_(m)	Sample stratigraphic depth in meters along the core, the sea-bottom = 0 m
Collector	Name of the sample collector
Sheet	Sheet of the geological map of Italy in which the core is located
Well	Core label
Systems_Tract	Sample's sequence stratigraphic characterization
Age	Inferred time interval of deposition (i.e., Holocene or late Pleistocene)
Substrate	Substrate recorded by the sample
Depositional_element	Sedimentary body or assemblage of bodies genetically related and deposited by the same medium
Facies_associations	Group of sedimentary facies used to define a particular sedimentary environment
Latitude	Core/sample coordinate expressed in grades and fraction of grades
Longitude	Core/sample coordinate expressed in grades and fraction of grades
Site_Altitude_(m)	Distance in meters of the site with respect to modern sea-level

Table 4.3 – Summary of temporal and geographical qualifiers reported in the dataset

The second part reports the sample taxonomic and abundance composition. The dataset is available on the AMS Acta repository (<http://doi.org/10.6092/unibo/amsacta/6101>; protected access until 29 March 2022). In addition, the relevant information is provided for each taxon identified. Specifically, the sample and species **ID** labels include a unique numerical or alphanumeric attribute (e.g., taxon-28), respectively. The **Ecosystem** label gives a broad environmental characterization for each taxon retrieved. Table 4.4 gives the identifiers adopted and the relative environmental characterization.

Ecosystems Label	Explanation
L	Land
F	Freshwater
F/B	Freshwater/Brackish
B	Brackish
B/M	Brackish/Marine
M	Marine

Table 4.4 - Environmental labels employed to characterize MAD taxa

Then, four commonly employed taxonomic ranks are reported separately and in descending order of **class, family, genus** and **species**. Although the higher taxonomic level employed here has been recognized for all specimens retrieved in the MAD samples (Table 4.5), increasingly higher percentages of fossil were not attributed to lower ranks and were left in open nomenclature. For example, about 35% of the total species are in open nomenclature mainly owing mainly to poor preservation of the examined specimens. Then, for each species name, its original **author** and **date** identifiers are reported to distinguish between homonyms of species-group names.

Class label	Explanation
P	Polyplacophora
G	Gastropoda
C	Cephalopoda
B	Bivalvia
S	Scaphopoda
Po	Polychaeta
Ma	Maxillopoda
Br	Brachiopoda
Ec	Echinoidea

Table 4.5 - Class rank employed to characterize MAD taxa.

The MAD dataset also reports, for each species considered the relevant auto-ecological information in order to characterize its life mode. Specifically, each species has been assigned (based on available literature) to generalized guilds in terms of: a) **type of feeding**; b) **substrate preference**; c) **degree of activity**. For point (c), a further classification has been provided in the case of immobile taxa. Table 4.6 gives specific information on each identifier employed for the afore-mentioned guilds.

Substrate relationship label	Explanation
IN	Infaunal
SI	Semi-infaunal
EP	Epifaunal
WB	Borer, nestler, ..., within burrows
EP-IN	Epifaunal to infaunal

NC	Nekton
Mobility label	Explanation
IM	Immobile
SE	Sedentary
AM	Actively mobile
Shell fixation label	Explanation
UN	Unattached
BA	Byssally (or other means) attached
CE	Cemented, by the shell or byssal cementation
Feeding type label	Explanation
SU	Suspension feeder
DE	(sub)surface (chemo symbiotic) deposit feeder
HE	Herbivores on rock plant, algal substrates
CAR	Carnivore
OM	Omnivorous
PAR	Parasite
SU-DE	Suspension (sub)surface (chemosymbiotic) deposit feeder
HE-CAR	Herbivore and carnivore
PAR-CAR	Parasite and carnivore

Table 4.6 – Life mode retrieved in MAD taxa

Finally, **family ID**, **genus ID** and **species ID** labels are identifiers that are invariant for each taxon-group at the taxonomic level considered (here, family, genus or species). That is, all taxa belonging to the same taxonomic-group at the level of family (e.g., Spæriidae), genus (e.g., *Pisidium*) or species (e.g., *Pisidium obtusale* and *Pisidium cf. obtusale*) will share the same ID. Open nomenclature taxa are not assigned an ID.

4.3. Future applications and outreach

Molluscan assemblages proved to be a powerful environmental tracker of high-frequency sea-level fluctuation that shaped the Quaternary history of coastal areas worldwide, meanwhile allowing high-resolution paleoenvironmental reconstructions (Meldahl et al., 1990; Roy et al., 1996; Schone et al., 2003; Goodwin et al., 2003; Tyler and Kowalewski, 2014; Bösken et al. 2018; West et al., 2018). For example, multivariate ordination of marine mollusk assemblages provided reliable depth estimates

for Quaternary depositional environments of the Po coastal plain (Scarponi and Kowalewski, 2004; Wittmer et al., 2014; Kowalewski et al., 2015; Scarponi et al., 2017). Hence, one of the purposes of this dataset is to test whether mollusk turnover in deeper marine succession of the MAD and central Adriatic, strongly correlate with their preferred depth as in the proximal basin area (the Po coastal plain). In fact, species turnover in offshore-settings could not be influenced by bathymetry as strongly as that of proximal settings. In addition, this dataset will provide an opportunity to depict Adriatic molluscan assemblages during the last glacial phase.

At the broader scale, the combined proximal-distal datasets (i.e., Po coastal plain-MAD) will provide documentation of marine macrobenthic ecosystems of the Adriatic across the last glacial-interglacial cycle and will be used to assess the ecological response of deltaic communities to long-term climate changes. In this respect, a previous study (Kowalewski et al., 2015) that compared deltaic mollusk assemblages between the present and previous interglacial periods, proved that marine communities of the penultimate interglacial reassembled unchanged following the last ice age. This recurrence of the same associations, in term of dominant species and other community descriptors, can indicate strong resilience if the community disintegrated upon perturbation (i.e., the last glacial maximum), but then recovered to a similar or even identical form after some time. Alternatively, it can indicate ecological persistence if the targeted associations continue through the perturbation. In this light, the MAD dataset that records coastal/deltaic dynamics of macrobenthic Adriatic communities at the time of the last glacial phase will shed light on and discriminate between the aforementioned long-term dynamics of Adriatic shallow marine communities.

In summary, the information reported in this dataset will enable reconstruction of the ecological response of the macrobenthic communities to climatic-driven late Quaternary sea-level oscillations. This will, in turn provide a reference framework for evaluating the severity and significance of anthropogenic climate changes on marine ecosystems.

Chapter 5

Manuscript I

5. Manuscript I

“Systematic vertical and lateral changes in quality and time resolution of the macrofossil record: Insights from Holocene transgressive deposits, Po coastal plain, Italy”

Authors: Daniele Scarponi ^a, Michele Azzarone ^a, Kristopher Kusnerik ^b, Alessandro Amorosi ^a, Kevin M. Bohacs ^c, Tina M. Drexler ^c, Michal Kowalewski ^b

^a Dipartimento di Scienze Biologiche, Geologiche e Ambientali, University of Bologna, Via Zamboni 67, 40126 Bologna, Italy

^b Florida Museum of Natural History, University of Florida, 1659 Museum Road, Gainesville, FL 32611, USA

^c ExxonMobil Upstream Research Company, 22777 Springwoods Village Parkway, Spring, TX 77389, USA

Status: Published in *Marine and Petroleum Geology*, volume 87, November 2017, pages 128-136

doi: doi.org/10.1016/j.marpetgeo.2017.03.031



Research paper

Systematic vertical and lateral changes in quality and time resolution of the macrofossil record: Insights from Holocene transgressive deposits, Po coastal plain, Italy



Daniele Scarponi ^{a, *}, Michele Azzarone ^a, Kristopher Kusnerik ^b, Alessandro Amorosi ^a, Kevin M. Bohacs ^c, Tina M. Drexler ^c, Michał Kowalewski ^b

^a Dipartimento di Scienze Biologiche, Geologiche e Ambientali, University of Bologna, Via Zamboni 67, 40126 Bologna, Italy

^b Florida Museum of Natural History, University of Florida, 1659 Museum Road, Gainesville, FL 32611, USA

^c ExxonMobil Upstream Research Company, 22777 Springwoods Village Parkway, Spring, TX 77389, USA

ARTICLE INFO

Article history:

Received 18 November 2016

Received in revised form

16 March 2017

Accepted 27 March 2017

Available online 28 March 2017

Keywords:

Taphonomy

Benthic invertebrates

Stratigraphic paleobiology

Holocene

Po plain

Sequence stratigraphy

ABSTRACT

In siliciclastic marine settings, skeletal concentrations are a characteristic feature of transgressive intervals that provide insights into biological and sequence-stratigraphic processes. To investigate taphonomic signatures of transgressive intervals, we analysed three cores along a depositional profile from the high resolution chrono- and stratigraphic framework of the Holocene Po coastal plain, in northern Italy. Coupled multivariate taphonomic and bathymetric trends delineated spatial and temporal gradients in sediment starvation/bypassing, suggesting that quality and resolution of the fossil record vary predictably along the studied depositional profile. Moreover, integration of taphonomic, bathymetric, and fossil density trends across the study area reveals distinctive signatures useful in characterizing facies associations and determining surfaces and intervals of sequence-stratigraphic significance. Within the southern Po plain succession, taphonomic degradation of macroskeletal remains increases from proximal/nearshore to distal/offshore locations. This trend is discernible for both biologically-driven (bioerosion) and physically-driven (e.g., dissolution, abrasion) shell alterations. Compared to the up-dip (most proximal) core, the down-dip core is distinguished by shell-rich lithosomes affected by ecological condensation (co-occurrence of environmentally non-overlapping taxa) and by higher taphonomic alteration. The onshore-offshore taphonomic trend likely reflects variation in sediment-accumulation along the depositional profile of the Holocene Northern Adriatic shelf, with surface/near-surface residence-time of macroskeletal remains increasing down dip due to lower accumulation rates. These results indicate that, during transgressive phases, changes in sea level (base level) are likely to produce down-dip taphonomic gradients across shelves, where the quality and resolution of the fossil record both deteriorate distally. Radiocarbon-calibrated amino acid racemisation dates on individual bivalve specimens and the chronostratigraphic framework for this profile suggest jointly that the high levels of taphonomic degradation observed distally developed over millennial time scales (~8ky). Whereas in proximal setting overall low taphonomic degradation and geochronologic constrains point to centennial-scale time-averaging during the late transgression phase. Patterns documented in the Holocene transgressive (and lowermost regressive) deposits of the southern Po Plain may be characteristic of siliciclastic-dominated depositional systems that experience high-frequency, base-level fluctuations.

© 2017 Elsevier Ltd. All rights reserved.

1. Introduction

In marine settings, skeletal concentrations often represent the geologic by-product of a complex interplay between the rate of

production of skeletal material (biogenic) and variations in clastic sediment supply/accumulation (Kidwell, 1986; Tomašových et al., 2006). In siliciclastic-dominated depositional settings, the close association of skeletal-rich deposits with prominent sequence-stratigraphic surfaces (e.g., Holland, 2000; Patzkowsky and Holland, 2012; Amorosi et al., 2014; Scarponi et al., 2014; Aucoin et al., 2016; Danise and Holland, 2017) suggests that taphonomically-complex, fossil-rich lithosomes are primarily a

* Corresponding author.

E-mail address: daniele.scarponi@unibo.it (D. Scarponi).

product of the interaction between sedimentation and accommodation. Consequently, variations in the taphonomic signature of siliciclastic fossiliferous deposits may be driven primarily by sedimentary inputs and depositional processes (i.e., R-sediment model of Kidwell, 1985, 1986), or by variations in the production rate of biogenic skeletal remains (i.e., the R-hardpart model; see Tomašových et al., 2006). This assumption has been successfully corroborated by qualitative and quantitative studies of several Quaternary (and older) siliciclastic successions around the globe (Kidwell, 1989; Meldahl, 1990; Abbott et al., 2005; Cantalamessa et al., 2005; Tomašových et al., 2006; Scarponi and Kowalewski, 2007; Zecchin and Caffau, 2011; Ávila et al., 2015; Scarponi et al., 2016; Brady, 2016).

Given these considerations, taphonomic characterization of marine fossil assemblages could aid environmental interpretation and may offer a potentially useful tool for identifying and delineating sequence-stratigraphic units and their bounding surfaces (e.g., Brett, 1998; Holland, 2000; Dominici, 2001; Huntley and Scarponi, 2012; Zecchin and Catuneanu, 2013; Horodyski et al., 2014; Giannetti and Monaco, 2015). This is especially true when stratigraphic interpretations are based on cores, for which information on the geometry of sedimentary bodies is exceedingly limited. In such cases the study of taphonomic and paleoecologic attributes of skeletal concentrations can provide an additional strategy for assessing the formational histories and stratigraphic development of cored successions. Here, we focus on the quantitative taphonomy of mainly transgressive fossiliferous lithosomes (with particular emphasis on marine deposits) from cores in the Holocene Po Plain succession (northern Italy) within the context of previously established, high-resolution facies, chronostratigraphic, and sequence-stratigraphic frameworks (Fig. 1; see Amorosi et al., 2017). Specifically, this study aims to: (1) compare taphonomic attributes of skeletal concentrations within and across genetically-related segments of the ~30-km long nearshore to shallow-marine dispersal system developed during the Holocene transgression; and (2) employ ecologic and taphonomic features of fossil assemblages to identify prominent sequence-stratigraphic surfaces (e.g., maximum flooding surface MFS) and intervals (e.g., condensed section CS), as well as investigate systematic changes along the studied profile.

2. Sequence-stratigraphic framework of the latest Quaternary Po plain succession

The latest Quaternary deposits (<30ky) of the southern Po Plain represent a few tens of meters thick succession of siliciclastic sediments. Extensive subsurface investigations conducted during the past few decades have led to a detailed reconstruction of the region's stratigraphic architecture (e.g., Amorosi et al., 1999; Scarponi and Kowalewski, 2004; Correggiari et al., 2005; Stefani and Vincenzi, 2005; Storms et al., 2008; Amorosi et al., 2016; Bruno et al., 2016; Calabrese et al., 2016; Scarelli et al., 2017). The lowermost part of this succession consists of alluvial facies deposited during the Last Glacial Maximum (30–18ky BP) and initial eustatic rise (18–14ky BP) phases, when sea level was approximately 120-to-90 m lower than today. Its upper portion (mainly Holocene in age), is dominated by a variety of transitional to shallow-marine deposits, accumulated during rapid eustatic rise (14–7ky BP) and subsequent highstand (6ky BP onward). In the study area, these genetically-related strata, up to 40 m in thickness, represent the Last Glacial Maximum (LGM) depositional sequence (Amorosi et al., 2017) which is dominated by aggradational alluvial and upper coastal plain facies associations (Lowstand systems tract—LST). The LST transitions upwards into retrogradational muddy lower coastal plain to shallow-marine deposits

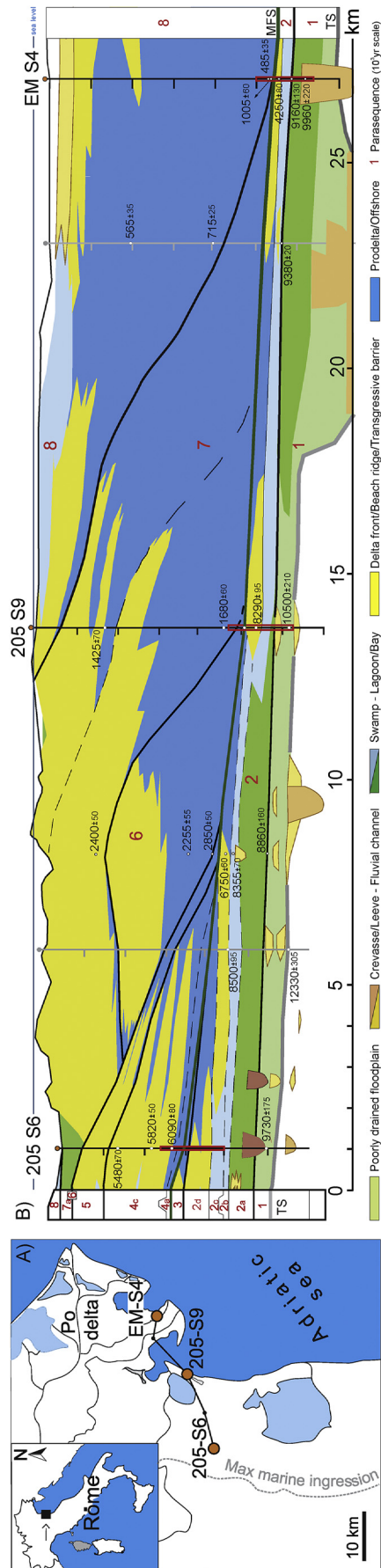


Fig. 1. A) Location of the study area with indication of the cross-section and position of the investigated cores: 205-S6 and 205-S9 were drilled by the Geological Survey of Emilia-Romagna (Italy), whereas EM-S4 was drilled as part of a collaborative research project supported by ExxonMobil Upstream Research Company (USA). B) Simplified and slightly modified cross-section (after Amorosi et al., 2017) illustrating the correlation of the studied cores, geochronology (radiocarbon calibrated BP), stratigraphic and parastratigraphic framework of the Holocene Last Glacial Maximum F-R sequence. The eight millennial scale parastratigraphic units are numbered in red, whereas lower-rank, centennial scale parastratigraphic units (indicated by letters) are delimited (where recognized) by dashed lines. Lastly, rectangles in red highlight the investigated portion of the three selected cores. (For interpretation of the references to colour in this figure legend, the reader is referred to the web version of this article.)

(Transgressive systems tract—TST) overlain by a mosaic of deltaic to coastal plain deposits reflecting the subsequent Holocene progradation (Highstand systems tract—HST). Eight higher-order depositional successions (meter-thick parasequences) that developed over centennial-to-millennial time scales characterize the internal structure of the LGM sequence (Fig. 1B). These parasequences, geochronologically well-constrained (Fig. 1B), can be defined by their characteristic bounding surfaces, internal stacking patterns, and geometric relations to surrounding strata (see Amorosi et al., 2017).

3. Methods

Three cores along a ~30-km down-dip transect across the southern Holocene Po Plain were investigated in this study (Fig. 1). Detailed (20-cm scale) stratigraphic description of the investigated portion of each core provides the depositional context for the fossiliferous deposits. Core 205-S6 is proximal to the shoreline at the time of maximum marine ingression (<5 km from shoreline), core 205-S9 is intermediate (~18 km), and core EM-S4 is distal (~30 km; Fig. 1). The brackish-to-marine (TST) and lowermost marine (HST) core sections were sampled at high resolution (~5 cm intervals, ~250 cm³ of sediment, commonly every 25 cm or more closely spaced in richly fossiliferous intervals) to quantitatively evaluate faunal composition, ecologic characteristics, and taphonomic attributes of macroskeletal assemblages (raw data are provided in supplementary material). In total, 50 samples were dried for 24 h at 40 °C, then soaked in ~4% H₂O₂ (≤12 h, depending on lithology) and wet sieved (see also Scarponi and Angeletti, 2008). The laboratory treatment is unlikely to have induced any notable alterations of the sampled shell material because we used a highly-diluted peroxide for a short interval of time. Sample-level bathymetric estimates were derived by employing non-metric multidimensional scaling (nMDS) of species abundance data. These water depth estimates were integrated with high-resolution facies analyses (Fig. 1). Lowermost HST deposits were investigated to constrain, at dm-scale resolution, the turnaround between transgressive and regressive stacking patterns.

nMDS is a dimension-reducing multivariate technique that ordines samples in a reduced space of 2 or 3 dimensions using arbitrarily scaled scores. This approach was also used to recognize and characterize backstepping-nearshore (here the main focus) from aggrading-shallow marine deposits (TST vs. lowermost HST). The nMDS ordination was conducted on a matrix of relative species abundance using Bray–Curtis distance. The acceptable value of stress (<0.20) resulted from nMDS performed in two dimensions (2 k). Bathymetric estimates were obtained by regressing nMDS 1 sample scores against sample-level bathymetric data obtained by specimen-weighted averaging of a subset of species with known bathymetric distribution. This method is fully explained in Wittmer et al. (2014); see EG-DC: posterior calibration of ordination scores using preferred depth of taxa; see also Tables S1 and S2 in supplementary material).

In order to investigate taphonomic-degradation patterns within cores and across the depositional gradient, percent volume of skeletal remains retrieved in each sample was recorded and 60 shells, or fragments larger than 2 mm, were randomly selected from each sample and inspected for taphonomic damage. Samples with scarce fossils content ($n < 60$ fragments/shells) were not examined. A total of 45 samples yielded sufficient material for taphonomic investigations. Each specimen was examined with a binocular microscope using 10× magnification, and six variables were recorded and scored following the protocol defined in Table 1. Fragments/shells varied in dimension from 2 to 40 mm. As shell/fragment size could potentially introduce an area-related bias (i.e.,

larger fragments offer more surface for examination), the analyses were computed focusing only on the more abundant size classes (2–6 mm). Sample size [n] remained reasonably adequate after the culling of specimens larger than 6 mm (n range: 35–59, mean n : 51; 2290 fragments/specimens total). The multivariate taphonomic relations between all samples were also explored using nMDS. The pairwise distances between samples were based on multivariate Euclidean distances using z-scored % values of taphonomic variables. That is, for each sample, a relative abundance score for each taphonomic state was computed separately for each taphonomic variable. For each taphonomic state, relative abundances were z-standardized (scaling to zero mean and unit variance) to ensure comparable weighting of all variables. The nMDS ordination was employed to visualize relative similarities of all samples in terms of their taphonomic signatures. The nMDS performed in 2 k returned a good value of stress (0.123). For each core, nMDS-derived taphonomic profiles were plotted along stratigraphic architecture to help delineate taphonomic trends and contrasted with nMDS-derived bathymetric profiles. Note that in the intermediate core, due to previously collected samples around MFS, transgressive deposits were explored only partly.

Finally, five ¹⁴C-calibrated amino-acid-racemisation ages were estimated for bivalves, including specimens of upper shoreface *Lentidium* and offshore *Corbula*. These specimens were recovered from within the top-most sample collected from a ~25 cm thick, densely packed fossiliferous interval in the offshore distal sector (EM-S4). These dates, along with others previously published (Scarponi et al., 2013; Campo et al., 2016, Fig. 1B), provide direct numerical insights into the geochronology and temporal resolution of the fossil record of the investigated region. Analyses were performed at the Amino Acid Geochronology Laboratory - Northern Arizona University (USA). All statistical analyses were performed using R (R Development Core, 2016) and PAST (Hammer et al., 2001) softwares.

4. Results

The nMDS ordination of taphonomic variables indicates that nMDS axis 1 is positively correlated with taphonomic damage: low axis-1 values point toward high taphonomic alteration of samples (Fig. 2). Specifically, samples with high axis-1 scores are typified by the absence or scarcity of bioerosion, dissolution, ornamentation loss, and immuration. A high degree of bioerosion, color alteration, and complete ornamentation loss characterize samples with lower (negative) nMDS axis-1 scores.

Samples are regularly distributed along axis 1 of the ordination plot (Fig. 2). Samples from proximal (205-S6) and intermediate (205-S9) cores are located in the mid-upper right quadrant of the nMDS plot and form adjacent, highly overlapping groups in the ordination space (Fig. 2). Samples retrieved from the distal (EM-S4) core are more widely dispersed in the nMDS space, but show only limited overlap with the intermediate core samples and no overlap with the proximal core samples (Fig. 2). Plots of nMDS axis-1 sample scores along core depth show that taphonomic profiles are variable from site to site, the overall taphonomic damage, however, tends to increase from proximal to distal locations (Figs. 3–4). In both proximal and distal cores, the major peak in the taphonomic damage is recorded in the facies associations related to deeper settings (i.e., shoreface transition and offshore, respectively), and in agreement with the maximum depth estimate (Fig. 3). In the intermediate core, peak damage occurs within the transgressive sand sheet—a meter-scale lithosome with strong evidence of physical reworking. However, no samples at the level of estimated maximum water depth (Fig. 3) were available for taphonomic analyses. Minor peaks in nMDS axis-1 scores are also

Table 1
Taphonomic variables and damage states used to score skeletal items from the Holocene Po Plain succession.

Taphonomic primer		
Variable	Evaluation of	State
Ornamentation(orn.)	sculpture state of shell/fragment	0 = pristine or well preserved; 1 = worn; 2 = lost/completely erased; 3 = smooth shell
Immuration (imm.)	precipitation of minerals on skeletons (e.g., carbonates or gypsum)	0 = pristine; 1 = traces; 2 = in part; 3 = coated
Fragmentation (frag.)	skeleton breakage	0 = whole valve or specimen; 1 = fragment,
Color (col.)	colors and patterns on shell surface	0 = pristine/fresh; 1 = faint/traces; 2 = discolored/not visible; 3 = secondary color/pattern
Dissolution (diss.)	dissolution on skeletal	0 = not visible, 1 = initial stage, 2 = advanced stage
Bioerosion (bioer.)	perforation or encrustation degree	0 = not visible; 1 = in part, 2 = completely covered

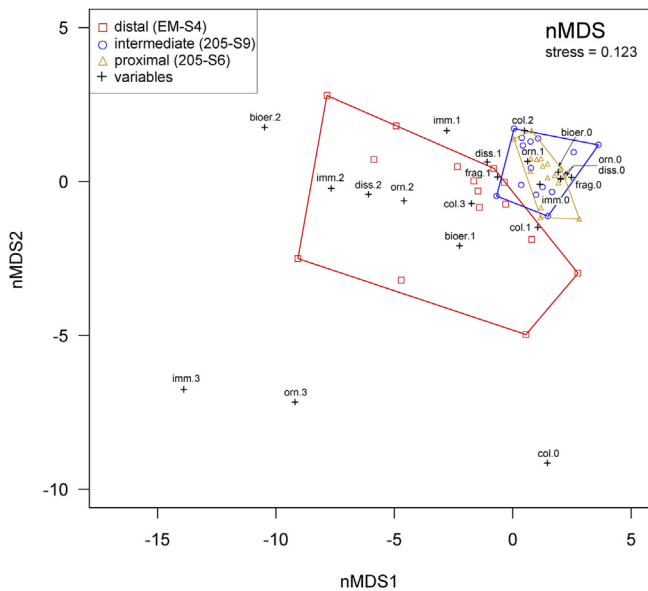


Fig. 2. nMDS in two dimensional space, based on Euclidean distance for z-standardized relative abundances of taphonomic variables of samples from the Holocene Po plain succession. Both taphonomic variables and samples are displayed.

observed at all three sites associated with facies shifts or across stratal boundaries (Fig. 3).

Finally, both bathymetric and taphonomic nMDS-derived trends coupled with ecologic information of recovered species appear to be diagnostic of the transgressive facies associations.

Specifically, lagoon/bay deposits commonly show barren or sparse, macroskeletal remains of mainly brackish taxa (e.g., *Cerastoderma glaucum*, *Abra segmentum*; Fig. 4C, F and I). These deposits are characterized by an overall invariant and/or upward decreasing (well to fairly preserved) taphonomic degradation coupled with invariant to deepening-upward bathymetric profiles (Fig. 3). ^{14}C -calibrated shelly material from outer-lagoon deposits from a companion core yielded centennial time estimates of time averaging (see Scarponi et al., 2013 locality 4). Minor spikes in the taphonomic damage profile are mainly associated with lithofacies changes.

Transgressive sand sheet—TrSS intervals are characterized by fossiliferous, ecologically mixed assemblages of brackish to shallow marine taxa (e.g., *Cerastoderma*, and tellinids respectively; Fig. 4E and H), with intermediate taphonomic degradation that increases basinwards (Fig. 3B–C). Previously ^{14}C -calibrated amino acid racemisation (AAR) dates from the topmost of this fossiliferous sand sheet in the intermediate core yielded age-offset of ~3.9 ky (Scarponi et al., 2013, Fig. 3B). Within this facies association the vertical changes in taphonomic damage follow a v-shaped pattern

characterized by an increasing and then decreasing-upward trend (Fig. 3B–C). These taphonomic changes developed within a bathymetrically invariant setting in the intermediate core (Fig. 3B). In the distal core, the bathymetric profile initially appears substantially invariant (i.e., observed changes are within the uncertainty of the estimate ± 1.8 m in Fig. 3), followed by shallowing. In contrast, fossiliferous and lithologically similar lower-shoreface deposits that also developed across a bathymetrically invariant trend, can be easily distinguished from TrSS by their overall low shell damage, reversed taphonomic degradation trend (first decreasing and then increasing upward; Fig. 3A), and ecologically coherent (lower shoreface) monotaxic *Chamelea gallina* assemblages (Fig. 4B), framed within a centennial-scale parasequence. This latter is nested within millennial-scale parasequence 2 (no radiometric data available; Fig. 1, Campo et al., 2016).

Offshore facies show variable taphonomic damage in relation to their position along the depositional profile (i.e., intermediate vs. distal). That is, offshore samples from the intermediate core show notably lower taphonomic degradation than offshore samples from the distal core (Figs. 3A, C and 4D, G). Only in the distal core we did observe a densely packed skeletal concentration (~25 cm thick) of highly-degraded (e.g., bioeroded and abraded) and ecologically non-overlapping mollusks in association with maximum water depth (>20 m; Figs. 3C, 4G and 5). These assemblages are dominated by species typical of Adriatic coralligenous assemblages that thrive in areas of minimal clastic sediment accumulation, low light and relatively low benthic-energy levels (Ballesteros, 2006). The ^{14}C -calibrated amino acid racemisation (AAR) ratios of the five shells did not include any outliers with aberrant amino acid signatures (see screening procedure in Scarponi et al., 2013). The ages were consistent within each of the two analysed species. Specifically, upper shoreface *Lentidium* valves yielded age estimates between 9.2 and 9.6ky, whereas, ages of offshore *Corbula* specimens ranged between 0.9 and 1.2ky (see Table S1 in supplementary material). These layers of ecologically mixed and highly damaged faunal remains (Fig. 3C) suggest the presence of a fossiliferous condensed section—CS in the distal core (Figs. 4G and 5).

5. Discussion and conclusion

5.1. Eco-taphonomic patterns and their driving factors

In back-barrier settings, taphonomic patterns are relatively consistent along the investigated depositional onshore-offshore profile. Scattered skeletal remains, characterized by low or decreasing upward taphonomic degradation, framed within a centennial-scale residence time, suggest relatively high net-accumulation rates. Preliminary estimates indicate average sedimentation rates of 2–6 mm/yr in transgressive back-barrier settings (Scarponi et al., 2013; Campo et al., 2016).

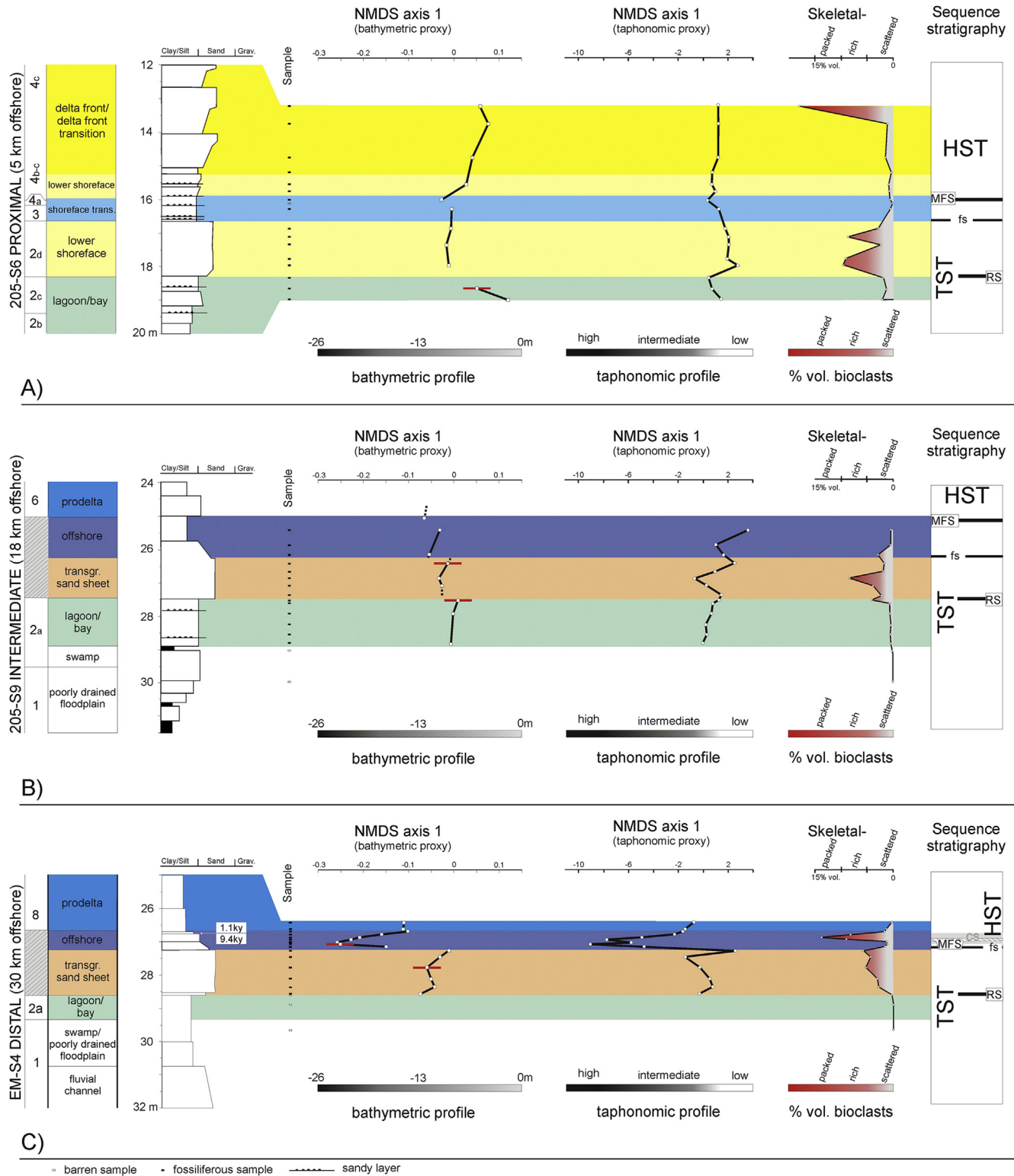


Fig. 3. Temporal trends across the three analysed cores. From left to right the columns represent (1) interpreted facies association and parasequence stack following Amorosi et al., 2017 (dashed, grey rectangle represents the portion of the core where parasequences are not resolvable), (2) core lithology; (3) vertical changes in faunal composition estimated by nMDS (Bray-Curtis distance) axes 1 scores based on faunal composition of samples; the red bar marks standard error (± 1.8 m) in the water depth estimates (see also Tables S1–2 in supplementary material); (4) vertical changes in taphonomic signatures estimated by nMDS (Euclidean distance), axes 1 scores based on z-standardized mean taphonomic scores of samples; (5) Density (% sample volume) of skeletal remains across cores. The boxes on the right side of the plots summarize sequence-stratigraphic interpretation based on the examined eco-taphonomic features. Abbreviations: TST—transgressive systems tract; HST—highstand systems tract; RS—ravinement surface; FS—flooding surface; MFS—maximum flooding surface. In the distal core, reported ages are mean ages based on ^{14}C -calibrated amino acid racemisation rates of *Corbula* (lower date) and *Lentidium* specimens (see also Table S3). (For interpretation of the references to colour in this figure legend, the reader is referred to the web version of this article.)

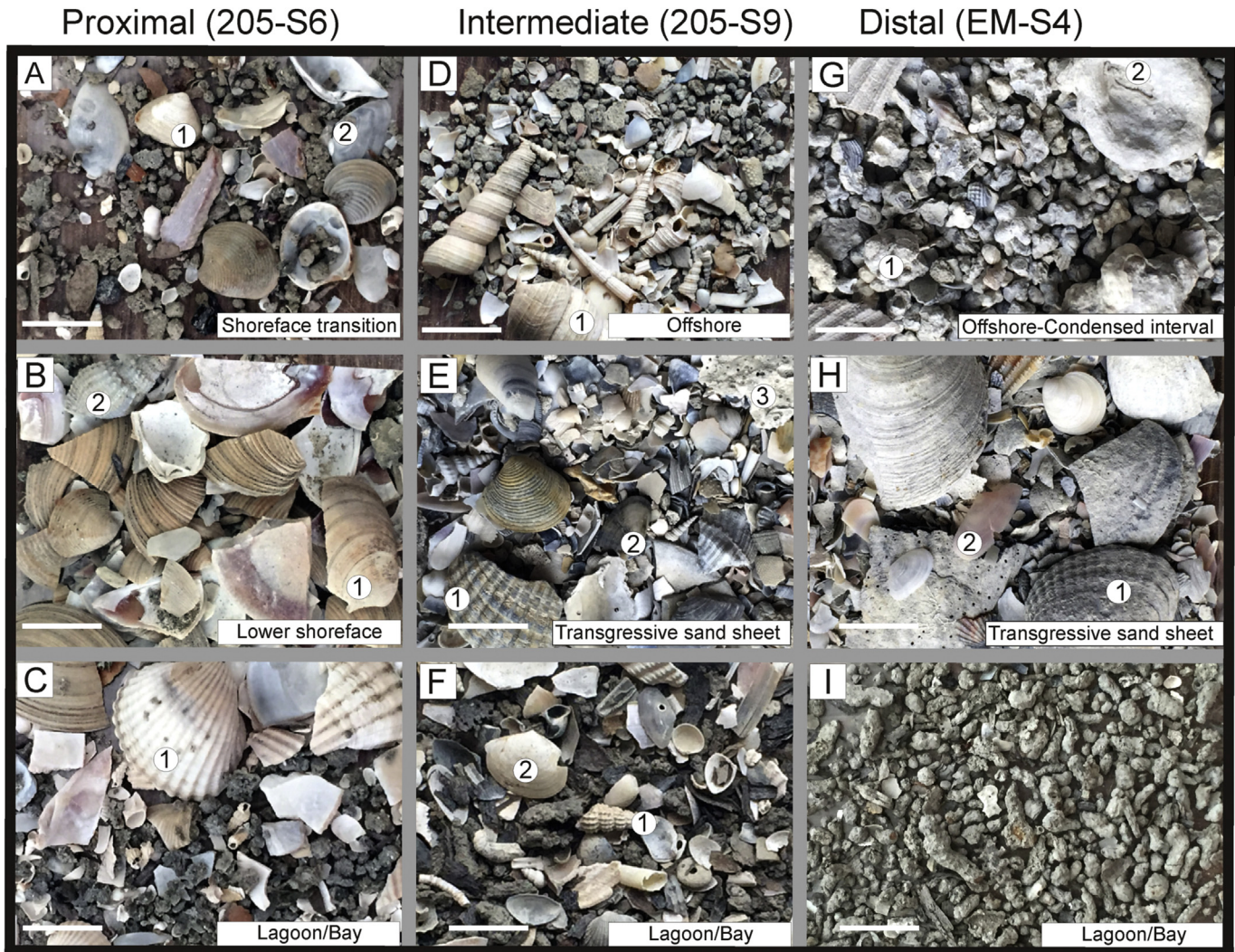


Fig. 4. Examples of macrofossil assemblages and taphonomic signatures retrieved along the depositional profile and across cores. A) Scattered fairly preserved, ecologically coherent assemblage (16.00 m core depth): 1—*Spisula subtruncata* specimen with decolored and smooth shell; 2—*Fabulina fabula* specimen with altered color. B) Richly fossiliferous, overall well preserved and monotaxic *Chamelea gallina* assemblage (17.80 m core depth): 1—*C. gallina* unique fragment with worn sculpture; 2—*Nassarius* specimen with well preserved sculpture and traces of color; 3—*Ostrea* fragment decolored and bioeroded. C) Scattered, overall well preserved, assemblage (18.70 m core depth): 1—*Cerastoderma glaucum* specimen with traces of color. D) Scattered, well preserved assemblage (25.45 m core depth): 1—*Turritella communis* fragment discolored, but otherwise well preserved. E) Richly fossiliferous, ecologically mixed assemblage showing overall intermediate taphonomic degradation (26.90 m core depth): 1—brackish *C. glaucum* and 2—upper shoreface *Donax*, common fragment with altered colors; 3—*Ostrea* fragment decolored and bioeroded. F) Scattered, overall well-preserved, ecologically-coherent assemblage (28.30 m core depth): 1—juvenile *C. glaucum* valve with altered color; 2—brackish *Abra segmentum* well preserved. G) Richly fossiliferous assemblage recording highest taphonomic damage (26.75 m core depth): 1—Trochidae specimen, partly immured, discolored, bioeroded; 2—Pectinidae, completely encrusted by calcareous algae. H) Richly fossiliferous and ecologically mixed assemblage with intermediate taphonomic damage (27.75 core depth): 1—*C. glaucum* worn specimen showing advanced stages of dissolution; 2—offshore *Atlantella* specimen well preserved with traces of color. I) Sample devoid of molluscs, only plant debris were retrieved (core depth 28.90 core depth). Scale bar = 10 mm. (For interpretation of the references to colour in this figure legend, the reader is referred to the web version of this article.)

Within the marine TST, taphonomic patterns change predictably along the depositional profile and show increasingly higher time-condensation, even for those samples that belong to the same facies association (i.e., TrSS and offshore) and show comparable faunal turnover and overlapping bathymetric profiles (e.g., the intermediate and distal portions; see Fig. 3). The basinward increase in taphonomic degradation coupled with increasingly poorer time resolution, suggests that changes in clastic supply, likely controlled by increasing distance from the shoreline and cyclonic oceanographic-circulation patterns (Amorosi et al., 2016), were the major drivers in shaping the taphonomic signature of skeletal assemblages, especially in intermediate and distal cores (i.e., >17 km offshore). These factors control the duration of sea-floor exposure of skeletal remains (Figs. 1 and 3B–C) and facilitate the

development of taphonomic feedback (*sensu* Kidwell and Bosence, 1991, Fig. 4G) and intense degradation. Found in intermediate and distal cores, a meter-thick transgressive sand sheet (TrSS; Figs. 3B–C and 5) represents ecologically-mixed fossiliferous sediments (Fig. 4E, H) and exhibits intermediate levels of fossil preservation. These characteristics of TrSS suggest that physical and biological reworking of skeletal-rich and skeletal-poor intervals outpaced net-accumulation rates for a substantial period, estimated 3–4 ky (see chapter 4). However, fairly preserved associations characterizing top TrSS in both intermediate and distal cores (Fig. 3B–C), point to episodic progradation during an overall transgression (see also Cattaneo and Steel, 2003). In the distal core this interpretation is also supported by a slight shallowing-upward tendency within uppermost TrSS and by a poorly fossiliferous thin



Fig. 5. Vertical stacking of facies associations in distal core EM-S4 (30 km offshore) with relevant sequence-stratigraphic units and surfaces as identified by taphonomic investigations. Core segments are 1 m in length. RS—ravinement surface; CS—condensed section; MFS—maximum flooding surface.

and laminated interval of silt/fine sand occasionally observed on top of the TrSS (see EM-S4, 27.10–27.20 m in Figs. 3C and 5). Additionally in the distal sector, the presence of an ecologically condensed interval overlying the TrSS (Fig. 4G) suggests that low accumulation rates persisted even longer, although this core is located only ~30 km offshore of its coeval shoreline (core EM-S4). Here, rates of net accumulation are difficult to quantify, but are estimated to be $<<1$ mm/yr (see Campo et al., 2016).

The results reported here demonstrate that fossil condensation is clearly delineated within marine deposits of distal location, by highly degraded and polytaxic skeletal concentrations that mix together ecologically non-overlapping species (Fig. 4G). This strong taphonomic signature recorded in this particular interval of core EM-S4 developed in less than 10ky (according to radiometric derived ages, Fig. 1; Table S3). Conversely, facies associations and the bathymetric changes across core 205-S6 (Fig. 3A) indicate that backstepping deposits developed close to the shoreline (<5 km) throughout the entire marine transgressive phase. Here, clearly defined highly fossiliferous horizons are recorded. These horizons contain ecologically coherent faunal assemblages, framed within centennial scale parasequences, with the relatively lowest levels of taphonomic degradation (Figs. 1 and 4B). The unexpectedly low level of taphonomic alteration – given the relatively high-energy setting (lower shoreface) in which those fossil horizons formed – highlights the overriding importance of clastic sediment supply that lowers the residence time of shells within the taphonomically active zone, as well as high biological productivity in nearshore settings at the time of late transgression. An overall high rate of clastic-sediment supply in such settings is also implied by the presence of scattered, fairly-preserved fossil remains in the deepest proximal facies (shoreface transition at time of maximum transgression; Figs. 1 and 4A). Here, given ecologically coherent associations characterizing these nearshore deposits (see also section

5.2), the net-sedimentation rates are inferred to be at least comparable with those recorded in back-barrier settings throughout the entire transgressive phase. This outcome is consistent with the predictions of the R-sedimentation model of Kidwell (1985, 1989). In the proximal portion of the gradient (<5 km offshore), however, variations in the production rate of biogenic skeletal remains (i.e., the R-hardpart model; Tomašových et al., 2006) may have also played a role in forming fossiliferous assemblages.

5.2. Eco-taphonomic patterns and implications for paleobiology

Back-barrier settings are characterized by ecologically congruent fossil assemblages with low levels of taphonomic alteration, which are indicative of relatively high net-sedimentation rates in a low-energy depositional environment. These ecological and taphonomic attributes indicate that back-barrier facies represent a high-quality and high-resolution fossil record, consistent with sub-millennial time-averaging of individual fossil horizons previously estimated via ^{14}C -calibrated amino acid dating (Scarponi et al., 2013). Back-barrier deposits are capped by a slightly diachronous ravinement surface [RS], which records marine flooding of older brackish depositional environments and is clearly separated from the transgressive surface [TS] recognized on top of the Younger Dryas paleosol (Campo et al., 2016). The reworked taxa with, at most, intermediate taphonomic degradation associated with the RS indicate a reduced temporal resolution, which is consistent with the time-averaging indicated by numerical dating of the RS shell lag (2–3ky in Scarponi et al., 2013). Lithosomes above the RS, capped by the MFS along dip, are suggestive of different patterns of sediment dispersal (see section 5.1).

These patterns indicate that the resolution and quality of the fossil record change predictably down-dip. Specifically, the proximal area is characterized by ecologically congruent, fairly preserved, monospecific fossil assemblages (Fig. 4B) due to sediment trapping at the time of maximum marine ingressions. These assemblages have centennial-scale resolution, as they occur within the centennial-scale parasequence 2d (Figs. 1B and 3A). In contrast, richly fossiliferous transgressive sand sheets (205-S9 and EM-S4 cores), are characterised by ecological mixing and generally intermediate preservation that deteriorates down-dip (Fig. 4E and H). These characteristics indicate an overall decline in the quality and resolution of the fossil record offshore (~18 km from shoreline). Quantitative estimates of time averaging in the topmost part of the transgressive sand sheet (TrSS) of 205-S9 core indicate substantial (multi-millennial) temporal mixing (~4 ky based on difference between means of dated *Lentidium* and *Corbula* shells; see horizon 6 g in Scarponi et al., 2013). In the distal core (EM-S4), vertically stacked TrSS and a condensed section contain highly degraded skeletal assemblages (Figs. 3C and 5) affected by strong taphonomic feedbacks (Fig. 4G), implying greater deterioration of the fossil record for the distal sector. Preliminary C^{14} -calibrated AAR dating on *Corbula* and *Lentidium* specimens retrieved from the top part of the CS indicates extensive time-averaging spanning at least 8ky (Fig. 3C, Table S3). This estimate is also in good agreement with the radiometrically calibrated chronostratigraphic framework for this profile (~7ky, Amorosi et al., 2017) and previously published radiometric data from a nearby core (Scardovari core in Correggiari et al., 2005 and references therein). In summary, transgressive lagoon/bay and nearshore facies are characterized by relatively high resolution and quality of the macrofossil record, whereas the more distal settings record stronger taphonomic alteration and record higher levels of temporal mixing. In the offshore distal setting, eco-taphonomic trends point to the development of strong taphonomic feedbacks and highest taphonomic degradation (suggestive of both stratigraphic and fossil

condensation). Amino acid racemisation dating indicates that such intense alteration can occur in a relatively short time span, less than 10ky.

5.3. Eco-taphonomic patterns and implication for sequence stratigraphy

The joint consideration of taphonomic, bathymetric, and fossil-density trends across the study cores provides a record of distinctive signatures that are useful in characterizing facies associations and identifying surfaces and intervals of sequence-stratigraphic significance.

Ravinement surface—RS. This ravinement surface, located a few meters above the TS, is associated with a sharp lithologic change within the TST (Figs. 3 and 5) across the study area. RS is commonly highlighted by a cm-thick interval of ecologically mixed taxa that record a bathymetric shift toward deeper settings (Fig. 3). Along the depositional profile, the RS is characterized by variable fossil packing and non-systematic fluctuations in taphonomic degradation. The lack of clear proximal-distal trend could reflect the primary influence of local conditions, such as local scours or inherited topography, that may have influenced the taphonomic signature and fossil packing.

Maximum Flooding Surface—MFS. In the deepest-water facies (shoreface transition) of the proximal core, a nMDS recorded deepening coupled with a peak in taphonomic damage suggest the position of the MFS at ~16.00 m core depth (Fig. 3A). In contrast, the fossil density profile does not show any distinctive signature (Fig. 3A), and the MFS is associated with sparse, fairly preserved macroskeletal remains (Fig. 4A). Conversely, in the distal part, the MFS lies within a ~15 cm thick, increasingly fossiliferous silty interval with highly-degraded remains in the lower part of the ecologically condensed section (26.90–27.05 m in Figs. 3C, 4G and 5). In the proximal and distal cores, the decreasing trend in bathymetric and taphonomic profiles associated with the low density of macrofaunal remains, marks the base of the highstand systems tract, which is represented by a thick, prograding delta front (proximal) to prodelta (intermediate-seaward) succession (Figs. 3 and 5).

Minor transgressive flooding surfaces—In the proximal core, 205-S6, bathymetric and taphonomic profiles fail to indicate any flooding surface other than the RS and MFS. However, at 16.60 m core depth, the sharp contact between fine/medium-grained sands and alternating silts and fine sand layers suggests a landward shift of facies (lower shoreface to shoreface transition) and points to a flooding event (Fig. 3A).

In the intermediate core, 205-S9, a significant bathymetric shift, coincident with a minor spike in fossil density (i.e., 26.15 m core depth Fig. 3B), suggests a flooding surface within the marine TST. However, only in the proximal portion of the depositional profile, the marine sedimentary package sandwiched between the RS and MFS can be subdivided into parasequences based on integrated eco-taphonomic and lithologic signatures. Conversely, in the distal and intermediate sectors, especially within the TrSS, the variability of investigated nMDS bathymetric estimates and a non-systematic variation in taphonomy and fossil density, may reflect stochastic fluctuation in assembling of macrofaunal remains (Fig. 3). This makes it difficult to clearly identify individual flooding surfaces (only a shallowing-upward trend characterizes the uppermost part of the TrSS).

5.4. Closing remarks

The integrated analyses of facies associations, taphonomic data, and their lateral changes along bathymetric profiles, made it

possible to characterize spatio-temporal trends in taphonomic degradation. These trends point to predictable changes in the quality and resolution of the fossil record, both spatially along the local depositional profile, and temporally through the transgressive systems tract: (1) transgressive nearshore deposits preserve a higher proportion of taphonomically pristine, internally simple and arguably less time-averaged skeletal concentrations than their distal counterparts; (2) taphonomic degradation along the investigated profile is inversely related to net sediment accumulation rates and positively related to distance offshore. This indicates that the quality and resolution of the macrofossil record improves proximally along the depositional profile.

These inferences may be applicable not only to the studied area—a siliciclastic, semi-enclosed, shallow basin influenced by a major river, but are likely transferrable to older successions accumulated within comparable depositional contexts. Finally, the quantitative approach applied here offers an independent strategy for testing sequence-stratigraphic interpretations and augmenting core-based sedimentary analyses with quantitative eco-taphonomic proxies.

Acknowledgements

The authors thanks Ronal J. Steel and an anonymous reviewer for constructive criticisms that improved the quality of this research report. The study was supported by ExxonMobil Upstream Research Company and the NSF grant EAR-1559196: “Stratigraphic Paleobiology and Historical Ecology of Po Basin”.

Appendix A. Supplementary data

Supplementary data related to this article can be found at <http://dx.doi.org/10.1016/j.marpetgeo.2017.03.031>.

References

- Abbott, S.T., Naish, T.R., Carter, R.M., Pillans, B.J., 2005. Sequence stratigraphy of the nukumaruan stratotype (Pliocene-Pleistocene, c. 2.08–1.63 Ma), Wanganui Basin, New Zealand. *J. R. Soc. N. Z.* 35 (1–2), 123–150.
- Amorosi, A., Bruno, L., Campo, B., Morelli, A., Rossi, V., Scarponi, D., Hong, W., Bohacs, K.M., Drexler, T.M., 2017. Global sea-level control on local parasequence architecture from the Holocene record of the Po Plain, Italy. *Mar. Pet. Geol.* 1–13.
- Amorosi, A., Colalongo, M.L., Pasini, G., Preti, D., 1999. Sedimentary response to Late Quaternary sea-level changes in the Romagna coastal plain (northern Italy). *Sedimentology* 46 (1), 99–121.
- Amorosi, A., Rossi, V., Scarponi, D., Vaiani, S.C., Ghosh, A., 2014. Biosedimentary record of postglacial coastal dynamics: high-resolution sequence stratigraphy from the northern Tuscan coast (Italy). *Boreas* 43, 939–954.
- Amorosi, A., Maselli, V., Trincardi, F., 2016. Onshore to offshore anatomy of a late Quaternary source-to-sink system (Po Plain-Adriatic Sea, Italy). *Earth-Sci. Rev.* 153, 212–237.
- Aucoin, C.D., Brett, C.E., Dattilo, B.F., Thomka, J.R., 2016. Sequence-stratigraphic model for repeated “butter shale” Lagerstätten in the Ordovician (Katian) of the Cincinnati, Ohio region, USA. *Can. J. Earth Sci.* 53 (8), 763–773.
- Ávila, S.P., Ramalho, R.S., Habermann, J.M., Quartau, R., Kroh, A., Berning, B., Johnson, M., Kirby, M.X., Zanon, V., Titschack, J., Goss, A., da Silva, C.M., Cachão, M., Madeira, J., 2015. Palaeoecology, taphonomy, and preservation of a lower Pliocene shell bed (coquina) from a volcanic oceanic island (Santa Maria Island, Azores). *Palaeogeogr. Palaeoclimatol. Palaeoecol.* 430, 57–73. <https://www.scopus.com/sourceid/13985?origin=recordpage>.
- Ballesteros, E., 2006. Mediterranean Coralligenous assemblages: a synthesis of present knowledge. *Oceanogr. Mar. Biodivers. Annu. Rev.* 44, 125–195.
- Brady, M., 2016. Middle to upper Devonian skeletal concentrations from carbonate-dominated settings of North America: investigating the effects of bioclastic input and burial rates across multiple temporal and spatial scales. *Palaios* 31 (6), 302–318.
- Brett, C.E., 1998. Sequence stratigraphy, paleoecology, and evolution: biotic clues and responses to sea-level fluctuations. *Palaios* 13 (3), 241–262.
- Bruno, L., Amorosi, A., Severi, P., Costagli, B., 2016. Late Quaternary Aggradation Rates and Stratigraphic Architecture of the Southern Po Plain, Italy. Basin Research. <http://dx.doi.org/10.1111/bre.12174>.
- Calabrese, L., Perini, L., Lorito, S., Luciani, P., Martini, A., Severi, P., Correggiari, A., Remia, A., 2016. 3D modelling of the Holocene succession in the southern Po Delta (Italy): from geology to applications. *Ger. J. Geol.* 167 (4), 339–352.

- Campo, B., Vaiani, S.C., Amorosi, A., 2016. Sequence stratigraphy and late Quaternary paleoenvironmental evolution of the Northern Adriatic coastal plain (Italy). *Palaeogeogr. Palaeoclimatol. Palaeoecol.* 466, 265–278.
- Cantalamesa, G., Di Celma, C., Ragaini, L., 2005. Sequence stratigraphy of the Punta Ballena Member of the Jama Formation (Early Pleistocene, Ecuador): insights from integrated sedimentologic, taphonomic and paleoecologic analysis of molluscan shell concentrations. *Palaeogeogr. Palaeoclimatol. Palaeoecol.* 216 (1), 1–25.
- Cattaneo, A., Steel, R.J., 2003. Transgressive deposits: a review of their variability. *Earth Sci. Rev.* 62, 187–228.
- Correggiari, A., Cattaneo, A., Trincardi, F., 2005. Depositional patterns in the Late-Holocene Po delta system. In: Bhattacharya, J.P., Giosan, L. (Eds.), *Concepts, Models and Examples*, vol. 83. SEPM, Special Publication, pp. 365–392.
- Danise, S., Holland, S., 2017. Faunal response to sea-level and climate change in a short-lived seaway: jurassic of the Western Interior, USA. *Palaeontology* 60, 213–232.
- Dominici, S., 2001. Taphonomy and paleoecology of shallow marine macrofossil assemblages in a collisional setting (late Pliocene–early Pleistocene, western Emilia, Italy). *Palaios* 16 (4), 336–353.
- Giannetti, A., Monaco, P., 2015. Definition of sequence through ichnocoenoses and taphofacies: an example from the Sàcaras Formation (early Cretaceous, eastern Spain). *Palaeogeogr. Palaeoclimatol. Palaeoecol.* 438, 70–80.
- Hammer, Ø., Harper, D.A.T., Ryan, P.D., 2001. PAST: paleontological statistics software package for education and data analysis. *Palaeontol. Electron.* 4 (1), 9.
- Holland, S.M., 2000. The quality of the fossil record: a sequence-stratigraphic perspective. *Paleobiology* 26, 148–168.
- Horodyski, R.S., Holz, M., Grahn, Y., Bossetti, E.P., 2014. Remarks on sequence stratigraphy and taphonomy of the malvinokaffric shelly fauna during the KACAK event in the apucarama sub-basin (paraná Basin) Brazil. *Int. J. Earth Sci.* 103, 367–380.
- Huntley, J.W., Scarponi, D., 2012. Evolutionary and ecological implications of trematode parasitism of modern and fossil northern Adriatic bivalvs. *Paleobiology* 38, 40–51.
- Kidwell, S.M., 1985. Palaeobiological and sedimentological implications of fossil concentrations. *Nature* 318 (6045), 457–460.
- Kidwell, S.M., 1986. Models for fossil concentrations: paleobiologic implications. *Paleobiology* 12 (1), 6–24.
- Kidwell, S.M., 1989. Stratigraphic condensation of marine transgressive records: origin of major shell deposits in the Miocene of Maryland. *J. Geol.* 1–24.
- Kidwell, S.M., Bosence, D.W., 1991. Taphonomy and Time-averaging of Marine Shelly Faunas. Taphonomy: Releasing the Data Locked in the Fossil Record. Plenum, New York, pp. 115–209.
- Meldahl, K.H., 1990. Sampling, species abundance, and the stratigraphic signature, of mass extinction: a test using Holocene tidal flat molluscs. *Geology* 18 (9), 890–893.
- Patzkowsky, M.E., Holland, S.M., 2012. *Stratigraphic Paleobiology: Understanding the Distribution of Fossil Taxa in Time and Space*, University of Chicago Press.
- R Core Team, 2016. R: a Language and Environment for Statistical Computing. R Foundation for Statistical Computing, Vienna, Austria. <https://www.R-project.org/>.
- Scarelli, F.M., Barboza, E.G., Cantelli, L., Gabbianelli, G., 2017. Surface and subsurface data integration and geological modelling from the Little Ice Age to the present, in the Ravenna coastal plain, northwest Adriatic Sea (Emilia-Romagna, Italy). *Catena* 151, 1–15.
- Scarponi, D., Angeletti, L., 2008. Integration of palaeontological patterns in the sequence stratigraphy paradigm: A case study from Holocene deposits of the Po Plain (Italy). *Geo Acta* 7, 1–13.
- Scarponi, D., Kowalewski, M., 2004. Stratigraphic paleoecology: bathymetric signatures and sequence overprint of mollusk associations from upper Quaternary sequences of the Po Plain, Italy. *Geology* 32 (11), 989–992.
- Scarponi, D., Kowalewski, M., 2007. Sequence-stratigraphic anatomy of diversity patterns: late Quaternary benthic mollusks of the Po Plain, Italy. *Palaios* 22 (3), 296–305.
- Scarponi, D., Kaufman, D., Amorosi, A., Kowalewski, M., 2013. Sequence stratigraphy and the resolution of the fossil record. *Geology* 41 (2), 239–242.
- Scarponi, D., Huntley, J.W., Capraro, L., Raffi, S., 2014. Stratigraphic paleoecology of the Valle di Manche section (Crotona Basin, Italy): a candidate GSSP of the middle pleistocene. *Palaeogeogr. Palaeoclimatol. Palaeoecol.* 402, 30–43.
- Scarponi, D., Della Bella, G., Dell'Angelo, B., Huntley, J.W., Sosso, M., 2016. Middle Miocene conoidean gastropods from western Ukraine (Paratethys): integrative taxonomy, palaeoclimatological and palaeobiogeographical implications. *Acta Paleontol. Pol.* 61, 327–344.
- Stefani, M., Vincenzi, S., 2005. The interplay of eustasy, climate and human activity in the late Quaternary depositional evolution and sedimentary architecture of the Po Delta system. *Mar. Geol.* 222–223, 19–48.
- Storms, J.E.A., Weltje, G.J., Terra, G.J., Cattaneo, A., Trincardi, F., 2008. Coastal dynamics under conditions of rapid sea-level rise: late Pleistocene to Early Holocene evolution of barrier-lagoon systems on the northern Adriatic shelf (Italy). *Quat. Sci. Rev.* 27 (11), 1107–1123.
- Tomašových, A., Fürsich, F.T., Olszewski, T.D., 2006. Modeling shelliness and alteration in shell beds: variation in hardpart input and burial rates leads to opposing predictions. *Paleobiology* 32 (2), 278–298.
- Wittmer, J.M., Dexter, T.A., Scarponi, D., Amorosi, A., Kowalewski, M., 2014. Quantitative bathymetric models for late Quaternary transgressive-regressive cycles of the Po Plain, Italy. *J. Geol.* 122 (6), 649–670.
- Zecchin, M., Caffau, M., 2011. Key features of mixed carbonate-siliciclastic shallow-marine systems: the case of the Capo Colonna terrace (southern Italy). *Ital. J. Geosci.* 130 (3), 370–379.
- Zecchin, M., Catuneanu, O., 2013. High-resolution sequence stratigraphy of clastic shelves I: units and bounding surfaces. *Mar. Pet. Geol.* 39 (3), 1–25.

Manuscript 1 Online Supplementary Material

“Systematic vertical and lateral changes in quality and time resolution of the macrofossil record: Insights from Holocene transgressive deposits, Po coastal plain, Italy”

Table S1—Summary of present-day mean bathymetric estimates of common species retrieved in our dataset and present also in the ENEA ecological dataset (see <http://www.santateresa.enea.it/wwwste/malaco/home.htm>). The ENEA census is part of a coordinated effort from multiple surveys that catalogued their collections of the Mediterranean molluscs and made them publicly available. The ENEA database includes information on: locality, sampling methods (dredging, immersion, etc.), water depth (m), substrate (sandy, rocky, muddy, etc.), and the number of individuals collected (both live and dead). These data were used to acquire independent quantitative estimates (weighted -by-specimens average) of the preferred water depth for species found in the core material (further details in Wittmer et al., 2014). Rank refers to abundance in the fossil Po Plain dataset.

Rank	Genus	Species	EG (m)
1	<i>Abra</i>	<i>alba</i>	-5.9
2	<i>Acteon</i>	<i>tornatilis</i>	-8
3	<i>Anomia</i>	<i>ephippium</i>	-25
4	<i>Atlantella</i>	<i>distorta</i>	-19.5
5	<i>Bittium</i>	<i>reticulatum</i>	-10.8
7	<i>Cerastoderma</i>	<i>glaucum</i>	-1.3
8	<i>Chamelea</i>	<i>gallina</i>	-7.7
9	<i>Donax</i>	<i>semistriatus</i>	-1.4
10	<i>Dosinia</i>	<i>lupinus</i>	-5.6
11	<i>Ecrobia*</i>	<i>ventrosa</i>	-0.95
13	<i>Fustiaria</i>	<i>rubescens</i>	-15.8
14	<i>Kurtiella</i>	<i>bidentata</i>	-13.1
16	<i>Lentidium</i>	<i>mediterraneum</i>	-2.9
17	<i>Loripinus</i>	<i>fragilis</i>	-15.1
18	<i>Lucinella</i>	<i>divaricata</i>	-14.9
19	<i>Mimachlamys</i>	<i>varia</i>	-14.9
23	<i>Nassarius</i>	<i>pygmaeus</i>	-9.8
28	<i>Nucula</i>	<i>nitidosa</i>	-19.4
29	<i>Papillicardium</i>	<i>papillosum</i>	-16.9
31	<i>Parvicardium</i>	<i>exiguum</i>	-9.7
35	<i>Pitar</i>	<i>rudis</i>	-16.7
47	<i>Spisula</i>	<i>subtruncata</i>	-6.6
58	<i>Timoclea</i>	<i>ovata</i>	-53.2
59	<i>Turritella</i>	<i>communis</i>	-18.3
92	<i>Corbula</i>	<i>gibba</i>	-13.5

Table S2 - Sample - Bathymetric estimates were obtained by regressing nMDS 1 sample scores (column c) against first approximation sample-level bathymetric data (column b) obtained by specimen weighted averaging of a subset of species per sample, with known bathymetric distribution (Table S1). As some samples are dominated by taxa for which EG estimates are not available, their sample depth estimate (column d) could be unreliable. Regressing nMDS1 samples scores against their preliminary bathymetric estimate returned more robust estimates, also congruent with the stratigraphic architecture of the examined succession. Ordinary least squares regression coefficients and tests employed for estimating sample water depth: slope 59.754; intercept = -8.536; $r^2 = 0.75$ $p_{(uncorr.)} = 6.9E-10$; standard error of the estimate = 1.8m.

Core label	Sample depth	nMDS1 sample score	Sample bathymetry	
			preliminary	definitive
E-S4	-26.45	-0.11127	-15.8	-15.2
E-S4	-26.66	-0.11218	-17.5	-15.2
E-S4	-26.71	-0.10178	-14.4	-14.6
E-S4	-26.77	-0.1593	-25.5	-18.1
E-S4	-26.9	-0.20807	-28.9	-21.0
E-S4	-26.96	-0.22719	-25.9	-22.1
E-S4	-26.99	-0.25736	-14.9	-23.9
E-S4	-27.05	-0.2503	-7.7	-23.5
E-S4	-27.15	-0.14933	-23.3	-17.5
E-S4	-27.22	-0.011836	-9.3	-9.2
E-S4	-27.49	-0.030347	-9.4	-10.3
E-S4	-27.79	-0.059577	-10.6	-12.1
E-S4	-28.14	-0.050552	-10.0	-11.6
E-S4	-28.4	-0.042198	-9.2	-11.1
E-S4	-28.61	-0.072426	-11.0	-12.9
S9	-24.4	-0.057832	-13.7	-12.0
S9	-24.9	-0.063887	-14.8	-12.4
S9	-25.4	-0.032914	-14.1	-10.5
S9	-25.9	-0.052786	-13.8	-11.7
S9	-26.4	-0.013184	-10.6	-9.3
S9	-26.9	-0.031693	-12.1	-10.4
S9	-27	-0.026503	-10.6	-10.1
S9	-27.45	0.0093278	-9.1	-8.0
S9	-27.9	-0.0014569	-9.9	-8.6
S9	-28.9	-0.0063341	-7.8	-8.9
S6	-13.2	0.055439	-5.1	-5.2
S6	-14	0.069198	-4.9	-4.4
S6	-14.75	0.036573	-7.6	-6.4
S6	-15.6	0.025202	-6.1	-7.0
S6	-16	-0.026809	-6.7	-10.1
S6	-16.3	-0.0059943	-8.2	-8.9
S6	-17	-0.0082538	-5.7	-9.0
S6	-17.4	-0.017171	-7.2	-9.6
S6	-18	-0.011726	-6.9	-9.2
S6	-18.7	0.048067	-6.1	-5.7
S6	-19	0.11509	-3.2	-1.7

Table S3 - Number, identification code, species name, amino acid racemization values, locality and sample depth along core, estimated ages, covariance screening for each analyzed right valve and mean ages per group of specimens. Age calibration procedure is explained in Scarponi et al. (2013). Abbreviation: Obs—number of analyzed valves per sample; Asp—aspartic acid; Glu—glutamic acid; Asp^x—Asp D/L derived age; Glu^x—Glu D/L derived age; x—the exponent that best linearizes the time versus D/L data; Y25%—specified cut off value between Asp and Glu derived ages, calculated on mean Asp and Glu D/L derived age; Yes—specimen that shows good Asp and Glu derived age covariation, the difference between the two ages is < 250 yr or 25% of its mean derived age.

Obs	Sample tag	Species	DL ratio		Core		Amino acid D/L age (yr)				Y25% (yr)	Y20% (yr)	Yes=retained No=discarded	Group mean age (yr)
			Asp	Glu	label	depth (m)	Asp ^x	Glu ^x	Mean	[Asp ^x -Glu ^x]				
1	12766A	<i>Lentidium</i>	0,311	0,164	EM-S4	26,7	8938	9982	9460	1044	2365	1892	YES	9414
2	12766B		0,283	0,156			8637	9812	9224	1175	2306	1845	YES	
3	12766C		0,322	0,168			9064	10054	9559	990	2390	1912	YES	
4	12767A	<i>Varicorbula</i>	0,197	0,046	EM-S4	26,7	941	953	947	12	237	189	YES	1090
5	12767B		0,212	0,052			1189	1277	1233	89	308	247	YES	

References

Scarponi, D., Kaufman, D., Amorosi, A., Kowalewski, M., 2013. Sequence stratigraphy and the resolution of the fossil record. *Geology*, 41(2), 239-242.

Wittmer, J. M., Dexter, T. A., Scarponi, D., Amorosi, A., Kowalewski, M., 2014. Quantitative bathymetric models for late Quaternary transgressive-regressive cycles of the Po Plain, Italy. *The Journal of Geology*, 122(6), 649-670.

Chapter **6**

Manuscript II

6. Manuscript II

“Surges in trematode prevalence linked to centennial-scale flooding events in the Adriatic”

Authors: Daniele Scarponi ^a, Michele Azzarone ^a, Michal Kowalewski ^b and John Warren Huntley ^c

^a Dipartimento di Scienze Biologiche, Geologiche e Ambientali, University of Bologna, Via Zamboni 67, 40126 Bologna, Italy

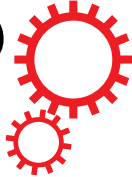
^b Florida Museum of Natural History, University of Florida, 1659 Museum Road, Gainesville, FL 32611, USA

^c Department of Geological Sciences, University of Missouri, 101 Geology Building, Columbia, MO, 65211, USA

Status: Published in *Scientific Reports*, volume 7, July 2017

doi: doi.org/10.1038/s41598-017-05979-6

SCIENTIFIC REPORTS



OPEN

Surges in trematode prevalence linked to centennial-scale flooding events in the Adriatic

Daniele Scarponi¹, Michele Azzarone¹, Michał Kowalewski² & John Warren Huntley³

The forecasts of increasing global temperature and sea level rise have led to concern about the response of parasites to anthropogenic climate change. Whereas ecological studies of parasite response to environmental shifts are necessarily limited to short time scales, the fossil record can potentially provide a quantitative archive of long-term ecological responses to past climate transitions. Here, we document multi-centennial scale changes in prevalence of trematodes infesting the bivalve host *Abra segmentum* through multiple sea-level fluctuations preserved in brackish Holocene deposits of the Po Plain, Italy. Prevalence values were significantly elevated ($p < 0.01$) in samples associated with flooding surfaces, yet the temporal trends of parasite prevalence and host shell length, cannot be explained by Waltherian facies change, host availability, salinity, diversity, turnover, or community structure. The observed surges in parasite prevalence during past flooding events indicate that the ongoing global warming and sea-level rise will lead to significant intensification of trematode parasitism, suppressed fecundity of common benthic organisms, and negative impacts on marine ecosystems, ecosystem services, and, eventually, to human well-being.

Understanding the historical impact of climate variability on heterocious parasites is prerequisite for forecasting parasite-host interactions in the near future and assessing the potential implications for ecosystem health, ecosystem services, and human well-being^{1–6}. However, ecological research on the response of parasites to anthropogenic warming is necessarily limited to short time scales of the most recent months and years^{7,8}. In this respect, the most promising avenue is offered by the latest Quaternary fossil record where, thanks to highly-resolved sequence and chrono-stratigraphic frameworks^{9–16}, past parasite-host interactions can be examined over geologically short (10^2 – 10^3 years), societally relevant time scales.

Digenean trematodes typically display a complex lifecycle with three hosts. The first intermediate host, where the parasite performs asexual reproduction of larvae (cercariae), is always a mollusk species. The newly emerged cercariae larvae infest the second intermediate host where the parasite is in an encysted, latent stage (metacercaria), waiting to be ingested by the third, definitive host, which is always a vertebrate organism that enables sexual reproduction of the adult parasite. A peculiarity of many trematode species, within the family Gymnophallidae, is that they have the same first and second intermediate individual hosts, skipping the intermediary, free-living cercariae stage¹⁵. It is usually in the second intermediate host stage that digeneans affect shell secretion in their molluscan hosts. Gymnophallids induce the active growth of characteristic pits with raised rims on the interior of their bivalve host's shells (Fig. 1)^{17–19} and schistosomatids and echinostomatids may alter the geochemical composition of their host's shells^{20,21}. Gymnophallid-induced pits are known from live-collected bivalve hosts and are readily preserved in the fossil record, providing a proxy for infestation by microscopic, non-biomineralized parasites²².

Previous quantitative analysis of a 9.6 ky record of Holocene estuarine deposits of the Pearl River²³ demonstrated that trematode prevalence peaked in the lower part of paralic transgressive deposits recording the generalized inundation of the regional coastal system coincident with Meltwater Pulse 1c, that took place between 9.5 and 9.2 ky²⁴. Similarly, significantly higher trematode prevalence was documented in host taxa from sediment-starved northern Adriatic strandline death assemblages, relative to that documented from comparable assemblages from the Po delta shoreline²⁵. These two coastal regimes serve respectively as modern analogues for

¹Dipartimento di Scienze Biologiche, Geologiche e Ambientali, University of Bologna, via Selmi 3, Bologna, I-40126, Italy. ²Florida Museum of Natural History, University of Florida, 1659 Museum Rd., Gainesville, FL, 32611, USA.

³Department of Geological Sciences, University of Missouri, 101 Geology Building, Columbia, MO, 65211, USA. Correspondence and requests for materials should be addressed to J.W.H. (email: huntleyj@missouri.edu)

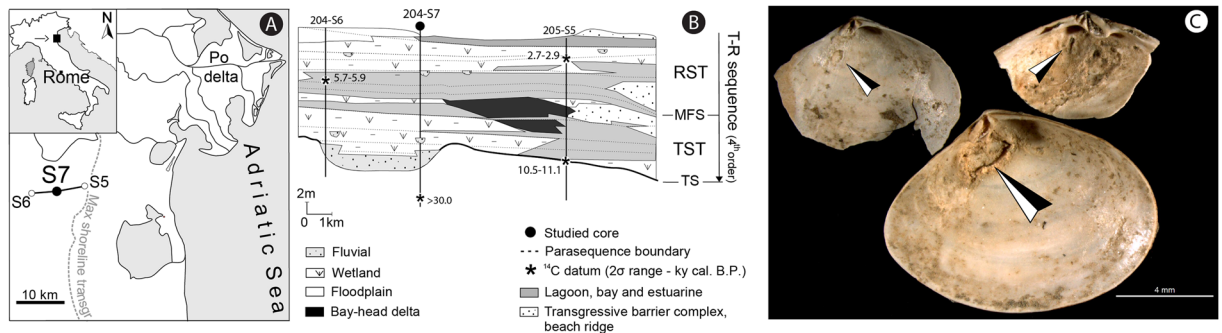


Figure 1. Location map, cross-section, and images of parasitized *Abra segmentum* valves. (A) Location map of investigated Po coastal plain sector, Italy (B) Schematic cross section (along dip) illustrating the stratigraphic stacking of facies across the investigated portion of the Holocene post-Last Glacial Maximum T-R sequence and location of the 204-S7 core. (C) Photomicrographs of *A. segmentum* with trematode-induced pits (black/white arrows). TS: transgressive surface, TST: transgressive systems tract, MFS: maximum flooding surface, RST: regressive systems tract, T-R: transgressive-regressive.

Holocene transgressive and prograding settings²⁶. This putative link between overall sea-level rise and prevalence, if demonstrated on societally relevant time scales, could serve as an analogue for the response of parasitism to global warming in the coming decades to centuries. Here we explicitly test the link between short term (10^2 – 10^3 years) flooding pulses and upsurges in parasite prevalence using the fossil record of bivalve hosts from a cored Holocene back-barrier succession (Fig. 1; Po coastal plain, Italy). Additionally, we test for correlative relationships between parasite prevalence and other environmental and ecological factors to identify or rule out driving factors of this pattern.

Coastal Po Plain Succession. The post-Last Glacial Maximum (post-LGM) transgressive-regressive sequence of the coastal Po Plain is a wedge-shaped genetically related package of latest Pleistocene-to-Holocene strata. In the studied core 204-S7, the T-R sequence is a few tens of meters thick (Fig. 1), with its base defined by the transgressive surface resting on top of a weakly developed, Younger Dryas age paleosol (Online Methods). Several higher-order depositional cycles (parasequences), defined by their characteristic bounding surfaces, internal stacking patterns, and geometric relations to surrounding strata, characterize the internal structure of the post-LGM sequence (Fig. 1)²⁷. These parasequences record high-frequency shifts in the local sea-level^{28,29} and a high-resolution chronostratigraphic framework indicates that they formed on millennial (and shorter) time scales (Online Methods). The strata in core 204-S7, from bottom to top, are composed of stacked fluvial channel facies associations (>9 ky; parasequence 1 in ref. 27), passing upwards into poorly-drained floodplain/wetland facies alternations, overlain by brackish (lagoon/estuary) and thinning upward swamp facies associations (parasequences 2-4; Figs 1A,B and 2B, Extended Data Fig. 1). The subsequent middle-to-late Holocene (parasequences 5-7; Fig. 2) record a mosaic of floodplain and wetland deposits (lower delta plain; <6 ky), which are overlain by parasequence 8 that details renewed brackish settings related to the most recent shift of the Po delta toward its present position²⁷.

Results

We collected 61 bulk samples from the top 20 meters of core 204-S7 (Fig. 2A; Online Methods). Forty-five out of 61 samples contained mollusk fossils (Extended Data Fig. 1), resulting in a matrix of 3,151 individuals from 26 genera and 31 species (Online Methods; Extended Data Table S1). A non-metric Multidimensional Scaling (nMDS) ordination displays a pronounced gradient with species distributed along the nMDS1 axis according to their salinity tolerance (Online Methods; Extended Table S2). These results were robust to a variety of filters and other ordination types (see Online Methods; Extended Data Figs 3 and 4; Table S3). The resulting nMDS1 sample scores positively correlate with preferred salinity values for extant taxa in modern ecosystems (see Extended Data Fig. 3 for taxon salinity data; Tables S3 and S4), and are, therefore, a proxy for salinity (Online Methods), a common ecological driver in back barrier settings³⁰.

The temporal trend of nMDS1 sample scores displays multiple orders of cyclicity. At the overall scale of the sedimentary package (Fig. 2B), the scores support the control of glacio-eustatic forcing on the development of the post-LGM sequence. Specifically, samples from parasequence one to four record the landward increasing influence of the Adriatic sea, while from parasequence four onward, the general trend toward lower salinity values is consistent with Po deltaic progradation into the Adriatic Sea (Figs 1B and 2A,B). At a higher resolution, the stratigraphic trajectory of nMDS1 sample scores highlights five flooding pulses depicted by major increases in salinity (in accordance with parasequence bounding surfaces of ref. 27), followed by a gradual return to reduced salinities (Fig. 2B). These abrupt and major salinity shifts are interpreted to represent non-Waltherian facies dislocations, with the overlying facies recording increased marine influence rather than a simple lateral shift to an adjacent environment relative to the underlying facies. The three salinity shifts recognized at 15.5, 12.3, and 1.1 m core depth (Fig. 2A) represent parasequence bounding surfaces developed over millennial time scales, whereas the remaining two are interpreted as higher frequency, centennial-scale pulses²⁷ representing short-lived, rapid transition from mesohaline to polyhaline dominated environments (Fig. 2B). Accordingly, parasequence 4, which

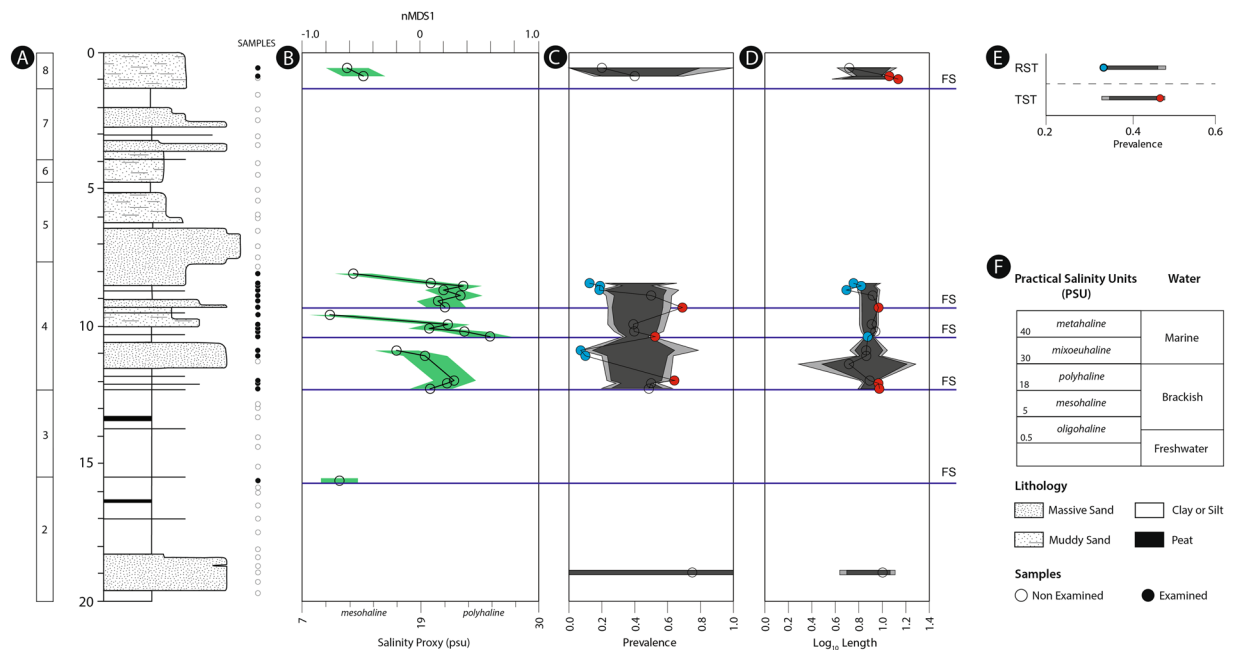


Figure 2. Detailed architectural, stratigraphic and bio-sedimentary (nMDS, *A. segmentum* trematode prevalence and shell length) features of core 204-S7. **(A)** Detailed stratigraphic column with 8 small-scale (millennial-scale sedimentary packages—parasequences defined in ref. 27 and the position of the studied samples: hollow circles represent samples with fewer than 15 specimens. **(B)** nMDS derived salinity trends along core highlighting back-barrier small-scale sedimentary packages and their internal architecture. Green field represents Standard Error of the Estimate (SEE) resulting from the RMA regression (see Extended Data Fig. S5) of nMDS derived salinity trends. **(C)** Prevalence of trematode pits among single samples recording more than 4 valves of *Abra segmentum*. **(D)** Mean log₁₀-transformed anterior-posterior length of single samples of *A. segmentum*. **(E)** Prevalence values of data pooled by TST and RST (defined by nMDS derived trend along core). **(F)** Reference scale for Practical Salinity Units (PSU) with associated type of water and legend for lithology and samples. Dark and light grey fields on panels C, D, and E represent 95% and 99% confidence intervals (CI) derived from 10,000 iteration randomizations, respectively. Red circles indicate values greater than 95% CI, blue circles indicate values less than 95% CI, and hollow circles (in panels C and D) indicate values that fall within 95% CI. FS indicates back barrier correlative of flooding surfaces; nMDS: non Metric Multidimensional Scaling.

marks the turnaround from retrogradation to progradation (Fig. 2B), consists of a set of three higher frequency (centennial scale) units bounded by stratigraphically significant (i.e., non-Waltherian) shifts of facies (Fig. 2B).

The thin-valved *Abra segmentum*—a genus which is parasitized by *Parvatrema rebecqui* in modern environments³¹—is the dominant species in core 204-S7 and displays a high prevalence of trematode-induced pits (34.4%; 348 infested of the total 1,012 valves). Anterior-posterior length of *A. segmentum* ranged between 1.5 and 22.3 mm (Extended Data Fig. 6). Single sample prevalence values range from 7.1% to 75.0% and display significant temporal variation (Fig. 2; Extended Data Table S4). At the systems tract level (i.e., a multi-millennial observational scale), there was a significant (i.e., outside the 95% confidence bounds estimated via randomization) difference in trematode prevalence values between the TST (44.9%) and RST (34.2%; Fig. 2E), consistent with previous findings^{23,26}. At the parasequence level, significantly elevated prevalence estimates are located in proximity to the millennial-scale flooding surface at 12.3 m and the centennial-scale flooding surfaces at 9.3 and 10.3 m (Fig. 2A,B). Significantly depressed prevalence estimates all occurred within these small-scale units (Fig. 2C).

Discussion

The results demonstrate a repeated association between significantly elevated prevalence and centennial scale flooding events, support the link between sea-level rise and increasing trematode activity, and can serve as historical analogues for ongoing and future anthropogenic climate change. Despite evidence for the consistent relationship between transgression and trematode prevalence, it is doubtful that a relative rise in sea level alone drove this pattern. Many factors that can influence the biota, including temperature, nutrient availability, salinity, host availability, diversity, and community structure, co-vary with sea level changes and should be tested as driving factors^{32,33}. Increasing temperature has been shown to increase reproductive output and infectivity of a diverse array of pathogens and parasites^{3,4} (but see refs 7, 8 and 34). As parasites derive nutrition from their hosts, it is not clear that changes in nutrient availability/productivity would directly control their distribution, however biological diversity is often related to productivity and its mode of delivery across a variety of scales and systems^{35,36}. Diversity and productivity often increase in concert until a tipping point above which diversity begins to decline, varying with the influence of consumers and disturbance level³⁷. In this way productivity could control the distribution and abundance of many taxa that might serve as intermediate or definitive hosts, though likely

	Arcsine Prevalence	nMDS1
<i>A. segmentum</i> abundance	ns	$R = +0.73, p = 0.001$
Mean shell length	$R = +0.68, p = 0.004$	ns
Standardized Richness (n = 15)	ns	$R = +0.81, p = 0.0001$
Dominance	ns	$R = -0.76, p = 0.0007$
Shannon (H)	ns	$R = +0.78, p = 0.0004$
Too fragmented to be certain	ns	$R = -0.76, p = 0.0007$
Salinity	ns	$R = +0.76, p = 0.0006$
nMDS1	ns	—
nMDS2	ns	ns

Table 1. Spearman rank correlation coefficients and p -values (when $p < \alpha = 0.05$; otherwise indicated as ns: non-significant) between arcsine-transformed trematode prevalence values of *Abra segmentum* from the 204-S7 core; nMDS1 sample scores; and environmental, ecological, and taphonomic variables. nMDS1: Non metric Multidimensional Scaling axis 1.

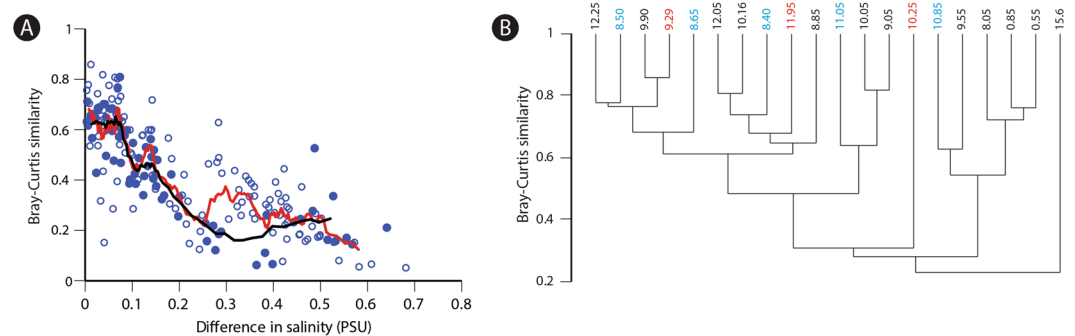


Figure 3. Turnover and ecological similarity of assemblages across core 204-S7. **(A)** Turnover estimated by pairwise comparison of Bray-Curtis similarity indices and environmental distance (nMDS1 salinity). Solid circles indicate pairwise comparisons between lagoonal muddy samples from core depths of 8.50–12.25 meters and the black line indicates the ten point running average. Hollow circles indicate all other comparisons. The red line indicates the ten point running average for all comparisons. **(B)** Q-mode cluster analysis (UPGMA algorithm, Bray-Curtis similarity). Samples with trematode prevalence values of *Abra segmentum* greater than and less than the 95% CI are indicated in red and blue, respectively. Note how the samples of either exceptionally low or high prevalence values are randomly distributed across the dendrogram.

in a non-linear manner. Salinity is a primary environmental driver of mollusk turnover in the studied system (Fig. 2B), and free-swimming larval (cercaria) production and survival time tend to decrease significantly in lowered salinity regimes in paralic environments; thereby reducing infestation of intermediate and/or definitive hosts^{38,39}. Here, however, as in ref. 23, the lack of correlation between salinity proxy and prevalence estimates (Table 1) suggests that salinity is not a strong driving factor of trematode prevalence at this spatial and temporal scale of observation.

The absence of correlation between preferred host (*A. segmentum*) abundance and prevalence (Table 1) rules out fluctuating host availability as a limiting factor of trematode distribution²³. The median shell length of infested valves of *A. segmentum* was significantly larger than that of their non-infested counterparts (Mann-Whitney U , $p = 2.21E-34$), likely due to the accumulation of parasites through ontogeny. Prevalence values were positively and significantly correlated with host shell length ($r = +0.68, p = 0.004$), however there were no significant associations between shell length and either flooding pulses or nMDS1 scores (Fig. 2C and Table 1). This suggests that other environmental or ecological factors, acting as drivers of host shell length, were unlikely to have indirectly driven the temporal trend of trematode prevalence. Similarly, the lack of correlative relationships between prevalence and standardized richness, dominance, and Shannon diversity (Table 1) suggests that fluctuating biodiversity did not exhibit direct/linear control over trematode-bivalve interactions.

The role of more complex, community-level factors that may have influenced the distribution of trematode parasites can be examined by evaluating the distribution of samples and their constituent taxa in the nMDS space and assessing faunal similarity using Bray-Curtis pairwise comparisons to measure faunal turnover throughout the length of the core (Fig. 3A). Samples retrieved from brackish muds only (8.50–12.25 m core depth) display a comparable amount of turnover to that identified when comparing samples from both freshwater and brackish environments. However, the dendrogram derived from the Q-mode cluster analysis of the samples included in the nMDS ordination demonstrates that samples recording elevated or subdued trematode prevalence were distributed haphazardly across the dendrogram topology. Consequently, community structure/turnover (Fig. 3B) is unlikely to have been a driving factor of trematode prevalence within Holocene lagoonal facies.

Sample nMDS1 scores were negatively correlated with the proportion of *Abra* valves that were too fragmented to evaluate in terms of infestation status. This pattern raises the question of how fragmentation might have influenced the parasite record (i.e., were valves with trematode pits more prone to fragmentation than non-infested valves?). All *Abra* valves were classified as either whole or broken, and the broken valves were further categorized into either “sufficiently complete” or “too fragmented” to determine infestation status. There was no significant difference in trematode prevalence values of whole and “sufficiently complete” broken valves (X^2 , $p = 0.16$). These results suggest that the proportion of “too fragmented” valves was unlikely to represent an important confounding factor in reconstructing the stratigraphic record of trematode dynamics.

Another potential factor affecting parasite prevalence is the fluctuating availability of habitat-area for trematodes during sea-level cycles. The geologically rapid creation of new habitat during flooding pulses and their subsequent destruction during progradation could exert a first order control on trematode prevalence during high frequency cycles. As sea level continues to rise, some settings will be more strongly influenced than others. For instance, densely populated lowlands, estuarine, and riverine settings would likely display the greatest increase in trematode habitat-area during relative sea level rise as a direct effect of flooding and, indirectly, by the landward rise of the groundwater table⁴⁰. Therefore, we hypothesize that gymnophallid trematode prevalence will be more strongly influenced by the creation of new habitat in brackish and freshwater settings than in shallow marine settings. Though not the direct topic of research here, an increase in wetlands created by sea level rise would generate new habitat for the gastropod intermediate hosts of *Schistosoma*⁴¹, the trematodes responsible for schistosomiasis in humans.

The fossil record of the northern Adriatic points to a significant association between the prevalence of heterocercous parasites and flooding events recording repeated climate-driven sea level shifts. From this historical perspective we posit that the ongoing anthropogenic warming and sea-level rise should trigger a significant upsurge in gymnophallid trematode prevalence and the expansion of wetland habitats ideal for schistosomatid intermediate hosts. The forecasted changes are expected to suppress the fecundity of common benthic organisms, exert negative impacts on ecosystems, impede ecosystem services, and, eventually, negatively affect human well-being.

References

- Ewing, D. A., Cobbold, C. A., Purse, B. V., Nunn, M. A. & White, S. M. Modelling the effect of temperature on the seasonal population dynamics of temperate mosquitoes. *Journal of Theoretical Biology* **400**, 65–79 (2016).
- Altizer, S., Ostfeld, R. S., Johnson, P. T. J., Kutz, S. & Harvell, C. D. Climate change and infectious diseases: From evidence to a predictive framework. *Science* **341**, 514–519 (2013).
- Poulin, R. Global warming and temperature-mediated increases in cercarial emergence in trematode parasites. *Parasitology* **132**, 143–151 (2006).
- Harvell, C. D. *et al.* Climate warming and disease risks for terrestrial and marine biota. *Science* **296**, 2158–2162 (2002).
- Stephens, P. R. The macroecology of infectious diseases: A new perspective on global-scale drivers of pathogen distributions and impacts. *Ecology Letters* **19**, 1159–1171 (2016).
- Paull, S. H. & Johnson, P. T. J. High temperature enhances host pathology in a snail–trematode system: Possible consequences of climate change for the emergence of disease. *Freshwater Biology* **56**, 767–778 (2011).
- de Montaudouin, X., Blanchet, H., Desclaux-Marchand, C., Lavesque, N. & Bachelet, G. Cockle infection by *Himasthla quissetensis* – I. From cercariae emergence to metacercariae infection. *Journal of Sea Research* **113**, 99–107 (2016).
- de Montaudouin, X. *et al.* Cockle infection by *Himasthla quissetensis* – II. The theoretical effects of climate change. *Journal of Sea Research* **113**, 108–114 (2016).
- Pandolfi, J. M. & Jackson, J. B. C. Ecological persistence interrupted in Caribbean coral reefs. *Ecology Letters* **9**, 818–826 (2006).
- Kidwell, S. M. & Tomašových, A. Implications of time-averaged death assemblages for ecology and conservation biology. *Annu. Rev. Ecol. Syst.* **44**, 539–563 (2013).
- Dietl, G. P. *et al.* Conservation paleobiology: Leveraging knowledge of the past to inform conservation and restoration. *Annu. Rev. Earth Planet Sci.* **43**, 79–103 (2015).
- Kowalewski, M., Wittmer, J. M., Dexter, T. A., Amorosi, A. & Scarponi, D. Differential responses of marine communities to natural and anthropogenic changes. *Proc. R. Soc. B.* **282**(1803) (2015).
- Kosnik, M. A. & Kowalewski, M. Understanding modern extinctions in marine ecosystems: The role of palaeoecological data. *Biol. Lett.* **12**(4), 20150951, doi:10.1098/rsbl.2015.0951 (2016).
- Scarponi, D., Kaufman, D., Amorosi, A. & Kowalewski, M. Sequence stratigraphy and the resolution of the fossil record. *Geology* **41**(2), 239–242 (2013).
- Scarponi, D., Huntley, J. W., Capraro, L. & Raffi, S. Stratigraphic paleoecology of the S. Mauro Marchesato Section (Crotone Basin, Italy): a candidate GSSP of the Middle Pleistocene. *Palaeogeography, Palaeoclimatology, Palaeoecology* **402**, 30–43 (2014).
- Tanabe, S., Nakanishi, T., Ishihara, Y. & Nakashima, R. Millennial-scale stratigraphy of a tide-dominated incised valley during the last 14 kyr: Spatial and quantitative reconstruction in the Tokyo Lowland, central Japan. *Sedimentology* **62**(7), 1837–1872 (2015).
- Littlewood, D. T. J. The evolution of parasitism in flatworms. In: (Eds) Maule, A. G. & Marks, N. J., *Parasitic Flatworms: Molecular Biology, Biochemistry, Immunology and Physiology* (2006).
- Bartoli, P. La Pénétration et l’installation des cercariae de *Gymnophallus fossarum* P. Bartoli, 1965 (Digenea, Gymnophallidae) chez *Cardium glaucum* Bruguière. *Bulletin du Museum National d’Histoire Naturelle, Zoologie* **117**, 319–334 (1973).
- Huntley, J. W. & De Baets, K. Trace fossil evidence of trematode-bivalve parasite-host interactions in deep time. *Advances in Parasitology* **90**, 201–231 (2015).
- Ong, J. H. L. *et al.* Effects of *Schistosoma mansoni* infection on inorganic elements in the snail *Biomphalaria glabrata*. *Journal of Helminthology* **78**, 343–346 (2004).
- White, M. M., Chejlava, M., Fried, B. & Sherma, J. Effects of various larval digeneans on the calcium carbonate content of the shells of *Helisoma trivolvis*, *Biomphalaria glabrata*, and *Physa* sp. *Parasitology Research* **95**, 252–255 (2005).
- De Baets, K., Dentzian-Dias, P. C., Upeniece, I., Verneau, O. & Donoghue, P. C. J. Constraining the deep origin of parasitic flatworms and host-interactions with fossil evidence. *Advances in Parasitology* **90**, 93–135 (2015).
- Huntley, J. W., Fürsich, F. T., Alberti, M., Hethke, M. & Liu, C. A complete Holocene record of trematode-bivalve infection and implications for the response of parasitism to climate change. *Proc. Natl. Acad. Sci. USA* **111**, 18150–18155 (2014).
- Zong, Y., Yim, W. S., Yu, F. & Huang, G. Late Quaternary environmental changes in the Pearl River mouth region, China. *Quaternary International* **206**(1), 35–45 (2009).
- Huntley, J. W. & Scarponi, D. Geographic variation of parasitic and predatory traces on mollusks in the northern Adriatic Sea, Italy: Implications for the stratigraphic paleobiology of biotic interactions. *Paleobiology* **41**, 134–153 (2015).

26. Huntley, J. W. & Scarponi, D. Evolutionary and ecological implications of trematode parasitism of modern and fossil northern Adriatic bivalves. *Paleobiology* **38**, 40–51 (2012).
27. Amorosi, A. *et al.* Global sea-level control on local parasequence architecture from the Holocene record of the Po Plain, Italy. *Marine and Petroleum Geology*, In Press (2017).
28. Wittmer, J. M., Dexter, T. A., Scarponi, D., Amorosi, A. & Kowalewski, M. Quantitative bathymetric models for late Quaternary transgressive-regressive cycles of the Po Plain, Italy. *The Journal of Geology* **122**(6), 649–670 (2014).
29. Scarponi, D. *et al.* Systematic vertical and lateral changes in quality and time resolution of the microfossil record: Insights from Holocene transgressive deposits, Po coastal plain, Italy. *Marine and Petroleum Geology* In Press (2017).
30. Amorosi, A., Rossi, V., Scarponi, D., Vaiani, S. C. & Ghosh, A. Biosedimentary record of postglacial coastal dynamics: high-resolution sequence stratigraphy from the northern Tuscan coast (Italy). *Boreas* **43**, 939–954 (2014).
31. Bartoli, P. & Gibson, D. I. Synopsis of the life cycles of Digenea (Platyhelminthes) from lagoons of the northern coast of the western Mediterranean. *Journal of Natural History* **41**, 25–28 (2007).
32. Patzkowsky, M. E. & Holland, S. M. Stratigraphic paleobiology: Understanding the distribution of fossil taxa in time and space. *University of Chicago Press* (2012).
33. Marcogliese, D. J. The distribution and abundance of parasites in aquatic ecosystems in a changing climate: More than just temperature. *Integrative and Comparative Biology*, 1–9, doi:10.1093/icb/icw036 (2016).
34. Lafferty, K. D. The ecology of climate change and infectious diseases. *Ecology* **90**, 888–900 (2009).
35. Bambach, R. K. Seafood through time: changes in biomass, energetics, and productivity in the marine ecosystem. *Paleobiology* **19**, 372–397 (1993).
36. Diaz, R. J. & Rosenberg, R. Spreading dead zones and consequences for marine ecosystems. *Science* **321**(5891), 926–929 (2008).
37. Worm, B., Lotze, H. K., Hillebrand, H. & Sommer, U. Consumer versus resource control of species diversity and ecosystem functioning. *Nature* **417**, 848–851 (2001).
38. Studer, A. & Poulin, R. Effects of salinity on an intertidal host–parasite system: Is the parasite more sensitive than its host? *Journal of Experimental Marine Biology and Ecology* **412**, 110–116 (2012).
39. Lei, F. & Poulin, R. Effects of salinity on multiplication and transmission of an intertidal trematode parasite. *Marine Biology* **158**, 995–1003 (2011).
40. Rotzoll, K. & Fletcher, C. H. Assessment of groundwater inundation as a consequence of sea-level rise. *Nature Climate Change* **3**, 477–481 (2013).
41. McManus, D. P. *et al.* Schistosomiasis in the People's Republic of China: The era of the Three Gorges Dam. *Clinical Microbiology Reviews* **23**, 442–466 (2010).

Acknowledgements

This work was supported by NSF awards EAR-1650745 (JWH) and EAR-1559196 (MK and DS), the Institute of Advanced Studies at the University of Bologna (JWH), the University of Missouri Research Council Faculty International Travel Award (JWH), the Unklesbay Fund of the Department of Geological Sciences at the University of Missouri (JWH), and RFO 2015, University of Bologna, Italy (DS). We thank Prof. Alessandro Amorosi (University of Bologna) for helpful discussion.

Author Contributions

D.S. and J.W.H. conceived the project; M.A., D.S., M.K., and J.W.H. collected and analyzed the data and produced the figures; M.A., D.S., M.K., and J.W.H. wrote the paper. All authors reviewed the manuscript.

Additional Information

Supplementary information accompanies this paper at doi:10.1038/s41598-017-05979-6

Competing Interests: The authors declare that they have no competing interests.

Publisher's note: Springer Nature remains neutral with regard to jurisdictional claims in published maps and institutional affiliations.



Open Access This article is licensed under a Creative Commons Attribution 4.0 International License, which permits use, sharing, adaptation, distribution and reproduction in any medium or format, as long as you give appropriate credit to the original author(s) and the source, provide a link to the Creative Commons license, and indicate if changes were made. The images or other third party material in this article are included in the article's Creative Commons license, unless indicated otherwise in a credit line to the material. If material is not included in the article's Creative Commons license and your intended use is not permitted by statutory regulation or exceeds the permitted use, you will need to obtain permission directly from the copyright holder. To view a copy of this license, visit <http://creativecommons.org/licenses/by/4.0/>.

© The Author(s) 2017

Manuscript 2 Online Supplementary Material

“Surges in trematode prevalence linked to centennial-scale flooding events in the Adriatic”

Methods

Sixty-one 10cm-thick bulk samples were collected on average every 22 cm from the top 20 meters of core 204-S7 (Fig. 2A), dried at 45°C, soaked in ~4% H₂O₂, and washed through a 1mm sieve (Scarponi and Angeletti, 2008). A total of 45 out of 61 samples contained mollusk fossils (Extended Data Fig. S1). For each of the fossiliferous samples, all complete or unique individual specimens (i.e., bivalve umbo/gastropod apex) were identified to the species level (when possible). The resulting taxon abundance matrix included 3,151 individuals from 26 genera and 31 species (Extended Data Table S1). Of the total matrix abundance 50% (i.e., 1012 out of 2022 valves) were represented by the brackish, deposit-feeding and infaunal bivalve *Abra segmentum* (Récluz, 1843). All *A. segmentum* valves were examined with an Askania stereo microscope (at 63x magnification) for the presence of oval- to irregular-shaped pits with raised rims (Fig. 1C), which are indicative of trematode infestation (Ruiz and Lindberg, 1989). Each valve was classified as parasitized, non-parasitized, or too fragmented to be certain. Prevalence was calculated as the number of parasitized valves divided by the total number of valves in a sample. Anterior-posterior length (APL) was measured for all whole valves. For all fragmented valves, APL was estimated based on chondrophore length by reduced major axis regression (RMA). A set of 23 right and 19 left complete valves (Extended Data Fig. S2) was used to relate chondrophore length to APL.

Multivariate ordinations were performed to explore the relationships between faunal composition and environmental gradients. Detrended Correspondence Analyses and non-metric Multidimensional Scaling (nMDS) ordinations returned comparable patterns while varying the taxon and sample thresholds; Extended Data Figs S3A-B; S4). Here we report the results of nMDS in 2-dimensions based on Bray-Curtis distances (metaMDS function; “vegan” package in R) with singleton taxa, monospecific samples, and samples with fewer than 15 specimens excluded from analysis. In the case of bivalves, each valve or unique fragment was counted as a 0.5 specimen (Kowalewski and Bambach, 2000). The final matrix for the nMDS ordination was composed of 20 samples, 17 species, and 2023 specimens (median sample size 75 specimens). Only nMDS axis 1 sample scores, obtained from a log-transformed matrix of specimen raw counts (which consider both shape and size of the count vectors), are reported here (Fig. 2; see Extended Data Fig. S4A-F for more detailed results).

An independent sample-level salinity proxy was calculated via the weighted average of a sub-set of taxa for which optimum salinity values were known (Extended Data Table S2). An RMA regression model between sample-level salinity estimates and nMDS1 scores was calculated so that a salinity proxy could be estimated for samples that were comprised of less than 30% of specimens from taxa for which optimum salinity values were known (Extended Data Table S3; Extended Data Fig. S5).

The extent of faunal turnover among samples along the core was assessed by the pairwise comparison of Bray-Curtis similarity values between samples and salinity estimates used as a proxy of “environmental distance” (Anderson et al., 2011). A Q-mode cluster analysis with paired-group UPGMA algorithm and Bray-Curtis similarity measure was applied to the data matrix utilized in the nMDS to determine the relationship between community structure and trematode prevalence. Finally, Spearman rank correlation analyses were carried out to test for potential interdependence between prevalence estimates and environmental and bio-ecological estimators (nMDS1 scores, shell length, indices of diversity and fragmentation). Randomizations (10,000 iterations each) were conducted for prevalence and shell length estimates to assess the range of values (95% and 99% confidence intervals) expected under the null model of no change through time. The analyses were carried out in R (R Development Core, 2016), PAST v.2.17c (Hammer et al., 2001), and SAS v.9.3 (Der and Everit, 2015).

Sequence Stratigraphic Framework Of The Latest Quaternary Po Plain Succession

The latest Quaternary (<30ky) succession of the Po Plain is a few tens of meters thick and extensive subsurface investigations conducted during the last decades have led to a detailed reconstruction of its stratigraphic architecture (e.g., Amorosi et al., 2005; Scarponi and Angeletti, 2008; Amorosi et al., 2014; Scarponi et al., submitted). This genetically related, wedge-shaped package of strata represents the Last Glacial Maximum (LGM) depositional sequence. The laterally extensive fluvial-channel and associated floodplain deposits of the lower part of the succession are interpreted to record progradation and aggradation during the LGM and early sea-level rise (30-14ky). LGM deposit are overlaid by a few meters of rapidly retrogradational stack of nearshore (barrier-lagoon-estuary system) to shallow marine fossil rich mudstones, in part filling the coastal accommodation created during rapid sea-level rise (14-7ky). Ensuing aggradation followed by progradation into the Adriatic Basin represents a distinctive stacking pattern generated by increasingly strong riverine sedimentation enhanced by the middle-late Holocene deceleration of sea-level rise (>6ky). Hence, in distal locations, the coastal accommodation created by the synergistic influence of eustasy, compaction, and subsidence during the early to middle Holocene was filled by a tract of shallowing upward marine and progradational deltaic facies. Whereas, in proximal locations, i.e. the targeted area of this study, the stratigraphic architecture of the LGM depositional sequence is dominated by aggradational alluvial and upper coastal plain facies associations, passing upwards into retrogradational muddy coastal plain to brackish deposits followed by a complex interplay of brackish and subaerial/freshwater (lower delta) plain deposits recording the relative decrease in Holocene sea-level rise.

Recurrent stacking of bedsets and their bounding surfaces have been mapped across shallow marine deposits of the coastal successions targeted here and have been traced landward. Following previous and ongoing investigations, several higher-order depositional cycles defined by their characteristic bounding flooding surfaces, internal stacking patterns, and geometric relations to surrounding strata characterize the internal structure of the LGM sequence and are interpreted here as parasequences (Amorosi et al., 2017). High-resolution chronostratigraphic control indicates that the majority of the parasequences formed on millennial time scales (with durations of about 2000 yrs), and a subset formed on centennial time periods (Scarponi et al., 2013; Amorosi et al., 2017).

Stratigraphic framework of core 204-S7

Core 204-S7, 40 meters-long (Extended Data Fig. S1), was drilled 0.5 m above sea level (Latitude 44.725577° N, Longitude 11.940878° E), south of Ostellato, Italy. The bottom of the core is comprised of two meters thick sedimentary package with sparse freshwater macrofossils and display an overall fining upward tendency (from medium sand to silty-clay), interpreted as fluvial-channel deposit. These coarse-grained deposits are capped by eight meters of multi-coloured (yellow to brown), macrofossil-barren, clay to silty-clay (~31 to ~38 m core depth), intercalated by thin sandy layers are interpreted as well-drained floodplain succession deposited during pre-glacial (>32ky) times (Amorosi et al., 2005).

The overlying 31.0-24.7m interval primarily records late glacial dynamics (i.e., lowstand deposition) and is characterized by a ~3m thick fluvial channel body, consisting of amalgamated medium sands with an erosional base resting on top of a stiff calcareous horizon (inceptisol). The sharp erosional surface located at 31m core depth on top of the inceptisol represents the sequence boundary of the Last Glacial Maximum 4th order depositional sequence (Amorosi et al, 2005). Whereas, the upper boundary of this fluvial package records a sharp transition to clayey-silt and silty-clay, in turn overlain by a two-meter-thick multi-coloured (yellow to brown) deposits characterized by relatively abundant macrofossil (mainly fragments) of land and freshwater mollusks, otherwise showing comparable features to those retrieved between 38-31m core depth. Hence, suggestive of overbank and well-drained floodplain deposits.

Between 24.7 and 20.8m core depth, emplaced on top of underlying muds, a 4m thick, amalgamated and coarse-grained but fining-upward body showing scanty freshwater mollusks is retrieved. This body is interpreted as the sedimentary output of a fluvial channel and the sharp contact delimitating this coarse-grained unit from underlying floodplain deposits is interpreted as the regional transgressive surface (TS) (Bruno et al., 2016). The ~1.0-meter-thick homogenous dark brown silty-clay with scanty freshwater mollusks reflect the first record in the core of coastal plain poorly drained deposits and/or temporary standing water bodies. At 19.60m, a sharp facies shift is recorded at the base of a ca. 1.3m thick medium sand with multiple centimeter-scale silt intercalations. This sandy lithosome records the first appearance in the core of scattered specimens of brackish taxa: *Cerastoderma glaucum* and *Abra segmentum* (Extended Data Table S1). Hence, the shift of facies from poorly drained floodplain/swamp to brackish settings is retained to represent a flooding surface. Another flooding surface identified by means of micro-sedimentary inferences (Amorosi et al., 2017), is located at 16.20m core depth, on top of a thin peat layer. The ~2m thick dark organic rich clay with silty intercalations recording freshwater gastropod (hydrobiids and *Teodoxus fluviatilis*) bracketed between coarse sand and the peat layer, records the rapid transition from a brackish setting to a poorly drained floodplain/swamp. The overlying ~4m thick grey clay interval (16.20 to 12.25m core depth) bearing scanty macrofossils records, based on micro-sedimentary inferences, a further parasequence boundary around 14.30m core depth. This flooding surface separates swamp deposits below from brackish to swamp deposits above.

The interval 12.60-7.70m core depth is characterized by fine to medium decimetric to metric sand bodies alternating with clay-silt organic rich deposits organized into stacking patterns of meter scale, coarsening-upward, of back barrier facies. This staking pattern and the associated stock of brackish species that tend to decrease in abundance from fine to coarse deposits represents the set of three small scale cycles thoroughly investigated in this study. The uppermost one is capped by grey, fine to medium sand fluvial package, 1.0m thick with internal fining-upward trends. This body is interpreted to reflect sand inputs into the lagoon by fluvial channels and it progressively infill. Between 6 and 1.5m core depth is characterized by an overall aggradational and cyclic staking pattern of muddy to sandy deposits with scattered freshwater and or pulmonate molluscs. Based on microfaunal and sedimentary inferences this interval records the repeated alternation of swamp, floodplain and overbank deposits ranging from one to few meters thick and recording the alternating development coastal plain dynamics related mainly to autogenic Po Delta dynamics. Within this interval three flooding surfaces delimiting millennial scale cycles are recognized at 6.2, ~5.0 and ~3.0m core depth. A last flooding surface at 1.5m core depth is clearly recorded by a sharp transition from poorly drained floodplain muds and silty-muds recording the brackish bivalve *Abra segmentum* representing the last developments of short-lived lagoon.

Biofacies-Refined Interpretation of Sequence Stratigraphic Architecture

The vertical trend of nMDS1 sample scores and their strong correlation with salinity, a common ecological driver in back barrier settings (see Amorosi et al., 2014), further demonstrates the utility of macrofossil data to augment stratigraphic interpretation in cored deposits.

At the scale of the overall sedimentary package examined (Fig. 2), the nMDS-derived salinity pattern supports the control of glacio-eustatic forcing on the development of the Late Glacial Depositional sequence. Specifically, the lower part (i.e., 20 to 10.30m in Fig. 2) of the v-shaped nMDS-derived salinity profile records the increasing influence of the sea (supported by the overall increase in salinity), which is consistent with a retrogradational stacking pattern of back barrier facies (i.e., floodplain to lagoon settings). Whereas the upper shift toward lower salinity values, recorded after 6 ky BP (see Amorosi et al. 2017), is consistent with progradational to aggradational stacking patterns of brackish, freshwater and poorly drained floodplain deposits of the regressive systems tract (Figs 1b-2a, b).

At a higher resolution, the stratigraphic trajectory of nMDS1 sample scores highlights five flooding pulses depicted by major increases in salinity (here interpreted as parasequence bounding surfaces), followed by a gradual return to previous conditions (see Fig. 2). These abrupt contacts (e.g., ~12‰ salinity shift at 9.5m core depth in Fig. 2), are interpreted to represent non-Waltherian facies dislocations, with the overlying facies recording increased marine influence rather than a simple lateral shift to an adjacent environment relative to the underlying facies.

The three salinity shifts recognized at 15.5, 12.3, and 1.1m core depth (Fig. 2) represent parasequence bounding surfaces developed over millennial time scales. Whereas the remaining two are interpreted as higher frequency (centennial) pulses representing short lived, conditions of these back-barrier settings. Accordingly, it is possible to subdivide parasequence 4, developed at the time of maximum marine ingression (Fig. 2B), into a set of three higher frequency (sub-millennial scale) units bounded by significant (i.e., non-Waltherian) shifts of facies indicating rapid transition from mesohaline to polyhaline dominated paleoenvironments (Fig. 2B).

Extended Data Table S1—Mollusc dataset: sixty-five bulk samples (10cm thick), collected at a vertical spacing of no more than 50 cm from core 204-S7 drilled ~24 km west of the modern shoreline. Nineteen of the 65 samples were barren, the remaining 46 samples yielded 3171 individuals from 26 genera and 32 species. Note: *Ecrobia* groups a stock of taxa very similar (*Ecrobia* and *Hydrobia*), mainly distinguishable by means of soft tissues.

Family	Well depth (m) Genus/Species	24.05	23.05	22.05	21.05	20.05	19.75	19.5	19.05	18.95
SEMELIDAE	<i>Abra segmentum</i>	0	0	0	0	0	0	0	1	4
SEMELIDAE	<i>Abra</i> sp.	0	0	0	0	0	0	0	0	0
CARDIIDAE	<i>Cerastoderma glaucum</i>	0	0	0	0	0	0	1	1	1
CORBULIDAE	<i>Lentidium mediterraneum</i>	0	0	0	0	0	0	0	0	0
LUCINIDAE	<i>Loripes orbiculatus</i>	0	0	0	0	1	0	0	2	0
MYTILIDAE	<i>Modiolus</i> sp.	0	0	0	0	0	0	0	0	0
MONTACUTIDAE	<i>Kurtiella bidentata</i>	0	0	0	0	0	0	0	0	0
SPHAERIDAE	<i>Pisidium amnicum_cf</i>	1	0	0	0	0	0	0	0	0
SPHAERIDAE	<i>Pisidium subtruncatum_cf</i>	0	0	0	0	2	0	0	0	0
VENERIDAE	<i>Polititapes aureus</i>	0	0	0	0	0	0	0	0	0
VENERIDAE	<i>Polititapes</i> sp.	0	0	0	0	0	0	0	0	0
MACTRIDAE	<i>Spisula</i> sp.	0	0	0	0	0	0	0	0	0
PLANORBIDAE	<i>Anisus leucostoma</i>	0	0	3	0	0	0	0	0	0
PLANORBIDAE	<i>Anisus vortex</i>	0	0	1	0	0	0	0	0	0
BITHYNIIDAE	<i>Bithynia tentaculata_cf</i>	2	0	8	0	0	0	0	0	0
Cerithiopsidae	<i>Cerithiopsis</i> sp.	0	0	0	0	0	0	0	0	0
CERITHIIDAE	<i>Bittium reticulatum</i>	0	0	0	0	0	0	0	1	1
CERITHIIDAE	<i>Cerithium vulgatum</i>	0	0	0	0	0	0	0	0	0
CERITHIIDAE	<i>Cerithium</i> sp.	0	0	0	0	0	0	0	0	0
PYRAMIDELLIDAE	<i>Chrysallida interstincta</i>	0	0	0	0	0	0	0	0	0
PYRAMIDELLIDAE	<i>Chrysallida</i> sp.1	0	0	0	0	0	0	0	0	0
HYDROBIIDAE	<i>Ecrobia ventrosa_gr.</i>	0	0	0	0	0	0	2	1	2
NASSARIIDAE	<i>Nassarius nitidus</i>	0	0	0	0	0	0	0	0	0
NASSARIIDAE	<i>Nassarius</i> sp.	0	0	0	0	0	0	0	0	0
SUCCINEIDAE	<i>Oxyloma</i> sp.	0	0	0	0	0	0	0	0	0
RISSOIDAE	<i>Pusillina lineolata</i>	0	0	0	0	0	0	0	0	0
RISSOIDAE	<i>Pusillina marginata</i>	0	0	0	0	0	0	0	0	0
RISSOIDAE	<i>Pusillina</i> sp.	0	0	0	0	0	0	0	0	0
RETUSIDAE	<i>Retusa mammillata</i>	0	0	0	0	0	0	0	0	0

12.55	12.45	12.25	12.05	11.95	11.55	11.35	11.05	10.85	10.55	10.25	10.16	10.05	9.9	9.55
2	1	35	98	50	8	1	33	14	0	218	80	21	51	16
0	0	0	0	0	0	0	0	0	0	0	0	0	0	0
0	2	10	11	15	0	1	9	2	0	44	28	7	12	0
0	0	0	0	0	0	0	0	0	0	3	0	0	0	0
0	1	30	67	46	2	3	11	3	0	240	73	19	31	0
0	0	1	0	0	0	0	0	0	0	3	2	0	0	0
0	0	0	1	0	0	0	0	0	0	0	0	0	0	0
0	0	0	0	0	0	0	0	0	0	0	0	0	0	0
0	0	0	0	0	0	0	0	0	0	0	0	0	0	0
0	0	0	0	0	0	0	0	0	0	0	0	0	0	0
0	0	0	0	0	0	0	0	0	0	0	0	0	0	0
0	0	0	0	0	0	0	0	0	0	3	1	0	1	0
0	0	0	0	0	0	0	0	0	0	0	1	0	0	0
0	0	0	0	0	0	0	0	0	0	0	0	0	0	0
0	0	0	0	0	0	0	0	0	0	0	0	0	0	0
0	0	0	0	0	2	0	0	0	0	0	0	1	0	3
0	0	0	0	0	0	0	0	0	0	2	0	0	0	0
0	0	6	27	45	3	2	3	4	0	118	33	14	24	0
0	0	0	0	0	0	0	0	0	0	0	0	0	0	0
0	0	0	1	0	0	0	0	0	0	0	1	0	0	0
0	0	0	0	0	0	0	0	0	0	3	2	0	3	0
0	0	0	0	0	0	0	0	0	0	2	0	0	0	0
0	0	16	24	59	2	6	2	4	0	120	17	5	18	6
0	0	0	0	0	0	0	0	0	0	1	0	0	0	0
0	0	0	0	0	0	0	0	0	0	1	0	0	0	0
0	0	0	0	0	0	0	0	0	0	0	1	0	0	0
0	0	7	0	4	0	0	0	0	0	20	0	0	0	0
0	0	0	1	0	0	0	0	0	0	0	0	0	0	0
0	0	0	0	0	0	0	0	0	0	0	0	0	2	0
0	0	0	1	1	0	0	1	0	0	7	1	0	0	0
0	0	0	0	0	0	0	0	0	0	0	0	0	0	0
0	0	0	0	1	2	0	0	0	0	2	12	1	3	0
0	0	0	0	6	0	0	0	1	0	0	0	1	0	0
0	0	0	3	0	0	0	0	0	0	0	0	0	0	0
0	0	0	0	0	0	0	0	0	0	0	0	0	0	0
0	0	0	0	0	0	0	0	0	0	0	0	0	0	0
0	0	0	0	0	0	0	0	0	0	0	0	0	0	0
0	0	0	0	0	0	0	0	0	0	0	0	0	0	0
0	0	0	0	0	0	0	0	0	0	0	0	1	0	0
0	1	0	0	0	0	0	0	0	0	0	0	0	0	0
2	5	105	234	227	19	13	59	28	0	787	252	70	145	25

9.27	9.05	8.95	8.85	8.65	8.5	8.4	8.05	7.85	7.55	7.05	6.55	6.05	5.95	5.45
44	18	1	47	59	124	54	4	0	0	1	0	0	0	0
0	0	0	0	1	0	0	0	0	0	0	0	0	0	0
5	6	0	34	31	29	18	0	0	0	0	0	0	0	0
0	0	0	1	1	0	0	0	0	0	0	0	0	0	0
39	28	0	23	16	30	29	3	0	0	0	0	0	0	0
0	0	0	0	1	0	0	0	0	0	0	0	0	0	0

0	0	0	0	0	0	0	0	0	0	0	418
0	0	0	0	0	0	0	0	0	0	0	4
0	0	0	0	0	0	0	0	0	0	0	2
0	0	0	0	0	0	0	0	0	0	0	11
0	0	0	0	0	0	0	0	0	0	0	2
0	0	0	0	0	0	0	0	1	11	12	513
0	0	0	0	0	0	0	0	0	0	0	2
0	0	0	0	0	0	0	0	0	0	0	1
0	0	0	0	0	0	0	0	0	0	0	1
0	0	0	0	0	0	0	0	0	0	0	37
0	0	0	0	0	0	0	0	0	0	1	6
0	0	0	0	0	0	0	0	0	0	0	3
0	0	0	0	0	0	0	0	0	0	0	29
0	0	0	0	0	0	0	0	0	0	0	8
0	0	0	0	0	0	0	0	0	0	0	28
0	0	0	0	0	0	0	0	0	0	0	12
0	0	0	0	0	0	0	0	3	0	0	6
0	0	0	0	0	0	0	0	0	0	0	1
0	0	0	0	0	0	0	0	0	0	0	2
0	0	0	0	0	0	0	0	0	0	0	5
0	0	0	0	0	0	0	0	0	0	0	1
0	0	0	0	0	0	1	0	0	0	1	5
0	1	1	0	0	0	2	0	9	31	26	

Extended Data Table S2—Summary of present-day salinity data used for environmental calibration of the mollusc nMDS axis 1 sample scores (nMDS1). The seven species used here were selected based on their abundance in 204-S7 core dataset (Extended Data Table S1) and to ensure continuous coverage along nMDS1. Preferred salinity of species (optima) and salinity range (min - max) were obtained from literature data (References). Midpoint is referred (if available) to the preferred salinity range (optima) of a targeted species.

Taxon	Salinity (psu)				References
	mi	max	optimal	midpoint	
<i>Loripes orbiculatus</i>	7	>35	20-35	27.5	Anistratenko 2011; Encyclopedia of Life, 2016; Cilenti et al., 2008
<i>Cerastoderma glaucum</i>	3	61	5.0-38.0	21.5	Gontikaki et al., 2003; Boyden and Russel, 1972
<i>Bithynia tentaculata</i>	0	6.3	0-4.2	2.1	Berezina, 2003
<i>Abra segmentum</i>	3	>35 (41)	9.0-12.0	10.5	CSB Database, 2016; Gontikaki et al., 2003
<i>Bittium reticulatum</i>	15	>35(38.4)	*	31.5	Nabozhenko, 2013; Encyclopedia of Life, 2016; Altobelli et al., 2008
<i>Retusa mammillata</i>	11	34	15.0-25.0	20	Zettler and Gosselck 2006; Chaban, 2004; Fleischer and Zettler, 2009
<i>Chrysallida interstincta</i>	15	>35	*	25	Funder S. et al., 2002; Rosemberg and Gofas, 2012

* No optimal salinity range recovered.

Extended Data Table S3—Sample salinity approximation based on weighted averaged salinity optima of the sub-set of the seven key species (Extended Data Table S2) retrieved in each sample. Abbreviation: # number, psu practical salinity unit. Highlighted in red those samples for which species preferred salinity estimate was available for only one or two species representing less 30% of total specimen abundance.

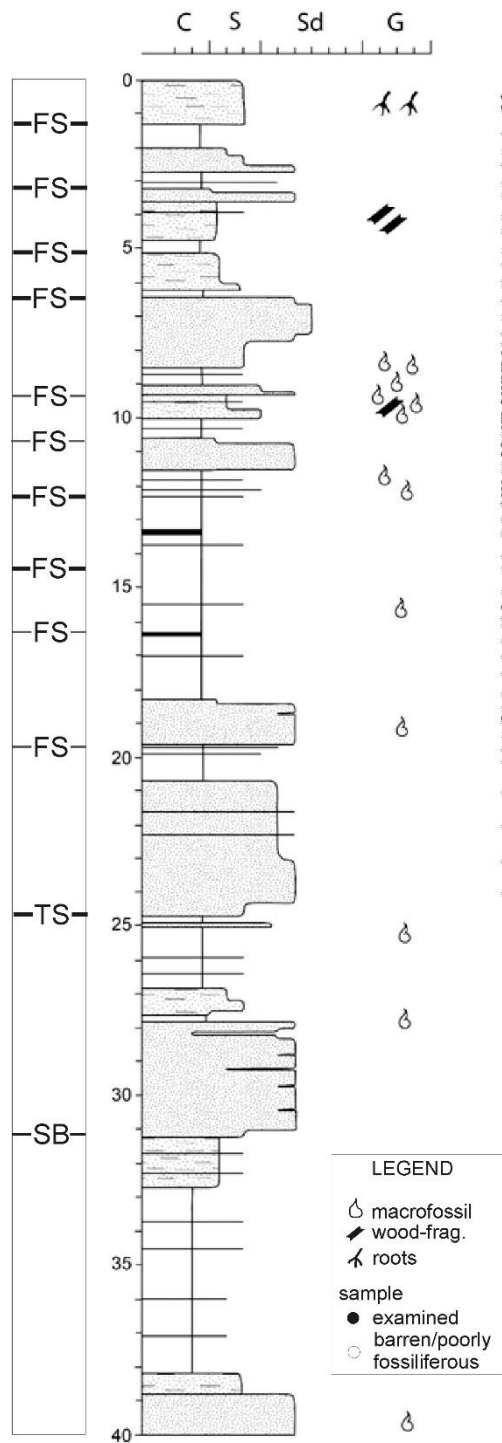
Core depth (m)	nMDS dataset sample species richness	# key species available for salinity computation	% specimens employed for first approximation sample salinity computation	Sample	
				weighted average salinity estimate (psu)	nMDS score
15.60	2	1	1.6	21.5	-0.75963
12.25	7	4	64.7	20.4	0.105331
12.05	7	5	82.4	20.9	0.238195
11.95	8	5	61.4	24.6	0.333406
11.05	6	5	94.1	17.7	0.076108
10.85	5	4	77.8	19.7	-0.24324
10.25	12	6	72.1	23.3	0.666585
10.16	9	6	82.0	22.4	0.427953
10.05	7	5	87.0	23.0	0.07666
9.90	7	5	78.1	22.3	0.270657
9.55	3	2	64.7	8.2	-0.81188
9.27	7	4	72.7	22.6	0.246792
9.05	7	5	88.1	23.8	0.185443
8.85	10	6	83.7	25.0	0.401588
8.65	13	5	69.0	17.1	0.26466
8.40	8	5	75.0	19.3	0.425677
8.50	7	5	70.4	18.7	0.103709
8.05	3	2	26.7	19.0	-0.74554
0.85	3	2	50.0	12.5	-0.54542
0.55	6	3	30.0	12.8	-0.71706

Extended Data Table S4—Trematode prevalence data for *Abra segmentum* from core 204-S7 samples. n = number of valves.

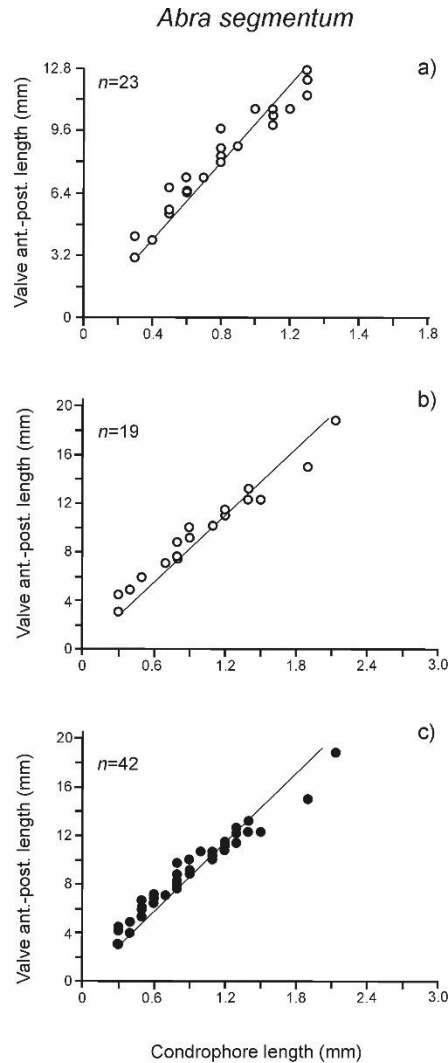
Core depth (m)	n	n with trematode pits	n too fragmented to determine infestation status	Prevalence	Prevalence Arcsine-transformed
18.95	4	3	1	0.750	1.047
12.25	35	17	12	0.486	0.771
12.05	98	49	22	0.500	0.785
11.95	39	25	7	0.641	0.928
11.35	1	0	0	0.000	0.000
11.05	30	3	9	0.100	0.322
10.85	14	1	5	0.071	0.271
10.35	212	111	53	0.524	0.809
10.16	73	29	24	0.397	0.682
9.9	51	20	15	0.392	0.677
9.29	42	29	3	0.690	0.981
8.85	40	20	7	0.500	0.785
8.65	27	5	0	0.185	0.445
8.5	111	21	32	0.189	0.450
8.4	32	4	6	0.125	0.361
0.96	3	2	0	0.667	0.955
0.85	20	8	5	0.400	0.685
0.55	5	1	1	0.200	0.464

Extended Data Table S5—Results of trematode prevalence 10,000 randomization iterations of individual valves. n_{valves} = number of valves examinable in a sample; Prevalence = number of valves with trematode pits divided by n_{valves} .

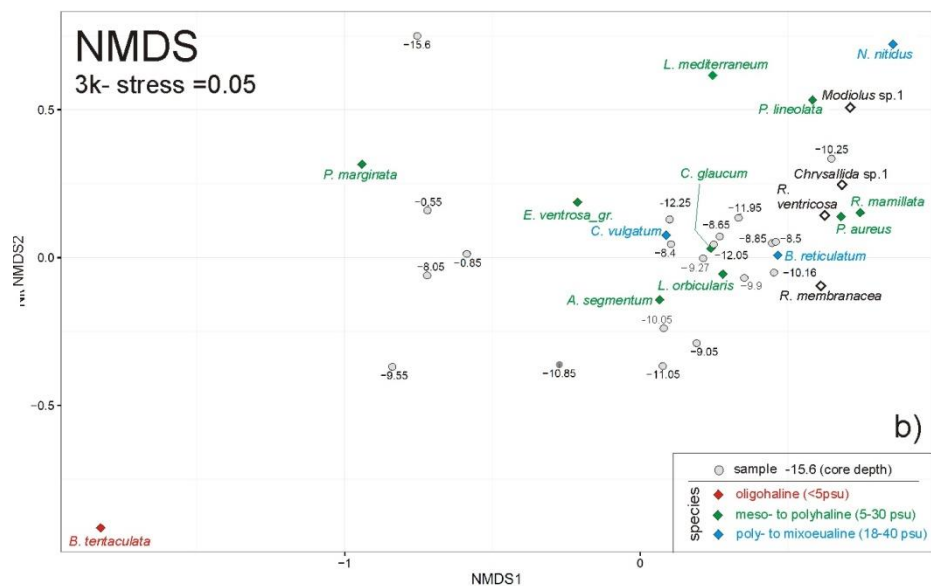
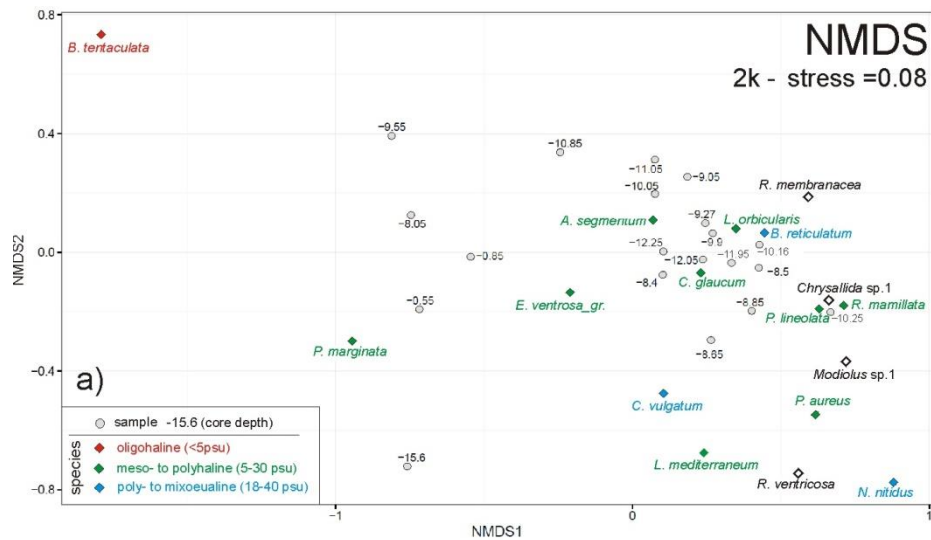
Sample core depth (m)	N valves	Prevalence	Results of 10,000 randomization iterations of individual valves for trematode prevalence				
			Mean	0.5%	2.5%	97.5%	99.5%
0.55	5	0.200	0.413	0.000	0.000	0.800	1.000
0.85	20	0.400	0.415	0.150	0.200	0.650	0.700
8.40	32	0.125	0.415	0.219	0.250	0.594	0.656
8.50	111	0.189	0.416	0.297	0.324	0.505	0.541
8.65	27	0.185	0.416	0.185	0.222	0.593	0.667
8.85	40	0.500	0.416	0.225	0.275	0.575	0.625
9.29	42	0.690	0.417	0.238	0.262	0.571	0.619
9.90	51	0.392	0.415	0.235	0.275	0.549	0.588
10.16	73	0.397	0.414	0.274	0.301	0.534	0.575
10.35	212	0.524	0.415	0.330	0.349	0.481	0.505
10.85	14	0.071	0.414	0.071	0.143	0.643	0.786
11.05	30	0.100	0.415	0.200	0.233	0.600	0.633
11.95	39	0.641	0.416	0.231	0.256	0.564	0.615
12.05	98	0.500	0.416	0.286	0.316	0.510	0.541
12.25	35	0.486	0.415	0.200	0.257	0.571	0.629
18.95	4	0.750	0.407	0.000	0.000	1.000	1.000



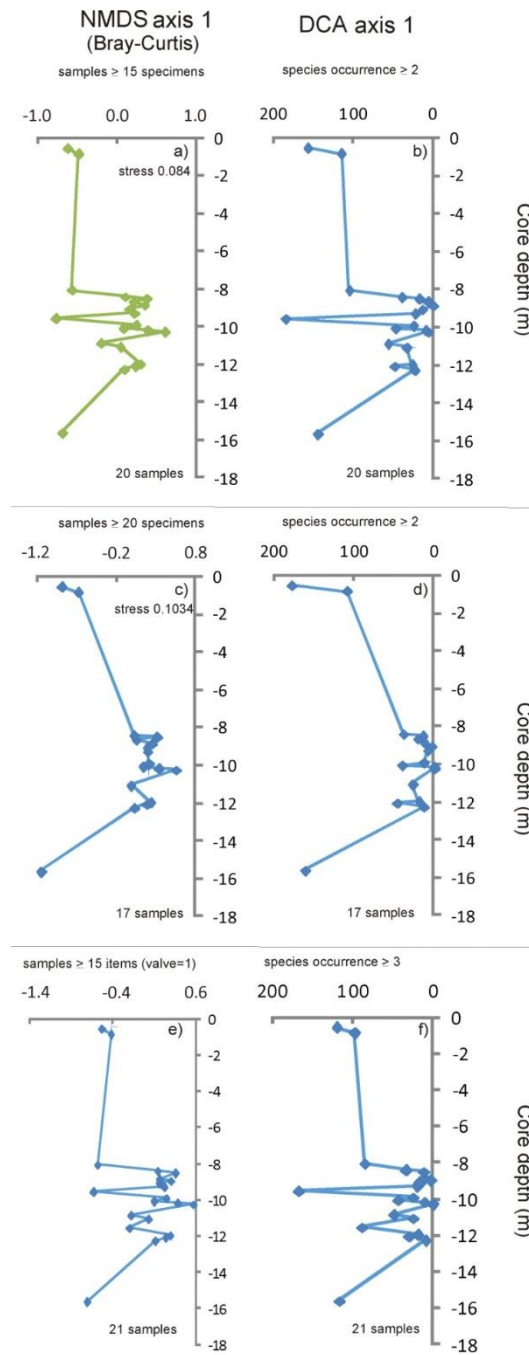
Extended Data Figure 1—204-S7 stratigraphic log showing position of samples, sequence boundary and flooding surfaces (millennial—thick line, and sub-millennial—thin line, time-scales). FS flooding surface; TS transgressive surface, SB sequence boundary.



Extended Data Figure 2—*Abra segmentum* valves were classified as either left or right, and anterior-posterior length (APL) was measured for all complete specimens. In the case of broken valves, we employed the chondrophore length (external portion; Fig. 1C) as a proxy for APL by means of reduced major axis regression (RMA). RMA was performed with intercept centered to 0 value and on a set of (a) 23 right, and (b) 19 left valves, and (c) a set of all valves measured. The RMA model of all valves was utilized for estimating APL of fragmented valves whose designation as a right or left valve was not possible. Estimation of anterior-posterior length was not employed for fragmented valves lacking the umbonal region. A) RMA regression for right valves. Regression coefficient and tests: Pearson $r = 0.97$; $r^2 = 0.94$; $p(\text{uncorr.}) < 0.05$; Slope 9.9566 (95% bootstrapped C.I. 9.46-10.34 based on 1999 iterations), Standard error 0.212. B) RMA regression for left valves. Regression coefficients and tests: Pearson $r = 0.99$; $r^2 = 0.97$; $p(\text{uncorr.}) < 0.05$; Slope 9.1483 (95% bootstrapped C.I. 8.54-9.57 based on 1999 iterations), Standard error 0.232. C) RMA regression for all valves. Regression coefficient and tests: Pearson $r = 0.98$; $r^2 = 0.96$; $p(\text{uncorr.}) < 0.05$; Slope 9.5008 (95% bootstrapped C.I. 9.06-9.86 based on 1999 iterations), Standard error 0.16659. Ant.=Anterior; Post.=posterior

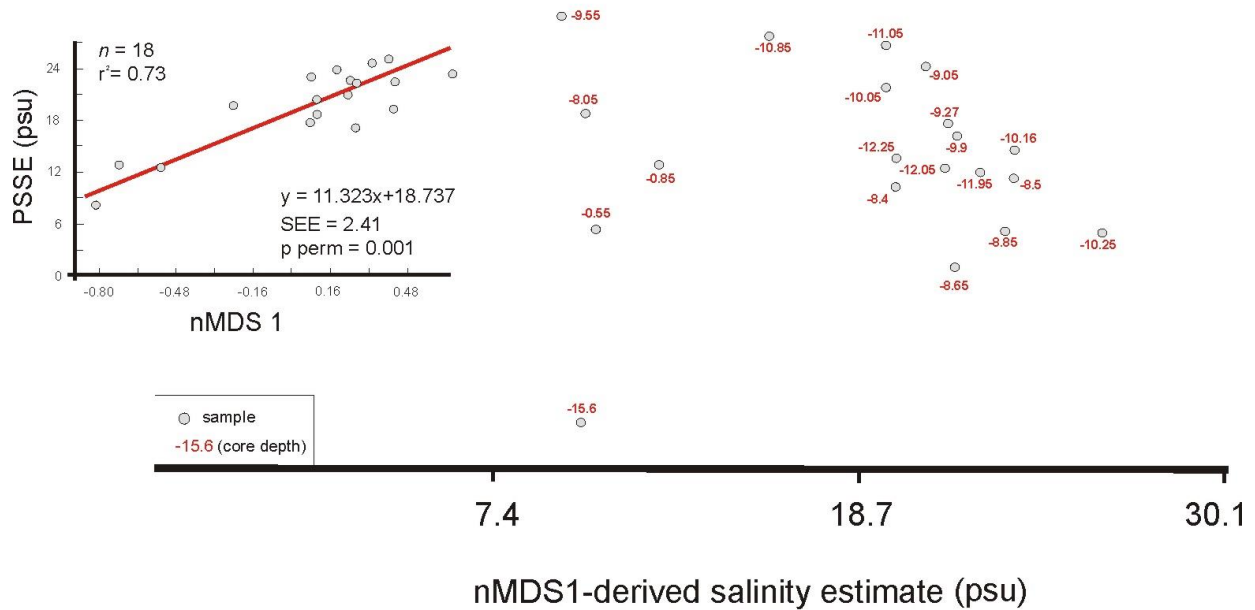


Extended Data Figure 3—Non-metric Multidimensional Scaling (nMDS) ordination was used to investigate the primary environmental gradient along which the samples could be ordinated. Only small samples ($n < 15$ specimens), singletons (1 occurrence), and congeneric specimens without species designations removed. Bray-Curtis similarity was used to develop nMDS ordinations; both (a) 2 dimension and (b) 3-dimensions outputs are reported. In both outputs, the indirect ordination analyses of the core data revealed a pronounced gradient, with species ordinated along the first nMDS axis, according to their salinity tolerance.

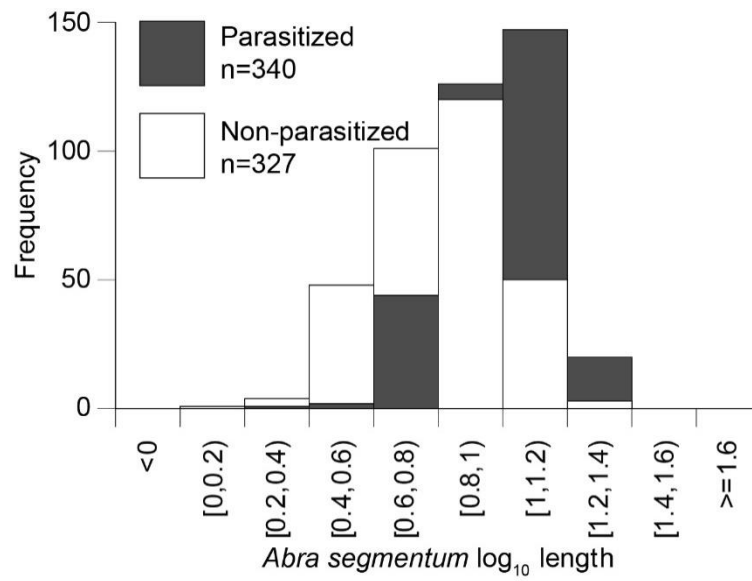


Extended Data Figure 4—non-metric Multidimensional Scaling (nMDS) and Detrended Correspondence Analysis ordinations varying rare taxa or sample thresholds returned comparable patterns. A-b) Matrix log-transformed, minimum sample size ≥ 15 specimens (valves counted as 0.5), only species occurring in one sample and samples with one species were excluded. C-d) As above, but minimum sample size ≥ 20 specimens (valves counted as 0.5). E-f) Matrix log-transformed, minimum sample size ≥ 15 specimens (valves counted as 1), only species occurring in less than three samples and samples with one species were excluded. The nMDS profile in green is reported in Figure 2.

NMDS
stress =0.08



Extended Data Figure 5—The species preferred salinity was independently estimated using the modern ecological data for mollusk (Extended Data Tables S2-3), and then correlated with the sample nMDS score along axis 1. Indeed, a recent study on comparable successions and based on averaging and Detrended Correspondence approaches, demonstrated that a posteriori ordination scores are a robust predictor of salinity for both samples and species across Holocene paralic succession of the Arno Plain (see Amorosi et al. 2014). The reduced major axis (RMA) linear regression (red line) is shown. The thick horizontal bottom line represents nMDS sample scores (Fig. Extended Data S3A) calibrated by means of RMA linear regression function. Abbreviations: nMDS1 = non-Metric Multidimensional Scaling axis one; n = sample size; p non param = permutation test on correlation; psu = practical salinity unit; r2 = coefficient of determination; SEE = standard error of the estimate; PSSE = provisory sample salinity estimate (see Extended Data Table S3).



Extended Data Figure 6—Size frequency distribution of *Abra segmentum* recovered in core 204-S7 classified by presence/absence of trematode-induced pits.

Extended Data References

- Altobelli, A., Hubina, T., Sponza, S., & Sisto, A. Effect of abiotic and biotic factors on the abundance of waterbirds in Grado-Marano Lagoon (Italy). In SPIE Remote Sensing, pp. 710404-710404 (2008, October). International Society for Optics and Photonics.
- Amorosi, A., Centineo, M. C., Colalongo, M. L., & Fiorini, F. Millennial-scale depositional cycles from the Holocene of the Po Plain, Italy. *Marine Geology*, 222, 7-18 (2005).
- Amorosi, A., Bruno, L., Rossi, V., Severi, P., & Hajdas, I. Paleosol architecture of a late Quaternary basin-margin sequence and its implications for high-resolution, non-marine sequence stratigraphy. *Global and Planetary Change*, 112, 12-25 (2014).
- Amorosi A. et al. Global sea-level control on local parasequence architecture from the Holocene record of the Po Plain, Italy. *Marine and Petroleum Geology* (2017).
- Anderson, M. J. et al., S. P. Navigating the multiple meanings of β diversity: a roadmap for the practicing ecologist. *Ecology letters*, 14(1), 19-28 (2011).
- Anistratenko, V. V., Khaliman, I. A., & Anistratenko, O. Y. *Molluscs the Sea of Azov*. Kiev: Naukova Dumka (2011).
- Bambach, R. K., & Kowalewski, M. How to count fossils. In *Geological Society of America Abstracts with Programs*, 32(7), 332 (2000).
- Berezina, N.A. Tolerance of Freshwater Invertebrates to Changes in Water Salinity. *Russian Journal of Ecology* 34, 261-266 (2003).
- Boyden, C. R., & Russell, P. J. C. The distribution and habitat range of the brackish water cockle (*Cardium* (*Cerastoderma*) *glaucum*) in the British Isles. *The Journal of Animal Ecology*, 719-734 (1972).
- Bruno, L., Amorosi, A., Severi, P., & Costagli, B. Late Quaternary aggradation rates and stratigraphic architecture of the southern Po Plain, Italy. *Basin Research* (2016).
- Caspian Sea Biodiversity (CSB) Database. Accessed thorough:
<http://www.caspianenvironment.org/biodb/eng/main.htm> on 07/05/2016.
- Chaban, E.M. Some materials for revision of opistobranchs of the family Retusidae (Mollusca:Cephalaspidea). *Annual Reports of the Zoological Institute Russian Accademy of Sciences* (2004).
- Cilenti, L. et al. Population structure and spatial distribution of *Loripes lacteus* (Linnaeus, 1758) in Varano lagoon, SE Italy. *Transitional Waters Bulletin*, 2(4), 63-70 (2010).
- Der, G., & Everitt, B. S. *Essential Statistics Using SAS University Edition*. Sas Institute (2015).
- Fleischer, D., Zettler, M.L. An adjustment of benthic ecological quality assessment to effects of salinity. *Marine Pollution Bulletin* 58, 351-357 (2009).
- Funder, S., Demidov, I., Yelovicheva, Y. Hydrography and mollusc faunas of the Baltic and the White Sea-North Sea seaway in the Eemian. *Palaeogeography, Palaeoclimatology, Palaeoecology*, 184, 275-304 (2002).
- Gontikaki, E., Antoniadou, C., Chintiroglou, C.C. Population structure of *Cerastoderma glaucum* and *Abra ovata* in Vouliagmeni Lagoon (Attiki). *Journal of Marine Biological Associations of the United Kingdom* 83, 1095-1097 (2003).
- Hammer, Ø., Harper, D.A.T., and P. D. Ryan. PAST: Paleontological Statistics Software Package for Education and Data Analysis. *Palaeontologia Electronica* 4(1): 9pp (2001).
- Nabozhenko. Reconstruction and dynamics of bivalvia taxocenosis (Mollusca: Bivalvia) of the Sea of Azov in the late Holocene in connection with change of salinity. *Proceedings of the Zoological Institute of the Russian Academy of Sciences Application No. 3, 2013, c. 182-191* (2013).
- Neal, J., & Abreu, V. Sequence stratigraphy hierarchy and the accommodation succession method. *Geology*, 37(9), 779-782 (2009).

Rosenberg, G., Gofas, S. *Chrysallida interstincta* (J. Adams, 1797) (2012). Accessed through: World Register of Marine Species at <http://www.marinespecies.org/aphia.php?p=taxdetails&id=140918> on 2012-05-11.

R Core Team. R: A language and environment for statistical computing. R Foundation for Statistical Computing, Vienna, Austria (2016). URL <https://www.R-project.org/>.

Scarponi, D., Angeletti, L. Integration of paleontological patterns in the sequence stratigraphy paradigm: A case study from Holocene deposits of the Po Plain (Italy). *GeoActa*, 7, 1-13 (2008).

Scarponi, D., Kaufman, D., Amorosi, A. and Kowalewski, M. Sequence stratigraphy and the resolution of the fossil record. *Geology*, 41/2, 239–242 (2013).

Scarponi, D. et al. Systematic vertical and lateral changes in quality and time resolution of the macrofossil record: insights from Holocene transgressive deposits, Po coastal plain, Italy. *Marine and Petroleum Geology* (submitted).

Zettler, M.L., Gosselck, F. Benthic assessment of marine areas of particular ecological importance within the German Baltic Sea EEZ. In: *Progress in Marine Conservation in Europe - Natura 2000 sites in German offshore waters*. H. von Nordheim, D. Boedeker, J.C. Krause (eds.) Springer Berlin (Chapter 8) (2006).

Chapter 7

Manuscript III

7. Manuscript III

“Stratigraphic signatures of mass extinction: ecological and sedimentary determinants”

Authors: Rafal Nawrot^a, Daniele Scarponi^b, Michele Azzarone^b, Troy A. Dexter^c, Kristopher M. Kusnerik^a, Jacalyn M. Wittmer^d, Alessandro Amorosi^b and Michal Kowalewski^a

^a Florida Museum of Natural History, University of Florida, 1659 Museum Road, Gainesville, FL 32611, USA

^b Dipartimento di Scienze Biologiche, Geologiche e Ambientali, University of Bologna, Via Zamboni 67, 40126 Bologna, Italy

^c Gerace Research Centre, University of the Bahamas, San Salvador, Bahamas

^d Department of Geological Sciences, State University of New York at Geneseo, One College Circle, Geneseo, NY 14454, USA

Status: Published in *Proceedings of the Royal Society B*, volume 285, issue 1886, September 2018

doi: doi.org/10.1098/rspb.2018.1191



Cite this article: Nawrot R, Scarponi D, Azzarone M, Dexter TA, Kusnerik KM, Wittmer JM, Amorosi A, Kowalewski M. 2018 Stratigraphic signatures of mass extinctions: ecological and sedimentary determinants. *Proc. R. Soc. B* **285**: 20181191. <http://dx.doi.org/10.1098/rspb.2018.1191>

Received: 29 May 2018

Accepted: 21 August 2018

Subject Category:

Palaeobiology

Subject Areas:

palaeontology, ecology, evolution

Keywords:

mass extinction, sequence stratigraphy, Signor–Lipps effect, sampling bias, stratigraphic palaeobiology, Holocene

Author for correspondence:

Rafał Nawrot

e-mail: rnawrot@flmnh.ufl.edu

Electronic supplementary material is available online at <https://dx.doi.org/10.6084/m9.figshare.c.4211948>.

Stratigraphic signatures of mass extinctions: ecological and sedimentary determinants

Rafał Nawrot¹, Daniele Scarponi², Michele Azzarone², Troy A. Dexter³, Kristopher M. Kusnerik¹, Jacalyn M. Wittmer⁴, Alessandro Amorosi² and Michał Kowalewski¹

¹Florida Museum of Natural History, University of Florida, 1659 Museum Road, Gainesville, FL 32611, USA

²Dipartimento di Scienze Biologiche, Geologiche e Ambientali, University of Bologna, Via Zamboni 67, 40126 Bologna, Italy

³Gerace Research Centre, University of the Bahamas, San Salvador, Bahamas

⁴Department of Geological Sciences, State University of New York at Geneseo, One College Circle, Geneseo, NY 14454, USA

id RN, 0000-0002-5774-7311; DS, 0000-0001-5914-4947; MA, 0000-0003-0197-6817; MK, 0000-0002-8575-4711

Stratigraphic patterns of last occurrences (LOs) of fossil taxa potentially fingerprint mass extinctions and delineate rates and geometries of those events. Although empirical studies of mass extinctions recognize that random sampling causes LOs to occur earlier than the time of extinction (Signor–Lipps effect), sequence stratigraphic controls on the position of LOs are rarely considered. By tracing stratigraphic ranges of extant mollusc species preserved in the Holocene succession of the Po coastal plain (Italy), we demonstrated that, if mass extinction took place today, complex but entirely false extinction patterns would be recorded regionally due to shifts in local community composition and non-random variation in the abundance of skeletal remains, both controlled by relative sea-level changes. Consequently, rather than following an apparent gradual pattern expected from the Signor–Lipps effect, LOs concentrated within intervals of stratigraphic condensation and strong facies shifts mimicking sudden extinction pulses. Methods assuming uniform recovery potential of fossils falsely supported stepwise extinction patterns among studied species and systematically underestimated their stratigraphic ranges. Such effects of stratigraphic architecture, co-produced by ecological, sedimentary and taphonomic processes, can easily confound interpretations of the timing, duration and selectivity of mass extinction events. Our results highlight the necessity of accounting for palaeoenvironmental and sequence stratigraphic context when inferring extinction dynamics from the fossil record.

1. Introduction

Stratigraphic distributions of last occurrences (LOs) of fossil taxa in sedimentary successions have been used to quantify onsets, durations and intensities of mass extinctions (e.g. [1–4]), track geographical and environmental variation in extinction rates [4–6], and relate those rates to concurrent changes in geochemical and sedimentological proxies [2,4,5]. This type of palaeontological data has been thus crucial for high-resolution reconstructions of the temporal and ecological dynamics of mass extinction events and identification of their extrinsic drivers. Nevertheless, the observed stratigraphic position of the LO of a species typically predates its actual time of extinction [7]. In addition, as demonstrated by Signor & Lipps [8], artificial truncation of the observed stratigraphic range of a taxon can simply arise from a random sampling process, which can make abrupt extinction events appear gradual in the fossil record. To correct for

this ‘Signor–Lipps effect’ [9], the timing and pattern of extinctions have been commonly estimated from stratigraphic data by assuming that fossil occurrences are essentially random and controlled primarily by sampling [7].

However, the focus on random sampling effects alone does not fully account for the complexity of the geological record and non-random nature of stratigraphic patterns [10]. Most outcrop- and core-based extinction studies implicitly assume that the positions of LOs logged at a given location provide an accurate chronology of extirpation or extinction events, especially so, if corrected for the Signor–Lipps effect. However, the local distribution of LOs is not only affected by sampling intensity, but also by systematic changes in facies and sediment accumulation rates that occur in response to regional or global drivers such as tectonic subsidence and eustatic change [11]. Consequently, a local stratigraphic expression of temporal variation in extinction rates is superimposed on ecological responses to lateral shifts of habitats through time, manifested in geological sections as vertical changes in composition and diversity of fossil assemblages. These changes can appear as sudden pulses in faunal turnover due to abrupt facies shifts, as well as due to non-deposition, stratigraphic condensation and erosion, often coincident with facies boundaries.

Numerical simulations that integrate eco-evolutionary and sequence stratigraphic models support those predictions: eco-stratigraphic processes can produce clusters of LOs concentrated at specific stratigraphic horizons such as flooding surfaces, surfaces of forced regression and sequence boundaries [10,12–15]. Such surfaces are typically associated with depositional hiatuses, stratigraphic condensation and non-Waltherian facies shifts [11,16]. Moreover, depositional architecture influences the stratigraphic distribution, taphonomic characteristics and temporal resolution of fossil concentrations [17–20], thus constraining the quantity and quality of palaeontological data retrievable from any given horizon.

The sequence stratigraphic control on fossil occurrences is worrisome because the fossil record of many prominent extinction events coincides with major sequence stratigraphic surfaces, suggesting that interpretations of these events may be partly, or even entirely, confounded by the stratigraphic architecture [10,21–23]. On the other hand, because trends in biodiversity and stratigraphic architecture may both be driven by common causative processes such as sea-level and climatic changes [24], it is difficult to distinguish clusters of LOs caused by elevated extinction rates from those generated by stratigraphic processes [10]. To avoid these uncertainties, we employ here the Holocene fossil record of living species to test the impact of the stratigraphic architecture on our ability to reconstruct the timing and tempo of past extinction events.

We evaluate how faithfully stratigraphic ranges of extant Adriatic molluscs are recorded in a series of cores that were drilled through a 40-metre-thick package of genetically related alluvial, coastal and shallow-marine strata of the Po Plain (northwest Italy). If the time when a given taxon was in existence was always accurately reflected by its stratigraphic range observed in local sections, LOs of extant species should coincide with the top of the succession. However, such a perfect record is implausible [8,25]. Here we test if the observed stratigraphic distribution of LOs can be explained by a random sampling alone (i.e. the Signor–Lipps effect), or is more consistent with combined effects of sampling and systematic variation in fossil occurrence rates

as predicted by the sequence stratigraphic model. Our approach can also be directly linked to mass extinction studies by following a simple thought experiment [25]: imagine that a catastrophic event has just wiped out all shallow marine and brackish molluscan fauna of the Adriatic Sea. The extinction horizon would then correspond to the modern sedimentary surface preserved in the rock record by subsequent sedimentation. We ask if this hypothetical extinction event could be correctly reconstructed from cores drilled across the Po Plain. By tracing the stratigraphic occurrences of extant species with known ecological preferences, in the context of the established regional depositional and sequence stratigraphic frameworks [26], we can directly assess the imprint of facies control, stratigraphic architecture and sampling on the stratigraphic distribution of LOs.

2. Material and methods

(a) Study area

The topmost 40-metre-thick succession of the Po coastal plain has been interpreted to represent the Last Glacial Maximum depositional sequence, which is currently accumulating in the Po Plain–Adriatic Sea system [27]. In the study area, the lowstand systems tract is primarily composed of fluvial and floodplain deposits of Late Pleistocene age. Overlying transgressive systems tract (TST) and highstand systems tract (HST) consist mainly of Holocene strata forming a transgressive–regressive, wedge-shaped succession, recently subdivided into a series of centennial units embedded within eight millennial-scale depositional units (parasequences in [26]; see ‘Geological setting’ in electronic supplementary material). The Holocene molluscan assemblages were studied in four cores for which environmental, sequence stratigraphic and chronostratigraphic interpretation have been previously established [19,20,26,28]. These cores form an L-shaped transect 35 km long that captures lateral variation in LO patterns along the depositional dip and strike (electronic supplementary material, figure S1). Fossiliferous deposits preserving estuarine, deltaic and marine assemblages occur up to the modern sedimentary surface in all four cores.

(b) Dataset

A total of 229 bulk samples, each representing an approximately 10 cm core interval, were collected with an average vertical spacing of 0.57 m (range 0.05–1.52 m). The standardized volume of samples allows us to track changes in fossil abundance (i.e. the density of identifiable fossils per unit of a core). See Kowalewski *et al.* [29] for the details of sample processing. Specimens lacking species-level identification and all terrestrial or exclusively freshwater species were excluded, resulting in the dataset encompassing 119 species and 38 093 specimens (electronic supplementary material, dataset S1). Stratigraphic ranges of species observed in the cores were extended to the Late Pleistocene based on their occurrence in the underlying marine strata of the Last Interglacial (Marine Isotope Stage 5e [29]).

(c) Estimating bathymetric preferences of species

We focused on water depth because it is one of the major factors controlling the distribution of marine benthic assemblages [15]. The independent estimates of the present-day bathymetric preferences of species were derived from the Italian Mollusc Census Database of the Italian National Agency for New Technologies, Energy and Sustainable Economic Development (ENEA; <http://www.santateresa.enea.it/wwwste/malaco/home.htm>), a compilation of benthic surveys along the Italian coast [30]. We only

considered sampling stations located on the Adriatic Sea shelf. The restricted dataset consisted of 403 samples collected from 0 to 124 m water depth and containing approximately 240 000 individuals of 439 species in total.

The bathymetric preference of a species was estimated as the mean water depths across all sampling stations at which that species was found, weighted by the number of specimens at each of those stations. Because brackish habitats tend to be underrepresented in the ENEA database, this procedure may overestimate water depths of species reaching peak abundance in brackish conditions. The counts of both live and dead individuals were combined to assure that the calculated parameters reflect an environmental distribution of a species as would be observed in the fossil record. Preferred water depth was estimated for 72 out of 119 species (60.5%) recorded in the cores which were present at five or more sampling stations in the ENEA database.

(d) Analytical methods

We tested whether the time and pattern of extinctions can be correctly estimated from the stratigraphic record under a simple model of a random distribution of fossil occurrences and constant sampling probability (uniform recovery potential) through time [7,31]. As recently noted by Wang & Marshall [7], this class of probabilistic methods continue to dominate palaeontological analyses, including the most recent studies.

First, we used empirically calibrated resampling simulations to assess if the stratigraphic patterns in LOs observed in the cores deviate significantly from the patterns that would be expected under uniform recovery potential of fossils. We designed two null models. The first model assumes a random distribution of species and uniform sampling intensity throughout the stratigraphic succession. The second model relaxes the latter condition by allowing the sample size to vary according to the trends in fossil abundance actually observed in the cores. See the electronic supplementary material for the details of the resampling procedures.

Second, we applied several methods of testing for abrupt versus stepwise or gradual extinction patterns: (i) a simple graphical approach based on the relationship between stratigraphic abundance (proportion of samples in which a given species was observed) and position of LO [25], (ii) a likelihood-ratio test for the simultaneous extinction of all species [32], and (iii) a two-step algorithm estimating the number of extinction pulses [33] (see the electronic supplementary material for details). We evaluated the ability of those methods to correctly identify the single simultaneous extinction event in each of the studied cores.

Finally, to test how accounting for systematic variation in fossil occurrence rates affects estimates of extinction times, we compared the performance of two methods for calculating confidence intervals (CIs) on the position of stratigraphic range endpoints. The classical method of Strauss & Sadler [34] assumes uniform recovery potential of fossils, while its generalization [35] allows recovery potential to vary with stratigraphic position according to a predefined recovery function. Following procedures of Holland [36], we estimated sample-level collection probabilities for each species using multivariate ordination (see the electronic supplementary material). For species with at least four occurrences in a given core, we calculated 50% and 95% CIs using both methods and compared the proportion of taxa for which the estimated range endpoint fell below the topmost sample in the core (the extinction horizon in our hypothetical scenario). All analyses were performed in R [37].

3. Results

Out of 119 extant species recorded in the cores, only six (5%) reach the top of the sedimentary succession (i.e. our

hypothetical extinction horizon). Thus, taken at face value, the observed stratigraphic ranges would provide a strongly distorted record of the timing and pattern of extinctions (figure 1). Moreover, LOs do not follow a simple gradual pattern predicted by the Signor–Lipps effect [8,25]. Instead, LOs form distinct clusters, the number and stratigraphic position of which depend on the location of the core along the depositional profile (figures 1 and 2*a*).

In the two proximal cores, a major peak at 7–9.5 m core depth precedes the cluster of LOs corresponding to the hypothetical extinction horizon at the top of the cores (figures 1 and 2*a*). The older cluster occurs below the shift from lagoonal to swamp facies association and above a series of closely spaced centennial-scale flooding surfaces within the earliest HST (parasequence 4). In the core 205-S5, another cluster of LOs is located in the middle part of the TST (16–18 m; parasequence 2), which also consists of a set of centennial-scale units deposited in back-barrier settings. The same interval in core 204-S7, located further updip, records swamp and floodplain deposits mostly devoid of macrofossils (figure 1).

In the downdip cores, LOs are strongly clustered around the maximum flooding surface (MFS; figures 1 and 2*a*). This interval includes a metre-thick, highly fossiliferous transgressive sand sheet, recording a millennial-scale condensation, and, in its lower part, ecologically mixed (reworked) faunal assemblages [19,20]. The unit is capped by a thin veneer of offshore clays and silts recording the maximum water depths within the studied succession [26,38], followed by a thick package of sparsely fossiliferous prodelta muds. Above them, a smaller peak in LOs is located around the centennial-scale flooding surface within the HST (8.5–10.5 and 15.5–18 m in core 205-S9 and 205-S14, respectively; parasequence 7). This cluster precedes the onset of a progradation of the southern Po delta lobes (Spina and Volano) and deposition of coarser-grained delta front facies.

Combining fossil occurrences across the cores reduces the magnitude of range truncation: for 30 out of 64 species recorded in more than one core, the positions of their LOs shifted upward to a younger parasequence (electronic supplementary material, figure S2). However, even for data merged across all four cores, only 16 species (13%) reach the youngest parasequence 8, and 67 species (56%) do not range beyond the condensed interval around the MFS. Capturing the full extent of their stratigraphic ranges would require sampling of sections located even further downdip recording more offshore environments.

Given that all sampled species are still living in the region, truncations of their stratigraphic ranges must reflect incomplete sampling or change in the local habitat (i.e. facies shifts). Facies control on the stratigraphic distribution of LOs can be assessed using bathymetric preferences of individual species derived from independent surveys of recent benthic fauna. While shallow-water and brackish-tolerant species are recorded up to the very top of the cores, LOs of taxa preferring more offshore conditions are concentrated in the late TST and earliest HST (figure 2*b*). The disappearance of deeper-water species from the upper part of the sequence can be linked to the onset of a fast regional progradation during the HST (parasequences 7–8). In the two distal cores, this progradation led to deposition of a thick, shallowing-upward deltaic wedge [26] (electronic supplementary material, figure S1). The same shallowing trend is manifested in the two proximal cores by a reduction of marine influence in back-barrier settings.

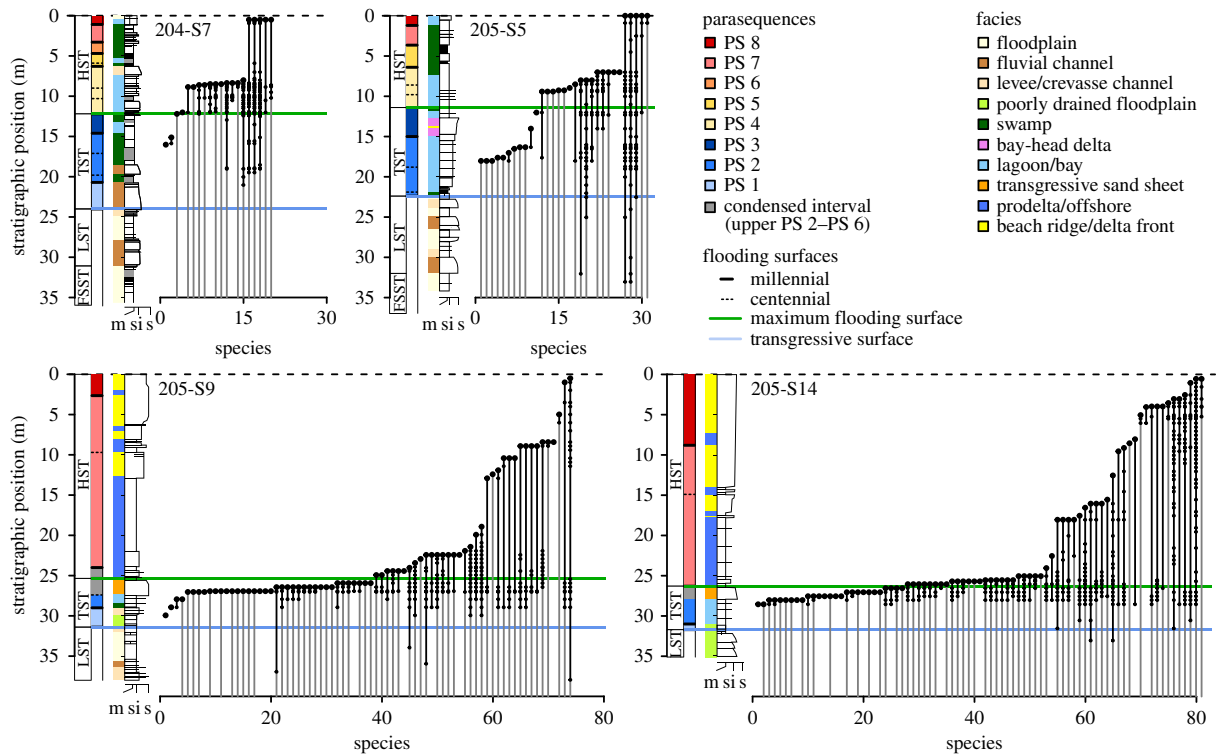


Figure 1. Stratigraphic ranges of extant mollusc species recorded in the proximal (cores 204-S7 and 205-S5, upper row) and distal (cores 205-S9 and 205-S14, lower row) parts of the Po coastal plain. Species are ordered according to their last occurrence below the hypothetical extinction horizon corresponding to the modern sediment surface (dashed horizontal line). Downward range extensions (marked in grey) are based on species occurrences in the underlying Late Pleistocene strata. Systems tracts, parasequences, facies associations and lithological logs are reported to the left of each range chart. Sequence stratigraphic interpretation follows Amorosi *et al.* [26]. FSST, falling stage systems tract; LST, lowstand systems tract; TST, transgressive systems tract, HST, highstand systems tract.

Systematic changes in fossil abundance represent another factor controlling the stratigraphic distribution of species. Because the volume of sediment sampled from each core interval was held constant, changes in shell density directly affect the number of specimens available for study and thus the likelihood of recording rare taxa. As a result, LOs of rare species should cluster in shell-rich horizons, where they are more likely to be sampled. Indeed, the position of LO clusters follows peaks in fossil abundance (figure 3*a,d*; electronic supplementary material, figures S3*a,d*).

The observed stratigraphic patterns in LOs depart significantly from the null model assuming both facies-independent distribution of species and uniform sampling intensity (model 1 in figure 3; electronic supplementary material, figure S3). Under those conditions, the probability of recording a given species depends only on its total abundance and remains constant throughout a core. In this model, the random truncation of stratigraphic ranges and differential sampling of rare versus common species lead to the classical Signor–Lipps pattern of downward smearing of LOs, stratigraphically manifested as a gradual decline in species diversity. By contrast, simulations incorporating vertical changes in fossil abundance always produce stepwise LOs patterns (model 2 in figure 3; electronic supplementary material, figure S3) and correctly predict the position and magnitude of many, though not all, LO clusters observed in the proximal cores. This suggests that some of the clusters of LOs can simply reflect a stratigraphic distribution of fossil-rich deposits. However, the distribution of LOs observed in the two distal cores is incongruent with the predictions of model 2. Variation in fossil abundance is thus insufficient to explain the position of LO clusters in these

cores underscoring the importance of facies control on the distribution of LOs.

Model 1 in our simulations corresponds to the assumption of uniform preservation and recovery of fossils that underlies many probabilistic methods for estimating the actual time or pattern of extinctions from fossil occurrences [7,31]. Such methods do not account for sequence stratigraphic control on LO patterns. The relationship between stratigraphic abundance and position of LOs [25] suggests two extinction pulses (electronic supplementary material, figure S4). False stepwise extinction patterns are also favoured by the maximum-likelihood estimates for the number of extinction pulses [33] (electronic supplementary material, figure S5), while the likelihood-ratio test [32] incorrectly rejects the hypothesis of simultaneous extinction of all species in three out of the four cores ($p = 0.17$ for core 205-S5 and $p < 0.001$ for the remaining cores). Because all species are extant, the CIs on their stratigraphic range endpoints should extend to the modern sedimentary surface. However, the classical method [34] based on the assumption of random fossil occurrence, systematically underestimates the extent of species ranges (electronic supplementary material, figure S6). Incorporation of facies-dependent occurrence probabilities derived from multivariate ordination [35,36] (electronic supplementary material, figures S8 and S9) reduces the bias in the estimates of extinction time (electronic supplementary material, figure S7). While the classical 95% CIs do not reach the top of the succession for 44%, 55%, 74% and 79% of species in core 205-S5, 204-S7, 205-S14 and 205-S9, application of the ordination-based CIs reduces these numbers to 0%, 12%, 52% and 23% of species, respectively.

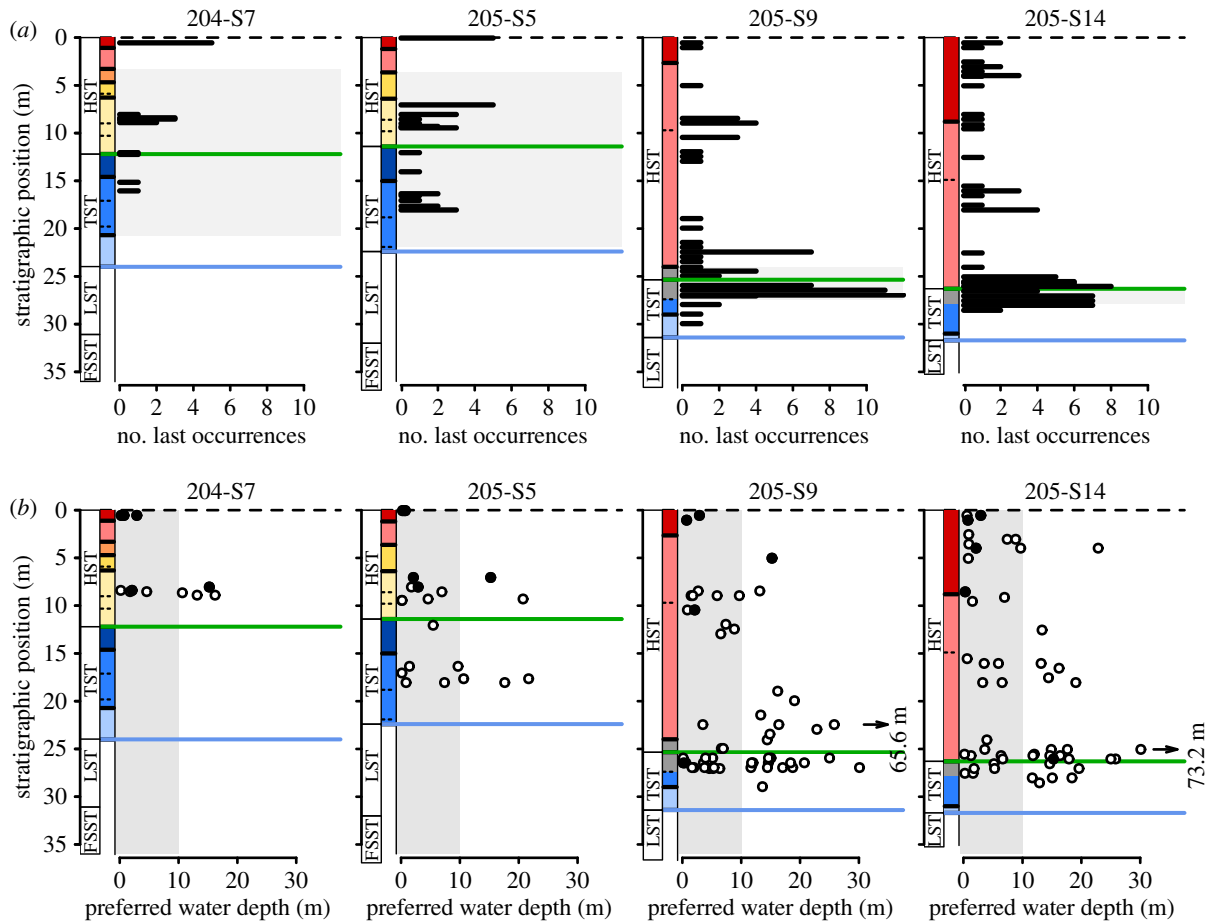


Figure 2. Clustering of LOs around the MFS (green line) associated with the disappearance of species preferring more offshore habitats. (a) The number of LOs observed at each sampled horizon. Grey rectangles delineate the stratigraphic interval isochronous with the strongly condensed portion of the two distal cores (the upper part of parasequence 2 to parasequence 6, see electronic supplementary material, figures S1 and S2). (b) Preferred water depth of mollusc species versus the stratigraphic position of their last occurrence. Water depths above the upper limit of the offshore transition zone (10 m) are marked in grey. Black points represent species reaching high abundance in brackish conditions. Arrows indicate outliers with much greater preferred water depth compared to the rest of the fauna. Note that several points representing different species can overlap. See figure 1 for the key to sequence stratigraphic units and parasequences.

4. Discussion

Non-random truncation of stratigraphic ranges of extant species observed in the Holocene strata of the Po Plain reveals pervasive effects of stratigraphic architecture on the distribution of LOs preserved in the fossil record. LOs of taxa tend to concentrate within intervals of stratigraphic condensation and strong facies shifts associated with flooding surfaces in the TST and lower HST (figures 1 and 2a). Literal reading of these patterns would falsely suggest a multiphase extinction event: a regionally synchronous interval of highly elevated extinction rates around the time of maximum marine ingression followed by smaller extinction pulses (figure 2a). Moreover, the relationship between the stratigraphic position of LOs and ecological affinities of species (figure 2b), if considered without a reference to the vertical facies changes, could be mistaken as a signature of habitat-selective extinction: early extinction of offshore taxa followed by a more protracted, stepwise decline of shallow-water and brackish fauna.

Such sequence stratigraphic control on the distribution of LOs, easy to identify in the Holocene strata, can severely hamper interpretations of more ancient records, especially when outcrop area is restricted to a narrow portion of a depositional profile, temporal resolution is low, and ecology of extinct taxa poorly known [10,21,22]. Because the nature and intensity of stratigraphic controls depend on the location along a

depositional profile, sequence architecture and tectonic setting [10,15,39], as well as on ecological and taphonomic characteristics of taxa [23,39–41], a variety of patterns in LOs can arise depending on the local context and taxonomic group under study. Indeed, contrasting interpretations of the number and timing of extinction pulses during the End-Permian mass extinction have been suggested to reflect different degrees to which sampling, facies control and stratigraphic incompleteness affect fossil occurrence patterns in individual sections [42].

The observed stratigraphic positions of LO clusters are consistent with the predictions of numerical simulations that modelled fossil occurrences as a function of bathymetry-dependent distribution of taxa and sequence stratigraphic architecture [10]. This agreement indicates that the effects of stratigraphic controls can be deduced from basic ecological and sequence stratigraphic principles, even when the models and empirical systems are only partly compatible. Whereas the numerical models simulated deposition over 10^6 – 10^7 years [10,12,14,39], the investigated succession represents only the last approximately 12 000 years. However, when considered in terms of the spatial extent, thickness of the strata, stratigraphic architecture and amplitude of the eustatic sea-level change, the studied succession is comparable to higher-order depositional sequences formed over much longer time scales. Consequently, the Quaternary fossil record of the Po Plain can serve as a good analogue for the field- or

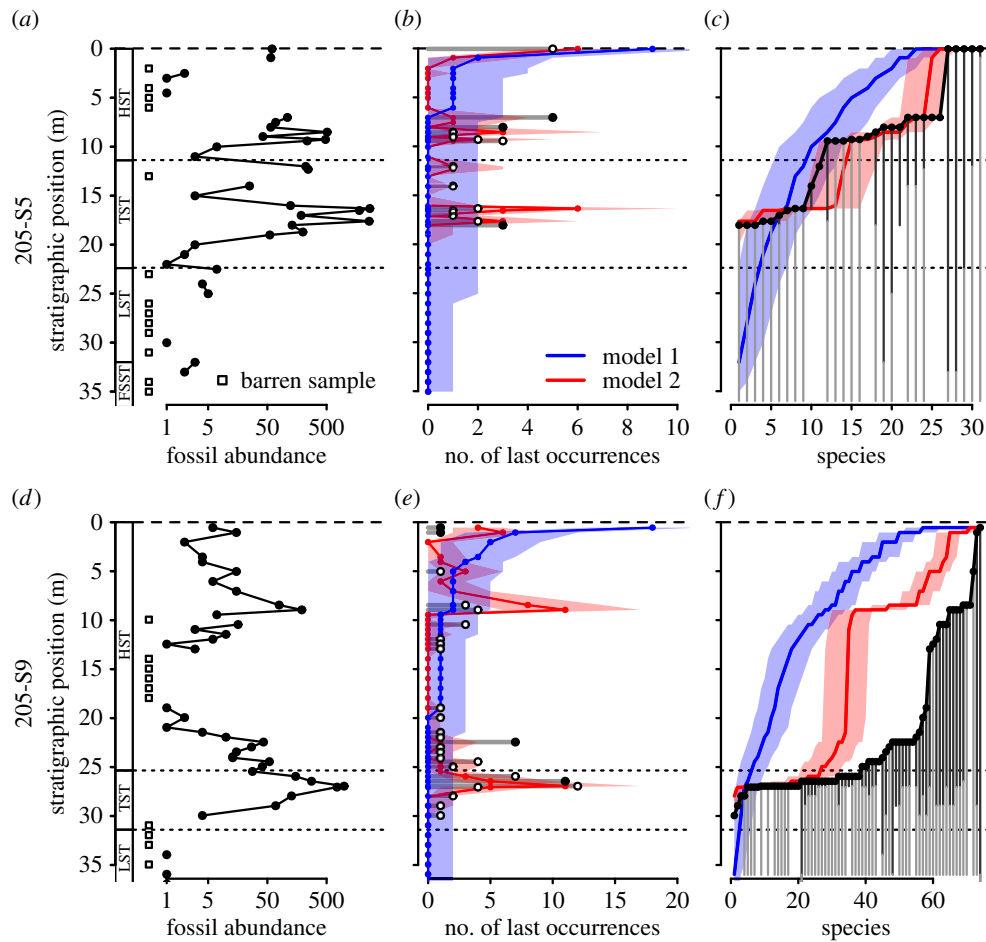


Figure 3. (a,d) Stratigraphic trends in fossil abundance (number of identifiable specimens per sample), and the results of two resampling models for (b,e) the expected number of LOs and (c,f) distribution of LOs (stratigraphic range endpoints) in cores (a–c) 205-S5 and (d–f) 205-S9. Model 1 assumes random distribution of species and uniform sampling. Model 2 also assumes random distribution of species but incorporates changes in fossil abundances observed throughout the cores. See the electronic supplementary material for details. Thick colour lines represent median values across 10 000 iterations and shading denotes 95% CIs. Filled black dots in (b) and (e) indicate the observed number of LOs that is significantly different from the number predicted for that stratigraphic position by either of the models. See figure 1 for the key to sequence stratigraphic units.

core-based mass extinction studies. Likewise, the discrepancy between the time interval covered by this study and typical species duration in molluscs (10^6 – 10^7 years) does not affect the results. Owing to its short temporal scale, the studied Holocene system is not affected by background extinctions, explicitly incorporated in the numerical models. Therefore, the observed clustering of LOs is produced solely by non-random truncation of stratigraphic ranges below a single mass extinction event (the modern sediment surface in our study). According to the models [10,12,13], the same types of sequence stratigraphic surfaces, at which these clusters were recorded, are expected to accumulate LOs of taxa even when extinction rate is constant through time. Consequently, the stratigraphic record of a mass extinction should be distorted even more severely in sedimentary successions spanning longer time scales, because LOs of the actual victims of a mass extinction would be clustered together with LOs of species that went extinct prior or after the event [10].

The stratigraphic distribution of species in Po Plain cores is controlled by both changes in depositional environments and vertical trends in fossil density. The first factor determines the composition of fossil assemblages that can be sampled at any given horizon, the second factor constrains the available sample size. Changes in environmental conditions and in fossil density are both driven by responses of sedimentary

systems to relative sea-level changes and are thus closely correlated: stratigraphic intervals marked by strong facies shifts and faunal turnover represent horizons where net sedimentation rates are reduced and skeletal accumulations are more likely to form [17,18,20]. Clustering of LOs at these horizons results from the combined effects of (i) direct environmental control on species distribution and hard part production rates, and (ii) taphonomic and sedimentary processes underlying formation and preservation of fossil concentrations.

Shell-rich beds should on average capture a greater share of the regional species pool relative to shell-poor strata, even if regional diversity remains stable through time and sample size is held constant. This inflation in sample-level richness is expected due to effects of higher time-averaging [43,44], positive feedback between bioclast accumulation and local epibenthic diversity [45,46] and enhanced preservation potential of skeletal elements [47]. This interplay between facies control and sampling bias is illustrated by the prominent peak in LOs bracketing the MFS in the two distal cores (figure 2a). Owing to environmental condensation [19,20], LOs of both offshore and shallow-water species are clustered together in this interval (figure 2b). The disappearance of offshore species results from the subsequent shallowing, while the concentration of LOs of shallow-water forms reflects over-sampling of rare species due to high fossil densities.

Our null models suggest that even in a highly unlikely scenario of identical environmental preferences of all species, non-random stratigraphic distribution of skeletal concentrations can produce clusters of LOs that mimic sudden or stepwise extinction patterns (model 2 in figure 3). Thus, distinct patterns in LOs can result solely from changes in fossil abundance produced by stratigraphic variation in sedimentation rates, fossil preservation and habitat-dependent hard part production rates, all of which can be controlled by stratigraphic architecture. In other words, rather than being uniform and randomly distributed, the effects of sampling are closely tied to the stratigraphic architecture and covary with patterns caused by facies changes. More intensive collecting effort concentrated only around the postulated extinction horizon is thus unlikely to mitigate the problem.

In contrast to our results, Meldahl [25] observed the classic gradual pattern of LOs produced by the Signor–Lipps effect in cores taken from a tidal channel in Bahia la Choya, northern Gulf of California. However, the 70-cm-long cores used in that study captured a single facies association and remained fossiliferous throughout their length. Our numerical simulations (model 1 in figure 3) show that gradual backward smearing of LOs below the extinction horizon would occur only under assumptions of (i) continuous and uniform sampling, and (ii) facies-independent distribution of species or constant environment through time. Such ideal conditions, translating to uniform recovery potential of fossil, are unrealistic in sedimentary successions deposited over time scales relevant for mass extinction studies [11]. Yet methods based on this simplifying assumption are still widely used to infer timing of extinctions from stratigraphic data [7]. Such methods fail to correctly reconstruct the actual extinction pattern among investigated mollusc species (electronic supplementary material, figures S4–S6), demonstrating that accounting for random sampling alone is not enough to avoid the effects of stratigraphic controls on LOs.

Systematic changes in occurrence rates and sampling probabilities of fossil are the rule rather than exception [13,48]. As a result, reliance on statistical procedures that account for the incomplete fossil record by assuming a uniform recovery potential of fossils can lead to incorrect inferences on the timing and mode of mass extinction events. Methods that relax this unrealistic assumption (e.g. [49,50]) or incorporate independent information on facies-specific occurrence rates and/or sampling effort [35,36,51] may provide more reliable estimates of extinction times, as demonstrated by our results (electronic supplementary material, figure S7). However, datasets restricted to individual outcrops or local composite sections are unlikely to fully capture an environmental and stratigraphic distribution of a taxon (electronic supplementary material, figure S2), while extrapolation of locally observed patterns to regional or global scales is problematic [23]. Combining data from multiple sections spanning different basins and depositional environments may reduce the effects of facies and sampling [42]. Such analyses cannot rely on biostratigraphic correlations, as important index fossil groups are not immune to the effects of stratigraphic architecture [22,23].

Overcoming sequence stratigraphic controls on fossil occurrence, although challenging, is not impossible [15,23,52,53]. Several strategies for distinguishing extinction-generated pulses of LOs from those produced by stratigraphic architecture have been suggested [10]: (i) clusters of LOs not associated with

sequence stratigraphic surfaces are likely to reflect elevated extinction rates; (ii) data from positionally updip or downdip sections can verify if a locally observed LOs correspond to the actual extinctions rather than facies-related disappearances; and (iii) fossil assemblages from environmentally equivalent strata located below and above a postulated extinction pulse can be compared to test if the extinction rates across this interval exceed background extinction rates. Also, multivariate analyses can be used to compare the magnitude of faunal turnover across the postulated event to the variation in assemblage composition that is expected from changes in depositional environments or stacking patterns [23]. Novel quantitative approaches for estimating environmental affinity of fossil taxa [53,54] should further increase our ability to disentangle consequences of mass extinction events from ecological responses to lateral habitat migration.

5. Conclusion

Stratigraphic distribution of extant species demonstrates that interactions between ecological preferences of organisms and processes of sediment accumulation produce systematic changes in occurrence rates and sampling probabilities of taxa along a sedimentary succession. The resulting non-random truncation of stratigraphic ranges leads to clustering of LOs at specific sequence stratigraphic positions distorting the relative chronology of species extinctions. Such patterns can easily confound interpretations of the timing, duration and ecological selectivity of mass extinction events. Importantly, the effects of these eco-stratigraphic processes cannot be removed by methods that correct the Signor–Lipps effect under a model of uniform preservation and recovery of fossils.

Research strategies that account for the effects of stratigraphic architecture are data-intensive and rely on placing fossil occurrences in a rigorous palaeoenvironmental and sequence stratigraphic framework. They also typically require integration of data across multiple sections or sedimentary basin, thus often sacrificing temporal and spatial resolution. These challenges imposed by the nature of the stratigraphic record must be acknowledged and addressed before high-resolution reconstructions of past extinction dynamics are attempted. However, more conservative interpretations of the stratigraphic distribution of fossil taxa will maximize the accuracy of palaeobiological interpretations and reduce the risk of using false extinction patterns to formulate and test eco-evolutionary hypotheses.

Data accessibility. The dataset and R code supporting this article are deposited at Dryad Digital Repository: <http://dx.doi.org/10.5061/dryad.j9c15ff> [55].

Authors' contributions. R.N., D.S. and M.K. designed the study; D.S., M.A., T.A.D., K.M.K., J.M.W., M.K. and A.A. collected the data; A.A. and D.S. provided sequence stratigraphic interpretations; R.N. analysed the data; R.N., D.S. and M.K. wrote the paper.

Competing interests. We declare we have no competing interests.

Funding. The study was supported by the NSF grant nos. EAR-0920075 and EAR-1559196.

Acknowledgements. We thank E. Jarochowska and A. Tomašových for numerous discussions, L. Bruno and B. Campo for sharing their unpublished data on the stratigraphy of the Po Plain, and R. W. Portell for curation of the mollusc samples used in this study. We are grateful to S. Holland and M. Aberhan for multiple suggestions that greatly improved this paper.

References

- Marshall CR, Ward PD. 1996 Sudden and gradual molluscan extinctions in the latest Cretaceous of western European Tethys. *Science* **274**, 1360–1363. (doi:10.1126/science.274.5291.1360)
- Jin YG, Wang Y, Wang W, Shang QH, Cao CQ, Erwin DH. 2000 Pattern of marine mass extinction near the Permian–Triassic boundary in South China. *Science* **289**, 432. (doi:10.1126/science.289.5478.432)
- Song H, Wignall PB, Tong J, Yin H. 2013 Two pulses of extinction during the Permian–Triassic crisis. *Nat. Geosci.* **6**, 52–56. (doi:10.1038/ngeo1649)
- Witts JD, Whittle RJ, Wignall PB, Crame JA, Francis JE, Newton RJ, Bowman VC. 2016 Macrofossil evidence for a rapid and severe Cretaceous–Paleogene mass extinction in Antarctica. *Nat. Commun.* **7**, 11738. (doi:10.1038/ncomms11738)
- Bond DPG, Wignall PB, Joachimski MM, Sun Y, Savov I, Grasby SE, Beauchamp B, Blomeier DPG. 2015 An abrupt extinction in the Middle Permian (Capitanian) of the Boreal Realm (Spitsbergen) and its link to anoxia and acidification. *GSA Bull.* **127**, 1411–1421. (doi:10.1130/B31216.1)
- He W-H *et al.* 2015 Late Permian marine ecosystem collapse began in deeper waters: evidence from brachiopod diversity and body size changes. *Geobiology* **13**, 123–138. (doi:10.1111/gbi.12119)
- Wang SC, Marshall CR. 2016 Estimating times of extinction in the fossil record. *Biol. Lett.* **12**, 20150989. (doi:10.1098/rsbl.2015.0989)
- Signor PW, Lipps JH. 1982 Sampling bias, gradual extinction patterns and catastrophes in the fossil record. *Geol. Soc. Am. Spec. Pap.* **190**, 291–296. (doi:10.1130/SPE190-p291)
- Raup DM. 1986 Biological extinction in earth history. *Science* **231**, 1528–1533. (doi:10.1126/science.11542058)
- Holland SM, Patzkowsky ME. 2015 The stratigraphy of mass extinction. *Palaeontology* **58**, 903–924. (doi:10.1111/pala.12188)
- Cataneanu O. 2006 *Principles of sequence stratigraphy*. New York, NY: Elsevier.
- Holland SM. 1995 The stratigraphic distribution of fossils. *Paleobiology* **21**, 92–109. (doi:10.1017/S0094837300013099)
- Holland SM. 2000 The quality of the fossil record: a sequence stratigraphic perspective. *Paleobiology* **26**, 148–168. (doi:10.1666/0094-8373(2000)26[148:TQOTFR]2.0.CO;2)
- Holland SM, Patzkowsky ME. 1999 Models for simulating the fossil record. *Geology* **27**, 491–494. (doi:10.1130/0091-7613(1999)027<0491:MFSTFR>2.3.CO;2)
- Patzkowsky ME, Holland SM. 2012 *Stratigraphic paleobiology: understanding the distribution of fossil taxa in time and space*. Chicago, IL: University of Chicago Press.
- Zecchin M, Cataneanu O. 2013 High-resolution sequence stratigraphy of clastic shelves I: Units and bounding surfaces. *Mar. Pet. Geol.* **39**, 1–25. (doi:10.1016/j.marpetgeo.2012.08.015)
- Kidwell SM. 1991 The stratigraphy of shell concentrations. In *Taphonomy: releasing the data locked in the fossil record* (eds PA Allison, DEG Briggs), pp. 211–290. New York, NY: Plenum Press.
- Brett CE. 1995 Sequence stratigraphy, biostratigraphy, and taphonomy in shallow marine environments. *Palaios* **10**, 597. (doi:10.2307/3515097)
- Scarponi D, Kaufman D, Amorosi A, Kowalewski M. 2013 Sequence stratigraphy and the resolution of the fossil record. *Geology* **41**, 239–242. (doi:10.1130/G33849.1)
- Scarponi D, Azzarone M, Kusnerik K, Amorosi A, Bohacs KM, Drexler TM, Kowalewski M. 2017 Systematic vertical and lateral changes in quality and time resolution of the macrofossil record: insights from Holocene transgressive deposits, Po coastal plain, Italy. *Mar. Pet. Geol.* **87**, 128–136. (doi:10.1016/j.marpetgeo.2017.03.031)
- Smith AB, Gale AS, Monks NEA. 2001 Sea-level change and rock-record bias in the Cretaceous: a problem for extinction and biodiversity studies. *Paleobiology* **27**, 241–253. (doi:10.1666/0094-8373(2001)027<0241:SLCARR>2.0.CO;2)
- Jarochowska E, Munnecke A. 2016 Late Wenlock carbon isotope excursions and associated conodont fauna in the Podlasie Depression, eastern Poland: a not-so-big crisis? *Geol. J.* **51**, 683–703. (doi:10.1002/gj.2674)
- Jarochowska E, Ray DC, Röstel P, Worton G, Munnecke A. 2018 Harnessing stratigraphic bias at the section scale: conodont diversity in the Homerian (Silurian) of the Midland Platform, England. *Palaeontology* **61**, 57–76. (doi:10.1111/pala.12326)
- Peters SE. 2006 Genus extinction, origination, and the durations of sedimentary hiatuses. *Paleobiology* **32**, 387–407. (doi:10.1666/05081.1)
- Meldahl KH. 1990 Sampling, species abundance, and the stratigraphic signature of mass extinction: a test using Holocene tidal flat molluscs. *Geology* **18**, 890–893. (doi:10.1130/0091-7613(1990)018<0890:SSAATS>2.3.CO;2)
- Amorosi A, Bruno L, Campo B, Morelli A, Rossi V, Scarponi D, Hong W, Bohacs KM, Drexler TM. 2017 Global sea-level control on local parasequence architecture from the Holocene record of the Po Plain, Italy. *Mar. Pet. Geol.* **87**, 99–111. (doi:10.1016/j.marpetgeo.2017.01.020)
- Amorosi A, Maselli V, Trincardi F. 2016 Onshore to offshore anatomy of a late Quaternary source-to-sink system (Po Plain–Adriatic Sea, Italy). *Earth-Sci. Rev.* **153**, 212–237. (doi:10.1016/j.earscirev.2015.10.010)
- Bruno L, Bohacs KM, Campo B, Drexler TM, Rossi V, Sammartino I, Scarponi D, Hong W, Amorosi A. 2017 Early Holocene transgressive palaeogeography in the Po coastal plain (northern Italy). *Sedimentology* **64**, 1792–1816. (doi:10.1111/sed.12374)
- Kowalewski M, Wittmer JM, Dexter TA, Amorosi A, Scarponi D. 2015 Differential responses of marine communities to natural and anthropogenic changes. *Proc. R. Soc. Lond. B* **282**, 20142990. (doi:10.1098/rspb.2014.2990)
- Bedulli D, Bassignani F, Bruschi A. 2002 Use of biodiversity hotspots for conservation of marine molluscs: a regional approach. *Mediterr. Mar. Sci.* **3**, 113–121. (doi:10.12681/mms.250)
- Marshall CR. 2010 Using confidence intervals to quantify the uncertainty in the end-points of stratigraphic ranges. *Paleontol. Soc. Pap.* **16**, 291–316. (doi:10.1017/S1089332600001911)
- Wang SC, Everson PJ. 2007 Confidence intervals for pulsed mass extinction events. *Paleobiology* **33**, 324–336. (doi:10.1666/06056.1)
- Wang SC, Zhong L. 2018 Estimating the number of pulses in a mass extinction. *Paleobiology* **44**, 199–218. (doi:10.1017/pab.2016.30)
- Strauss D, Sadler PM. 1989 Classical confidence intervals and Bayesian probability estimates for ends of local taxon ranges. *Math. Geol.* **21**, 411–427. (doi:10.1007/BF00897326)
- Marshall CR. 1997 Confidence intervals on stratigraphic ranges with nonrandom distributions of fossil horizons. *Paleobiology* **23**, 165–173. (doi:10.1017/S0094837300016766)
- Holland SM. 2003 Confidence limits on fossil ranges that account for facies changes. *Paleobiology* **29**, 468–479. (doi:10.1666/0094-8373(2003)029<0468:CLOFRT>2.0.CO;2)
- R Core Team. 2018 *R: a language and environment for statistical computing*. Version 3.4.4. Vienna, Austria: R Foundation for Statistical Computing. See <http://www.Rproject.org>.
- Scarponi D, Kowalewski M. 2004 Stratigraphic paleoecology: bathymetric signatures and sequence overprint of mollusk associations from upper Quaternary sequences of the Po Plain, Italy. *Geology* **32**, 989–992. (doi:10.1130/G20808.1)
- Holland SM, Patzkowsky ME. 2002 Stratigraphic variation in the timing of first and last occurrences. *Palaios* **17**, 134–146. (doi:10.1669/0883-1351(2002)017<0134:SVITTO>2.0.CO;2)
- Carlucci JR, Westrop SR. 2015 Trilobite biofacies and sequence stratigraphy: an example from the Upper Ordovician of Oklahoma. *Lethaia* **48**, 309–325. (doi:10.1111/let.12107)
- Wittmer JM, Dexter TA, Scarponi D, Amorosi A, Kowalewski M. 2014 Quantitative bathymetric models for late Quaternary transgressive–regressive cycles of the Po Plain, Italy. *J. Geol.* **122**, 649–670. (doi:10.1086/677901)
- Wang Y, Sadler PM, Shen S, Erwin DH, Zhang Y, Wang X, Wang W, Crowley JL, Henderson CM. 2014 Quantifying the process and abruptness of the end-Permian mass extinction. *Paleobiology* **40**, 113–129. (doi:10.1666/13022)
- Scarponi D, Kowalewski M. 2007 Sequence stratigraphic anatomy of diversity patterns: Late Quaternary benthic

- mollusks of the Po Plain, Italy. *Palaios* **22**, 296–305. (doi:10.2110/palo.2005.p05-020r)
44. Tomašových A, Kidwell SM. 2010 Predicting the effects of increasing temporal scale on species composition, diversity, and rank-abundance distributions. *Paleobiology* **36**, 672–695. (doi:10.1666/08092.1)
45. Kidwell SM, Jablonski D. 1983 Taphonomic feedback: ecological consequences of shell accumulation. In *Biotic interactions in recent and fossil benthic communities* (eds MJ Tavesz, PL McCall), pp. 195–248. New York, NY: Plenum Press.
46. Gutiérrez JL, Jones CG, Strayer DL, Iribarne OO. 2003 Mollusks as ecosystem engineers: the role of shell production in aquatic habitats. *Oikos* **101**, 79–90. (doi:10.1034/j.1600-0706.2003.12322.x)
47. Tomašových A, Schlögl J. 2008 Analyzing variations in cephalopod abundances in shell concentrations: the combined effects of production and density-dependent cementation rates. *Palaios* **23**, 648–666. (doi:10.2110/palo.2008.p08-033r)
48. Holland SM. 2016 The non-uniformity of fossil preservation. *Phil. Trans. R. Soc. B* **371**, 20150130. (doi:10.1098/rstb.2015.0130)
49. Roberts DL, Solow AR. 2003 Flightless birds: when did the dodo become extinct? *Nature* **426**, 245. (doi:10.1038/426245a)
50. Wang SC, Everson PJ, Zhou HJ, Park D, Chudzicki DJ. 2016 Adaptive credible intervals on stratigraphic ranges when recovery potential is unknown. *Paleobiology* **42**, 240–256. (doi:10.1017/pab.2015.37)
51. Labandeira CC, Johnson KR, Wilf P. 2002 Impact of the terminal Cretaceous event on plant–insect associations. *Proc. Natl. Acad. Sci. USA* **99**, 2061–2066. (doi:10.1073/pnas.042492999)
52. Zuschin M, Harzhauser M, Mandic O. 2011 Disentangling palaeodiversity signals from a biased sedimentary record: an example from the Early to Middle Miocene of Central Paratethys Sea. *Geol. Soc. Lond. Spec. Publ.* **358**, 123–139. (doi:10.1144/SP358.9)
53. Sheets HD, Mitchell CE, Melchin MJ, Loxton J, Štorch P, Carlucci KL, Hawkins AD. 2016 Graptolite community responses to global climate change and the Late Ordovician mass extinction. *Proc. Natl. Acad. Sci. USA* **113**, 8380–8385. (doi:10.1073/pnas.1602102113)
54. Myers CE, Stigall AL, Lieberman BS. 2015 PaleoENM: applying ecological niche modeling to the fossil record. *Paleobiology* **41**, 226–244. (doi:10.1017/pab.2014.19)
55. Nawrot R, Scarponi D, Azzarone M, Dexter TA, Kusnerik KM, Wittmer JM, Amorosi A, Kowalewski M. 2018 Data from: Stratigraphic signatures of mass extinctions: ecological and sedimentary determinants. Dryad Digital Repository. (<http://dx.doi.org/10.5061/dryad.j9c15ff>)

Manuscript 3 Online Supplementary Material

Stratigraphic signatures of mass extinctions: ecological and sedimentary determinants

Supplementary materials and methods

1. Geological setting

Many previous studies describe in detail the stratigraphic architecture of the Po-Adriatic Sea systems, especially for the latest Quaternary (e.g., [1–8]). Here we provide a brief outline focused only on the main stratigraphic features of the targeted area. For an in-depth discussion of stratal geometries and environmental evolution of the investigated succession, we refer to the above-mentioned papers and references therein.

The Pliocene-Quaternary sedimentary infill of the basin beneath the Po coastal plain is >7 km thick and records a stacking of 3rd order tectono-stratigraphic sequences bounded by major unconformities, each representing a major event of deformation related to the structuring of the Apennine foredeep [7,9]. High-resolution studies of the latest Quaternary succession of the study region [10,11] documented a set of higher frequency (4th order) wedge-shaped packages of strata, in which internal organization was interpreted as being driven primarily by glacio-eustatic changes. Within the study area, the topmost 40-m-thick succession has been interpreted to represent the Last Glacial Maximum (LGM) depositional sequence [3]. The sequence boundary was placed at a notable paleosol developed at the beginning of the last maximum glacial phase (<34 ka cal BP [2]). The lowstand systems tract (LST) is mainly composed of laterally extensive sand fluvial bodies associated with pedogenically modified floodplain deposits. The onset of an overall retrogradational stacking pattern (represented by a vertical transition from coastal to marginal marine facies) highlights the transgressive surface (TS) or maximum regressive surface. The TS, being associated with a weakly developed palaeosol attributed to the Younger Dryas cold spell, is the most distinct surface that can be recognized regionally in cores [8]. Above the TS, the Holocene deposits of the Po coastal plain record a transgressive-regressive, wedge-shaped succession, recently subdivided into a series of centennial units embedded within eight millennial-scale depositional units (parasequences in [3]). Parasequences 1 to 3 show a distinct retrogradational stacking pattern of alluvial to estuarine and marginal marine depositional systems in tune with a stepped post-glacial eustatic sea-level rise. Parasequences 4 to 8, in turn, are characterized by a multifaceted and aggradational to increasingly progradational pattern of coastal/deltaic depositional systems. The maximum flooding surface (MFS), marking the turnaround between transgressive and normal regressive stacking patterns, is interpreted to be at the base of parasequence 4 ([3]; figure S1)

To track the lateral variation in the stratigraphic distribution of species along the depositional dip and strike, we focused on four cores forming a 35-km-long L-shaped transect across the southern Po Plain (figure S1). The two proximal (updip) cores (204-S7 and 205-S5) located in proximity to the maximum extent of Holocene marine ingressions are dominated by floodplain, coastal swamp and brackish (lagoon/bay) facies associations. The downdip cores (205-S9 and 205-S14) represent a more distal setting, ~18 km seaward from the shoreline during the maximum ingressions, and record transition from brackish, through nearshore to shallow-marine depositional environments.

2. Resampling models

We designed two null models aimed at separating the effects of random range truncations, stratigraphic trends in fossil abundance, and facies control on species occurrence. The first model makes two assumptions: random distribution of species and uniform sampling intensity (constant number of individuals sampled per horizon) throughout the stratigraphic succession. The second model relaxes the second of those assumptions by allowing the sample size to vary vertically

according to the trends in fossil abundance actually observed in the cores. The assumption of random distribution of fossils made by both models corresponds to a scenario in which either (1) the probability of species occurrence is uniform across all facies (i.e. species lack any environmental preferences and their preservation potential is the same in all environments), or (2) sedimentary environment remains constant through time.

For both models, all samples in a given core were first pooled together. For each core depth corresponding to an actually sampled horizon, a random sample of individuals was taken from the pool without replacement, while preserving their species identities. In the first model, the number of randomly drawn individuals was constant and equal to the average sample size in the core. In the second model, the number of specimens was set to be the same as actually observed at the particular core depth. Such random samples were assigned to all horizons sampled in the core. The simulated dataset was then used to construct a range chart and identify the stratigraphic positions of LOs for each species. This procedure was repeated 10,000 times. Repeated simulations indicated that analytical outcomes were highly reproducible at 10,000 iterations.

The number of LOs that was actually observed at each sampled stratigraphic horizon was compared to the median number of LOs at that depth calculated across all resampling iterations. The corresponding 95% confidence intervals were calculated using the percentile method [12]. The observed pattern of stratigraphic range end-points was compared to the null expectation by first ranking all species in simulated range charts according to their LOs and then calculating for each rank the median core depth at which the LO occurred together with corresponding 95% confidence intervals.

3. Inferring time and pattern of extinctions from fossil occurrences

We tested whether the effects of sequence-stratigraphic controls can be removed by methods that correct for the Signor–Lipps effect by estimating the time or pattern of extinctions from fossil occurrences under a simple model of uniform preservation and recovery of taxa. As noted by Wang & Marshall [13], this class of probabilistic methods continue to dominate palaeontological analyses, including the most recent studies. Whereas several methods relaxing the assumption of uniform fossil recovery has been proposed (e.g., [14–18]), they remain rarely used in empirical studies [13]. A systematic evaluation of different statistical approaches used to estimate times of extinction from stratigraphic data is beyond the scope of our study (see reviews in [13,19]).

(a) Assessing the pattern of extinctions. We applied a simple graphical method proposed by Meldahl [20] to distinguish between gradual, stepwise, and sudden extinction patterns based on the relationship between stratigraphic abundance and position of LO (figure S4). Stratigraphic abundance is the proportion of stratigraphic intervals (core samples in our case) in which a given species was observed. Because the magnitude of artificial truncation of stratigraphic ranges is likely to be smaller for common taxa (i.e., those with high stratigraphic abundance), their LOs should better approximate the stratigraphic positions of extinction events. Simulations suggest that gradual, stepwise, and sudden extinction pattern produce different graphical relations between stratigraphic abundance and LO [20]. This method implicitly assumes that probability of collecting a taxon is constant throughout a stratigraphic section. However, if a given species is tied to a specific facies, both its stratigraphic abundance and the position of the LO may primarily reflect the stratigraphic distribution of that facies.

We supplement the qualitative approach of Meldahl [20] with a formal test of the null hypothesis of the simultaneous extinction of all species using the likelihood ratio test of Wang and Everson [21]. The null hypothesis is true in our hypothetical scenario: given that all species found in the cores are known to be extant in the region, their true stratigraphic range-end points correspond to the modern sedimentary surface. We also applied the recently proposed generalization of this method [22],

which directly estimates the number of extinction pulses. In both cases, species recorded only once in a given core were excluded prior to the analyses. For each core, we calculated the relative support for extinction scenarios ranging from a single (i.e., simultaneous extinction) to five extinction pulses (figure S5) using the original R code provided in the supplementary material to Wang and Zhong's [22] paper.

The two-step algorithm of Wang and Zhong [22], first determines the maximum likelihood estimate (MLE) for each possible number of pulses. In the second step, MLEs for different number of pulses are compared using Akaike information criterion (AIC) and Bayesian information criterion (BIC). To increase the accuracy of the estimated number of pulses, a k -nearest neighbour classifier is applied to the set of AIC and BIC weights (see [22] for details). The algorithm predicts the number of extinction pulses most consistent with the observed fossil occurrences under the assumption of uniform preservation and recovery of fossils throughout the extent of their stratigraphic ranges. It also estimates the confidence level associated with each number of pulses, which can be interpreted as posterior probabilities in Bayesian framework.

(b) Confidence limits on stratigraphic ranges. We compared the performance of two methods for calculating confidence intervals on the position of the true end-points of stratigraphic ranges: the classical method of Strauss and Sadler [23], which assumes random occurrence and thus constant sampling probability of fossil, and its generalization [15], which allows recovery potential to vary with stratigraphic position according to a predefined recovery function. We estimated species recovery functions using multivariate ordination [24] (see below). For species with at least four occurrences in a given core, we calculated 50% and 95% confidence intervals using both methods (figures S6 and S7) and compared the proportion of taxa for which the estimated range end-point fell below the topmost sample in the core (the extinction horizon in our hypothetical scenario). We calculated the stratigraphic length (measured in thickness of strata) of the confidence interval (r_c) as a fraction (α) of the observed stratigraphic range (R) [19,23]:

$$r_c = \alpha R \quad (1)$$

This fraction depends on the number of horizons at which a taxon was found (H) and on the chosen confidence level (C) [23]:

$$\alpha = (1 - C)^{-1/(H-1)} - 1 \quad (2)$$

As demonstrated by Marshall [15], equation (1) can be generalized as the relationships between the probability of collecting a taxon within its known stratigraphic range (R) and the probability of observing it within a distance (r_c) beyond that range. These probabilities can be expressed as integrals of the fossil recovery potential curve [15]:

$$\int_b^{b+r_c} f(h) dh = \alpha \int_a^b f(h) dh \quad (3)$$

where a is the stratigraphic position of the first occurrence of a taxon, b is the position of the LO, α is given by equation (2), and $f(h)$ is the density distribution function of fossil recovery potential, i.e. the function describing how the probability of collecting a taxon varies with stratigraphic position. Calculation of generalized confidence intervals requires establishing fossil recovery potential of a species. Following Holland [24], we estimated sample-level collection probabilities for each species using a multivariate ordination technique, detrended correspondence analysis (DCA). DCA places samples and species in the same ordination space in a way that maximizes the compositional variation in the dataset along the first ordination axis. DCA axis 1 scores can be thus considered as a measure of the relative position of samples along the primary environmental gradient controlling taxonomic composition of the assemblages. In marine settings axis 1 usually corresponds to water depth and environmental variables that are correlated with it [25,26]. Parameters of species response curves, which describe how the probability of collecting a given species changes along this

gradient, can be estimated from DCA results using a simple Gaussian model [24,27,28]. The model is based on three parameters: preferred environment (PE; mean of the Gaussian curve), environmental tolerance (ET; standard deviation of the Gaussian curve), and peak abundance of a species (PA; the probability of finding the species at its PE represented by the height of Gaussian curve). PE can be estimated by the DCA axis 1 score of the species, ET by the standard deviation of axis 1 scores of all samples containing the species, and PA by the proportion of samples in which the species was found located within one ET of the PE of that species (see [24] for further details).

DCA ordination of the total dataset was performed with R package “vegan” [29]. Prior to the analysis, samples that were devoid of fossils or contained only a single species, as well as species occurring in only one sample were removed [28], resulting in the dataset containing 83 species and 143 samples. The relative abundance data were log-transformed to down-weight the effects of very abundant species. In the resulting DCA ordination samples tend to be distributed along axis 1, according to their position along the onshore-offshore gradient (figure S8). Specifically, samples representing swamp and lagoon/bay facies associations tend to have negative axis 1 scores, beach ridge/delta front samples have intermediate scores, and prodelta and offshore transition samples have high axis 1 scores. Higher axis 1 scores can be thus interpreted as indicating an increase in marine influence and/or water depths. Moreover, axis 1 scores of species are positively correlated with their preferred water depth ($r = 0.50$; 95% confidence interval: 0.28–0.68; $P < 0.001$). The correlation is weaker than observed in the previous quantitative bathymetric models for Po Plain Quaternary succession [4,11]. This reflects our focus on species rather than genera (used in the previous studies), inclusion of rare taxa, and a large share of samples from the proximal cores (204-S7 and 205-S5). These onshore cores capture predominately floodplain and back-barrier habitats, in which assemblage composition is controlled by environmental factors that can be poorly correlated with water depth, like salinity [4,30].

Based on the above evidence, DCA axis 1 can be used as a quantitative proxy for tracking shifts in the position of each core along the onshore-offshore gradient throughout the stratigraphic succession (figure S9). Probability of collecting a species from a given sampling horizon can be estimated based on the axis 1 score of that sample and species response curves derived from the DCA. These estimates can be used to track stratigraphic changes in species recovery potential (figure S9B) and thus allow for estimating the generalized confidence intervals on stratigraphic ranges [24]. For a given species, we summed recovery potential across all sampling horizons that were located within the observed stratigraphic range of the species. The resulting sum was multiplied by factor α [as defined in equation (2)] to obtain the total recovery potential expected within the extent of a confidence interval r_c above the observed range [equation (3)]. To find the top of the confidence interval we cumulatively added recovery potentials for samples located above the observed LO of a species, from the lowermost to the highest sampling horizon, until the summed recovery potential was greater than or equal to that recorded within the observed range [31]. The stratigraphic position of the last sample included in this procedure marked the top of the confidence interval. If the sum of recovery potentials across all samples located above the LO of a species, including the topmost sample in the core, was still smaller than the total recovery potential within the observed range, we assumed that the confidence interval extends beyond the modern sedimentary surface. This procedure was done separately for each of the four cores.

References

1. Amorosi A, Centineo MC, Colalongo ML, Pasini G, Sarti G, Vaiani SC. 2003 Facies architecture and latest Pleistocene–Holocene depositional history of the Po Delta (Comacchio Area), Italy. *J. Geol.* **111**, 39–56. (doi:10.1086/344577)
2. Campo B, Amorosi A, Vaiani SC. 2017 Sequence stratigraphy and late Quaternary paleoenvironmental evolution of the Northern Adriatic coastal plain (Italy). *Palaeogeogr. Palaeoclimatol. Palaeoecol.* **466**, 265–278. (doi: 10.1016/j.palaeo.2016.11.016)
3. Amorosi A, Bruno L, Campo B, Morelli A, Rossi V, Scarponi D, Hong W, Bohacs KM, Drexler TM. 2017 Global sea-level control on local parasequence architecture from the Holocene record of the Po Plain, Italy. *Mar. Pet. Geol.* **87**, 99–111. (doi:10.1016/j.marpetgeo.2017.01.020)
4. Wittmer JM, Dexter TA, Scarponi D, Amorosi A, Kowalewski M. 2014 Quantitative bathymetric models for late Quaternary transgressive-regressive cycles of the Po Plain, Italy. *J. Geol.* **122**, 649–670. (doi:10.1086/677901)
5. Pellegrini C, Maselli V, Gamberi F, Asioli A, Bohacs KM, Drexler TM, Trincardi F. 2017 How to make a 350-m-thick lowstand systems tract in 17,000 years: The Late Pleistocene Po River (Italy) lowstand wedge. *Geology* **45**, 327–330. (doi:10.1130/G38848.1)
6. Scarponi D, Azzarone M, Kusnerik K, Amorosi A, Bohacs KM, Drexler TM, Kowalewski M. 2017 Systematic vertical and lateral changes in quality and time resolution of the macrofossil record: Insights from Holocene transgressive deposits, Po coastal plain, Italy. *Mar. Pet. Geol.* **87**, 128–136. (doi:10.1016/j.marpetgeo.2017.03.031)
7. Zecchin M, Donda F, Forlin E. 2017 Genesis of the Northern Adriatic Sea (Northern Italy) since early Pliocene. *Mar. Pet. Geol.* **79**, 108–130. (doi:10.1016/j.marpetgeo.2016.11.009)
8. Amorosi A, Maselli V, Trincardi F. 2016 Onshore to offshore anatomy of a late Quaternary source-to-sink system (Po Plain–Adriatic Sea, Italy). *Earth-Sci. Rev.* **153**, 212–237. (doi:10.1016/j.earscirev.2015.10.010)
9. Pieri M, Groppi G. 1981 *Subsurface geological structure of the Po Plain*. Rome: C.N.R.
10. Amorosi A, Colalongo ML, Fusco F, Pasini G, Fiorini F. 1999 Glacio-eustatic Control of continental–shallow marine cyclicity from Late Quaternary deposits of the southeastern Po Plain, northern Italy. *Quat. Res.* **52**, 1–13. (doi:10.1006/qres.1999.2049)
11. Scarponi D, Kowalewski M. 2004 Stratigraphic paleoecology: Bathymetric signatures and sequence overprint of mollusk associations from upper Quaternary sequences of the Po Plain, Italy. *Geology* **32**, 989–992. (doi:10.1130/G20808.1)
12. Kowalewski M, Novack-Gottshall P. 2010 Resampling methods in paleontology. *Paleontol. Soc. Pap.* **16**, 19–54. (doi:10.1017/S1089332600001807)
13. Wang SC, Marshall CR. 2016 Estimating times of extinction in the fossil record. *Biol. Lett.* **12**, 20150989. (doi:10.1098/rsbl.2015.0989)
14. Marshall CR. 1994 Confidence intervals on stratigraphic ranges: partial relaxation of the assumption of randomly distributed fossil horizons. *Paleobiology* **20**, 459–469. (doi:10.1017/S0094837300012938)
15. Marshall CR. 1997 Confidence intervals on stratigraphic ranges with nonrandom distributions of fossil horizons. *Paleobiology* **23**, 165–173. (doi:10.1017/S0094837300016766)

16. Roberts DL, Solow AR. 2003 Flightless birds: when did the dodo become extinct? *Nature* **426**, 245. (doi:10.1038/426245a)
17. Bradshaw CJA, Cooper A, Turney CSM, Brook BW. 2012 Robust estimates of extinction time in the geological record. *Quat. Sci. Rev.* **33**, 14–19. (doi:10.1016/j.quascirev.2011.11.021)
18. Wang SC, Everson PJ, Zhou HJ, Park D, Chudzicki DJ. 2016 Adaptive credible intervals on stratigraphic ranges when recovery potential is unknown. *Paleobiology* **42**, 240–256. (doi:10.1017/pab.2015.37)
19. Marshall CR. 2010 Using confidence intervals to quantify the uncertainty in the end-points of stratigraphic ranges. *Paleontol. Soc. Pap.* **16**, 291–316. (doi:10.1017/S1089332600001911)
20. Meldahl KH. 1990 Sampling, species abundance, and the stratigraphic signature of mass extinction: A test using Holocene tidal flat molluscs. *Geology* **18**, 890–893. (doi:10.1130/0091-7613(1990)018<0890:SSAATS>2.3.CO;2)
21. Wang SC, Everson PJ. 2007 Confidence intervals for pulsed mass extinction events. *Paleobiology* **33**, 324–336. (doi:10.1666/06056.1)
22. Wang SC, Zhong L. 2018 Estimating the number of pulses in a mass extinction. *Paleobiology* **44**, 199–218. (doi:10.1017/pab.2016.30)
23. Strauss D, Sadler PM. 1989 Classical confidence intervals and Bayesian probability estimates for ends of local taxon ranges. *Math. Geol.* **21**, 411–427. (doi:10.1007/BF00897326)
24. Holland SM. 2003 Confidence limits on fossil ranges that account for facies changes. *Paleobiology* **29**, 468–479. (doi:10.1666/0094-8373(2003)029<0468:CLOFRT>2.0.CO;2)
25. Patzkowsky ME, Holland SM. 2012 *Stratigraphic paleobiology: understanding the distribution of fossil taxa in time and space*. Chicago: University of Chicago Press.
26. Tyler CL, Kowalewski M. 2014 Utility of marine benthic associations as a multivariate proxy of paleobathymetry: A direct test from Recent coastal ecosystems of North Carolina. *PLOS ONE* **9**, e95711. (doi:10.1371/journal.pone.0095711)
27. Holland SM. 1995 The stratigraphic distribution of fossils. *Paleobiology* **21**, 92–109. (doi:10.1017/S0094837300013099)
28. Holland SM, Miller AI, Meyer DL, Dattilo BF. 2001 The detection and importance of subtle biofacies within a single lithofacies: The Upper Ordovician Kope formation of the Cincinnati, Ohio region. *Palaios* **16**, 205–217. (doi:10.1669/0883-1351(2001)016<0205:TDAIOS>2.0.CO;2)
29. Oksanen J *et al.* 2017 vegan: Community Ecology Package. R package version 2.4-3.
30. Scarponi D, Azzarone M, Kowalewski M, Huntley JW. 2017 Surges in trematode prevalence linked to centennial-scale flooding events in the Adriatic. *Sci. Rep.* **7**, 5732. (doi:10.1038/s41598-017-05979-6)
31. Labandeira CC, Johnson KR, Wilf P. 2002 Impact of the terminal Cretaceous event on plant–insect associations. *Proc. Natl. Acad. Sci.* **99**, 2061–2066. (doi:10.1073/pnas.042492999)

Supplementary figures

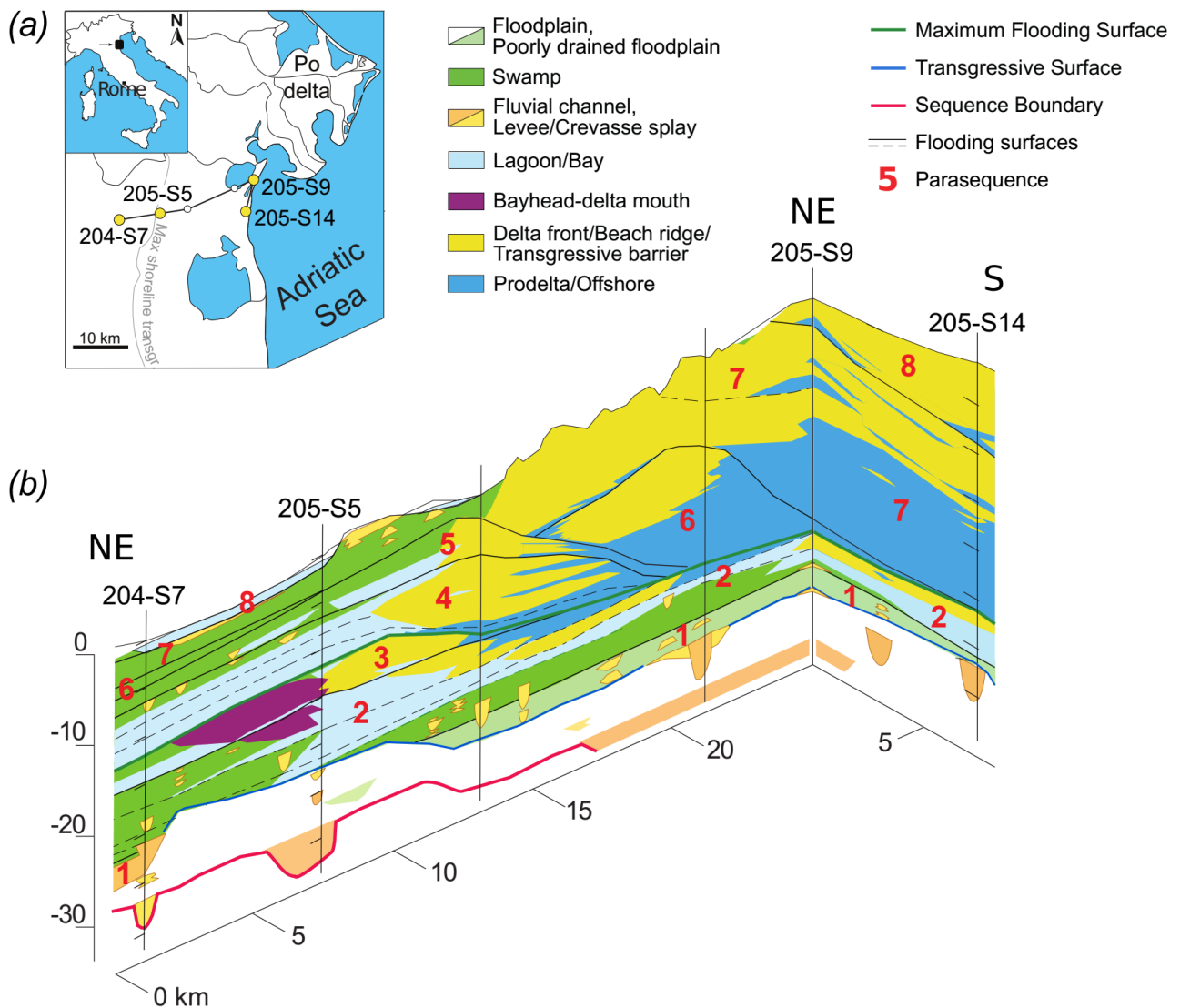


Figure S1. Location of the investigated cores (a) and cross-section of the latest Pleistocene–Holocene succession of the Po coastal plain (b; based on [3] and unpublished data of L. Bruno and B. Campo) illustrating the regional facies architecture and sequence-stratigraphic framework. Millennial-scale parasequences are numbered in red. See figure 1 for the key to sequence stratigraphic units.

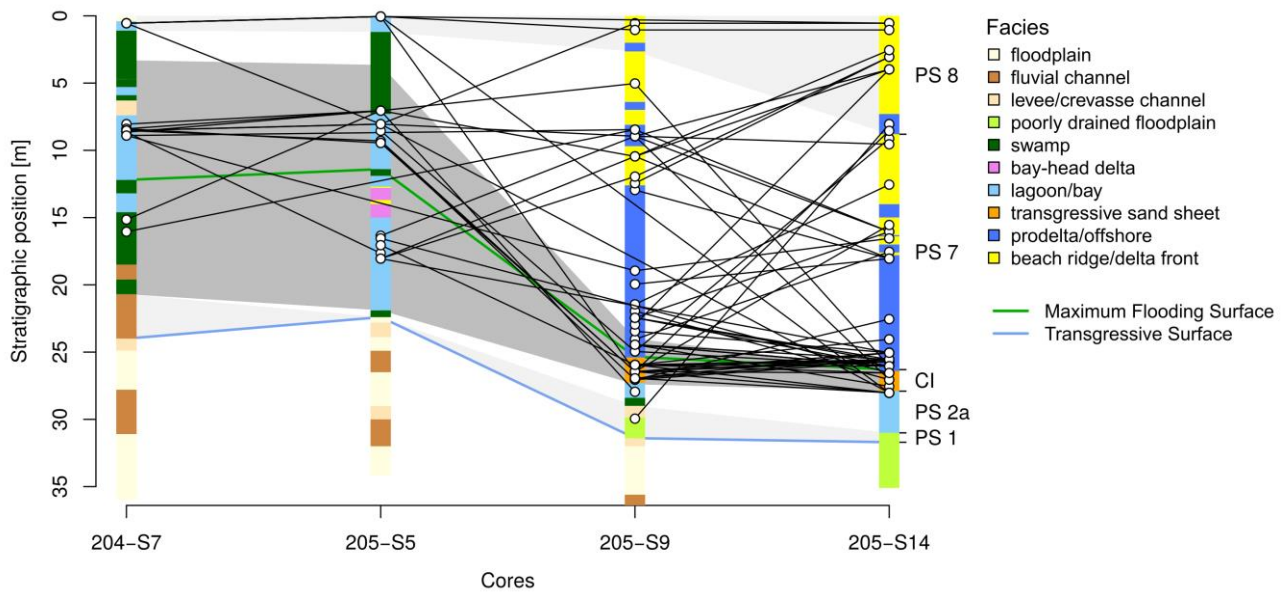


Figure S2. Tangled-fence diagram showing variation in the timing of LOs across individual cores. Lines connect stratigraphic positions of the LO of a single species in different cores. Only species recorded in more than one core are shown. Shading delineates approximately isochronous core intervals correlated based on the parasequence framework (see [3] for details). In the two distal cores (205-S9 and 205-S14), individual parasequences cannot be distinguished around the MFS due to strong condensation. This condensed interval (shaded in dark gray) correlates with the a much more stratigraphically expanded interval in the proximal cores that encompasses multiple parasequences ranging from the upper part of parasequence 2 to the parasequence 6. PS 1, parasequence 1; PS 2a, lowermost part of the parasequence 2; CI, condensed interval; PS 7, parasequence 7; PS 8, parasequence 8.

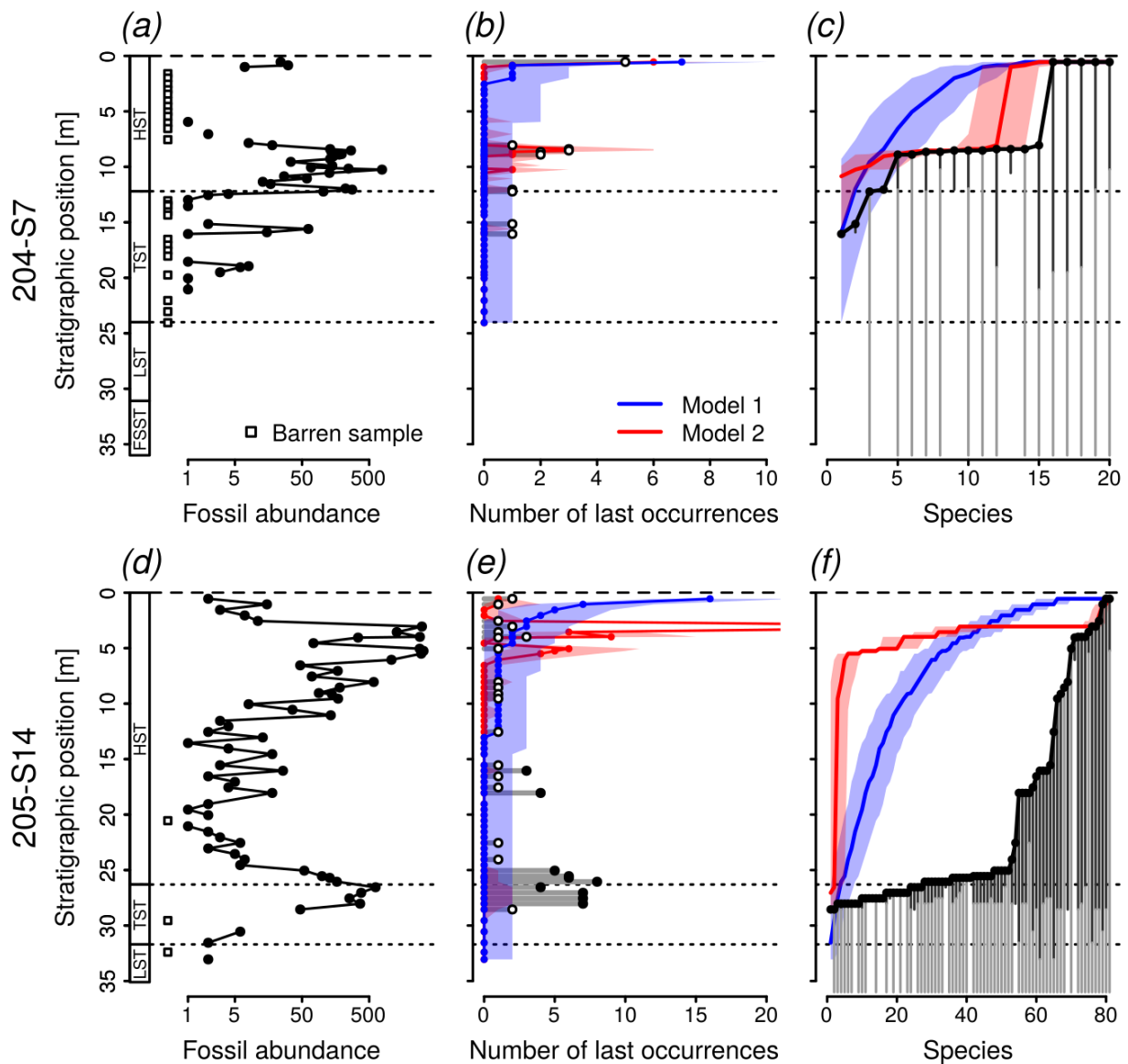


Figure S3. Stratigraphic trends in fossil abundance (number of identifiable specimens per sample; *a, d*) in cores 204-S7 and 205-S14, and the results of two resampling models for the expected number of last occurrences (*b, e*) and distribution of stratigraphic range end points (*c, f*). See figure 3 for further details and figure 1 for the key to sequence stratigraphic units.

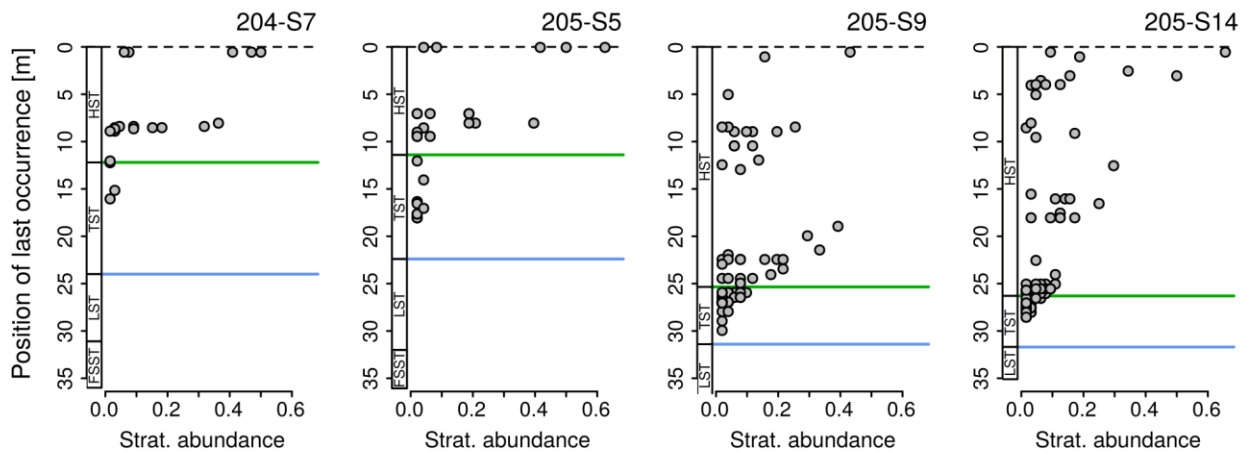


Figure S4. Plots of stratigraphic abundance (proportion of samples in which a species was recorded) versus the stratigraphic position of last occurrence support stepwise extinction pattern in three of the studied cores. In core 205-S14 the observed distribution is more consistent with a gradual extinction scenario. See figure 1 for the key to sequence stratigraphic units.

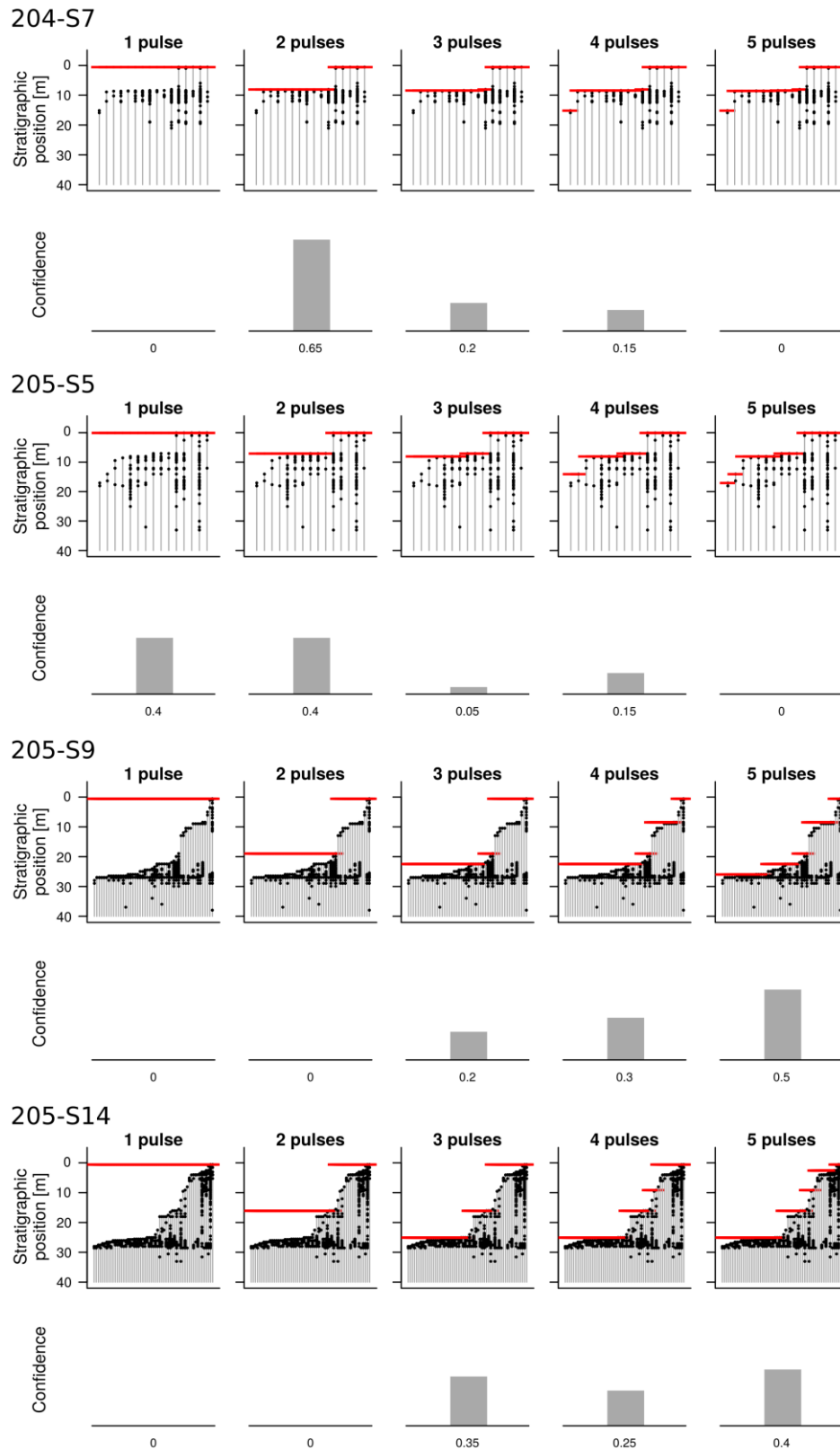


Figure S5. Maximum likelihood estimates for the positions of extinction pulses in each core for scenarios involving 1–5 pulses (upper rows) and corresponding confidence levels (lower rows) calculated using the two-step algorithm of Wang and Zhong [22]. Species recorded only once in a given core were excluded prior to the analyses. With the exception of core 205-S5, stepwise extinction scenarios are overwhelmingly better supported compared to a single extinction event.

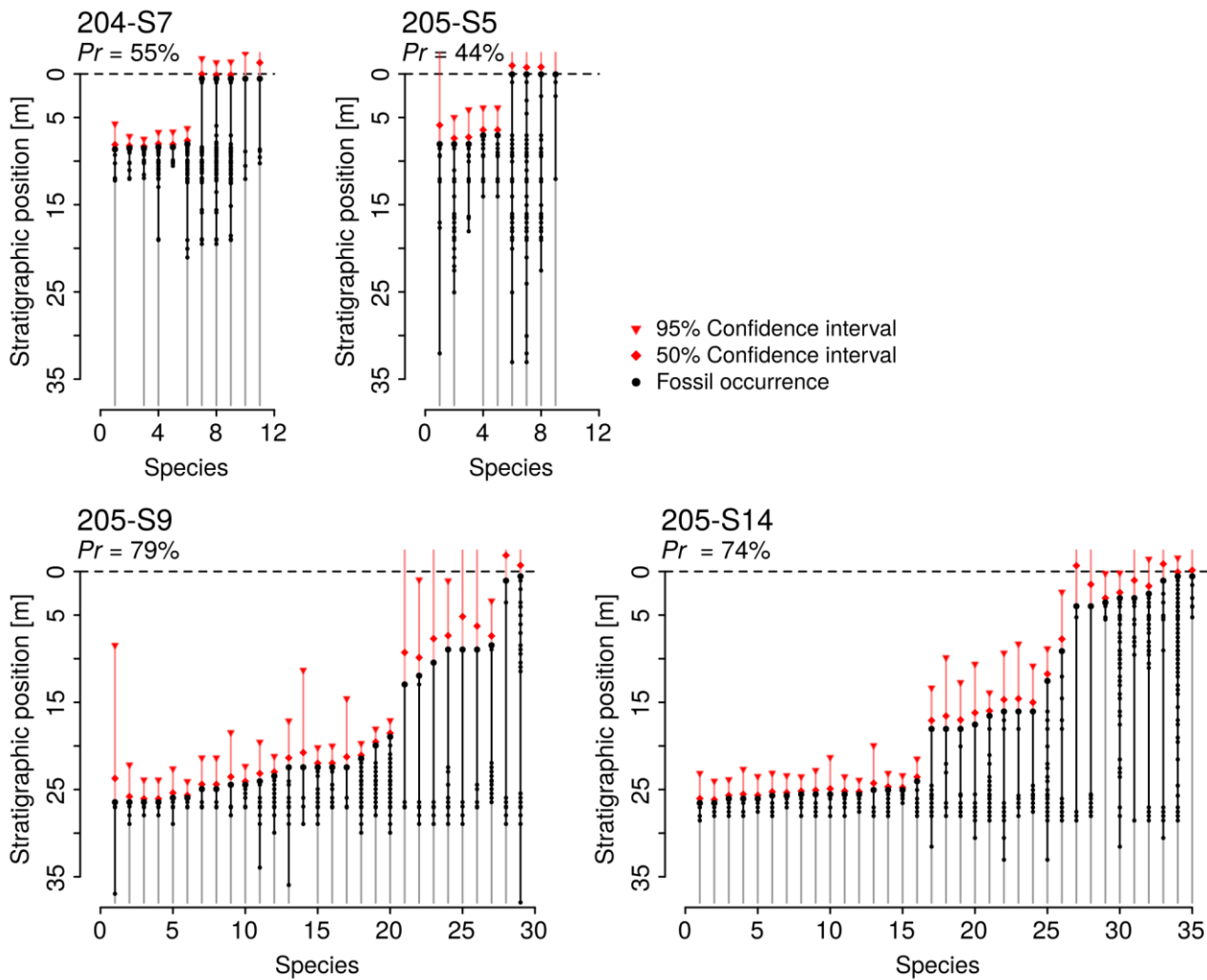


Figure S5. Stratigraphic ranges with their 50% (diamonds) and 95% confidence intervals (triangles) for mollusc species with at least four occurrences in a given core. Confidence intervals were calculated using the classical method of Strauss and Sadler [23], which is assuming random occurrence and thus constant sampling probability through the taxon's range. The percentage of species for which the 95% confidence interval do not reach the topmost sample in a given core (Pr) is also shown. Note, that since all species are extant, the resulting range extensions of all species should reach the top of the succession (dashed horizontal line; the position of a sudden extinction event in our hypothetical scenario).

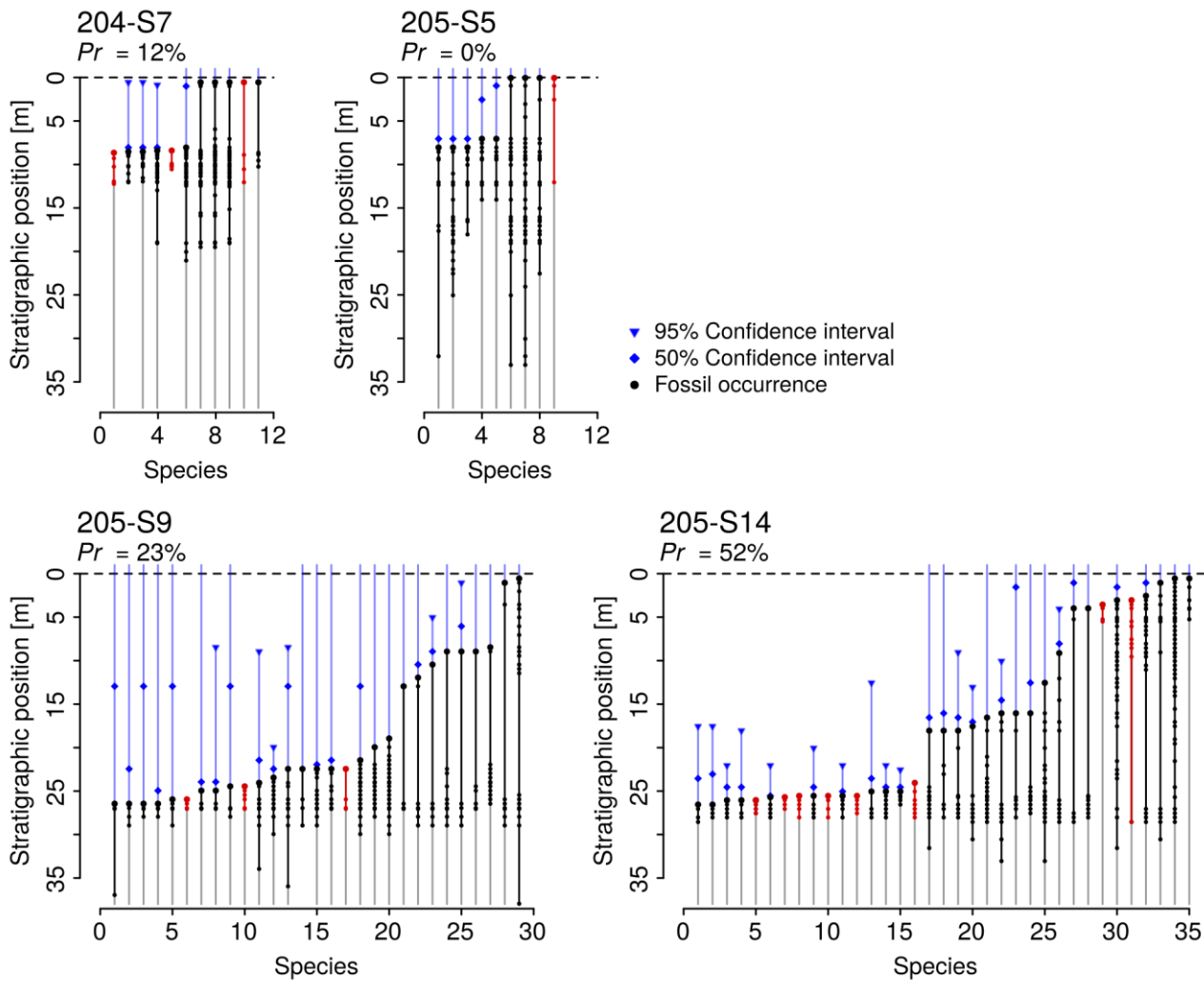


Figure S7. Stratigraphic ranges with their 50% (diamond) and 95% confidence intervals (triangles) for mollusc species with at least four occurrences in a given core. Confidence intervals were calculated following the procedures of Holland [24] by using sample-level estimates of species occurrence rates derived from the DCA ordination of the complete dataset. The percentage of species for which the 95% confidence interval do not reach the topmost sample in a given core (Pr) is also shown. Although this approach yields improved estimates compared to classical confidence intervals (figure S6), it tends to underestimate the ranges of taxa confined to the transgressive sand sheet in the two distal cores, suggesting that mixing of ecologically non-overlapping species in these deposits hampers the correct estimation of the parameters of their response curves. For 13 species (marked in red), the parameters of response curves, and consequently the confidence intervals on their stratigraphic ranges, could not be estimated from the ordination results. The DCA axis 1 scores of these species lie far outside the observed range of sample scores, which may indicate that their preferred habitat is not represented in the studied cores [28].

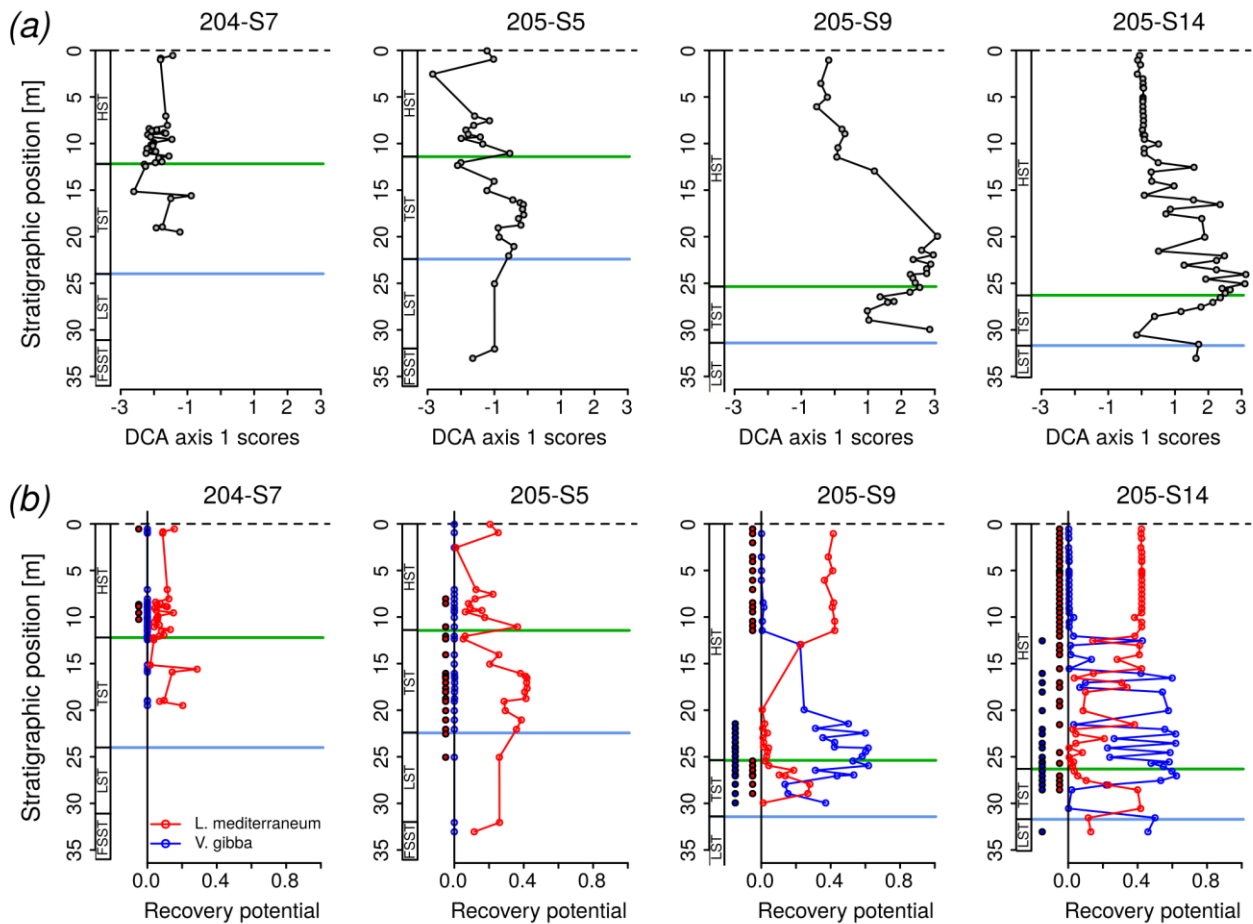


Figure S9. Stratigraphic patterns in DCA axis 1 sample scores along the four cores (a) and examples of recovery potential curves (b) for two species of corbulid bivalves (*Lentidium mediterraneum* and *Varicorbula gibba*) with contrasting environmental preferences. Note that the recovery potential of these species is neither constant, nor changing monotonically along the sedimentary succession. The observed fossil occurrences are shown to the left of the recovery potential curves (filled dots). In the distal cores (205-S9 and 205-S14), the two species co-occur within the condensed deposits below the MFS containing ecologically mixed faunal assemblages. See figure 1 for the key to sequence stratigraphic units.

Chapter **8**

Manuscript IV

8. Manuscript IV

“Early-Middle Pleistocene benthic turnover and oxygen isotope stratigraphy from the Central Mediterranean (Valle di Manche, Crotone Basin, Italy): Data and trends”

Authors: Michele Azzarone ^a, Patrizia Ferretti ^b, Veronica Rossi ^a, Daniele Scarponi ^a, Luca Capraro ^c, Patrizia Macrì ^d, John W. Huntley ^e, Costanza Faranda ^f

^a Dipartimento di Scienze Biologiche, Geologiche e Ambientali, University of Bologna, Via Zamboni 67, 40126 Bologna, Italy

^b Consiglio Nazionale delle Ricerche, Istituto per la Dinamica dei Processi Ambientali (CNR-IDPA), Via Torino 155, I-30172, Venezia Mestre, Italy

^c Dipartimento di Geoscienze, Università di Padova, Via G. Gradenigo 6, I-35131 Padova, Italy

^d Istituto Nazionale di Geofisica e Vulcanologia, Via di Vigna Murata 605, I-00143 Roma, Italy

^e Department of Geological Sciences, University of Missouri, 101 Geology Building, Columbia, MO 65211, USA

^f Dipartimento di Scienze, University of Roma Tre, Largo San Leonardo Murialdo 1, 00146 Roma, Italy

Status: Published in *Data in Brief*, volume 17, April 2018, pages 1099-1107

doi: doi.org/10.1016/j.dib.2018.02.017



ELSEVIER

Contents lists available at ScienceDirect

Data in Brief

journal homepage: www.elsevier.com/locate/dib

Data Article

Early-Middle Pleistocene benthic turnover and oxygen isotope stratigraphy from the Central Mediterranean (Valle di Manche, Crotone Basin, Italy): Data and trends

Michele Azzarone^{a,*}, Patrizia Ferretti^b, Veronica Rossi^a,
 Daniele Scarponi^a, Luca Capraro^c, Patrizia Macri^d,
 John W. Huntley^e, Costanza Faranda^f

^a Dipartimento di Scienze Biologiche, Geologiche e Ambientali, Università di Bologna, Piazza di Porta San Donato 1, I-40126 Bologna, Italy

^b Consiglio Nazionale delle Ricerche, Istituto per la Dinamica dei Processi Ambientali (CNR-IDPA), Via Torino 155, I-30172, Venezia Mestre, Italy

^c Dipartimento di Geoscienze, Università di Padova, Via G. Gradenigo 6, I-35131 Padova, Italy

^d Istituto Nazionale di Geofisica e Vulcanologia, Via di Vigna Murata 605, I-00143 Roma, Italy

^e Department of Geological Sciences, University of Missouri, 101 Geology Building, Columbia, MO 65211, USA

^f Dipartimento di Scienze, University of Roma Tre, Largo San Leonardo Murialdo 1, 00146 Roma, Italy

ARTICLE INFO

Article history:

Received 2 January 2018

Received in revised form

5 February 2018

Accepted 8 February 2018

ABSTRACT

Ostracod faunal turnover and oxygen isotope data (foraminifera) along the Valle di Manche (VdM) section are herein compiled. Specifically, the material reported in this work includes quantitative palaeoecological data and patterns of ostracod fauna framed within a high-resolution oxygen isotope stratigraphy ($\delta^{18}\text{O}$) from *Uvigerina peregrina*. In addition, the multivariate ostracod faunal stratigraphic trend (nMDS axis-1 sample score) is calibrated using bathymetric distributions of extant molluscs sampled from the same stratigraphic intervals along the VdM section. Data and analyses support the research article “Dynamics of benthic marine communities across the Early-Middle Pleistocene boundary in the

DOI of original article: <https://doi.org/10.1016/j.palaeo.2017.12.042>

* Corresponding author.

E-mail address: michele.azzarone2@unibo.it (M. Azzarone).

<https://doi.org/10.1016/j.dib.2018.02.017>

2352-3409/© 2018 The Authors. Published by Elsevier Inc. This is an open access article under the CC BY license (<http://creativecommons.org/licenses/by/4.0/>).

Mediterranean region (Valle di Manche, Southern Italy): biotic and stratigraphic implications” Rossi et al. [1].

© 2018 The Authors. Published by Elsevier Inc. This is an open access article under the CC BY license (<http://creativecommons.org/licenses/by/4.0/>).

Specifications Table

Subject area	<i>Earth Science</i>
More specific subject area	<i>Palaeoecology and Oxygen Isotope Stratigraphy</i>
Type of data	<i>Tables, Figures and Text file</i>
How data were acquired	<i>Field and dissecting microscope observations. Isotope ratio mass spectrometry</i>
Data format	<i>Raw and analysed</i>
Experimental factors	
Experimental features	
Data source location	<i>San Mauro Marchesato (Crotone, Southern Italy)</i>
Data accessibility	<i>The data are available with this article</i>

Value of the data

- Valle di Manche (VdM) is a key-section within the Mediterranean Basin as it straddles the Early-Middle Pleistocene boundary and contains a record of the Matuyama–Brunhes reversal. The abundance data of benthic organisms here presented complement the available documentation for the VdM section.
- The multidisciplinary approach adopted provides a viable strategy for quantifying stratigraphic and palaeontological patterns, which allowed for an improved reconstruction of depositional environments.
- The data here presented could be compared to other Mediterranean siliciclastic successions that record Early-Middle Pleistocene high frequency sea level fluctuations.

1. Data

We report data from ostracod fauna (39 samples, > 3600 valves; [Appendix 1](#)) and stable isotope data from the benthic foraminifera *Uvigerina peregrina* sampled at high resolution along the 38m-thick investigated interval of the Valle di Manche section (Crotone Basin, Southern Italy [[2,3](#)]).

2. Experimental design, materials and methods

Concerning the ostracod fauna, each valve was counted as one individual ([Appendix 1](#)). *Uvigerina peregrina* specimens were picked from the > 150 µm coarse fraction of 229 sediment samples (Table 2 in [[3](#)]), which were previously disaggregated using distilled water.

2.1. Unconstrained gradient analysis

Detrended correspondence analysis (DCA) and non-metric multi-dimensional scaling (nMDS) are two widely employed indirect ordination methods in palaeoecology. As both ordination techniques

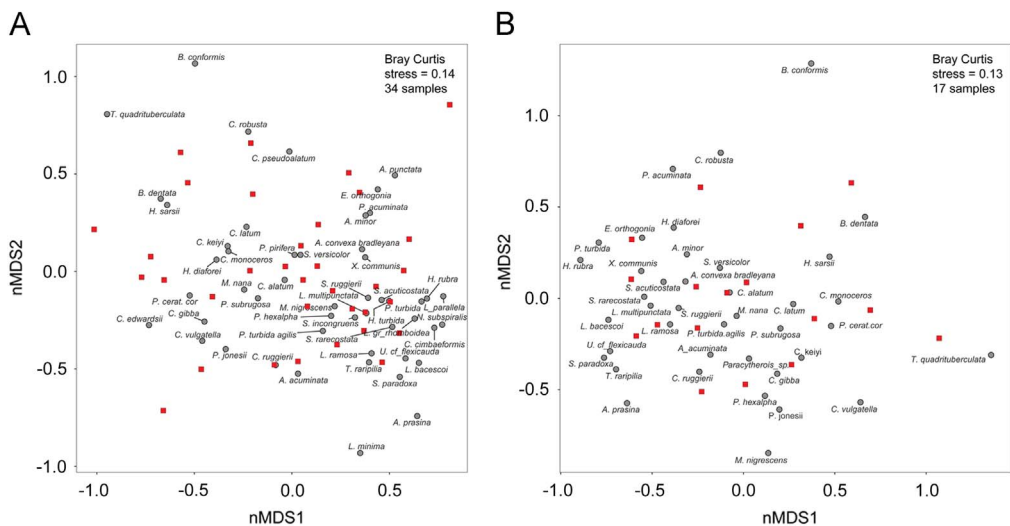


Fig. 1. Non-metric multidimensional scaling outputs performed on data matrices with different taxonomic and numerical resolution. A) Samples ≥ 20 specimens and species recorded in more than one sample (i.e., 34 samples/51 species matrix). B) Samples ≥ 20 specimens and species recorded in more than two samples (i.e., 17 samples/34 species matrix; Fig. 1B). Square and circle symbols represent sample and species, respectively.

have different strengths and weaknesses, the best approach is to use both methods as a crosscheck on the robustness of the outputs [4,5]. Faunal counts were log-transformed to prevent distortion due to very abundant species. Then, DCA and nMDS were performed on a set of abundance matrices derived varying sample and taxon thresholds. In this work, we focus on nMDS outputs (2-dimensions and based on Bray-Curtis distance; Fig. 1, Table 1A), as for DCA outputs we refer to [1]. Stratigraphic plots of nMDS and DCA axis-1 sample scores are also displayed (Table 1A; Fig. 2 A, C, E and B, D, F respectively). Ordination analyses were performed in R 3.3.2 [6] with “vegan” package and PAST software [7].

2.2. Ostracod and mollusc faunal trends along Valle di Manche (VdM) section

Reduced Major Axis (RMA) regression was performed to explore the relationship between ostracod and mollusc faunal composition along the Valle di Manche section (Table 1). The multiple DCA and nMDS axis 1 sample scores obtained from ostracods (Table 1A) were correlated via RMA to the scores previously obtained from DCA on the mollusc matrix (see [8]; Table 1A). All analyses returned high and significant correlation coefficients (Table 1B).

2.3. Oxygen isotope stratigraphy and age model

Between 10 and 15 specimens of *U. peregrina* were analysed in order to reduce statistical variability. After being lightly crushed, to remove organic contaminants, the selected specimens were soaked in hydrogen peroxide (3%). Then, analytical grade acetone was added, and the samples cleaned ultrasonically, after which the excess liquid was removed. All stable isotope analyses were carried out on an automated continuous flow carbonate preparation GasBench II device, attached to a Thermo Scientific Delta V Advantage Isotope Ratio Mass Spectrometer. Measurements of $\delta^{18}\text{O}$ were determined relative to the Vienna Peedee belemnite (VPDB) standard, with an analytical precision that is better than 0.1‰.

The chronology for the Valle di Manche section was developed by tuning the *Uvigerina peregrina* $\delta^{18}\text{O}$ signal to the stacked planktonic oxygen isotope record derived from the Mediterranean Sea [9,10]. In the initial stages, we produced an alternative age model by making use of the time scale of

Table 1

A - Sample information and major axis sample scores obtained from non-Metric Multidimensional Scaling (nMDS) and Detrended Correspondence Analysis (DCA) on Valle di Manche ostracod and mollusc datasets. A1) Mollusc sample label. A2) DCA axis 1 sample score; A3) Stratigraphic offset with respect to the adjacent ostracod sample. A4) Ostracod sample label. A5–6) nMDS axis 1 sample score obtained from a reduced ostracod matrix (employing absolute–Abs and relative–Rel abundances) comparable to the mollusc one (i.e., 17 samples see Scarponi et al., 2014). Stress values = 0.19 and 0.16, respectively. A7–8) As for A5–6 but employing DCA. A9–10) nMDS axis 1 sample score obtained from the 51×34 ostracod matrix employing absolute–Abs and relative–Rel abundances. Stress values = 0.20 and 0.19, respectively. A11–12) As for A9–10 but employing DCA. B. Linear correlation (RMA) coefficients (r–Pearson) and p-values ($\alpha=0.05$) between ordination of ostracod matrices (i.e., DCA- 1 or nMDS-1) and mollusc DCA axis 1 sample score (after [8]).

A) Ordination analyses and sample information from the Valle di Manche section

<i>after Scarponi et al. (2014)</i>				Ostracod samples							
Label	DCA-1	S-offset	Label	Matrix 17 samples				Matrix 34 samples			
				nMDS-1		DCA-1		nMDS-1		DCA-1	
				Abs	Rel	Abs	Rel	Abs	Rel	Abs	Rel
1)	2)	3) (cm)	4)	5)	6)	7)	8)	9)	10)	11)	12)
Bk22	196	20	SMA50	-0.24433	-0.25854	22	0	0.121	0.128	15	31
Bk21	117	0	SMA42	-0.05252	-0.04989	87	73	0.012	0.014	94	74
Bk20	95	-40	SMA38	0.14789	0.084843	143	127	-0.067	-0.047	135	137
Bk19	122	0	SMA30	-0.10886	-0.10742	67	57	0.051	0.052	79	80
Bk18	67	-10	SMA18	-0.03471	-0.02284	109	61	0.043	0.042	83	88
Bk17	0	40	SMA10	0.41237	0.41683	264	237	-0.307	-0.282	255	238
Bk16	9	-30	SMA8	0.31321	0.33418	206	218	-0.245	-0.237	235	195
Bk15	51	0	SMA4	0.16096	0.18789	173	151	-0.133	-0.160	174	152
Bk14	90	40	SMA-8	0.073954	0.078073	142	106	-0.051	-0.072	118	102
Bk13	98	-20	SMA-14	-0.16361	-0.16797	91	41	0.055	0.048	80	76
Bk12	223	10	SMB14	-0.18192	-0.21069	29	11	0.145	0.145	20	8
Bk11	198	10	SMB20	-0.14185	-0.15454	56	14	0.090	0.095	38	56
Bk9	164	30	SMB40	-0.24981	-0.20625	0	30	0.117	0.096	45	26
Bk8	80	20	SMB52	-0.04612	-0.05474	96	70	0.026	0.019	91	99
Bk7	59	10	SMB56	-0.02318	0.030985	84	157	0.037	0.025	134	137
Bk6	4	0	SMB60	0.35609	0.32507	181	257	-0.224	-0.229	267	236
Bk5	272	60	SMB76	-0.21757	-0.22499	2	5	0.136	0.136	24	20

B) Linear correlation: ordination axis 1 ostracod-sample scores vs. DCA axis 1 mollusc-sample score

Ostracod (17 samples matrix) vs. Mollusc matrix

<i>nMDS-1 absolute abundance</i>	$r = -0.844, p<0.05$
<i>nMDS-1 relative abundance</i>	$r = -0.873, p<0.05$
<i>DCA-1 log-transformed raw values</i>	$r = -0.881, p<0.05$
<i>DCA-1 relative abundance</i>	$r = -0.880, p<0.05$

Ostracod (34 samples matrix) vs. Mollusc matrix

<i>nMDS-1 absolute abundance</i>	$r = 0.849, p<0.05$
<i>nMDS-1 relative abundance</i>	$r = 0.864, p<0.05$
<i>DCA-1 log-transformed raw value</i>	$r = 0.894, p<0.05$
<i>DCA-1 relative abundance</i>	$r = -0.905, p<0.05$

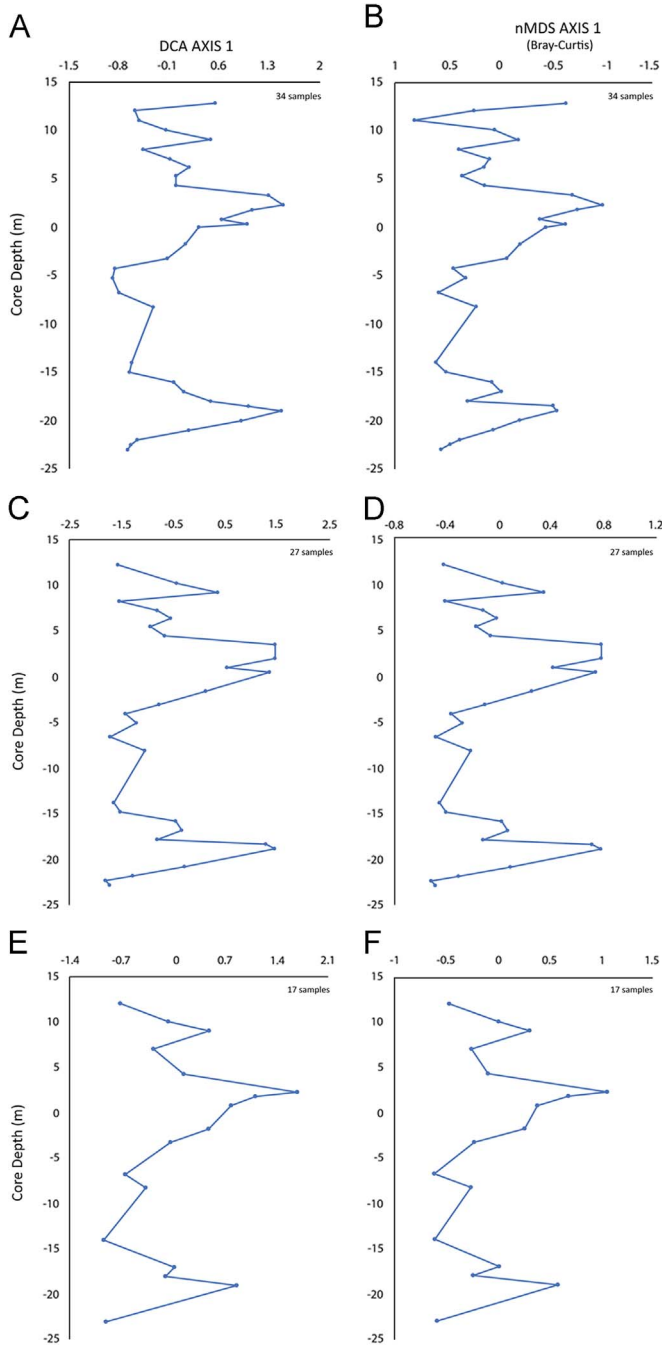


Fig. 2. Multiple stratigraphic plots of Detrended Correspondence Analysis (A, C, E) and non-Metric Multidimensional Scaling (B, D, F) axis 1 sample scores. A-B) Sample ≥ 20 specimens and species singletons excluded. C-D) Sample ≥ 25 specimens and species occurrence ≥ 5 samples. E-F) Ostracod dataset comparable (in sample size and sampling resolution) to the mollusc dataset reported in [13]; sample size ≥ 20 specimens and species singletons excluded.

Table 2

A) Sample information and ostracod DCA sample axis 1 score obtained from the 51 species/34 samples matrix of Valle di Manche section (DCA performed with PAST 3.11). B) Bathymetric calibration of ostracod samples. Reduced major axis regression coefficients: slope $a=0.46884$; intercept $b=24.175$; $r=-0.92$; $p=7.87 \cdot 10^{-6}$; standard error of the estimates = 14.3 m. C) Pearson linear correlation coefficient (r) and p (uncorr.) values ($\alpha=0.05$) between DCA 1 sample scores and % of sand in each sample are shown. Regression models performed with PAST 3.11.

Label	A) Ostracod Samples: age, grain size and DCA score					B) Water depth	
	Position (m)	Age (ka)	Sample weight (gr)	Sand fraction (> 63 μm)		DCA1 sample score	Water depth (m)
				(gr)	(%)		
SMA53	12.81	741.8	46.9	2.67	5.7	164	101
SMA50	12.06	744.4	48.0	6.14	12.8	15	31
SMA46	11.06	747.8	50.8	1.44	2.8	4	26
SMA42	10.06	751.2	46.9	8.57	18.3	94	68
SMA38	9.06	754.6	48.8	3.26	6.7	135	87
SMA34	8.06	758.0	47.4	9.01	19.0	34	40
SMA30	7.06	761.2	45.4	14.39	31.7	79	61
SMA26	6.21	764.0	47.7	5.13	10.8	55	50
SMA22	5.31	767.0	54.9	1.48	2.7	41	43
SMA18	4.31	770.1	55.0	3.33	6.1	83	63
SMA14	3.31	773.4	57.2	3.20	5.6	242	138
SMA10	2.31	777.5	55.3	3.43	6.2	255	144
SMA8	1.81	780.0	56.2	5.11	9.1	235	134
SMA4	0.81	784.5	55.0	1.89	3.4	174	106
SMA2	0.31	786.3	58.5	1.52	2.6	238	136
SMA-1	0.00	787.5	51.8	2.58	5.0	151	95
SMA-8	-1.75	794.0	46.6	3.91	8.4	118	79
SMA-14	-3.25	795.6	46.4	6.79	14.6	80	62
SMB4	-4.25	796.7	54.9	11.41	20.8	0	24
SMB8	-5.25	797.7	57.1	7.82	13.7	2	25
SMB14	-6.75	799.3	56.2	3.52	6.3	20	34
SMB20	-8.25	800.9	55.1	4.81	8.7	38	42
SMB40	-14.00	811.6	54.0	4.96	9.2	45	45
SMB44	-15.00	813.8	50.1	19.76	39.4	20	34
SMB48	-16.00	827.3	54.5	21.30	39.1	66	55
SMB52	-17.00	839.4	55.5	6.05	10.9	91	67
SMB56	-18.00	846.3	55.0	18.22	33.1	134	87
SMB58	-18.50	850.6	53.8	6.11	11.4	240	137
SMB60	-19.00	855.8	56.4	6.79	12.0	267	149
SMB64	-20.00	861.9	53.5	1.30	2.4	204	120
SMB68	-21.00	863.6	54.9	6.80	12.4	162	100
SMB72	-22.00	865.3	54.9	4.57	8.3	52	49
SMB74	-22.50	866.1	50.4	4.05	8.0	25	36
SMB76	-23.00	867.0	54.6	8.54	15.6	24	35

C) DCA score vs. % of sand - linear correlation
 $r = 0.291$ $r^2 = 0.085$ $p = 0.094$

Konijnendijk and collaborators [11], which is also based on a stacked and averaged suite of oxygen isotope records from the eastern Mediterranean, in this case from benthic foraminifera. This initial tuning approach was based on the assumption that the correlation of the benthic $\delta^{18}\text{O}$ signal from the VdM succession to a benthic record from the Mediterranean region appeared to be a more advisable choice than the use of a planktonic $\delta^{18}\text{O}$ stack as a tuning target. However, the benthic $\delta^{18}\text{O}$ from VdM and the benthic $\delta^{18}\text{O}$ stack of [11] have little in common at either low or high frequency, as the suite of cores used by [11] reflects the dynamics of different (i.e. deeper) water masses. Serious discrepancies between the dataset from VdM and the benthic $\delta^{18}\text{O}$ stack in the time interval from ca. 860 to 815 ka (MIS 21), lead to difficulties in developing a tuned timescale (see Figure 10 in [3]). This is an interval

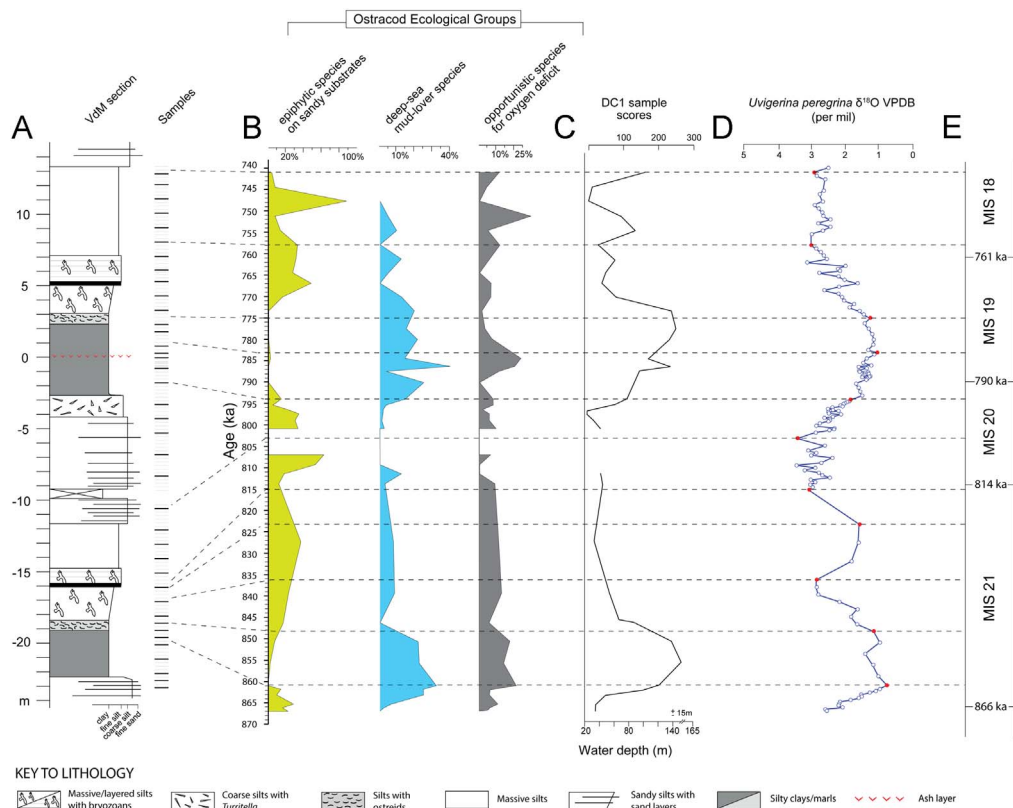


Fig. 3. Data summary of the high-resolution chronostratigraphic and palaeoenvironmental inferences retrieved at Valle di Manche (VdM). A) Physical stratigraphy of VdM section along with location of the 229 collected samples, in bold the 39 samples analysed for the ostracod fauna. B) Ostracod ecological groups distinguished on the basis of different ecological preferences, in terms of substrate and oxygen conditions, of the species recorded along the VdM section. C) Stratigraphic pattern in DCA-calibrated water depth based on the 34×51 ostracod matrix (see also Fig. 2A). D) *U. peregrina* oxygen isotope stratigraphy of the VdM section. E) Marine Isotope Stages (MIS) straddling the Early-Middle Pleistocene transition. Red dots represent the control points employed for reconstructing the VdM section age model. Panel A is plotted versus stratigraphic depth. Panels B–E are plotted versus age.

when some sources of uncertainty arise in the time scale developed by [11], as changes in insolation forcing are generally relatively small between 700–950 ka, no sapropel layers are present, and proxies lack a characteristic pattern to tie to insolation, making the resulting chronology dubious [12]. For these reasons, this initial age model was rejected.

On the other hand, transfer of the time scale by Wang and collaborators [9] proved very straightforward. As each version of the age model was developed, the age of every sample was estimated by linear interpolation between the control points. We closely monitored changes in sedimentation rate when defining age–depth correlations. If substantial changes in sedimentation rates were generated by the use of specific age controls, we evaluated whether the implied changes in the flux of biogenic and/or detrital sediment were reasonable and justified within the geological setting of the VdM section. According to our age model, the studied record spans the time interval from ca. 870 ka to 740 ka (Table 2A and Fig. 3). For more information on *U. peregrina* oxygen isotope data, we refer to [3].

2.4. Environmental proxies calibration

Sand percentages within samples (a proxy for substrate texture) is interpreted as a driver of ostracod turnover along sedimentary successions. In this work, sand percentage was plotted against DCA axis-1 sample scores (Table 2A) via linear correlation (least squares) to evaluate the role of substrate in driving ostracod faunal changes (Table 2C). Sand fraction includes both biotic and abiotic grains > 63 µm (Table 2A).

A linear correlation model (RMA) was also applied for bathymetry estimates of ostracod samples (Table 2B). Given the lack of quantitative water-depth information on ostracods species here recovered, water-depth calibrations rely on bathymetry inferences available for mollusc species retrieved in concomitance or proximity of the horizons sampled for ostracods (Table 1A column 3).

Sample-level bathymetry was calculated via the weighted average of a sub-set of extant mollusc species for which optimum bathymetry values were known (see Appendix 2 in [8]). Among the 14 extant taxa reported in [8], all cemented species (i.e., *Anomia ephippium*, *Heteranomina squamula*) were excluded from calibration, as they commonly show low association between ordination scores and bathymetry [13,14]. Then, a RMA regression between sample-level bathymetry estimates and DCA axis-1 ostracod sample scores was calculated (Table 2B).

Information collected at Valle di Manche and relative climatic, environmental and chronostratigraphic inferences are summarised in Fig. 3.

Funding sources

This research was funded by the University of Padova (Progetto di Ateneo 2011 and Dotazione Ordinaria della Ricerca (DOR) to LC) and University of Bologna (Ricerca Fondamentale Orientata, 2016 D. Scarponi).

Transparency document. Supporting information

Supplementary data associated with this article can be found in the online version at <http://dx.doi.org/10.1016/j.dib.2018.02.017>.

Appendix A. Supporting information

Supplementary data associated with this article can be found in the online version at <http://dx.doi.org/10.1016/j.dib.2018.02.017>.

References

- [1] V. Rossi, M. Azzarone, L. Capraro, C. Faranda, P. Ferretti, P. Macri, D. Scarponi Response of benthic marine communities to Early-Middle Pleistocene environmental changes and sequence stratigraphic implications (Valle di Manche section, Southern Italy), *Palaeogeogr. Palaeoclimatol. Palaeoecol.* (in press).
- [2] L. Capraro, P. Macri, D. Scarponi, D. Rio, The lower to Middle Pleistocene Valle di Manche section (Calabria, Southern Italy): state of the art and current advances, *Quat. Int.* 383 (2015) 36–46. <http://dx.doi.org/10.1016/j.quaint.2014.08.055>.
- [3] L. Capraro, P. Ferretti, P. Macri, D. Scarponi, F. Tateo, E. Fornaciari, G. Bellini, G. Dalan, The Valle di Manche section (Calabria, Southern Italy): a high-resolution record of the Early-Middle Pleistocene transition (MIS 21-MIS 19) in the Central Mediterranean, *Quat. Sci. Rev.* 165 (2017) 31–48. <http://dx.doi.org/10.1016/j.quascirev.2017.04.003>.
- [4] D. Scarponi, M. Azzarone, M. Kowalewski, J.W. Huntley, Surges in trematode prevalence linked to centennial-scale flooding events in the Adriatic, *Sci. Rep.* 7 (2017) 5732. <http://dx.doi.org/10.1038/s41598-017-05979-6>.
- [5] M. Zuschin, R. Nawrot, M. Harzhauser, O. Mandic, A. Tomašových, Taxonomic and numerical sufficiency in depth-and salinity-controlled marine paleocommunities, *Paleobiology* (2017) 1–16. <http://dx.doi.org/10.1017/pab.2016.49>.
- [6] R. Core Team, R: A language and environment for statistical computing. *R Foundation for Statistical Computing*, Vienna, Austria URL (<https://www.R-project.org/>), 2016.
- [7] Ø. Hammer, D.A.T. Harper, *Paleontological Data Analysis*, Wiley-Blackwell, New York (2005) 368.

- [8] D. Scarponi, J.W. Huntley, L. Capraro, S. Raffi, Stratigraphic paleoecology of the Valle di Manche section (Crotona Basin, Italy): a candidate GSSP of the Middle Pleistocene, *Palaeogeogr. Palaeoclimatol. Palaeoecol.* 402 (2014) 30–43. <http://dx.doi.org/10.1016/j.palaeo.2014.02.032>.
- [9] P. Wang, J. Tian, L.J. Lourens, Obscuring of long eccentricity cyclicity in Pleistocene oceanic carbon isotope records, *Earth Planet. Sci. Lett.* 290 (3–4) (2010) 319–330. <http://dx.doi.org/10.1016/j.epsl.2009.12.02>.
- [10] L.J. Lourens, Revised tuning of Ocean Drilling Program Site 964 and KC01B (Mediterranean) and implications for the d18O, tephra, calcareous nannofossil, and geomagnetic reversal chronologies of the past 1.1 Myr, *Paleoceanography* 19 (2004) PA3010. <http://dx.doi.org/10.1029/2003PA000997>.
- [11] T.Y.M. Konijnendijk, M. Ziegler, L.J. Lourens, On the timing and forcing mechanisms of late Pleistocene glacial terminations: insights from a new high-resolution benthic stable oxygen isotope record of the eastern Mediterranean, *Quat. Sci. Rev.* 129 (2015) 308–320. <http://dx.doi.org/10.1016/j.quascirev.2015.10.005>.
- [12] T.Y.M. Konijnendijk, M. Ziegler, L.J. Lourens, Chronological constraints on Pleistocene sapropel depositions from high-resolution geochemical records of ODP Sites 967 and 968, *Newslett. Stratigr.* 47/3 (2014) 263–282. <http://dx.doi.org/10.1127/0078-0421/2014/0047>.
- [13] D. Scarponi, M. Kowalewski, Stratigraphic paleoecology: bathymetric signatures and sequence overprint of mollusk associations from upper Quaternary sequences of the Po Plain, Italy, *Geology* 32 (2004) 989–992. <http://dx.doi.org/10.1130/G20808.1>.
- [14] J.M. Wittmer, T.A. Dexter, D. Scarponi, A. Amorosi, M. Kowalewski, Quantitative bathymetric models for late quaternary transgressive-regressive cycles of the Po Plain, Italy, *J. Geol.* 122 (6) (2014) 649–670. <http://dx.doi.org/10.1086/677901>.

Manuscript 4 Online Supplementary Material

“Early-Middle Pleistocene benthic turnover and oxygen isotope stratigraphy from the Central Mediterranean (Valle di Manche, Crotone Basin, Italy): Data and trends.

	**		**			**		**	**		**
Ostracod taxon/Sample position (m)	SMA53	SMA50	SMA46	SMA42	SMA38	SMA34	SMA30	SMA26	SMA22	SMA18	SMA14
	12.81	12.06	11.06	10.06	9.06	8.06	7.06	6.21	5.31	4.31	3.31
<i>Aurila convexa</i> (Baird, 1850)	0	8	16	7	2	43	33	19	35	9	0
<i>Cimbaurila cimbaeformis</i> (Seguenza, 1883) **	0	0	0	0	0	0	0	0	0	0	0
<i>Aurila cruciata</i> (Ruggieri, 1950) */**	0	0	0	0	0	0	0	0	0	0	0
<i>Aurila interpretis</i> (Uliczny, 1969) */**	0	0	0	0	0	0	0	0	0	0	0
<i>Aurila prasina</i> (Barbeito-Gonzalez, 1971)	0	0	0	1	0	0	0	0	0	0	0
<i>Aurila punctata</i> (Münster, 1830) **	0	0	5	0	0	0	0	0	3	0	0
<i>Aurila</i> sp. */**	0	0	0	0	0	0	0	0	0	1	0
<i>Callistocythere</i> group (Ruggieri, 1953) */**	2	0	2	0	4	2	24	8	0	6	0
<i>Carinocythereis carinata</i> (Roemer, 1838) */**	0	0	0	0	0	0	0	0	0	0	0
<i>Cluthia keiyi</i> (Neale, 1975)	0	0	0	0	0	0	3	2	1	4	0
<i>Costa edwardsii</i> (Roemer, 1838) **	1	0	0	0	0	0	0	0	0	0	0
<i>Cythereis</i> sp. */**	0	0	0	0	0	0	0	0	0	0	0
<i>Cytheromorpha nana</i> (Bonaduce, Ciampo and Masoli, 1975) */**	0	0	0	0	0	0	0	0	0	0	0
<i>Cytheromorpha fuscata</i> (Brady, 1869) */**	0	0	0	0	0	0	0	0	0	0	0
<i>Eucythere curta</i> (Ruggieri, 1975) */**	0	0	0	0	0	0	0	0	0	0	0
<i>Eucythere pubera</i> (Bonaduce, Ciampo and Masoli, 1975) */**	0	0	0	0	0	0	0	0	0	0	0
<i>Eucytherura orthogonia</i> (Colalongo and Pasini, 1980)	0	0	0	0	0	0	2	5	2	0	0
<i>Hiltermannicythere rubra</i> (G.W. Muller, 1894)	0	2	0	0	0	0	1	0	0	0	0
<i>Hiltermannicythere turbida</i> (G.W. Muller, 1894) **	0	0	0	0	0	0	0	0	0	0	0
<i>Loxococoncha geometrica</i> (Bonaduce, Ciampo and Masoli, 1975) */**	0	0	0	1	0	0	0	0	0	0	0
<i>Loxococoncha minima</i> (Bonaduce et al., 1975) **	1	0	0	0	0	0	0	0	0	0	0
<i>Loxococoncha parallela</i> (G.W. Muller, 1894) **	0	0	0	0	0	0	0	0	0	0	0
<i>Loxococoncha gr. rhomboidea</i> (Fischer, 1855) **	0	0	0	0	0	0	0	0	0	0	0
<i>Loxococoncha</i> sp. */**	0	0	0	0	0	0	0	0	0	0	0
<i>Macrocypris</i> sp. */**	0	0	0	0	0	0	2	0	0	0	0
<i>Neocytherideis subspiralis</i> (Brady, Crosskey and Robertson, 1874) **	0	0	0	0	0	1	0	0	0	0	0
<i>Neocytherideis</i> sp. */**	0	0	0	0	0	0	0	0	0	0	0
<i>Occultocythereis</i> sp. */**	0	0	0	1	0	0	0	0	0	0	0
<i>Paracytheridea hexalpa</i> (Doruk, 1980)	0	0	0	0	0	2	2	0	0	0	0
<i>Paracytheridea</i> sp. */**	0	0	0	0	0	0	0	0	0	0	0
<i>Pontocypris acuminata</i> (G.W. Muller, 1894)	0	0	0	0	0	0	0	0	0	0	0
<i>Pontocythere turbida</i> (G.W. Muller, 1894)	0	0	0	0	0	1	2	0	0	0	0
<i>Propontocypris pirifera</i> (G.W. Muller, 1894) **	0	0	0	0	0	1	0	0	0	0	0
<i>Sagmocythere versicolor</i> (G.W. Muller, 1894)	2	3	0	0	7	15	6	7	8	27	7
<i>Semicytherura acuticostata</i> (G.O. Sars, 1866)	0	0	0	0	0	0	0	0	0	0	0
<i>Semicytherura incongruens</i> (G.W. Muller, 1894) **	0	0	0	0	1	0	0	0	0	0	0
<i>Semicytherura marialuisae</i> (Faranda and Gliozzi, 2008) */**	0	0	0	0	0	0	0	0	0	0	0
<i>Semicytherura paradoxa</i> (G.W. Muller, 1894)	0	4	0	0	0	0	2	0	0	0	0
<i>Semicytherura rarecostata</i> (Bonaduce, Ciampo and Masoli, 1975)	0	1	0	0	0	4	4	0	0	0	0
<i>Semicytherura ruggierii</i> (Pucci, 1955)	0	48	1	13	5	29	17	22	5	12	0
<i>Semicytherura sulcata</i> (G.W. Muller, 1894) */**	0	0	0	0	0	0	0	0	0	0	0
<i>Semicytherura</i> sp. */**	0	0	0	0	0	0	0	0	0	0	0
<i>Hemicytherura diaforei</i> (Ruggieri, 1953)	2	0	0	0	0	0	3	0	0	0	0
<i>Microcytherura angulosa</i> (Seguenza, 1880) */**	0	0	0	0	0	0	0	0	0	0	0
<i>Microcytherura nigrescens</i> (G.W. Muller, 1894)	0	0	0	0	0	0	0	0	1	0	0
<i>Microcytherura</i> sp. */**	0	0	0	0	0	0	0	0	0	0	0
<i>Monoceratina mediterranea</i> (Sissingh, 1972) */**	0	0	0	0	0	0	0	0	0	0	0
<i>Tuberculocythere quadrituberculata</i> (Colalongo and Pasini, 1980)	0	0	0	0	0	0	0	0	0	0	0

<i>Microxestoleberis nana</i> (G.W. Muller, 1894)	0	0	0	0	0	0	0	4	0	0	0	0
<i>Microxestoleberis xenomys</i> (Barbeito-Gongalez, 1971) */**	0	0	0	2	0	0	0	0	0	0	0	0
<i>Urocythereis</i> cf. <i>U. flexicauda</i> (Bonaduce, Ciampo and Masoli, 1975)	0	2	0	2	0	0	0	0	0	0	0	0
<i>Xestoleberis communis</i> (G.W. Muller, 1894)	0	0	0	0	0	2	2	0	1	0	0	0
<i>Xestoleberis</i> sp. */**	0	0	0	0	0	0	0	0	0	1	0	0
<i>Palmoconcha turbida</i> (G.W. Muller, 1894)	0	2	0	1	0	3	3	0	0	1	0	0
<i>Palmoconcha subrugosa</i> (Ruggieri 1967)	3	0	0	11	2	2	2	0	2	5	0	0
<i>Pterygocythereis coronata</i> (Roemer, 1838)	0	0	0	0	0	0	2	0	0	2	2	0
<i>Pterygocythereis jonesii</i> (Baird 1850)	0	0	0	0	0	0	0	0	0	0	0	0
<i>Pterygocythereis</i> sp. */**	0	0	0	0	0	0	0	0	0	0	0	0
<i>Leptocythere bacescoi</i> (Rome 1942)	0	2	0	2	0	0	2	0	0	0	0	0
<i>Leptocythere levis</i> (G.W. Muller, 1894) */**	0	0	0	0	0	0	0	0	0	0	0	0
<i>Leptocythere macella</i> (Ruggieri, 1975) */**	0	0	0	0	0	0	0	0	0	0	0	0
<i>Leptocythere multipunctata</i> (Seguenza 1883)	0	8	0	0	0	8	8	2	2	5	0	0
<i>Leptocythere ramosa</i> (Rome 1942)	0	0	0	1	0	0	1	0	0	1	0	0
<i>Leptocythere rara</i> (G.W. Muller, 1894) */**	0	0	0	0	0	0	0	0	0	0	0	0
<i>Leptocythere transiens</i> (Pucci, 1956) */**	0	0	0	0	0	0	0	0	0	0	0	0
<i>Leptocythere</i> sp. */**	0	0	0	0	0	0	0	0	0	0	0	0
<i>Cytherella alverium</i> (Bonaduce, Ciampo and Masoli, 1975) */**	0	0	0	2	0	0	0	0	0	0	0	0
<i>Cytherella gibba</i> (Aiello, Barra, Bonaduce and Russo, 1996)	2	5	0	7	0	0	3	2	0	0	0	8
<i>Cytherella robusta</i> (Colalongo and Pasini, 1980)	0	0	0	0	0	0	0	0	1	0	0	0
<i>Cytherella vulgatella</i> (Aiello, Barra, Bonaduce and Russo, 1996)	0	0	0	12	0	2	0	0	0	0	0	2
<i>Cytherella</i> sp. */**	0	0	0	0	0	0	0	0	0	1	0	0
<i>Argilloecia acuminata</i> (G.W. Muller, 1894)	2	1	0	2	0	8	5	0	0	0	0	0
<i>Argilloecia minor</i> (G.W. Muller, 1894)	0	1	0	2	0	0	0	0	2	0	0	0
<i>Argilloecia robusta</i> (Bonaduce, Ciampo and Masoli, 1975) */**	0	0	0	0	0	0	0	0	0	0	0	0
<i>Argilloecia</i> sp. */**	0	0	0	0	0	0	0	0	1	0	0	0
<i>Bairda conformis</i> (Terquem, 1878)	0	0	0	0	0	0	0	0	0	0	0	2
<i>Bairda</i> sp. */**	0	0	0	0	0	0	0	0	0	0	0	0
<i>Bosquetina tarentina</i> (Baird, 1850)	2	2	0	0	5	0	0	6	1	0	0	16
<i>Bosquetina</i> sp. */**	0	0	0	0	1	0	0	0	0	0	0	0
<i>Cytheropteron aduncum</i> (Colalongo and Pasini, 1980) */**	0	0	0	0	0	0	0	0	0	0	0	0
<i>Cytheropteron agile</i> (Colalongo and Pasini, 1980) */**	0	0	0	0	0	0	0	0	0	0	0	0
<i>Cytheropteron alatum</i> (Sars, 1866)	0	0	0	0	0	0	1	0	0	0	0	0
<i>Cytheropteron</i> cf. <i>C. ionicum</i> (Colalongo and Pasini, 1980) */**	0	0	0	0	0	0	0	0	0	0	0	0
<i>Cytheropteron latum</i> (G.W. Muller, 1894)	0	0	0	0	0	0	0	0	0	1	0	0
<i>Cytheropteron monoceros</i> (Bonaduce, Ciampo and Masoli, 1975)	0	0	0	4	2	0	13	4	0	4	7	0
<i>Cytheropteron pseudoalatum</i> (Colalongo and Pasini, 1980) **	0	0	0	0	0	0	1	0	4	0	0	0
<i>Cytheropteron rectum</i> (Colalongo and Pasini, 1980) */**	0	0	0	0	0	0	0	0	0	6	0	0
<i>Cytheropteron ruggierii</i> (Pucci 1955)	6	4	0	2	0	4	4	0	0	0	0	3
<i>Cytheropteron trapezium</i> (Colalongo and Pasini, 1980) */**	0	0	0	0	0	0	0	0	0	0	0	0
<i>Cytheropteron</i> sp. */**	0	0	0	0	0	0	1	0	0	0	0	1
<i>Henryhowella sarsii</i> (G.W. Muller, 1894)	0	0	0	0	2	0	8	0	0	0	0	23
<i>Krithe</i> group (Brady, Crosskey and Robertson, 1874) */**	21	6	1	13	11	2	3	12	5	0	0	75
<i>Parakrithe</i> group (van den Bold, 1958) */**	0	1	0	9	0	0	9	4	1	0	0	7
<i>Paracytheroismediterranea</i> (Bonaduce, Ciampo and Masoli, 1975)	0	0	0	0	0	0	0	1	0	8	0	0
<i>Triebelina raripilia</i> (G.W. Muller, 1894)	0	0	0	0	0	0	0	0	0	0	0	0
Total Abundance	44	100	25	95	42	129	173	94	75	94	153	

			**	**	*/**			**	**	**		*/**	*/**
SMA10	SMA8	SMA4	SMA2	SMA-1	SMA-4	SMA-8	SMA-14	SMB4	SMB8	SMB14	SMB20	SMB26	SMB32
2.31	1.81	0.81	0.31	0.00	-0.75	-1.75	-3.25	-4.25	-5.25	-6.75	-8.25	-10.5	-12.00
0	0	2	0	0	0	9	0	9	24	20	27	0	9
0	0	0	0	0	0	0	0	8	11	4	0	0	0
0	0	0	0	0	0	0	0	1	0	0	0	0	0
0	0	0	0	0	0	0	0	0	0	1	0	0	0
0	0	0	0	0	0	0	0	0	0	0	0	0	0
0	0	0	0	0	0	0	0	1	0	0	0	0	0

0	0	0	0	0	0	0	0	0	0	0	1	0	0
0	0	2	0	0	0	9	6	7	10	9	2	0	12
0	0	0	0	0	0	0	0	0	1	0	0	0	0
2	0	3	0	0	0	0	2	0	0	0	0	0	0
0	1	0	0	0	0	0	0	0	0	0	0	0	0
0	0	0	0	0	0	0	0	1	0	0	0	0	0
0	0	0	0	0	0	0	0	0	1	0	0	0	0
0	0	0	0	0	0	0	0	0	0	0	0	0	0
0	0	0	0	0	0	0	0	1	0	0	0	0	0
0	0	0	0	0	0	0	0	0	0	0	0	0	0
0	0	0	0	0	0	0	0	0	0	0	0	0	0
0	0	0	0	0	0	0	0	1	6	3	0	0	0
0	0	0	0	0	0	0	0	0	0	0	0	0	0
0	0	0	0	0	0	0	0	0	0	0	0	0	0
0	0	0	0	0	0	0	0	0	0	0	0	0	0
0	0	0	0	0	0	0	0	0	0	0	0	0	0
0	0	0	0	0	0	0	0	1	2	3	0	0	0
0	0	0	0	0	0	0	0	1	1	0	0	0	0
0	0	0	0	0	0	0	0	0	0	0	0	0	0
0	0	0	0	0	0	0	0	0	0	0	0	0	0
0	0	0	0	0	0	0	0	1	0	0	0	0	0
0	0	0	0	0	0	0	0	0	0	2	0	0	0
0	0	0	0	0	0	0	0	0	0	0	0	0	0
0	0	0	0	0	0	3	0	1	0	0	0	0	0
0	0	0	0	0	0	0	0	1	1	0	0	0	0
0	0	0	0	0	0	0	0	1	0	0	1	0	0
0	0	0	0	0	0	0	0	0	0	0	0	0	0
0	0	0	0	0	0	0	0	0	0	0	0	0	0
0	0	4	0	4	0	6	3	4	8	11	4	0	0
0	0	2	0	0	0	0	0	2	1	1	0	0	0
0	0	0	0	0	0	0	0	0	1	0	0	0	4
0	0	0	0	0	0	0	0	0	1	0	0	0	0
0	0	0	0	0	0	0	0	1	0	0	0	0	0
0	0	1	0	0	0	0	0	4	2	3	1	0	0
0	2	0	0	0	0	3	24	41	9	7	11	0	0
0	0	0	0	0	0	0	0	0	0	0	0	0	0
0	0	0	0	0	0	0	0	0	0	2	0	0	0
0	0	0	0	0	0	0	0	0	0	0	0	0	0
0	0	0	0	0	0	0	0	0	0	1	0	0	0
0	0	0	0	0	0	3	2	4	0	0	0	0	0
0	0	0	0	0	0	0	0	0	0	0	0	0	0
0	0	0	0	0	0	0	0	0	0	0	0	0	0
2	0	2	0	0	0	0	0	0	0	0	0	0	0
0	0	0	0	0	0	0	1	0	0	0	0	0	0
0	0	0	0	0	0	0	0	0	0	0	0	0	0
0	0	0	0	0	0	0	3	1	3	2	0	0	0
0	0	0	0	0	0	0	2	1	3	1	0	0	0
0	0	0	0	0	0	2	0	1	0	0	0	0	0
0	4	1	0	1	0	0	0	0	2	6	0	0	2
0	5	21	19	2	0	6	3	0	3	0	6	0	0
2	19	10	2	6	0	0	3	1	1	0	0	0	0
0	0	2	0	1	0	0	2	0	0	0	0	0	0
0	0	0	0	0	0	0	0	0	1	0	0	0	0
0	0	0	0	0	0	0	1	0	0	0	0	0	0
0	0	0	0	0	0	0	0	0	0	0	0	0	0
0	0	0	0	0	0	0	1	0	0	0	0	0	0
0	0	2	2	2	0	0	8	6	15	15	12	0	0
0	0	0	0	1	0	0	1	0	5	0	0	0	0
0	0	0	0	0	0	0	0	0	1	0	0	0	0
0	0	0	0	0	0	0	0	0	0	1	0	0	0
0	0	0	0	0	0	0	0	1	0	0	1	0	0
0	0	0	0	0	0	0	0	0	0	0	0	0	0
2	20	5	5	2	0	12	10	2	1	1	0	0	0
0	0	0	3	0	0	0	0	0	0	1	0	0	0
2	4	6	0	0	0	3	2	0	1	0	0	0	0
0	0	0	0	0	0	0	0	0	0	1	0	0	0
0	0	4	0	0	0	0	1	0	0	0	2	0	0
0	0	0	0	0	0	0	0	0	0	0	0	0	0
0	0	0	0	0	0	0	2	0	0	0	0	0	0
0	0	0	0	0	0	0	0	2	1	0	0	0	0

0	0	0	0	0	0	0	0	0	0	0	0	0	0
0	0	0	0	0	0	0	0	1	1	0	0	0	0
3	24	9	4	0	1	0	0	0	0	0	0	0	0
0	0	0	0	0	0	0	0	0	0	0	0	0	0
0	0	1	0	0	0	0	0	0	0	0	0	0	0
0	0	0	0	0	0	2	0	0	0	0	0	0	0
0	0	0	0	0	0	0	0	0	0	0	0	0	0
0	0	0	0	0	0	0	0	0	0	0	0	0	0
1	0	0	0	0	0	0	0	0	0	1	0	0	0
2	7	17	2	0	0	14	0	1	1	0	2	0	0
0	0	0	0	0	0	0	0	0	0	0	0	0	0
0	0	0	0	0	0	0	0	0	0	0	0	0	0
0	0	6	6	4	2	0	13	2	3	1	5	0	0
0	0	0	0	0	0	0	0	0	0	0	0	0	0
0	0	0	0	0	0	0	0	0	0	0	0	0	0
8	32	2	30	1	1	0	1	1	0	1	0	0	0
43	65	33	17	3	0	42	7	3	2	8	10	0	5
0	0	0	0	0	0	0	0	0	0	0	0	0	0
0	0	0	4	0	0	3	2	0	1	0	0	0	0
0	0	0	0	0	0	0	1	0	0	1	0	0	0
67	183	135	94	27	4	117	102	113	124	107	85	0	32

*/**		**	**			**		*/**	**	**	**	**	
SMB36	SMB40	SMB44	SMB48	SMB52	SMB56	SMB58	SMB60	SMB62	SMB64	SMB68	SMB72	SMB74	SMB76
-13.00	-14.00	-15.00	-16.00	-17.00	-18.00	-18.50	-19.00	-19.50	-20.00	-21.00	-22.00	-22.50	-23.00
5	25	10	50	24	11	8	2	0	3	6	9	10	19
0	0	0	0	0	0	0	0	0	0	0	0	2	0
0	0	0	0	0	0	0	0	0	0	0	0	0	0
0	0	0	0	0	0	0	0	0	0	0	0	0	0
0	0	0	0	0	0	0	0	0	0	0	0	0	3
0	0	0	2	0	7	0	0	0	1	7	12	1	0
0	0	0	0	0	0	0	0	0	0	0	2	0	0
0	0	3	4	3	2	0	2	0	1	2	14	10	8
0	0	0	0	0	0	0	0	0	0	0	0	0	0
0	0	0	0	0	0	4	0	0	0	0	1	0	0
0	0	0	0	0	0	0	0	0	0	2	0	0	0
0	0	0	0	0	0	0	0	0	0	0	0	0	0
0	0	0	0	0	0	0	0	0	0	0	0	0	0
0	0	0	0	0	0	0	0	0	0	0	0	0	2
0	0	0	0	0	0	0	0	0	0	0	0	0	0
0	0	0	0	0	0	0	0	0	0	0	0	0	1
0	0	0	0	0	4	0	0	0	0	0	0	0	2
0	5	0	0	0	0	0	0	0	0	0	0	0	0
0	0	0	0	0	0	0	0	0	0	2	0	0	2
0	0	0	0	0	0	0	0	0	0	0	0	0	0
0	0	0	0	0	0	0	0	1	0	0	1	2	1
0	0	0	0	0	0	0	0	1	0	0	0	0	0
0	0	0	0	0	0	0	0	0	0	0	0	0	0
0	0	0	0	0	0	0	2	0	0	0	0	0	0
0	0	0	0	0	0	0	0	0	0	0	0	0	0
0	0	2	0	0	0	0	0	0	0	0	0	0	0
0	0	0	0	0	0	0	0	0	0	0	0	1	0
0	0	0	0	0	0	0	0	0	0	0	0	0	0
0	0	0	6	0	0	0	0	0	0	0	0	1	0
0	0	0	0	0	0	0	0	0	0	0	0	0	0
0	0	0	0	0	1	0	0	0	0	1	0	0	0
0	5	0	0	0	0	0	0	0	0	0	3	0	0
0	0	0	0	0	0	0	3	0	0	0	0	3	0
0	3	0	9	10	6	0	2	0	2	10	0	0	0
0	3	0	0	4	0	0	0	0	0	1	3	0	4
0	0	0	2	0	0	0	0	0	0	0	2	1	0
0	0	0	0	0	0	0	0	0	0	0	0	0	0
0	0	0	0	0	0	0	0	0	0	0	0	0	4
0	0	6	2	0	1	0	0	0	0	9	4	16	2
4	19	38	19	6	11	0	0	0	0	11	17	24	21
0	0	0	0	3	0	0	0	0	0	0	0	0	0
0	2	0	0	3	0	0	1	0	0	0	2	3	0

0	0	0	0	0	2	2	0	0	0	0	0	0	0
0	0	0	0	0	0	0	0	0	0	0	0	0	0
0	0	0	0	0	0	0	0	0	0	0	1	0	0
0	0	9	2	0	0	0	0	0	0	0	0	0	0
0	0	0	0	0	0	6	0	0	0	0	0	0	0
0	0	0	0	0	0	2	0	1	5	0	0	0	0
0	0	0	0	0	0	0	1	0	0	0	0	0	0
0	0	0	0	0	0	0	0	0	0	0	0	0	0
0	3	0	0	0	0	0	0	0	0	0	0	0	8
0	0	3	0	0	7	3	0	0	0	0	0	0	2
0	0	0	0	0	0	0	0	0	0	0	0	0	0
0	0	0	0	0	0	0	0	0	1	1	3	4	0
0	0	9	16	11	0	2	2	0	1	7	10	0	4
0	0	0	8	0	2	2	0	0	0	0	0	1	1
0	0	0	0	0	0	0	0	0	1	0	0	1	0
0	0	0	0	0	0	0	0	0	0	0	0	0	0
0	22	0	0	0	0	0	0	0	0	0	4	8	8
0	9	0	0	0	0	0	0	0	0	0	0	0	0
0	0	0	0	0	0	0	0	0	0	0	0	0	0
0	3	12	0	4	2	0	0	0	2	4	12	21	12
0	2	3	1	2	0	0	0	0	0	0	1	5	1
0	0	0	0	0	0	0	0	0	0	0	0	0	0
0	0	0	0	0	0	0	0	0	0	0	0	0	0
0	0	0	0	0	0	0	1	0	0	0	2	0	0
0	0	0	0	0	0	0	0	0	0	0	0	0	0
0	0	0	0	5	0	2	0	3	0	0	0	0	5
0	3	0	0	0	4	22	16	0	3	11	0	0	3
0	0	0	0	0	0	0	0	0	0	0	0	2	0
0	0	0	0	0	0	0	0	0	0	0	0	0	0
0	0	0	0	2	0	0	0	4	0	0	0	0	2
0	0	0	0	0	4	0	0	0	0	0	0	0	0
0	0	0	0	0	0	0	0	0	0	0	0	0	0
0	0	0	0	0	2	16	19	0	0	0	0	2	0
0	0	0	0	0	10	0	10	0	0	0	0	0	0
0	0	0	0	0	0	0	0	0	0	1	0	0	0
0	0	0	2	3	15	0	20	0	1	0	0	0	0
0	0	0	0	0	0	0	0	0	0	0	0	0	0
0	0	0	0	0	0	0	0	0	0	0	0	0	0
0	0	0	0	3	0	0	0	0	0	0	0	0	0
0	0	0	3	0	0	0	0	0	0	0	0	0	0
0	0	0	0	0	0	0	0	0	0	0	0	0	0
0	0	0	0	0	0	0	0	0	0	0	0	0	0
0	0	0	0	3	0	0	0	0	0	0	0	0	0
0	0	0	0	1	0	0	0	0	0	0	0	0	0
0	0	0	1	0	0	0	4	0	0	3	0	1	0
0	16	0	0	5	0	19	18	1	3	32	0	0	0
0	12	4	4	11	20	8	33	0	5	22	5	8	11
0	0	0	0	0	0	0	0	1	0	0	0	0	0
0	0	0	0	1	0	0	0	1	3	0	0	0	0
0	0	0	0	0	0	0	0	0	0	0	0	0	0
9	132	102	145	103	111	104	152	19	33	145	124	136	126

Chapter 9

Concluding remarks

9. Concluding remarks

The case studies reported in this Ph.D. thesis utilize the stratigraphic paleobiology approach to investigate mollusk-dominated fossil benthic associations retrieved from Quaternary sedimentary successions of Italy. The research described in these chapters offers an improved understanding of how to collect and use macrofossil to assess the response of late Quaternary ecosystems to climate-driven environmental changes. On one hand, these studies focus on how stratigraphic imprint can distort biological dynamics recorded in the geological record. On the other hand, investigations carried out during my Ph.D. highlight the importance of the macrobenthic record to interpret environmental gradients and thus refine (sequence) stratigraphic interpretation of the investigated sedimentary record.

The Mid Adriatic Deep dataset (Chapter 4) when merged with the previously assembled Po plain dataset, will be pivotal for acquiring a historical perspective on modern ecosystems that have been shaped by long term (glacial/interglacial) climatic oscillations. Furthermore, the understanding of long-term dynamics of macrobenthic communities (i.e., resilience, persistence or stochastic reassembly) to long-term natural changes will provide us with an important reference framework for assessing recent anthropogenic changes affecting deltaic ecosystems.

In the first case study (Chapter 5) the high-resolution sequence stratigraphic architecture of the transgressive succession of the Po coastal plain served as a framework for evaluating taphonomic trends and time resolution of the macrofossil record along a down-dip profile: nearshore to shallow marine settings. Along the investigated profile, resolution and quality of the macrofossil record both decline down-dip. Compared to distal settings, proximal settings (<5 km from shoreline at time of maximum marine ingression) are distinguishable by high (centennial-scale) resolution and overall well-preserved and ecologically coherent fossil assemblages. The onshore-to-offshore degradation of quality and resolution of the macrobenthic record likely reflects increasing surface/near-surface resident time of macroskeletal remains down-dip, due to decreasing sediment accumulation rates. Individually dated mollusks suggest that the strong taphonomic degradation and ecological condensation affects distally developed successions with the estimated time-averaging manifested over multi-millennial time scales (~8 ka). In addition, the integrated taphonomic, bathymetric and fossil density trends highlight distinctive signatures useful in interpreting past environments and identifying surfaces/intervals of sequence stratigraphic significance.

The second case study (Chapter 6), targets Holocene bivalves within brackish succession of the Po coastal plain. These deposits represent a well-preserved fossil record, framed within a high-resolution chronostratigraphic framework (see Chapter 5). The research focuses on documenting parasite-host dynamics over geological short-lived (centennial scale) and small amplitude sea-level oscillations. Specifically, we investigated the parasite-induced malformations (*pits*) visible on the

inner part of the valves of the thin-shelled *Abra segmentum*, which is the most abundant bivalve in the targeted cored succession. The study documents that prevalence values of trematodes parasites infesting the bivalve host *Abra segmentum* were significantly elevated ($p \ll 0.05$) in samples associated with centennial-time scale flooding surfaces. These evidences suggest that the fossil record can provide a quantitative archive also of parasite-host interactions developed at societally-relevant time scales. Furthermore, the historical perspective acquired here could be used to shed light on the response of heterocious parasites to ongoing anthropogenic warming and sea-level rise.

The third study (Chapter 7) investigates distribution of Last Occurrences (LOs) of macrobenthic species along a down-dip transect in the Po coastal plain transgressive-regressive succession to examine potential effects of the sequence stratigraphic architecture on mass extinction patterns. The results show that if a hypothetical mass extinction took place today, the LOs would not always follow the gradual smearing-backward predicted by the Signor-Lipps effect. Instead, the LOs would typically cluster along intervals of stratigraphic condensation/strong facies-shifts, mimicking sudden extinction pulses. These clusters of LOs are particularly evident in the two distal cores in accordance with the results highlighted in Chapter 5, which documented multi-millennial time and stratigraphic condensation in the distal part of the studied profile. The resultant complex but completely false extinction pattern highlights the necessity of accounting for paleoenvironmental and sequence stratigraphic context when inferring extinctions from the fossil record. The sequence stratigraphic architecture of relevant fossiliferous successions could easily confound the timing, duration and selectivity of mass-extinction events.

The fourth case study (Chapter 8) focused on the well-known Pleistocene benthic fauna from Valle di Manche section (Southern Italy). This succession - with its well-established stratigraphic and chronological frameworks - offers the opportunity to test the robustness of paleoecological patterns derived by the application of different ordination analyses. Concomitantly, these analyses also serve to assess the main environmental driver(s) of faunal turnover. The investigation concluded that, even when notably varying the analytical sample threshold, stratigraphic plots of axis-1 sample scores obtained by detrended correspondence analysis (DCA) and non-metric multidimensional scaling (nMDS) yielded consistent outcomes, which invariably pointed to bathymetry as the main driver of faunal turnover. Consequently, the results suggest that combined use of DCA and nMDS can help to assess the robustness of the analytical outcomes to the choice of the ordination method used and help us to better define the main environmental driver of faunal turnover.

References

- AGIP, (1977). Temperature sotterranee. Inventario dei dati raccolti dall'AGIP durante la ricerca e la produzione di idrocarburi in Italia, Edizioni AGIP, 1930 p.
- Alteriis, G. (1995). Different foreland basins in Italy: examples from the central and southern Adriatic Sea. *Tectonophysics*, 252(1-4), 349-373.
- Amorosi, A., and Colalongo, M. L. (2005). The linkage between alluvial and coeval nearshore marine successions: evidence from the Late Quaternary record of the Po River Plain, Italy. *Fluvial Sedimentology* VII, 255-275.
- Amorosi, A., Colalongo, M. L., Fusco, F., Pasini, G., and Fiorini, F. (1999). Glacio-eustatic control of continental–shallow marine cyclicity from late Quaternary deposits of the southeastern Po Plain, northern Italy. *Quaternary Research*, 52(1), 1-13.
- Amorosi, A., Colalongo, M. L., Fiorini, F., Fusco, F., Pasini, G., Vaiani, S. C., and Sarti, G. (2004). Palaeogeographic and palaeoclimatic evolution of the Po Plain from 150-ky core records. *Global and Planetary Change*, 40(1-2), 55-78.
- Amorosi, A., Centineo, M. C., Colalongo, M. L., and Fiorini, F. (2005). Millennial-scale depositional cycles from the Holocene of the Po Plain, Italy. *Marine Geology*, 222, 7-18.
- Amorosi, A., Colalongo, M. L., Dinelli, E., Lucchini, F., and Vaiani, S. C. (2007). Cyclic variations in sediment provenance from late Pleistocene deposits of the eastern Po Plain, Italy. *Special Papers-Geological Society Of America*, 420, 13.
- Amorosi, A., Pavesi, M., Lucchi, M. R., Sarti, G., and Piccin, A. (2008). Climatic signature of cyclic fluvial architecture from the Quaternary of the central Po Plain, Italy. *Sedimentary Geology*, 209(1-4), 58-68.
- Amorosi, A., Rossi, V., Sarti, G., and Mattei, R. (2013). Coalescent valley fills from the late Quaternary record of Tuscany (Italy). *Quaternary International*, 288, 129-138.
- Amorosi, A., Bruno, L., Campo, B., and Morelli, A. (2015). The value of pocket penetration tests for the high-resolution palaeosol stratigraphy of late Quaternary deposits. *Geological Journal*, 50(5), 670-682.
- Amorosi, A., Maselli, V., and Trincardi, F. (2016). Onshore to offshore anatomy of a late Quaternary source-to-sink system (Po Plain–Adriatic Sea, Italy). *Earth-Science Reviews*, 153, 212-237.
- Amorosi, A., Bruno, L., Campo, B., Morelli, A., Rossi, V., Scarponi, D., ... and Drexler, T. M. (2017). Global sea-level control on local parasequence architecture from the Holocene record of the Po Plain, Italy. *Marine and Petroleum Geology*, 87, 99-111.
- Andrews, J. T., & Voelker, A. H. (2018). “Heinrich events” (& sediments): A history of terminology and recommendations for future usage. *Quaternary Science Reviews*, 187, 31-40.
- Antonoli, F., Ferranti, L., Fontana, A., Amorosi, A., Bondesan, A., Braitenberg, C., ... and Mastronuzzi, G. (2009). Holocene relative sea-level changes and vertical movements along the Italian and Istrian coastlines. *Quaternary International*, 206(1-2), 102-133.
- Aquater (1976). Elaborazione dei dati geofisici relativi alla Dorsale Ferrarese: Rapporto Inedito per ENEL.

- Aquater (1977). Elaborazione dei dati geofisici relativi alla struttura del Trino Vercellese: Rapporto Inedito per ENEL.
- Aquater (1978). Interpretazione dei dati geofisici delle strutture plioceniche e Quaternarie della Pianura Padana e Veneta: Rapporto Inedito per ENEL.
- Aquater-ENEL (1981), Elementi di neotettonica del territorio italiano: Volume Speciale, Roma.
- Argnani, A., and Gamberi, F. (1995). Stili strutturali al fronte della catena appenninica nell'Adriatico centro-settentrionale. *Studi Geologici Camerti*, 1, 19-27.
- Artegiani, A., Paschini, E., Russo, A., Bregant, D., Raicich, F., and Pinardi, N. (1997). The Adriatic Sea general circulation. Part I: Air–sea interactions and water mass structure. *Journal of physical oceanography*, 27(8), 1492-1514.
- Artegiani, A., Paschini, E., Russo, A., Bregant, D., Raicich, F., and Pinardi, N. (1997). The Adriatic Sea general circulation. Part II: baroclinic circulation structure. *Journal of physical oceanography*, 27(8), 1515-1532.
- Artoni, A. (2007). Growth rates and two-mode accretion in the outer orogenic wedge-foreland basin system of Central Apennine (Italy). *Bollettino-Società Geologica Italiana*, 126 (3), 531.
- Asioli, A. (1996). High resolution foraminifera biostratigraphy in the Central Adriatic basin during the last deglaciation: a contribution to the PALICLAS Project. *Memorie-Istituto Italiano di Idrobiologia*, 55, 197-218.
- Asioli, A., Trincardi, F., Lowe, J. J., Ariztegui, D., Langone, L., and Oldfield, F. (2001). Sub-millennial scale climatic oscillations in the central Adriatic during the Lateglacial: palaeoceanographic implications. *Quaternary Science Reviews*, 20(11), 1201-1221.
- Astori, A., Castaldini, D., Burrato, P., and Valensise, G. (2002). Where the Alps meet the Apennines. In *Active tectonic and seismicity of the central Po Plain. SAFE (Slow Active Faults in Europe). Semester meeting, Mantova* (pp. 20-23).
- Azzarone, Michele (2019) Mid Adriatic Deep Dataset. Alma Mater Studiorum Università di Bologna. DOI <http://doi.org/10.6092/unibo/amsacta/6101>
- Bally, A. W. (1986). Balanced sections and seismic reflection profiles across the Central Apennines. *Memorie Società Geologica Italiana*, 35, 257-310.
- Bartolini, C., Caputo, R., and Pieri, M. (1996). Pliocene–Quaternary sedimentation in the Northern Apennine Foredeep and related denudation. *Geological Magazine*, 133(3), 255-273.
- Bassetti, M. A., Berne, S., Jouet, G., Taviani, M., Dennielou, B., Flores, J. A., Gaillot, A., Gelfort, R., Lafuerza, S., and Sultan, N. (2008). The 100-ka and rapid sea level changes recorded by prograding shelf sand bodies in the Gulf of Lions (western Mediterranean Sea). *Geochemistry, Geophysics, Geosystems*, 9(11).
- Berger, A. (1988). Milankovitch theory and climate. *Reviews of geophysics*, 26(4), 624-657.
- Berné, S., Rabineau, M., Flores, J. A., and Sierro, F. (2004). The impact of Quaternary global changes on strata formation: exploration of the shelf edge in the NW Mediterranean Sea. *Oceanography*, 17(4), 92-103.
- Bigi, G., Cosentino, D., Parotto, M., Sartori, R., and Scandone, P. (1992). Modello strutturale tridimensionale d'Italia in scala 1: 500 000. *CNR-Centro Nazionale delle Ricerche, Roma*.

- Bigi, S., Conti, A., Casero, P., Ruggiero, L., Recanati, R., & Lipparini, L. (2013). Geological model of the central Periadriatic basin (Apennines, Italy). *Marine and Petroleum Geology*, *42*, 107-121.
- Boessenecker, R. W., Perry, F. A., and Schmitt, J. G. (2014). Comparative taphonomy, taphofacies, and bonebeds of the Mio-Pliocene Purisima Formation, Central California: strong physical control on marine vertebrate preservation in shallow marine settings. *PLoS One*, *9*(3), e91419.
- Bolotov, I. N., Besspalaya, Y. V., & Usacheva, O. V. (2012). Ecology and evolution of hydrobionts in hot springs of the Subarctic and Arctic: formation of similar assemblages, adaptation of species, and microevolutionary processes. *Biology Bulletin Reviews*, *2*(4), 340-348.
- Bond, G., Showers, W., Cheseby, M., Lotti, R., Almasi, P., deMenocal P., Priore, P., Cullen, H., Hajdas, I. and Bonani, G. (1997). A pervasive millennial-scale cycle in North Atlantic Holocene and glacial climates. *Science*, *278*(5341), 1257-1266.
- Bonelli Jr, J. R., and Patzkowsky, M. E. (2008). How are global patterns of faunal turnover expressed at regional scales? Evidence from the Upper Mississippian (Chesterian Series), Illinois Basin, USA. *Palaïos*, *23*(11), 760-772.
- Bösken, J., Sümegei, P., Zeeden, C., Klasen, N., Gulyás, S., & Lehmkuhl, F. (2018). Investigating the last glacial Gravettian site 'Ságvár Lyukas Hill' (Hungary) and its paleoenvironmental and geochronological context using a multi-proxy approach. *Palaeogeography, Palaeoclimatology, Palaeoecology*, *509*, 77-90.
- Bouchet P. (2006). The magnitude of marine biodiversity. In: C.M. Duarte (ed.). *The exploration of marine biodiversity. Scientific and technological challenges*: 31-62. Fundación BBVA, Bilbao.
- Bouchet, P.; Bary, S.; Héros, V.; Marani, G. (2016). How many species of molluscs are there in the world's oceans, and who is going to describe them?, *in*: Héros, V. *et al.* (Ed.) *Tropical Deep-Sea Benthos* 29. *Mémoires du Muséum national d'Histoire naturelle* (1993), 208: pp. 9-24
- Bourne, A. J., Lowe, J. J., Trincardi, F., Asioli, A., Blockley, S. P. E., Wulf, S., Matthews, I.P., Piva, A. and Vigliotti, L. (2010). Distal tephra record for the last ca 105,000 years from core PRAD 1-2 in the central Adriatic Sea: implications for marine tephrostratigraphy. *Quaternary Science Reviews*, *29*(23-24), 3079-3094.
- Boyd, R. (2006). Estuarine and incised-valley facies models. *Facies models revisited*, 171-235.
- Bradley, R. S. (1999). *Paleoclimatology: reconstructing climates of the Quaternary* (Vol. 68). Elsevier.
- Broecker, W. S., and Denton, G. H. (1989). The role of ocean-atmosphere reorganizations in glacial cycles. *Geochimica et Cosmochimica Acta*, *53*(10), 2465-2501.
- Bruno, L., Amorosi, A., Severi, P., and Costagli, B. (2017). Late Quaternary aggradation rates and stratigraphic architecture of the southern Po Plain, Italy. *Basin Research*, *29*(2), 234-248.
- Burrato, P., Ciucci, F., and Valensise, G. (2003). An inventory of river anomalies in the Po Plain, Northern Italy: evidence for active blind thrust faulting. *Annals of Geophysics*.
- Butler, R. W. (1982). Hangingwall strain: a function of duplex shape and footwall topography. *Tectonophysics*, *88*(3-4), 235-246.

- Campo, B., Amorosi, A., and Vaiani, S. C. (2017). Sequence stratigraphy and late Quaternary paleoenvironmental evolution of the Northern Adriatic coastal plain (Italy). *Palaeogeography, Palaeoclimatology, Palaeoecology*, 466, 265-278.
- Castellarin, A. (2013). Alps-Apennine and Po Plain-frontal Apennines relations. In Vai, F., & Martini, I. P. (Eds.), *Anatomy of an orogen: the Apennines and adjacent Mediterranean basins*. Springer.
- Cattaneo, A., Correggiari, A., and Trincardi, F. (2002). Recognition of turbidite elements in the late-Quaternary Adriatic basin: where are they and what do they tell us. In *Turbidite Systems and Deep-Sea Fans in the Mediterranean and Black Seas: Commission for the Scientific Exploration of the Mediterranean Sea (CIESM), Workshop Series* (No. 17, pp. 27-32).
- Cattaneo, A., Correggiari, A., Langone, L., and Trincardi, F. (2003). The late-Holocene Gargano subaqueous delta, Adriatic shelf: sediment pathways and supply fluctuations. *Marine Geology*, 193(1-2), 61-91.
- Cattaneo, A., and Steel, R. J. (2003). Transgressive deposits: a review of their variability. *Earth-Science Reviews*, 62(3-4), 187-228.
- Catuneanu, O. (2017). Sequence stratigraphy: Guidelines for a standard methodology. In *Stratigraphy and Timescales* (Vol. 2, pp. 1-57). Academic Press.
- Carey, J. S., Sheridan, R. E., and Ashley, G. M. (1998). Late Quaternary sequence stratigraphy of a slowly subsiding passive margin, New Jersey continental shelf. *AAPG bulletin*, 82(5), 773-791.
- Chappell, J. (1974). Geology of coral terraces, Huon Peninsula, New Guinea: a study of Quaternary tectonic movements and sea-level changes. *Geological Society of America Bulletin*, 85(4), 553-570.
- Ciabatti, M., Curzi, P. V., and Ricci Lucchi, F. (1987). Quaternary sedimentation in the central Adriatic Sea. *Giornale di geologia*, 49(1), 113-125.
- Correggiari, A. (1996). Late Pleistocene and Holocene evolution of the north Adriatic Sea. *Il Quaternario*, 2, 697-704.
- Correggiari, A., Cattaneo, A., and Trincardi, F. (2005). The modern Po Delta system: lobe switching and asymmetric prodelta growth. *Marine Geology*, 222, 49-74.
- Costa, M. (2003). The buried, Apenninic arcs of the Po Plain and northern Adriatic Sea (Italy); a new model. *Bollettino della Società geologica italiana*, 122(1), 3-23.
- Cruz Jr, F. W., Burns, S. J., Karmann, I., Sharp, W. D., Vuille, M., Cardoso, A. O., Ferrari, J.A., Silva Dias P.L. and Viana Jr, O. (2005). Insolation-driven changes in atmospheric circulation over the past 116,000 years in subtropical Brazil. *Nature*, 434(7029), 63.
- Danise, S., and Holland, S. M. (2017). Faunal response to sea-level and climate change in a short-lived seaway: Jurassic of the Western Interior, USA. *Palaeontology*, 60(2), 213-232.
- Dansgaard, W., Johnsen, S. J., Clausen, H. B., Dahl-Jensen, D., Gundestrup, N. S., Hammer, C. U., Hvidberg C.S., Steffensen, A.E., Sveinbjörnsdottir, A. E., Jouzel, J. and Bond, G. (1993). Evidence for general instability of past climate from a 250-kyr ice-core record. *Nature*, 364(6434), 218.
- DeCelles, P. G., and Giles, K. A. (1996). Foreland basin systems. *Basin research*, 8(2), 105-123.

- Deplazes, G., Lückge, A., Peterson, L. C., Timmermann, A., Hamann, Y., Hughen, K. A., Röhl, U., Laj, C., Cane, M. A., Sigman D. M. and Haug, G. H. (2013). Links between tropical rainfall and North Atlantic climate during the last glacial period. *Nature Geoscience*, 6(3), 213.
- Doglionni, C., Mongelli, F., and Pieri, P. (1994). The Puglia uplift (SE Italy): an anomaly in the foreland of the Apenninic subduction due to buckling of a thick continental lithosphere. *Tectonics*, 13(5), 1309-1321.
- Doglionni, C., Harabaglia, P., Martinelli, G., Mongelli, F., and Zito, G. (1996). A geodynamic model of the Southern Apennines accretionary prism. *Terra Nova*, 8(6), 540-547.
- Dominici, S., and Kowalke, T. (2007). Depositional dynamics and the record of ecosystem stability: Early Eocene faunal gradients in the Pyrenean Foreland, Spain. *Palaios*, 22(3), 268-284.
- Dominici, S., Danise, S., and Benvenuti, M. (2017). Pliocene stratigraphic paleobiology in Tuscany and the fossil record of marine megafauna. *Earth-Science Reviews*.
- Dowdeswell, J. A., Maslin, M. A., Andrews, J. T., and McCave, I. N. (1995). Iceberg production, debris rafting, and the extent and thickness of Heinrich layers (H-1, H-2) in North Atlantic sediments. *Geology*, 23(4), 301-304.
- ENEA (2017) website - http://www.santateresa.enea.it/wwwste/banchedati/bd_ambmar.html. Accessed on 09/15/2017
- Fantoni, R., and Franciosi, R. (2010). Tectono-sedimentary setting of the Po Plain and Adriatic foreland. *Rendiconti Lincei*, 21(1), 197-209.
- Fontana, A., Mozzi, P., & Marchetti, M. (2014). Alluvial fans and megafans along the southern side of the Alps. *Sedimentary Geology*, 301, 150-171.
- Foote, M. (1996). Models of morphological diversification. *Evolutionary paleobiology*. University of Chicago Press, Chicago, 62-86.
- Foote, M., and Raup, D. M. (1996). Fossil preservation and the stratigraphic ranges of taxa. *Paleobiology*, 22(2), 121-140.
- Francani, V., Piccin, A., Credali, M., Berra, F., Battaglia, D., Gattinoni, P., Rigamonti, I., Rosselli, S. (2016). *Note illustrative della Carta Geologica d'Italia alla scala 1:50.000. Foglio 118* - Milano. ISPRA, Piacenza.
- Gambi, M. C., Fresi, E., and Giangrande, A. (1982). Descrittori efficaci di comunità bentoniche. *Naturalista Siciliano*, 489-497.
- Garzanti, E., Vezzoli, G., and Andò, S. (2011). Paleogeographic and paleodrainage changes during Pleistocene glaciations (Po Plain, northern Italy). *Earth-Science Reviews*, 105(1-2), 25-48.
- Ghielmi, M., Minervini, M., Nini, C., Rogledi, S., Rossi, M., and Vignolo, A. (2010). Sedimentary and tectonic evolution in the eastern Po-Plain and northern Adriatic Sea area from Messinian to Middle Pleistocene (Italy). *Rendiconti Lincei*, 21(1), 131-166.
- Ghielmi, M., Minervini, M., Nini, C., Rogledi, S., and Rossi, M. (2013). Late Miocene–Middle Pleistocene sequences in the Po Plain–Northern Adriatic Sea (Italy): the stratigraphic record of modification phases affecting a complex foreland basin. *Marine and Petroleum Geology*, 42, 50-81.
- Gladstone W. (2002). The potential value of indicator groups in the selection of marine reserves. *Biological Conservation*; 104:211-220

- Goodwin, D. H., Schone, B. R., and Dettman, D. L. (2003). Resolution and fidelity of oxygen isotopes as paleotemperature proxies in bivalve mollusk shells: models and observations. *Palaios*, 18(2), 110-125.
- Goudeau, M. L. S., Grauel, A. L., Bernasconi, S. M., & de Lange, G. J. (2013). Provenance of surface sediments along the southeastern Adriatic coast off Italy: an overview. *Estuarine, Coastal and Shelf Science*, 134, 45-56.
- Grant, K. M., Rohling, E. J., Bar-Matthews, M., Ayalon, A., Medina-Elizalde, M., Ramsey, C. B., Satow, C. and Roberts, A. P. (2012). Rapid coupling between ice volume and polar temperature over the past 150,000 years. *Nature*, 491(7426), 744.
- Gutiérrez, J. L., Jones, C. G., Strayer, D. L., and Iribarne, O. O. (2003). Mollusks as ecosystem engineers: the role of shell production in aquatic habitats. *Oikos*, 101(1), 79-90.
- Haszprunar, G., & Wanninger, A. (2012). Molluscs. *Current Biology*, 22(13), R510-R514.
- Holland, S. M. (1995). The stratigraphic distribution of fossils. *Paleobiology*, 21(1), 92-109.
- Holland, S. M. (2000). The quality of the fossil record: a sequence stratigraphic perspective. *Paleobiology*, 148-168.
- Holland, S. M., and Allen, J. (2008). The habitat of primitive vertebrates; the need for sedimentary geology in paleontology. *The Sedimentary Record*, 6(4), 4-7.
- Holland, S. M., and Christie, M. (2013). Changes in area of shallow siliciclastic marine habitat in response to sediment deposition: implications for onshore-offshore paleobiologic patterns. *Paleobiology*, 39(4), 511-524.
- Holland, S. M., Miller, A. I., Meyer, D. L., and Dattilo, B. F. (2001). The detection and importance of subtle biofacies within a single lithofacies: the Upper Ordovician Kope Formation of the Cincinnati, Ohio region. *Palaios*, 16(3), 205-217.
- Huntley, J. W., Fürsich, F. T., Alberti, M., Hethke, M., and Liu, C. (2014). A complete Holocene record of trematode–bivalve infection and implications for the response of parasitism to climate change. *Proceedings of the National Academy of Sciences*, 111(51), 18150-18155.
- Huntley, J. W., and Scarponi, D. (2015). Geographic variation of parasitic and predatory traces on mollusks in the northern Adriatic Sea, Italy: implications for the stratigraphic paleobiology of biotic interactions. *Paleobiology*, 41(1), 134-153.
- Kidwell, S. M. (1993). Patterns of time-averaging in the shallow marine fossil record. *Short Courses in Paleontology*, 6, 275-300.
- Kidwell, S. M., and Holland, S. M. (2002). The quality of the fossil record: implications for evolutionary analyses. *Annual Review of Ecology and Systematics*, 33(1), 561-588.
- Kingston, D. R., Dishroon, C. P., & Williams, P. A. (1983). Global basin classification system. *AAPG bulletin*, 67(12), 2175-2193.
- Kowalewski, M., Wittmer, J. M., Dexter, T. A., Amorosi, A., and Scarponi, D. (2015). Differential responses of marine communities to natural and anthropogenic changes. *Proceedings of the Royal Society of London B: Biological Sciences*, 282(1803), 20142990.

- Li, L., Zhang, X., Yun, H., & Li, G. (2017). Complex hierarchical microstructures of Cambrian mollusk *Pelagiella*: insight into early biomineralization and evolution. *Scientific reports*, 7(1), 1935.
- Lisiecki, L. E., and Raymo, M. E. (2005). A Pliocene-Pleistocene stack of 57 globally distributed benthic $\delta^{18}O$ records. *Paleoceanography*, 20(1).
- Little, M. G., Schneider, R. R., Kroon, D., Price, B., Summerhayes, C. P., and Segl, M. (1997). Trade wind forcing of upwelling, seasonally, and Heinrich events as a response to sub-Milankovitch climate variability. *Paleoceanography*, 12(4), 568-576.
- Livani, M., Scrocca, D., Arecco, P., & Doglioni, C. (2018). Structural and Stratigraphic Control on Salient and Recess Development Along a Thrust Belt Front: The Northern Apennines (Po Plain, Italy). *Journal of Geophysical Research: Solid Earth*.
- Lobo, F. J., and Ridente, D. (2014). Stratigraphic architecture and spatio-temporal variability of high-frequency (Milankovitch) depositional cycles on modern continental margins: an overview. *Marine Geology*, 352, 215-247.
- Maselli, V., Trincardi, F., Cattaneo, A., Ridente, D., and Asioli, A. (2010). Subsidence pattern in the central Adriatic and its influence on sediment architecture during the last 400 kyr. *Journal of Geophysical Research: Solid Earth*, 115(B12).
- Maselli, V., Hutton, E. W., Kettner, A. J., Syvitski, J. P., and Trincardi, F. (2011). High-frequency sea level and sediment supply fluctuations during Termination I: an integrated sequence-stratigraphy and modeling approach from the Adriatic Sea (Central Mediterranean). *Marine Geology*, 287(1-4), 54-70.
- Maslin, M., Seidov, D., and Lowe, J. (2001). Synthesis of the nature and causes of rapid climate transitions during the Quaternary. *The Oceans and Rapid Climate Change*, 9-52.
- Mattavelli, L., Ricchiuto, T., Grignani, D., and Schoell, M. (1983). Geochemistry and habitat of natural gases in Po basin, Northern Italy. *AAPG bulletin*, 67(12), 2239-2254.
- McClennen, C. E., Ammerman, A. J., and Schock, S. G. (1997). Framework stratigraphy for the Lagoon of Venice, Italy: revealed in new seismic-reflection profiles and cores. *Journal of Coastal Research*, 745-759.
- McMullen, S. K., Holland, S. M., and O'Keefe, F. R. (2014). The occurrence of vertebrate and invertebrate fossils in a sequence stratigraphic context: the Jurassic Sundance Formation, Bighorn Basin, Wyoming, USA. *Palaios*, 29(6), 277-294.
- Meldahl, K. H. (1990). Sampling, species abundance, and the stratigraphic signature, of mass extinction: A test using Holocene tidal flat molluscs. *Geology*, 18(9), 890-893.
- Milankovitch, M. (1930). Mathematische klimalehre und astronomische theorie der klimaschwankungen. *Handbuch der Klimatologie 1*.
- Milankovitch, M. K. (1941). Kanon der Erdbestrahlung und seine Anwendung auf das Eiszeitenproblem. *Royal Serbian Academy Special Publication*, 133, 1-633.
- Mikkelsen, P. M., and Cracraft, J. (2001). Marine biodiversity and the need for systematic inventories. *Bulletin of Marine Science*, 69(2), 525-534.
- Morton, J. E. (1967). Molluscs. London: Hutchinson

- Muttoni, G., Carcano, C., Garzanti, E., Ghielmi, M., Piccin, A., Pini, R., Rogledi, S. and Sciunnach, D. (2003). Onset of major Pleistocene glaciations in the Alps. *Geology*, *31*(11), 989-992.
- Nordsieck, F. (1968). Die europäischen Meeres-Gehäuse-schnecken. 273 pp.
- Nordsieck, F. (1972). *Die europäischen Meeresschnecken:(Opisthobranchia mit Pyramidellidae: Rissoacea); vom Eismeer bis Kapverden, Mittelmeer und Schwarzes Meer*. G. Fischer.
- Nordsieck, F. (1982). *Die europäischen Meeres-Gehäuseschnecken (Prosobranchia): vom Eismeer bis Kapverden, Mittelmeer und Schwarzes Meer*. G. Fischer.
- Oliverio, M. (2003). The Mediterranean molluscs: the best known malacofauna of the world... so far. *Biogeographia—The Journal of Integrative Biogeography*, *24*(1).
- Ori, G. G., and Friend, P. F. (1984). Sedimentary basins formed and carried piggyback on active thrust sheets. *Geology*, *12*(8), 475-478.
- Ori, G. G., Roveri, M., and Vannoni, F. (1986). Plio-Pleistocene sedimentation in the Apenninic-Adriatic foredeep (Central Adriatic Sea, Italy). In *Foreland basins* (Vol. 8, pp. 183-198). International Association of Sedimentologists.
- Pace, P., Scisciani, V., Calamita, F., Butler, R. W., Iacopini, D., Esetime, P., & Hodgson, N. (2015). Inversion structures in a foreland domain: Seismic examples from the Italian Adriatic Sea. *Interpretation*, *3*(4), SAA161-SAA176.
- Paillard, D., and Labeyriet, L. (1994). Role of the thermohaline circulation in the abrupt warming after Heinrich events. *Nature*, *372*(6502), 162.
- Parenzan, P. (1970). Carta d'identità delle conchiglie del Mediterraneo Vol. 1. (Gasteropodi) *Taranto, Bios Taras*: 1-283.
- Parenzan, P. (1974). Carta d'identità delle conchiglie del Mediterraneo Vol. 2, part 1 (Bivalvi), *Taranto, Bios Taras*: 1-277 + 46 plates.
- Parenzan, P. (1976). Carta d'identità delle conchiglie del Mediterraneo Vol. 2, part 2 (Bivalvi), *Taranto, Bios Taras*: 283-546 + 56 plates. [+ Vol. 3 (Bibliografia): 1-50].
- Patzkowsky, M. E., and Holland, S. M. (1999). Biofacies replacement in a sequence stratigraphic framework; Middle and Upper Ordovician of the Nashville Dome, Tennessee, USA. *Palaios*, *14*(4), 301-317.
- Patzkowsky, M. E., and Holland, S. M. (2012). *Stratigraphic paleobiology: understanding the distribution of fossil taxa in time and space*. University of Chicago Press.
- Petersen, S. V., Schrag, D. P., & Clark, P. U. (2013). A new mechanism for Dansgaard-Oeschger cycles. *Paleoceanography*, *28*(1), 24-30.
- Pellegrini, C., Maselli, V., and Trincardi, F. (2016). Pliocene–Quaternary contourite depositional system along the south-western Adriatic margin: changes in sedimentary stacking pattern and associated bottom currents. *Geo-Marine Letters*, *36*(1), 67-79.
- Pellegrini, C., Maselli, V., Gamberi, F., Asioli, A., Bohacs, K. M., Drexler, T. M., and Trincardi, F. (2017a). How to make a 350-m-thick lowstand systems tract in 17,000 years: The Late Pleistocene Po River (Italy) lowstand wedge. *Geology*, *45*(4), 327-330.

- Pellegrini, C., Bohacs, K. M., Drexler, T. M., Gamberi, F., Rovere, M., & Trincardi, F. (2017b). Identifying the sequence boundary in over- and under-supplied contexts: the case of the late Pleistocene Adriatic continental margin. In *Sequence Stratigraphy: the Future Defined, Proceedings of the 36th Annual Perkins-Rosen Research Conference* (pp. 160-182).
- Pellegrini, C., Asioli, A., Bohacs, K. M., Drexler, T. M., Feldman, H. R., Sweet, M. L., Maselli, V., Rovere, M., Gamberi, F., Dalla Valle, G. and Trincardi, F. (2018). The late Pleistocene Po River lowstand wedge in the Adriatic Sea: Controls on architecture variability and sediment partitioning. *Marine and Petroleum Geology*, *96*, 16-50.
- Picotti, V., Capozzi, R., Bertozzi, G., Mosca, F., Sitta, A., and Tornaghi, M. (2007). The Miocene petroleum system of the Northern Apennines in the central Po Plain (Italy). In *Thrust Belts and Foreland Basins* (pp. 117-131). Springer, Berlin, Heidelberg.
- Picotti, V., and Pazzaglia, F. J. (2008). A new active tectonic model for the construction of the Northern Apennines mountain front near Bologna (Italy). *Journal of Geophysical Research: Solid Earth*, *113*(B8).
- Pieri, M., and Groppi, G. (1981). *Subsurface geological structure of the Po Plain, Publication 414 del Progetto Finalizzato Geodinamica*. CNR. Internal report.
- Piva, A., Asioli, A., Schneider, R. R., Trincardi, F., Andersen, N., Colmenero-Hidalgo, E., Dennielou, B., Flores J. A. and Vigliotti, L. (2008). Climatic cycles as expressed in sediments of the PROMESS1 borehole PRAD1-2, central Adriatic, for the last 370 ka: 1. Integrated stratigraphy. *Geochemistry, Geophysics, Geosystems*, *9*(1).
- Ponder, W., and Lindberg, D. R. (Eds.). (2008). *Phylogeny and Evolution of the Mollusca*. University of California Press.
- Regione Emilia-Romagna and ENI-AGIP. (1998). Riserve idriche sotterranee della Regione Emilia-Romagna. Di Dio, G., ed. Florence, S.EL.CA. s.r.l., 120 pp.
- Regione Lombardia, and E.N.I. Divisione A.G.I.P. (2002), *Geologia degli acquiferi Padani della Regione Lombardia*: Firenzer, S.EL.CA. s.r.l., 130 pp.
- Ricci Lucchi, F. (1986). The Oligocene to Recent foreland basins of the northern Apennines. In *Foreland basins* (Vol. 8, pp. 105-139). Blackwell Scientific Oxford.
- Ricci Lucchi, F. (1990). Turbidites in foreland and on-thrust basins of the northern Apennines. *Palaeogeography, Palaeoclimatology, Palaeoecology*, *77*(1), 51-66.
- Rahmstorf, S., Crucifix, M., Ganopolski, A., Goosse, H., Kamenkovich, I., Knutti, R., Lohmann, G., Marsh, R., Mysak, L. A., Wang, Z. and Weaver, A. J. (2005). Thermohaline circulation hysteresis: A model intercomparison. *Geophysical Research Letters*, *32*(23).
- Ridente, D., and Trincardi, F. (2002). Eustatic and tectonic control on deposition and lateral variability of Quaternary regressive sequences in the Adriatic basin (Italy). *Marine geology*, *184*(3-4), 273-293.
- Ridente, D., & Trincardi, F. (2005). Pleistocene “muddy” forced-regression deposits on the Adriatic shelf: a comparison with prodelta deposits of the late Holocene highstand mud wedge. *Marine Geology*, *222*, 213-233.

- Ridente, D., & Trincardi, F. (2006). Active foreland deformation evidenced by shallow folds and faults affecting late Quaternary shelf-slope deposits (Adriatic Sea, Italy). *Basin Research*, *18*(2), 171-188.
- Ridente, D., Fogliani, F., Minisini, D., Trincardi, F., and Verdicchio, G. (2007). Shelf-edge erosion, sediment failure and inception of Bari Canyon on the Southwestern Adriatic Margin (Central Mediterranean). *Marine Geology*, *246*(2-4), 193-207.
- Ridente, D., Fracassi, U., Di Bucci, D., Trincardi, F., and Valensise, G. (2008a). Middle Pleistocene to Holocene activity of the Gondola Fault Zone (Southern Adriatic Foreland): deformation of a regional shear zone and seismotectonic implications. *Tectonophysics*, *453*(1-4), 110-121.
- Ridente, D., Trincardi, F., Piva, A., Asioli, A., and Cattaneo, A. (2008b). Sedimentary response to climate and sea level changes during the past~ 400 ka from borehole PRAD1–2 (Adriatic margin). *Geochemistry, Geophysics, Geosystems*, *9*(9).
- Ridente, D., Trincardi, F., Piva, A., and Asioli, A. (2009). The combined effect of sea level and supply during Milankovitch cyclicity: Evidence from shallow-marine $\delta^{18}O$ records and sequence architecture (Adriatic margin). *Geology*, *37*(11), 1003-1006.
- Rizzini, A., and Dondi, L. (1979). Messinian evolution of the Po basin and its economic implications (hydrocarbons). *Palaeogeography, Palaeoclimatology, Palaeoecology*, *29*, 41-74.
- Rossi, M. (2017). Outcrop and seismic expression of stratigraphic patterns driven by accommodation and sediment supply turnarounds: Implications on the meaning and variability of unconformities in syn-orogenic basins. *Marine and Petroleum Geology*, *87*, 112-127.
- Rossi, V., Azzarone, M., Capraro, L., Faranda, C., Ferretti, P., Macrì, P., and Scarponi, D. (2018). Dynamics of benthic marine communities across the Early-Middle Pleistocene boundary in the Mediterranean region (Valle di Manche, Southern Italy): Biotic and stratigraphic implications. *Palaeogeography, Palaeoclimatology, Palaeoecology*, *495*, 127-138.
- Roy, K., Valentine, J. W., Jablonski, D., and Kidwell, S. M. (1996). Scales of climatic variability and time averaging in Pleistocene biotas: implications for ecology and evolution. *Trends in Ecology and Evolution*, *11*(11), 458-463.
- Royden, L., Patacca, E., and Scandone, P. (1987). Segmentation and configuration of subducted lithosphere in Italy: An important control on thrust-belt and foredeep-basin evolution. *Geology*, *15*(8), 714-717.
- Ruddiman W.R. (2014). *Earth's Climate Past and Future*. Third Edition, W.H. Freeman and Company New York, 429pp
- Scarponi, D., and Kowalewski, M. (2004). Stratigraphic paleoecology: Bathymetric signatures and sequence overprint of mollusk associations from upper Quaternary sequences of the Po Plain, Italy. *Geology*, *32*(11), 989-992.
- Scarponi, D., and Kowalewski, M. (2007). Sequence stratigraphic anatomy of diversity patterns: Late Quaternary benthic mollusks of the Po Plain, Italy. *Palaios*, *22*(3), 296-305.
- Scarponi, D., Kaufman, D., Amorosi, A., and Kowalewski, M. (2013). Sequence stratigraphy and the resolution of the fossil record. *Geology*, *41*(2), 239-242.

- Scarponi, D., Huntley, J. W., Capraro, L., and Raffi, S. (2014). Stratigraphic paleoecology of the Valle di Manche section (Crotone Basin, Italy): a candidate GSSP of the Middle Pleistocene. *Palaeogeography, Palaeoclimatology, Palaeoecology*, 402, 30-43.
- Scarponi, D., Azzarone, M., Kusnerik, K., Amorosi, A., Bohacs, K. M., Drexler, T. M., and Kowalewski, M. (2017). Systematic vertical and lateral changes in quality and time resolution of the macrofossil record: Insights from Holocene transgressive deposits, Po coastal plain, Italy. *Marine and Petroleum Geology*, 87, 128-136.
- Schöne, B., Tanabe, K., Dettman, D. L., and Sato, S. (2003). Environmental controls on shell growth rates and $\delta^{18}\text{O}$ of the shallow-marine bivalve mollusk *Phacosoma japonicum* in Japan. *Marine Biology*, 142(3), 473-485.
- Schwarzacher, W. (2000). Repetitions and cycles in stratigraphy. *Earth-Science Reviews*, 50(1), 51-75
- Seidov, D., and Maslin, M. (2001). Atlantic Ocean heat piracy and the bipolar climate see-saw during Heinrich and Dansgaard–Oeschger events. *Journal of Quaternary Science: Published for the Quaternary Research Association*, 16(4), 321-328.
- Selley, R. C., & Sonnenberg, S. A. (2014). *Elements of petroleum geology*. Academic Press.
- Sierro, F. J., Andersen, N., Bassetti, M. A., Berné, S., Canals, M., Curtis, J. H., Dennielou B., Flores, J. A., Frigola, J., Gonzalez-Mora, B., Grimalt, J. O., Hodell, D. A., Jouet, G., Perez-Folgado, M. and Schneider, R. (2009). Phase relationship between sea level and abrupt climate change. *Quaternary Science Reviews*, 28(25-26), 2867-2881.
- Somoza, L., Hernández-Molina, F. J., De Andrés, J. R., and Rey, J. (1997). Continental shelf architecture and sea-level cycles: Late Quaternary high-resolution stratigraphy of the Gulf of Cádiz, Spain. *Geo-Marine Letters*, 17(2), 133-139.
- Storms, J. E., Weltje, G. J., Terra, G. J., Cattaneo, A., and Trincardi, F. (2008). Coastal dynamics under conditions of rapid sea-level rise: Late Pleistocene to Early Holocene evolution of barrier–lagoon systems on the northern Adriatic shelf (Italy). *Quaternary Science Reviews*, 27(11-12), 1107-1123.
- Terry, R. C., and Novak, M. (2015). Where does the time go?: Mixing and the depth-dependent distribution of fossil ages. *Geology*, 43(6), 487-490.
- Tinti, S., Maramai, A., and Favali, P. (1995). The Gargano promontory: An important Italian seismogenic-tsunamigenic area. *Marine Geology*, 122(3), 227-241.
- Torre, M., Di Nocera, S., and Ortolani, F. (1988). Evoluzione post-tortoniana dell'Appennino meridionale. *Memorie della Società Geologica Italiana*, 41, 47-56.
- Trincardi, F., and Correggiari, A. (2000). Quaternary forced regression deposits in the Adriatic basin and the record of composite sea-level cycles. *Geological Society, London, Special Publications*, 172(1), 245-269.
- Trincardi, F., Correggiari, A., and Roveri, M. (1994). Late Quaternary transgressive erosion and deposition in a modern epicontinental shelf: the Adriatic semienclosed basin. *Geo-marine letters*, 14(1), 41-51.
- Trincardi, F., Cattaneo, A., Asioli, A., Correggiari, A., and Langone, L. (1996). Stratigraphy of the late-Quaternary deposits in the central Adriatic basin and the record of short-term climatic events. *Memorie-Istituto Italiano di Idrobiologia*, 55, 39-70.

- Trincardi, F., Cattaneo, A., Correggiari, A., and Ridente, D. (2004). Evidence of soft sediment deformation, fluid escape, sediment failure and regional weak layers within the late Quaternary mud deposits of the Adriatic Sea. *Marine Geology*, 213(1-4), 91-119.
- Trobec, A., Busetti, M., Zgur, F., Baradello, L., Babich, A., Cova, A., Gordini E., Romeo R., Tomini I., Poglajen S., Diviaco P., Vrabek M. (2018). Thickness of marine Holocene sediment in the Gulf of Trieste (northern Adriatic Sea). *Earth System Science Data*, 10(2), 1077-1092.
- Tyler, C. L., and Kowalewski, M. (2014). Utility of marine benthic associations as a multivariate proxy of paleobathymetry: a direct test from recent coastal ecosystems of North Carolina. *PLoS one*, 9(4), e95711.
- Tyler, C. L., & Kowalewski, M. (2017). Surrogate taxa and fossils as reliable proxies of spatial biodiversity patterns in marine benthic communities. *Proc. R. Soc. B*, 284(1850), 20162839
- Trincardi, F., Argnani, A., and Correggiari, A. (2011). Note Illustrative della Carta Geologica dei Mari Italiani alla scala 1: 250.000. *EL. CA, fogli Ancona NK*, 33-1.
- Valentine, J. W. (2004). *On the origin of phyla*. University of Chicago Press.
- Vannoli, P., Burrato, P., and Valensise, G. (2015). The seismotectonics of the Po Plain (northern Italy): Tectonic diversity in a blind faulting domain. *Pure and Applied Geophysics*, 172(5), 1105-1142.
- Van Wagoner, J. C. (1995). Overview of sequence stratigraphy of foreland basin deposits: terminology, summary of papers, and glossary of sequence stratigraphy.
- West, C. F., Burchell, M., & Andrus, C. F. T. (2018). Molluscs and Paleoenvironmental Reconstruction in Island and Coastal Settings: Variability, Seasonality, and Sampling. In *Zooarchaeology in Practice* (pp. 191-208). Springer, Cham.
- Wittmer, J. M., Dexter, T. A., Scarponi, D., Amorosi, A., and Kowalewski, M. (2014). Quantitative bathymetric models for late Quaternary transgressive-regressive cycles of the Po Plain, Italy. *The Journal of Geology*, 122(6), 649-670.
- Zecchin, M., Praeg, D., Ceramicola, S., and Muto, F. (2015). Onshore to offshore correlation of regional unconformities in the Plio-Pleistocene sedimentary successions of the Calabrian Arc (central Mediterranean). *Earth-Science Reviews*, 142, 60-78.
- Zecchin, M., and Catuneanu, O. (2013). High-resolution sequence stratigraphy of clastic shelves I: units and bounding surfaces. *Marine and Petroleum Geology*, 39(1), 1-25.
- Zhang, X., Lohmann, G., Knorr, G., & Purcell, C. (2014). Abrupt glacial climate shifts controlled by ice sheet changes. *Nature*, 512(7514), 290.
- Ziemen, F. A., Kapsch, M. L., Klockmann, M., & Mikolajewicz, U. (2018). Heinrich events show two-stage climate response in transient glacial simulations. *Climate of the Past Discussions*, 1-22.
- Wells, F. E. (1998). Superfamily Stromboidea. Pages 766–769 in P. L. Beesley, G. J. B. Ross, and A. Wells, eds. *Mollusca: the southern synthesis*. Fauna of Australia. Vol. 5, part B. CSIRO, Melbourne.

Acknowledgements

I was always fascinated by fossils and the window that they open on the history of life on Earth. Thanks to my parents when I was child, I collected numerous books and booklets on a wide range of topics on paleontology, which fed my passion and my curiosity. I was captured by dinosaurs and the mysterious prehistoric world depicted in a multitude of movies, documentaries, and books after the release of Jurassic Park in 1993; however, the shells that I was able to collect a few kilometers from my childhood city held my attention more. From this point, the choice of a geology degree became obvious, and my interest continued to grow as I discovered the works of Darwin and other classic scientific authors.

These three years of Ph.D. study passed rapidly. During this journey, I finally was able to “evolve” from being an amateur and to enter the world of scientific research. For this, I thank the wonderful people that guided me through the faceted and complex but captivating world of paleontology.

To avoid an entire chapter to acknowledge people to whom I am grateful, I thank everyone who shared my journey. However, several key figures deserve special thanks.

First, I thank Daniele Scarponi, my Ph.D. advisor, who indefatigably accompanied me through these three years. His patience and his incredible trust as well as the invaluable suggestions were keystones for my professional growth over the course of my Ph.D. research.

I am also grateful for Michal Kowalewski, who warmly welcomed and accompanied me in the Florida Museum of Natural History, providing precious guidance through the foreign world of multivariate ordination analysis, at least to me.

Thanks also go to John Warren Huntley for offering kind advice and collaboration to guide me through the exploration of parasitism in the fossil record.

I appreciate the opportunity granted to me by the CNR-ISMAR in Bologna to access and sample their cores. This research was indispensable for the assemblage of the Mid Adriatic Deep dataset.

I'm also thankful for Claudio Pellegrini, who offered patient assistance during the sampling sessions of cores at CNR-ISMAR, and for Veronica Rossi for fruitful collaboration. I thank both for their kind review on the complex passages of this thesis.

Hoping to not forget anyone and who helped me through these years, I am concluding by thanking Monica Caffara and Andrea Gustinelli, who assisted in the analysis of parasites in living bivalves at the Veterinary Department of UniBo.

I am also grateful for all the friends whom I met during these three years, particularly Giulia and Ilenia, my officemates. With them, I shared laughs and difficulties that made this voyage an unforgettable one.

Outside the academic world, I am grateful for my family, who have always been present and supportive, especially when I needed them most.

Finally, a special thank to Barbara for her incredible support of my work.

Michele